Cover: *Neutrophil Engulfing MRSA* is a photograph by National Institute of Allergy and Infectious Diseases (NIAID)/National Institutes of Health (Frank DeLeo), uploaded on June 29, 2016.

Universiteit Antwerpen

Insight in methicillin-resistant *Staphylococcus aureus* (MRSA) biofilms: identification of key determinants in biofilm formation of highly pathogenic and globally successful MRSA clones

Inzicht in methicilline-resistente Staphylococcus aureus (MRSA) biofilms: identificatie van belangrijke genetische determinanten die bijdragen tot biofilm vorming van zeer pathogene en wereldwijd succesvolle klonen

Dissertation for the degree of **Doctor in Medical Sciences** at University of Antwerp, to be defended by:

Sarah De Backer

Supervisor: Prof. Dr. Surbhi Malhotra-Kumar

Co-supervisor: Prof. Dr. Herman Goossens

Laboratory of Medical Microbiology

Faculteit Geneeskunde en Gezondheidswetenschappen

2019

Promotor:

Prof. Dr. Surbhi Malhotra-Kumar

Laboratory of Medical Microbiology, University of Antwerp, Belgium

Co-promotor:

Prof. Dr. Herman Goossens

Laboratory of Medical Microbiology, University of Antwerp, Belgium

Member of the examination and reading committee:

Internal jury (Universiteit Antwerpen):

Prof. Dr. Phillipe Jorens (voorzitter)

Intensive Care Unit, Universitair Ziekenhuis Antwerpen (UZA), Belgium

Prof. Dr. Ir. Sarah Lebeer

Laboratory of Applied Microbiology and Biotechnology, University of Antwerp, Belgium

External jury:

Prof. Dr. Patrick Van Dijck

Laboratory of Molecular Cell Biology, KU Leuven, Belgium

Dr. Cuong Vuong

AiCuris Anti-infective Cures GmbH, Wuppertal, Germany

Prof. Dr. Jodi Lindsay

Institute of Infection and Immunity, London, The United Kingdom

"In the average adult are 100 trillion human cells and 1500 trillion microbes. At best you are little more than 10% you. We're all just petri dishes with shoes."

- Anyletter (schuhlelewis.blogspot.com)

SDB is supported by funding from Research Foundation Flanders (FWO, applicant number 1128818N).

Table of contents

List of figures 12

List of tables 15

List of abbreviations 17

Abstract 19

Nederlandstalig abstract 21

Chapter 1: Introduction on methicillin-resistant *Staphylococcus aureus* - exploring the biofilm 23

1.1. Methicillin-resistant *Staphylococcus aureus*: exploring the biofilm 24

1.1.1. Abstract 24

1.1.2. Introduction 24

1.1.3. Biofilm formation by staphylococci 25

1.1.4. Biofilm formation by methicillin-sensitive *S. aureus* (MSSA) 29

1.1.5. Biofilm formation by methicillin-resistant *S. aureus* 31

1.1.6. Methicillin resistance and the biofilm phenotype 32

1.1.7. Molecular underpinnings of MRSA outbreaks 33

1.1.8. Conclusions and outlook 36

1.1.9. Addendum 36

Chapter 2: Scope of the thesis 43

2.1. Research hypothesis 44

2.2. Aims 45

2.3. References 46

Chapter 3: Experimental work 47

3.1. Differential gene expression analysis to identify MRSA transcriptional signatures associated with the planktonic and biofilm phenotypes 48

3.1.1. Transcriptome sequencing analysis investigates global changes in *Staphylococcus aureus* biofilm gene expression and reveals a key role of arginine biosynthesis across pandemic methicillin-resistant USA300, EMRSA-15 and ST239-SCC*mec*III clones 49

3.1.1.1. Abstract 49
3.1.1.2. Introduction 50
3.1.1.3. Materials and methods 51
3.1.1.4. Results 55
3.1.1.5. Discussion 66
3.1.1.6. Addendum 70
3.2. A *bursa aurealis* transposon library to screen MRSA knockout mutants for biofilm-associated targets 85
3.2.1. Screening of a *bursa aurealis* transposon mutant library for genes involved in the PIA/PNAG-independent biofilm phenotype formed by methicillin-resistant *Staphylococcus aureus* USA300. 86
3.2.1.1. Abstract 86
3.2.1.2. Introduction 86
3.2.1.3. Materials & methods 87
3.2.1.4. Results & discussion 91
3.2.1.5. Conclusion 97
3.2.1.6. Addendum 98
3.3. Identification of biofilm-associated candidate genes using *in vitro* biofilm models of staphylococcal infection and comparative genomics 110
3.3.1. Enzymes catalysing the TCA- and urea cycles influence the matrix composition of biofilms formed by methicillin-resistant *Staphylococcus aureus* USA300 111
3.3.1.1. Abstract 111
3.3.1.2. Introduction 112
3.3.1.3. Materials and methods 114
3.3.1.4. Results 119
3.3.1.5. Discussion 125
3.3.1.6. Addendum 127
3.3.2. Fatty acid kinase A is an important determinant of biofilm formation in methicillin-resistant *Staphylococcus aureus* USA300. 132
3.3.2.1. Abstract 132
3.3.2.2. Background 133

3.3.2.3. Methods 134
3.3.2.4. Results 138
3.3.2.5. Discussion 144
3.3.2.6. Conclusions.....146
3.3.2.7. Addendum 146
3.4. Characterization of biofilm-associated candidate genes as a critical determinant of MRSA pathogenic success. 155
3.4.1. Remarkable geographical variations between India and Europe in carriage of the staphylococcal surface protein-encoding s*asX/sesI* and in the population structure of methicillin-resistant *Staphylococcus aureus* belonging to clonal complex 8 156
3.4.1.1. Abstract 156
3.4.1.2. Introduction.....157
3.4.1.3. Methods 158
3.4.1.4. Results 159
3.4.1.5. Discussion 164
3.4.1.6. Addendum 166

Chapter 4: Concluding insights.....171
4.1. General discussion.....172
4.2. Future perspectives.....174
4.3. Summary 177
4.4. Nederlandstalige samenvatting 180
4.5. References.....184

Acknowledgements 189
Addendum: Curriculum vitae 191
Articles in international peer-reviewed journals 191
Articles under submission in international peer-reviewed journals.....192
Oral presentations in international meetings 192
Poster presentations in international meetings.....193

List of figures

Figure 1| Phases of biofilm development in *S. aureus*..... 28

Figure 2| Major regulatory networks directing biofilm formation by *S. aureus*..... 30

Figure 3| Model of the alteration of *S. aureus* virulence, biofilm or colonization capacity exerted by the acquisition of methicillin resistance gene *mecA*..... 34

Figure 4| Experimental workflow for RNA-sequencing of biofilm and planktonic pandemic USA300, EMRSA-15 and ST239-SCC*mec*III MRSA phenotypes. ... 53

Figure 5| Biofilm formation of pandemic USA300, EMRSA-15, and ST239-SCC*mec*III MRSA clones under flow conditions..... 56

Figure 6| Metabolic functions of differentially up- and down-expressed genes (|$\log_2$(fold change)|>1) in pandemic USA300, EMRSA-15, and ST239-SCC*mec*III MRSA clones ageing biofilm cells. 58

Figure 7| Expression of the ADI-pathway in ageing biofilm cultures of pandemic USA300, EMRSA-15 and ST239-SCC*mec*III MRSA clones..... 60

Figure 8| Expression of the pyrimidine nucleotide biosynthesis pathway and the high-affinity K^+-specific transport system in ageing biofilm cultures of pandemic USA300, EMRSA-15 and ST239-SCC*mec*III MRSA clones..... 62

Figure 9| Expression of ACME-element associated genes and biofilm formation of corresponding knockout mutants in USA300..... 64

Figure 10| Expression of the urea cycle in ageing biofilm cultures of pandemic USA300, EMRSA-15 and ST239-SCC*mec*III MRSA clones..... 65

Figure 11| $\log_2$(fold change) of genes involved in arginine biosynthesis and the urea cycle under biofilm conditions for pandemic USA300, EMRSA-15 and ST239-SCC*mec*III MRSA clones 67

Figure 12| Visualization of the mapping of bursa aurealis transposon insertion UAS391-Ery^S mutants against *S. aureus* FPR3757 and USA300 UAS391..... 88

Figure 13| Gene functional assignment of *bursa aurealis* transposon UAS391-Ery^S mutants with a change in biofilm formation..... 92

Figure 14| Schematic representation of pBursa plasmid with the *bursa aurealis* transposon and pFA545 plasmid carrying *bursa aurealis* transposase, and their insertion in ten selected *bursa aurealis* transposon UAS391-Ery^S mutants..... 94

Figure 15| Identification and characterization of the ten *bursa aurealis* insertion UAS391-Ery^S mutant genes involved in biofilm formation 96

Figure 16| Schematic representation of the urea and tricarboxylic acid (TCA) cycles 113

Figure 17| Effect of TCA- and urea cycle knockouts on the biofilm phenotype by USA300 UAS391-Ery^S.....122

Figure 18| Static biofilm matrix structure obtained from fluorescent microscopy observations of *S. aureus* USA300 UAS391-Ery^S, and TCA- and urea cycle knockouts. 123

Figure 19| Enzymatic treatment of pre-formed 24h (no flow) or 17h (flow) old biofilms of UAS391-Ery^S, ATCC®25923™ and urea or TCA-cycle knockouts. 125

Figure 20| Whole-genome maps of USA300 strains.....139

Figure 21| Biofilm formation of USA300 strains in the dynamic shear flow assay 139

Figure 22| Biofilm formation of USA300 strains in the dynamic shear flow assay 140

Figure 23| Transcription levels of the *fakA* gene in UAS391, TCH1516, FPR3757, JE2 and in corresponding transductant strains 144

Figure 24| Circular phylogram reflecting evolutionary relationships between Indian and European clinical strains based on *sasX* homology and compared to ST239 reference sequences 160

Figure 25| Formation of biofilms by 9 Indian and 33 European CC8 strains isolated from either hospital-associated infection specimens or nasal screening samples 161

Figure 26| Characterization of the *sasX*, *sasX*-1 and *sesI*-carrying ϕSPβ-like prophage 162

Figure 27| Maximum likelihood phylogenetic tree based on the core genome SNPs of CC8 strains from India and Europe.....163

Supplementary figure 1| Phenotypic characterization of pandemic USA300, EMRSA-15, and ST239-SCC*mec*III MRSA clones.....70

Supplementary figure 2| Volcano plot of pandemic USA300, EMRSA-15, and ST239-SCC*mec*III MRSA clones RNAseq data.....71

Supplementary figure 3| Quantification of relative gene expression in pandemic USA300, EMRSA-15, and ST239-SCC*mec*III MRSA clones 71

Supplementary figure 4| PCA plot of pandemic USA300, EMRSA-15 and ST239-SCC*mec*III MRSA clones..... 72

Supplementary figure 5| Relative quantification of gene expression in UAS391-Ery^S and the corresponding *bursa aurealis* insertion UAS391-Ery^S mutants..... 98

Supplementary figure 6| Background absorption-corrected 24h growth curves for UAS391, UAS391-Ery^S and ten selected *bursa aurealis* insertion mutants. 99

Supplementary figure 7| Background absorption-corrected 24h growth curves for UAS391-Ery^S as well as TCA- and urea cycle knockouts 128

Supplementary figure 8| Quantification relative gene expression in UAS391-Ery^S and the corresponding TCA- and urea cycle knockout mutants..... 129

Supplementary Figure 9| Comparative genome alignment of USA300, TCH1516, FPR3757 and UAS391 147

Supplementary Figure 10| Multiple alignments of *fakA* gene sequences in *S. aureus* and *S. epidermidis* 147

Supplementary figure 11| MLST typing of Indian and European MRSA 167

Supplementary figure 12| Alignment of SasX, SasX-1 and SesI protein of Indian (IN) and European (EU) isolates exemplified by TW20, EU_ST239_7 and RP62A, respectively. EU_ST239_7 shows an additional change within SasX-1, which is highlighted in red. 167

Supplementary figure 13| Histogram of pairwise SNP differences between 64 study strains (Hamming distance) 167

List of tables

Table 1| *Bursa aurealis* transposon insertion mutants in USA300-JE2 and other *S. aureus* knockout isolates used in the differential gene expression study 51

Table 2| Bacterial strains and plasmids used during the TCA- and urea cycle study. 114

Table 3| Overview of relative gene expression, formed biofilm mass, growth rate and staining results in the TCA- and urea cycle study.....119

Table 4| USA300 strains used for clonal, genomic, and phenotypic analyses during the fatty acid kinase A study.....135

Table 5| Single nucleotide polymorphisms (SNPs) between TCH1516/FPR3757 and UAS391 142

Supplementary table 1| Gene-specific primers used for RT-PCR validation of RNA-Seq results.. 72

Supplementary table 2| Expression of 7 housekeeping genes (log_2 (fold-change)) under aging biofilm growth of pandemic USA300, EMRSA-15 and ST239-SCC*mec*III MRSA clones 72

Supplementary Table 3| Differentially expressed genes (log_2 (fold-change)) of urea cycle, arginine biosynthesis, pyrimidine biosynthesis, nitrite/nitrate respiration and cation transport as well as ACME-element associated genes (only in USA300) under ageing biofilm growth of pandemic USA300, EMRSA-15 and ST239-SCC*mec*III MRSA clones 73

Supplementary Table 4| Top differentially expressed genes with |fold-change>3| and FDR p-value correction<0.001 in biofilms of USA300 UAS391. 74

Supplementary Table 5| Top differentially expressed genes with |fold-change>3| and FDR p-value correction<0.001 in biofilms of EMRSA-15 H-EMRSA-15. 76

Supplementary Table 6| Top differentially expressed genes with |fold-change>3| and FDR p-value correction<0.001 in biofilms of ST239-*SCCmecIII*. 80

Supplementary Table 7| Primers used during the *bursa aurealis* transposon library study 99

Supplementary Table 8| Overview of *bursa aurealis* transposon insertion mutants with an increase in biofilm formation capacity as compared to UAS391-Ery^S.....99

Supplementary Table 9| Overview of *bursa aurealis* transposon insertion mutants with a decrease in biofilm formation capacity as compared to UAS391-Ery^{S} 103
Supplementary Table 10| Primers used during the TCA- and urea cycle study 129
Supplementary Table 11| Complete list of SNPs in genes representing divergent alleles in UAS391 and TCH1516 and their putative gene functions 147
Supplementary Table 12| Complete list of SNPs in genes representing divergent alleles in UAS391 and FPR3757 and their putative gene functions 150
Supplementary Table 13| Primers used in the *S. aureus* surface protein *sasX*/*sesI* study. 168
Supplementary table 14| Table of ST239 reference isolates used in the *S. aureus* surface protein *sasX*/*sesI* study with corresponding accession numbers. 168
Supplementary Table 15| Characteristics of MRSA isolates carrying *sasX*, *sasX*-1 or *sesI* in the *S. aureus* surface protein *sasX*/*sesI* study 169

List of abbreviations

ACME	arginine catabolic mobile element
ACP	enoyl-acyl carrier protein
ADI	arginine deiminase
AMP	antimicrobial peptide
ATCC	american type culture collection
ATP	adenosine triphosphate
BHI	brain-heart infusion
BLAST	basic local alignment tool
CA	community-associated
CA-MRSA	community-associated methicillin-resistant *S. aureus*
CC	clonal complex
DEG	differentially expressed gene
DNA	deoxyribonucleic acid
ECM	extracellular matrix
eDNA	extracellular DNA
EU	Europe
FASII	fatty acid synthesis
FnBP	fibronectin-binding proteins
HA	hospital-associated
HA-MRSA	hospital-associated methicillin-resistant *S. aureus*
HMM	hidden markov models
I	intermediate
IN	India
KEGG	kyoto encyclopaedia of genes and genomes
LB	luria-berthani
LPXTG	Leu-Pro-X-Thr-Gly
LTA	lipoteichoic acid
MGE	mobile genetic element
MOSAR	masterin hospital antimicrobial resistance and its spread in the community
MRSA	methicillin-resistant *S. aureus*
MSCRAMM	microbial surface components recognizing adhesive matrix molecules
MSSA	methicillin-sensitive *S. aureus*
NARSA	network on antimicrobial resistance in *S. aureus*
NGS	next-generation sequencing
NTML	nebraska transposon mutant library
ORF	open reading frame
PBP2a	penicillin-binding protein 2a

PBS	phosphate buffered saline
PCR	polymerase chain reaction
PDH	pyruvate dehydrogenase
PIA	polysaccharide intercellular adhesin
PNAG	Poly-N-acetylglucosamine
PSM	phenol-soluble modulin
R	resistant
RAP	RNAIII activating protein
RNA	ribonucleic acid
rpm	rounds per minute
rRNA	ribosomal RNA
RT-PCR	real-time polymerase chain reaction
S	susceptibility
SATURN	specific antibiotic therapies on the prevalence of human host resistant bacteria
SCC*mec*	staphylococcal chromosome mec
SERAM	secretable expanded repertoire adhesive molecules
SMART	single modular architecture research tool
SNP	single nucleotide polymorphism
sRNA	small RNA
ST	sequence type
TCA	tricarboxylic acid
Tn	transposon
TRAP	target of RAP
VAP	ventilator-associated pneumonia
WGA	wheat germ agglutinin
WGM	whole-genome mapping
WGS	whole-genome sequencing
WTA	wall-teichoic acid

Abstract

This thesis addresses *Staphylococcus aureus* that are a common cause of skin and soft tissue infections, but also several invasive, life-threatening infections such as pneumonia, endocarditis, osteomyelitis, septic arthritis, sepsis, and toxic shock syndrome. In addition to multidrug resistance (methicillin-resistant *S. aureus*, MRSA), the phenomenal success of *S. aureus* is also attributable to higher virulence due to the presence of virulence-specific factors, such as extracellular toxins, surface structures facilitating tissue colonization, immune evasion and tissue destruction, as well as prolonged persistence of *S. aureus* infections linked to the formation of sessile matrix-encased microcolonies termed biofilms. These biofilms are notoriously difficult to eradicate, with sessile populations being up to 1000-fold more resistant than their planktonic counterparts. Despite the important role of *S. aureus* biofilms in disease, our comprehension of the molecular mechanisms promoting biofilm formation is incomplete. Recent studies of *S. aureus* biofilm development hint that the extracellular matrix consists of proteins, DNA and/or polysaccharide (polysaccharide intercellular adhesin, PIA/PNAG). However, it has become evident that clinical MRSA isolates are not only dependent on PIA/PNAG for biofilm formation. Protein-mediated biofilm formation has emerged as another option to PIA/PNAG, and many surface adhesins, such as Bap, Spa, FnBPA, FnBPB, and SasG have been implicated in this divergent biofilm mechanism.

We aim to dissect the fundamental aspects underlying the pathogenic success of *S. aureus*/MRSA, and results are likely to have both diagnostic and therapeutic implications.

Three highly pathogenic and globally successful MRSA clones, USA300-UAS391, EMRSA-15 H-EMRSA-15 and ST239-SCC*mec*III EU_ST239_16, were characterized as prolific biofilm formers and therefore used as a model to look for commonalities in the global formation of MRSA biofilms. MRSA transcriptional signatures associated with *in vitro* planktonic and biofilm phenotypes were identified by means of differential gene expression analysis and requested from the publicly available NARSA knockout library. Additionally, in order not to overlook other important genes with non-significant up-regulation in the transcriptome analysis, screening of a high-throughput USA300-UAS391 transposon library revealed many mutants displaying changes in biofilm formation capacity. Interesting 'hits' were functionally validated for biofilm formation in both static and shear flow *in vitro* biofilm assays. The relevance of these mutations was also further confirmed by transduction experiments to look for similar phenotypic effects and complementation to demonstrate restoration of the wild type phenotype when a functional protein was present. As such, fatty acid kinase A (*fakA*), intermediates

of the TCA-cycle (*fumC*, *sdhA* and *sdhB*), and staphylococcal surface protein X (*sasX*) were marked as important determinants contributing to the pathogenic success of MRSA.

As biofilm formation is an important virulence factor for *S. aureus*, our delineation of factors that define virulence in the entire range of infectious MRSA strains will permit the rational design of anti-biofilm drugs that can be combined with conventional antibiotics, thus restoring efficacy the latter show to staphylococci in a non-biofilm status. Interestingly, this research opens the possibility of a single target affecting two key aspects of MRSA pathogenesis; β-lactam resistance and biofilm formation.

Nederlandstalig abstract

Deze thesis spitst zich toe op *Staphylococcus aureus*; de voornaamste oorzaak van huidinfecties, maar ook van verschillende invasieve en levensbedreigende infecties zoals longontsteking, endocarditis, osteomyelitis, septische artritis, sepsis en het toxic shock syndroom. Naast multidrug resistentie (methicilline-resistente *S. aureus*, MRSA), kan het fenomenale succes van *S. aureus* worden toegewezen aan een wijd arsenaal van virulentiefactoren, zoals extracellulaire toxines, oppervlaktestructuren die zorgen voor kolonisatie, ontwijking van het immuunsysteem en weefselvernietiging, alsook de verlengde persistentie van *S. aureus* infecties door de vorming van sessiele, matrix-omhulde microkolonies genaamd biofilms. Deze biofilms zijn berucht vanwege het feit dat dit fenotype bijna 1000 keer resistenter is tegen antibiotica dan de planktonische variant, waardoor deze biofilm-geassocieerde infecties zeer moeilijk te behandelen zijn. Ondanks de belangrijke rol van *S. aureus* biofilms in ziekte, is ons begrip van de moleculaire mechanismen die bijdragen tot de vorming van dergelijke biofilms nog steeds erg beperkt. Recente studies suggereren dat de extracellulaire matrix van de ontwikkelende *S. aureus* biofilm bestaat uit proteïnen, DNA en/of polysachariden (polysaccharide intercellulair adhesine, PIA/PNAG). Desondanks is het duidelijk geworden dat verschillende klinische *S. aureus* stammen niet afhankelijk zijn van PIA/PNAG voor biofilmvorming. Proteïne-gemedieerde biofilmvorming lijkt een toepasselijk alternatief te zijn voor PIA/PNAG en vele oppervlakte adhesines, zoals Bap, Spa, FnBPA, FnBPB, en SasG werden reeds geïmpliceerd in dit afwijkend biofilmmechanisme.

Wij beogen om de fundamentele aspecten die ten grondslag liggen aan het pathogene succes van *S. aureus*/MRSA, te ontleden. Resultaten zullen vermoedelijk zowel diagnostische als therapeutische implicaties hebben.

Drie sterk pathogene en globaal succesvolle MRSA klonen, USA300-UAS391, EMRSA-15 H-EMRSA-15 en ST239-SCC*mec*III EU_ST239_16, werden gekarakteriseerd als sterke biofilmvormers en daarom gebruikt als een model om te kijken naar gelijkenissen in de algemene vorming van MRSA biofilms. Transcriptionele MRSA kenmerken die geassocieerd waren met het *in vitro* planktonische en biofilm fenotype werden allereerst geïdentificeerd door middel van genexpressie-analyse en vervolgens opgevraagd bij de publiekelijk beschikbare NARSA knockout bibliotheek. Om geen andere belangrijke genen met niet-significante opregulatie in de transcriptoomanalyse te missen, werd een USA300-UAS391 transposon bibliotheek gescreend. Dit onthulde een groot aantal mutanten met sterke veranderingen in biofilmvormingscapaciteit. Interessante 'hits' werden functioneel gevalideerd voor biofilmvorming in zowel een statisch als dynamisch

in vitro biofilmexperiment. De relevantie van deze mutaties werd verder bevestigd door middel van transductie-experimenten waarbij gekeken werd naar gelijkaardige fenotypische effecten en complementatie om herstel van het originele fenotype te bevestigen wanneer een functioneel proteïne aanwezig was. Zodoende konden we vetzuur kinase A (*fakA*), tussenproducten van de TCA-cyclus (*fumC*, *sdhA*, en *sdhB*), en het staphylococcus oppervlakte proteine X (*sasX*) identificeren als belangrijke determinanten die bijdragen tot het pathogene succes van MRSA.

Omdat biofilmvorming een belangrijke virulentiefactor van *S. aureus* is, kan onze identificatie van factoren die kenmerkend zijn voor virulentie in een complete collectie van infectieuze MRSA stammen bijdragen tot het rationeel ontwerp van anti-biofilm drugs die gecombineerd kunnen worden met conventionele antibiotica, waardoor deze opnieuw dezelfde effectiviteit zullen vertonen als tegen staphylococci in een non-biofilm status. Dit onderzoek biedt ook de mogelijkheid van een enkel doelwit dat twee aspecten van MRSA pathogenese beïnvloedt: namelijk β-lactam resistentie en biofilmvorming.

<u>Chapter 1</u>: Introduction on methicillin-resistant *Staphylococcus aureus* - exploring the biofilm

"*Attack of the killer slime: it's not a B-movie, it's a biofilm*."

- Erica Mitchell

1.1. Methicillin-resistant Staphylococcus aureus: exploring the biofilm

Unpublished.

1.1.1. Abstract

The ability of *Staphylococcus aureus* to form biofilms is a key virulence factor for this pathogen that facilitates a prolonged persistence of infection and increases human morbidity and mortality. Bacteria change dramatically during the transition to a biofilm growth state: phenotypically; transcriptionally; and metabolically, making them hard to eradicate and highlighting the need for research into molecular mechanisms involved in biofilm formation. However, the biofilm phenotype expressed by *S. aureus* is also influenced by the production of penicillin-binding protein (PBP) 2a – encoded by the *mec* gene, which is responsible for methicillin resistance. The most well-known mechanism of biofilm formation is the production of the *icaADBC* operon-encoded polysaccharide intercellular adhesin (PIA) or poly-N-acetylglucosamine (PNAG), which is commonly employed by methicillin-sensitive *S. aureus* (MSSA). Methicillin-resistant *S. aureus* (MRSA), in contrast, expresses an Atl/FnBP-mediated biofilm phenotype. While the different mechanisms of MSSA and MRSA do not appear to influence their colonization capacity, the acquisition of methicillin resistance is also associated with an overall down-regulation of virulence gene expression. This makes MRSA optimally adapted to the hospital environment, which is characterized by immunocompromised patients in need of intensive antibiotic treatment and life-supporting medical devices. However, the formation of biofilms has also emerged as a tenacious survival strategy for MRSA infecting otherwise healthy individuals. This suggests that biofilm factors, along with colonization, antibiotic resistance and virulence factors may have an established role in contributing to global MRSA outbreaks.

Here, we review the mechanisms of MSSA and MRSA biofilm production and discuss specific pathogenesis factors exemplifying why biofilm-forming capacity is a major key factor underpinning successful MRSA spread in both healthcare and community settings.

1.1.2. Introduction

As an opportunistic pathogen, *Staphylococcus aureus* can colonize the human skin, forming a risk factor for infection of an implanted device or for infections ranging from boils to sepsis and pneumonia [1]. Although *S. aureus* infections used to be easily curable with penicillin and methicillin, the widespread emergence of β-lactamase and

the acquisition of the staphylococcal cassette chromosome *mec* (*SCCmec*) encoding an alternative penicillin-binding protein PBP2a with decreased affinity for β-lactams have rendered these antibiotics largely ineffective [2]. Based on the type of this *SCCmec* element (and the genetically distinct *S. aureus* lineage), MRSA clones can be defined. Only a few clonal types of MRSA are successful in hospitals (healthcare-acquired MRSA, HA-MRSA; *SCCmec* type I-III), with separate clones of MRSA spreading in the community (community-acquired MRSA, CA-MRSA; IV-V *SCCmec* elements) [3, 4]. HA-MRSA and CA-MRSA show significant differences in terms of distribution of toxin and antibiotic resistance genes. While HA-MRSA tends to be more multidrug-resistant than CA-MRSA, the latter tends to be more virulent as evidenced by its propensity to infect and cause fulminant infections in healthy individuals [5]. Another 'virulent' strategy employed by *S. aureus* is the formation of biofilms *in vivo*, which facilitates a prolonged persistence of infections [6]. In a biofilm, the community of cells remains attached to a solid support, embedded in a matrix of extracellular polymeric substances, and shows altered growth and metabolic activity, gene expression and protein production in comparison to their planktonic counterparts [7, 8]. Moreover, being part of a biofilm also confers resistance to antibiotics that are otherwise active against planktonic MRSA and this presents a major problem to clinicians for the treatment of MRSA infections [9]. Therefore, developing therapeutic or diagnostic approaches for targeting biofilm-related infections requires a thorough understanding of the molecular mechanisms underlying biofilm formation.

Here, we review biofilm development by methicillin-sensitive *S. aureus* (MSSA) and methicillin-resistant *S. aureus* (MRSA) and explore the underpinnings of linked biofilm formation, antibiotic resistance, and virulence gene expression in MRSA outbreaks.

1.1.3. Biofilm formation by staphylococci

1.1.3.1. Initial attachment

Staphylococci*,* especially *S. aureus,* have an amazing capacity to attach to indwelling medical devices through direct interaction with the device's polymer surface or by establishing connections to a surface conditioning film of blood plasma and host matrix material.

Upon passive contact with a surface, *S. aureus* may directly attach to abiotic surfaces [10, 11]. Binding includes autolysin activity (major autolysin Atl) [12], which is controlled by wall teichoic acids (WTAs) [13]. However, in clinical practice, indwelling devices are never bare surfaces and become rapidly covered by host matrix material, such as collagens, fibronectins, and fibrinogen [14]. Here, specific staphylococcal surface

proteins interact with those human matrix proteins. The most important surface-expressed staphylococcal binding proteins are the MSCRAMMs (microbial surface components recognizing adhesive matrix molecules) family [15]. MSCRAMMS contain a conserved Leu-Pro-X-Thr-Gly (LPXTG) motif and are covalently linked to cell wall peptidoglycan by the sortase enzyme SrtA [16, 17]. Most well-known examples are the fibronectin-binding proteins (FnBPA, FnBPB), the clumping factors (ClfA, ClfB), and the serine-aspartate repeat family proteins (SdrC, SdrD, SdrE) [18-21]. Other surface proteins mediating attachment in a non-covalently linked way belong to the SERAM (secretable expanded repertoire adhesive molecules) family [22]. Members include the extracellular adherence protein Eap, the extracellular matrix, and plasma binding protein Emp and the giant 1.1MDa cell wall-associated fibronectin-binding protein Ebh [23-25].

1.1.3.2. Proliferation/maturation

After attachment, cells will proliferate into microcolonies and start secreting polymeric molecules to form a glue-like extracellular matrix (ECM) which is mainly constituted out of polysaccharides, proteins, nucleic acids and lipids [10, 11]. Although there are structural differences in the matrix formed by MRSA and MSSA (methicillin-sensitive *S. aureus*), which will be addressed later on, the matrix has a general function in providing mechanical stability, mediating adhesion to surfaces, interconnecting and immobilizing cells, and acting as an external digestive system by keeping extracellular enzymes close to the cells [8]. Intricate channel networks flow through these complex biofilm structures and facilitate efficient nutrient uptake as well as outflow of metabolic waste products [26]. Nevertheless, staphylococci in a biofilm are generally slow growing, characterized by a general down-regulation of active cell processes, such as protein, DNA and cell wall biosynthesis [7, 27]. Other metabolic changes include a switch to fermentative acid-producing processes due to low oxygen concentrations in the biofilm [7, 27-29]. To limit the subsequent deleterious effects of reduced pH, urease and arginine deiminase (ADI) pathways, producing pH-alkalizing ammonia compounds, have been reported to be up-regulated [7, 27].

1.1.3.3. Detachment (dispersal)

Upon reaching a specific cell density, a quorum sensing mechanism using self-produced proteases [30], phenol-soluble modulins (PSMs) [31] and nucleases [32, 33] is triggered, which will release cells from the biofilm to spread through blood and other body fluids in order to reinitiate biofilm formation at sites distal from the infection nidus [10, 11]. PSMs are staphylococcal peptides with an α-helical, amphipathic structure, which gives them surfactant-like characteristics [34]. *S. aureus* produces four PSMα peptides, which are encoded in the *psmα* operon, two PSMβ peptides encoded in the

psmβ operon, and the RNAIII-encoded δ-toxin [35]. The *S. aureus* PSMα peptides and the δ-toxin belong to the group of short α-type PSMs (~20–25 aa), whereas the PSMβ peptides belong to the β-type PSMs, which are about double in size compared with α-type PSMs [31]. *S. aureus* also secretes ten proteases, including seven serine proteases (SspA and SplA-F), two cysteine proteases (SspB and ScpA), and one metalloprotease (Aur) [36]. Additionally, *S. aureus* is known to produce two secreted nucleases, one encodes an unnamed nuclease A (*nuc1*), and the other encodes a thermonuclease (*nuc2*) [37]. Interestingly, recent experimental studies in *Streptococcus pneumoniae* have reported that cells detaching from a biofilm have a greater association with cytotoxicity for transition to invasive disease and mortality than the equivalent planktonic ones [38]. This urgently warrants further research, as typical therapeutic strategies proposed to increase the efficacy of antibiotics involves the induction of biofilm dispersal [39].

1.1.3.4. Redefining the stages of staphylococcal biofilm formation (**Fig. 1**)

The recent use of the BioFlux1000 system, a microfluidic flow-cell device integrated with a fluorescence microscope, allowed to study *S. aureus* biofilm formation in a real-time manner, revealing a five-stage developmental process including: (i) attachment, (ii) multiplication, (iii) exodus, (iv) maturation and, (v) dispersal [40].

After attaching to a surface and prior to the production of an ECM, *S. aureus* cells produce a variety of factors that help to stabilize cell-to-cell interactions [41]. Moormeier et al. called this stage 'multiplication' and showed, by means of a 25 mutant strain screen from the Nebraska Transposon Mutant Library (NTML), that cell wall-associated proteins (such as *fnbA/B*, *clfA/B*, *embp*, *ebps*, *spa*, *sasC,* and *sasG*) are not involved during the multiplication stage, while subsequent screening of an *atl*::ΦΝΣ mutant suggested the involvement of autolysis and the subsequent release of extracellular genomic DNA (eDNA) [41]. Regulation of autolysis and DNA release will be discussed later. Once attachment to tissue or matrix-covered devices was accomplished, microcolony formation coincides with an early dispersal event which results in a restructuring of the biofilm and was called 'exodus' [40]. By testing an *agr*::*tet* mutant in UAMS-1 and an *agrA*::ΦΝΣ JE2 transposon mutant for biofilm formation, Moormeier et al. showed that the *agr* quorum sensing circuit and PSMs are not required for this event [41]. Instead, the authors observed that the growing biofilm became DNaseI sensitive after 6h of development and proved that mass exodus of the bulk of the biofilm population was mediated by the function of staphylococcal nuclease in the degradation of eDNA [41]. Nuc expression is commonly controlled by the two-component SaeRS system, which is also involved in the repression of extracellular proteases [42].

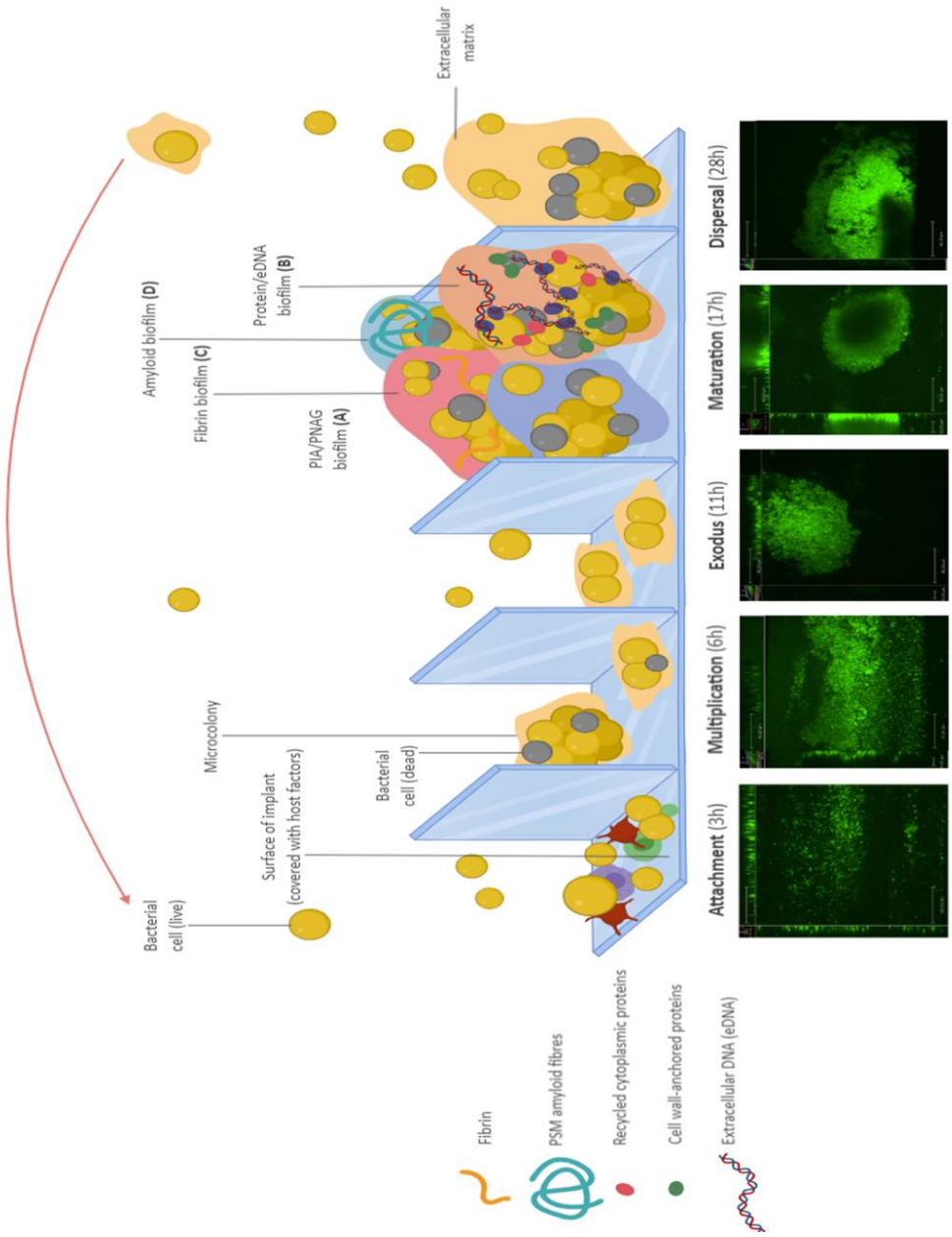

Figure 1: Phases of biofilm development in *S. aureus*. Biofilm development as envisioned by Moormeier, et al. includes initial attachment, multiplication, maturation, exodus and final dispersal or detachment. Types of biofilm: **(A)** Polysaccharide-type biofilm is dependent on expression of PIA/PNAG by *icaADBC*; **(B)** Surface proteins (black) such as Bap, FnBPs and SasG, cytoplasmic proteins (pink) and eDNA released following cell lysis (autolysin, green) mediate cell-to-cell contact; **(C)** Fibrinogen which is converted into fibrin by coagulase is recruited into the biofilm scaffold; **(D)** PSMs can accumulate as amyloid aggregates to promote biofilm accumulation.

1.1.3.5. Regulation of staphylococcal biofilm formation (**Fig. 2A**)

Many regulators adapt staphylococcal biofilm gene expression to changing environmental conditions. The major global regulators, staphylococcal accessory regulator (*sarA)* and accessory gene regulator (*agr)*, have been associated with biofilm formation [1]. The *agr* locus consists of five genes (*agrA*, *agrC*, *agrD*, *agrB* and *hld*), but is composed of two divergent transcripts, RNAII and RNAIII, which are under the control of two distinct promoters, P2, and P3 [43]. Dunman et al. identified 140 genes that are upregulated and 34 that are down-regulated by *agr* in a cell density-dependent manner [44]. The main Agr effector molecule RNAIII commonly represses the transcription of a number of cell wall-associated adherence factors (e.g. *spa*, *coA*, *fnbA/B*) and activates that of several detergent-like PSM peptides (e.g. PSMα1–4, PSMβ1–2, PSMγ, PSMδ, PSMε, and PSM-*mec*) [44, 45], serine and cysteine proteases (e.g. SspA, SplA-F, SspB, ScpA and Aur), and nucleases *(*e.g. *nuc1, nuc2)* [36, 46]. Agr is positively regulated by SarA, and expression of the *sarA* gene commonly results in down-regulation of protease activity, allowing for the development of an immature biofilm [47, 48]. SarA controls the expression of over more than 120 proteins [44], including a diverse range of surface-related adhesive proteins, such as Spa, FnBPA, FnBPB, and SdrC [49]. Additional levels of control are achieved through the *sigB* operon product σ^B in *S. aureus* (regulated by operon genes *rsbU*, *rsbW,* and *rsbV*) [50]. In *S. aureus*, σ^B is activated by signal transduction in response to high temperature, high osmolarity, antibiotics, or extreme pH [51]. σ^B has been shown to regulate an excess of 200 genes, including several genes involved in biofilm formation [50]. Specifically, it is involved in the activation of several virulence factors such as α-haemolysin, adhesins, proteases, and thermonucleases, and this transcriptional factor also positively regulates *sarA* and downregulates *agr*-RNAIII [52]. Also, factors necessary for the initial stages of biofilm formation, including ClfA, ClfB, FnBPA, and coagulase, are regulated by σ^B [53].

*1.1.4. Biofilm formation by methicillin-sensitive S. aureus (MSSA) (**Fig. 2B**)*

MSSA strains commonly fabricate an *icaADBC* operon-encoded polysaccharide intercellular adhesin or poly-N-acetylglucosamine (PIA/PNAG)-dependent biofilm [54]. PIA/PNAG is a glycan of β-1,6-linked 2-acetamido-2-deoxy-D-glucopyranosyl residues with a net positive charge that enhances intercellular aggregation and surface attachment of cells [55, 56]. PIA/PNAG biosynthesis is accomplished by the products of the *ica* (intercellular adhesion) gene locus, which comprises the *icaA*, *icaD*, *icaB*, and *icaC* genes, and a divergently transcribed repressor, *icaR* [12, 57]. IcaA is an N-acetylglucosamine transferase, which together with IcaD produces an N-acetylglucosamine oligomer. IcaC is the PIA/PNAG exporter, while surface-located IcaB

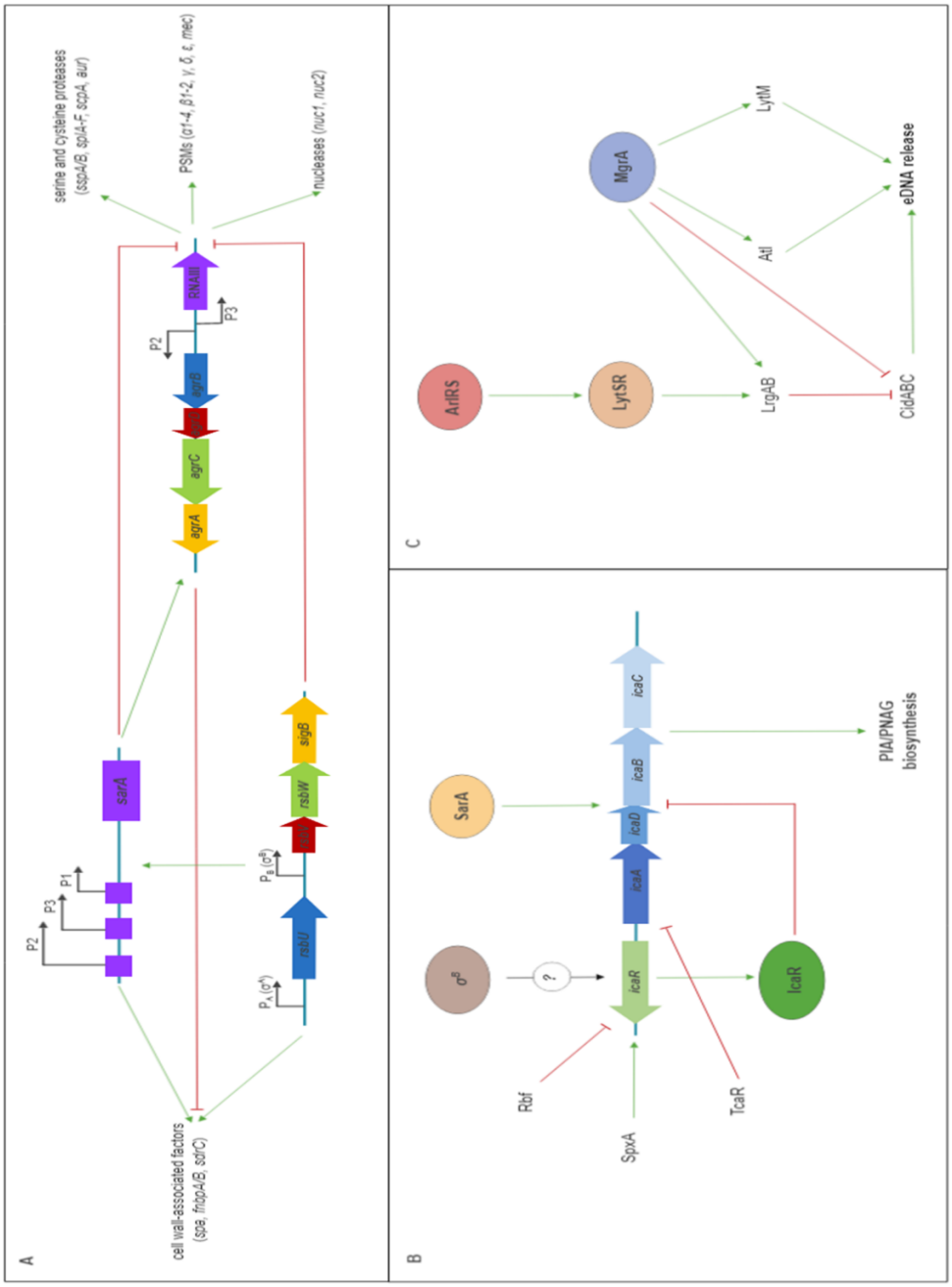

Figure 2: Major regulatory networks directing biofilm formation by *S. aureus*. **(A)** The regulatory cascades of the most important systems governing general biofilm formation (*sarA*, *agr*, *sigB*) are depicted; **(B)** model of *ica*-dependent biofilm formation; **(C)** model of *ica*-independent biofilm formation. Lines ending in arrows (green) indicate activation or induction, while those ending with lines (red) indicate deactivation or repression.

is a PIA/PNAG deacetylase [58]. The regulation of *icaADBC* expression is mediated by a number of regulatory factors including global regulatory proteins SarA and σ^B [59]. SarA positively affects *icaADBC* expression by directly binding to the *icaADBC* promotor [60, 61]. σ^B regulation appears to be indirect. Cerca et al. looked at *icaADBC* and *icaR* expression in σ^B-deleted derivatives of *S. aureus* strains SA113 and Newman, and σ^B was found to be a positive regulator of both *icaR* and *icaADBC* [62]. However, Valle et al. reported that mutation of σ^B in the same strains had no significant effect on *ica* expression or biofilm [63]. TcaR was identified as another (weak) repressor of *ica* operon transcription [64]. TcaR is a member of the MarR family of transcriptional regulators and controls expression of the teicoplanin-associated locus. IcaR transcription is also activated by the SpxA (global regulator of stress response genes) protein, leading to decreased *ica* operon expression [65]. The protein regulator of biofilm formation, Rbf, however, represses transcription of IcaR [66]. Additionally, many environmental factors including oxygen, glucose, ethanol, osmolarity, temperature, and antibiotics such as tetracycline have been shown to also play a role in the regulation of *ica* [67, 68].

*1.1.5. Biofilm formation by methicillin-resistant S. aureus (**Fig. 2C**)*

In contrast, the *ica* locus was found to be redundant for MRSA biofilm formation [54, 69]. Among the factors implied for cell-cell and cell-surface interactions occurring during biofilm development are the LPXTG-anchored surface proteins such as the fibronectin binding proteins [70], protein A [71], SasG [72, 73], and biofilm-associated protein (BAP) [74]. It has also been suggested that cytoplasmic proteins, such as enolase (*eno*) and GAPDH, play an important role in the matrix where they associate with cells upon a drop in pH [75, 76]. In addition, amyloids have recently come forward as an important proteinaceous constituent of many microbial biofilms, including *S. aureus*. Amyloids are insoluble fibrous aggregates of PSMs that contain parallel β-sheets, instead of the α-helical form that gives their surfactant properties [77, 78]. Amyloids are infamous for being relatively resistant to protease digestion and insoluble in detergents. Additionally, surface-associated proteins with amyloidogenic properties have also been reported. Taglialegna et al. reported recently that the Bap protein of *S. aureus* could also self-assemble into functional amyloid aggregates [79]. eDNA is also thought to be an important structural component of *S. aureus* biofilms [80]. In *S. aureus*, autolytic activity from a subpopulation of cells promotes in the release of genomic DNA that adds to cell adhesion during biofilm maturation [81]. Isolates of *S. aureus* produce several autolysins, including Atl and LytM, for example. These hydrolases act in specific peptidoglycan links and are crucial for mechanisms that involve cell wall

maturation, separation of daughter cells and cell wall degradation [82]. The chemical nature of the long charged DNA molecule is assumed to adapt the cell surface properties and to promote cell-to-cell and cell-to-surface adhesion and to serve a structural role in the *S. aureus* biofilm matrix [33]. Additionally, while different biofilm matrix types have long time been believed to exist, matrix components are also capable of interacting [83]. For example, the *S. aureus* protein β-toxin is adept to binding with eDNA [84]. The presence of eDNA also enhances the polymerization of amyloidogenic peptides [77]. Last, interactions between eDNA and polysaccharides have also been observed in biofilms. In *P. aeruginosa*, two main biofilm matrix components (eDNA and the polysaccharide Psl) collaborate by physically interacting in a biofilm to form a web of Psl–eDNA fibres [85]. Inhibition of biofilm expression by decreasing eDNA content is accomplished by the SarA homolog global transcriptional regulator MgrA, which down-regulates the peptidoglycan hydrolase LytM [86]. Additionally, both LytM and Atl autolysins are up-regulated by the two-component system YycGF (WalK/R, formed by *walR*, *walk*, *walH*, *walI*, and *walJ*) [82]. Autolysis is also regulated by the ArlRS two-component system, which regulates the expression of at least 114 genes [87]. ArlRS positively impacts the *lytRS* system [87]. LytR and LytS positively regulate the expression of two genes, *lrgA,* and *lrgB*, that inhibit the activity of murein hydrolases (cleavage of structural components of the bacterial cell wall) [88]. *LrgAB* works together with *cidABC* like bacteriophage holin/antiholin systems [89]. *CidA*, the holin in this system, oligomerizes in the cell membrane, which results in the formation of a pore that is utilized for the transport of the murein hydrolase. *LrgAB* functions as the antiholin and prevents the activity of *cidA* [33]. *LrgAB* is positively regulated by *mgrA*, which also negatively regulates *cidABC* [74].

1.1.6. Methicillin resistance and the biofilm phenotype

MRSA and MSSA are differentiated by carriage of the methicillin resistance gene *mecA*, which is carried on the staphylococcal cassette chromosome *mec* (*SCCmec*) that was presumably acquired by horizontal transfer from a coagulase-negative *Staphylococcus* species [90]. Pozzi et al., showed that high-level expression of the *mecA*-product, PBP2a or penicillin-binding protein 2a, was associated with a mutation in the c-di-AMP phosphodiesterase gene *gdpP*, resulting in pleiotropic effects by blocking *icaADBC*-dependent polysaccharide type biofilm development and promoting an alternative PBP2a-mediated biofilm, where the accessory gene regulator and extracellular protease production was repressed, and virulence in a mouse device-infection model was attenuated [91]. Whether PBP2a expression works in a direct or indirect manner (e.g. via altered cell wall architecture) on biofilm

production, remains to be determined. Possibly, the peptidoglycan altered cell wall architecture and permeability in MRSA strains associated with oxacillin resistance may facilitate PBP2a-promoted cell-cell interactions that are not possible between MSSA cells [91]. The cell wall architecture changes could also block the export of PIA/PNAG to the cell surface, which is accompanied by the redeployment of FnBPs [92].

However, while earlier studies reported differences between methicillin-resistant and –sensitive isolates, more recent studies indicate that both MRSA and MSSA form almost exclusively protein-dependent biofilms [93, 94]. For example, the clinical MRSA strain 132 has been shown to alternate between a proteinaceous and an exopolysaccharidic biofilm matrix [95].

1.1.7. Molecular underpinnings of MRSA outbreaks

1.1.7.1. Biofilm meets virulence

Most common diseases caused by MRSA are not different from those caused by MSSA and mostly include skin, soft-tissue, respiratory, bone, joint, endovascular infections and sepsis [96]. In addition, the different mechanisms of biofilm formation employed by MRSA and MSSA do not appear to impair the ability of either to colonize implanted biomaterial *in vivo* [91]. However, high-level PBP2a expression in MRSA is commonly associated with repression of the *agr* operon [91], which blocks the coordinated induction of toxin and enzyme secretion [97]. Indeed, a study of 104 patients with *S. aureus* bacteraemia found that MSSA bacteraemia correlated with significantly higher rates of infective endocarditis and a significantly higher illness severity score from invasive disease than MRSA [98]. Instead, MRSA seems to deploy the formation of biofilms as a tenacious survival strategy resulting in prolonged persistence of infections. Retention of biofilm forming capacity and antibiotic resistance are likely more advantageous than metabolically costly toxin production in a hospital setting where there is a large pool of immunocompromised patients that often require intensive antibiotic treatments and implanted medical devices [54]. Interestingly, it was recently shown that highly virulent MRSA prevalent in the community are even better biofilm formers than HA-MRSA [99]. These results are in line with the high virulence but low-antibiotic resistance profile of CA-MRSA, which makes biofilm formation an important survival mechanism against antimicrobial killing. As such, biofilm formation may be an important factor underpinning MRSA outbreaks in both environments. Indeed, there is evidence to suggest that increased capacity to form biofilms and adhere to epithelial cells may have been linked for

example to the spread of the so-called Brazilian MRSA clone sequence type (ST) 239 [100], the likely predecessor of the Chinese sasX-positive ST239 strains.

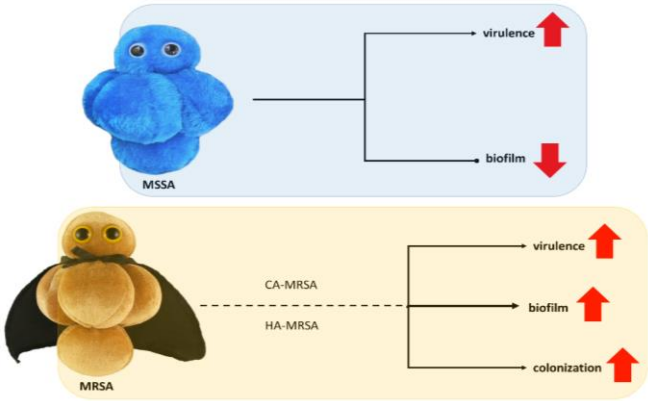

Figure 3: Model of the alteration of *S. aureus* virulence, biofilm or colonization capacity exerted by the acquisition of methicillin resistance gene *mecA*. Images were obtained from Giantmicrobes, Inc., https://www.giantmicrobes.com/us/.

Here, we will explore identified molecular factors, involved in high virulence or exceptional good colonization capacity, that lie at the basis of the epidemiological success of MRSA and also contribute to improved biofilm formation capacity.

1.1.7.1.1. Alpha-toxin

Alpha-toxin is a secreted 33 kDa pore-forming, multimeric, haemolytic toxin encoded by the *hla* gen [101], lysing red blood cells, epithelial cells, T cells, macrophages, and leukocytes [102, 103]. The host cells are lysed by forming β-barrel pores in the membrane which causes leakage of the cell's content [104]. Most MSSA and MRSA isolates have been shown to carry alpha-toxin; a study of 994 respiratory *S. aureus* isolates from 34 countries determined that the *hla* gene was expressed by 99% of MSSA and 83.2% of MRSA, with higher levels of expression in MSSA [105]. However, Caiazza and O'Toole were the first to describe a positive *in vitro* correlation between alpha-toxin production and biofilm formation using MSSA strain NCTC 8325-4 and *hla* knockout derivatives [106]. Alpha-toxin could promote biofilm formation by facilitating cell-to-cell interactions, resulting in macrocolony formation [107]. Anderson et al., showed in an *ex vivo* model using porcine vaginal mucosal tissue, that high alpha-toxin producing strains produced more biofilm and were more cytolytic than their *hla*-knocked-out counterparts [108, 109]. It was suggested that alpha-toxin might aid biofilm formation by disrupting the host epithelium, and thus exposing the ECM needed for attachment, nutrients and bacterial adhesion [108].

1.1.7.1.2. SasX protein

SasX, was first identified by whole-genome sequencing of a Chinese hospital MRSA strain of ST239 [110], but began spreading to other STs within the last years [111]. This protein has no homology with other proteins deposited in genetic databases, except for the ϕSPβ prophage-encoded *SesI* of *Staphylococcus epidermidis* [112]. SasX is a member of the family of surface-located proteins that are attached to the bacterial cell wall by the sortase enzyme [15]. The protein was found to mediate adhesion to nasal epithelial cells harvested from human volunteers and promoted nasal colonization in a murine colonization model [113]. Furthermore, in mouse models of lung and skin infection SasX enhanced virulence. This contribution to virulence appears to be linked to SasX-mediated promotion of biofilm formation and aggregation, which results in increased resistance to neutrophil phagocytosis and survival in human blood [113]. The precise molecular interactions underlying aggregation and adhesion behavior mediated by SasX are currently unknown, although an increase in cell-cell interactions or receptor-mediated binding to epithelial cells have been suggested [114].

1.1.7.1.3. PSM-*mec*

PSM-*mec* is a secreted virulence factor that belongs to the amphipathic, α-helical PSM peptide toxins [115]. Whilst all known PSMs are core genome-encoded, PSM-*mec* is found in specific sub-types of *SCCmec* elements (type II or III) commonly carried by ST5, ST36, ST45, ST225 and ST239 MRSA strains [116]. Interestingly, this gene is not found in CA-MRSA or MSSA, but also HA-MRSA strains having type-I *SCCmec* or type-IV *SCCmec* that do not carry the *psm-mec* ORF, have been isolated from hospitals in European countries and Australia [117]. The transcription product of the *psm-mec* toxin acts as a regulatory RNA and suppresses the expression of core genome-encoded toxin genes such as PSMα production [115]. It was also demonstrated that introducing the *psm-mec* ORF into Newman, MW2, and FRP3757 strains increased biofilm formation. Psm-*mec* mRNA was shown to promote *S. epidermidis* biofilm formation through up-regulation of bacterial autolysis and the release of eDNA [118].

1.1.7.1.4. Arginine catabolic mobile element (ACME)

In resemblance to the situation seen with *sasX*, the ACME element originally carried by *S. epidermidis*, was first described in the CA-MRSA strain USA300 [119], but has recently also been reported to spread to other sequence types such as ST5 in Japan [120]. The 31-kb genomic island primarily contains an arginine deiminase operon (*arc* genes), and an oligopeptide permease operon (*opp* genes) [119, 121], which are used for pH adjustment of the acid environment on the skin by ammonia

production [122]. Acquisition of one ACME gene, *speG*, allows USA300 strains to withstand levels of polyamines (e.g., spermidine) produced in skin that are toxic to other closely related *S. aureus* strains [122]. *SpeG*-mediated polyamine tolerance also enhanced adherence to fibrinogen/fibronectin, and resistance to antibiotic and keratinocyte-mediated killing [123]. Both these functions are believed to underlie the high propensity of USA300 to form biofilms [99]. Interestingly, while the enhanced skin colonization capacities are important for sustainable spread of USA300 in the community, the rising additional success of USA300 as an HA-MRSA may also be due to ACME-mediated promotion of colonization and biofilm formation [124].

1.1.8. Conclusions and outlook

Biofilm formation by *S. aureus* represents a virulence determinant of utmost importance and seems to have evolved as a coordinated response to optimally exploit the infection milieu. The contribution of multiple matrix components (albeit separately or combined), multifactorial regulation and maturation of metabolically distinct subpopulations of cells in the newly proposed developmental biofilm model, allow the overall population to be better adapted to environmental stresses. As such, MRSA has become almost perfectly adapted to the hospital setting where there is a large pool of immunocompromised individuals that often require intensive antibiotic therapies and implanted medical devices. Indeed, MRSA is often found at higher incidence in the healthcare setting than the community and spread may therefore be regarded as clinically more significant. But biofilms seem to be potentially also more relevant for survival of CA-MRSA as these do normally not carry genes that confer resistance to specific antibiotics as are present in hospital-acquired strains. This explains why the increasing isolation of CA-MRSA from patients in healthcare settings has begun to blur the clinical distinction between HA-MRSA and CA-MRSA, giving rise to the existence of highly virulent and hardly treatable “superpathogens”.

Ultimately, a more comprehensive understanding of the complexity of biofilm development in, not only MRSA, but general *S. aureus* is urgently needed. MSSA isolates also cause outbreaks but are rarely investigated. Furthermore, the association of β-lactam resistance and biofilm formation opens the promising possibility of a single target affecting two key aspects of MRSA pathogenesis.

1.1.9. Addendum

1.1.9.1. Acknowledgements

SDB is supported by funding from Research Foundation Flanders (FWO, applicant number 1128818N). The described research is part of IWT-SBO project (#140746) and FWO research project (#GOD3516N).

1.1.9.2. References

1. Archer, N.K., et al., *Staphylococcus aureus biofilms: properties, regulation, and roles in human disease.* Virulence, 2011. **2**(5): p. 445-59.
2. Jansen, W.T., et al., *Novel mobile variants of staphylococcal cassette chromosome mec in Staphylococcus aureus.* Antimicrob Agents Chemother, 2006. **50**(6): p. 2072-8.
3. Chambers, H.F. and F.R. Deleo, *Waves of resistance: Staphylococcus aureus in the antibiotic era.* Nat Rev Microbiol, 2009. **7**(9): p. 629-41.
4. Lindsay, J.A., *Evolution of Staphylococcus aureus and MRSA during outbreaks.* Infect Genet Evol, 2014. **21**: p. 548-53.
5. Deurenberg, R. and E.E. Stobberingh, *The molecular evolution of hospital- and community-associated methicillin-resistant Staphylococcus aureus.* Curr Mol Med, 2009. **9**(2): p. 100-15.
6. Donlan, R.M., *Biofilms: microbial life on surfaces.* Emerg Infect Dis, 2002. **8**(9): p. 881-90.
7. Beenken, K.E., et al., *Global gene expression in Staphylococcus aureus biofilms.* J Bacteriol, 2004. **186**(14): p. 4665-84.
8. Flemming, H.C. and J. Wingender, *The biofilm matrix.* Nat Rev Microbiol, 2010. **8**(9): p. 623-33.
9. Jones, S.M., et al., *Effect of vancomycin and rifampicin on meticillin-resistant Staphylococcus aureus biofilms.* Lancet, 2001. **357**(9249): p. 40-41.
10. Otto, M., *Staphylococcal biofilms.* Curr Top Microbiol Immunol, 2008. **322**: p. 207-28.
11. Otto, M., *Staphylococcal Biofilms.* Microbiol Spectr, 2018. **6**(4).
12. Heilmann, C., et al., *Evidence for autolysin-mediated primary attachment of Staphylococcus epidermidis to a polystyrene surface.* Mol Microbiol, 1997. **24**(5): p. 1013-24.
13. Schlag, M., et al., *Role of staphylococcal wall teichoic acid in targeting the major autolysin Atl.* Mol Microbiol, 2010. **75**(4): p. 864-73.
14. Arciola, C.R., D. Campoccia, and L. Montanaro, *Implant infections: adhesion, biofilm formation and immune evasion.* Nat Rev Microbiol, 2018. **16**(7): p. 397-409.
15. Foster, T.J., et al., *Adhesion, invasion and evasion: the many functions of the surface proteins of Staphylococcus aureus.* Nat Rev Microbiol, 2014. **12**(1): p. 49-62.
16. Clarke, S.R. and S.J. Foster, *Surface Adhesins of Staphylococcus aureus.* 2006. **51**: p. 187-224.
17. Mazmanian, S.K., et al., *Staphylococcus aureus sortase, an enzyme that anchors surface proteins to the cell wall.* Science, 1999. **285**(5428): p. 760-3.
18. Abraham, N.M. and K.K. Jefferson, *Staphylococcus aureus clumping factor B mediates biofilm formation in the absence of calcium.* Microbiology, 2012. **158**(Pt 6): p. 1504-12.
19. Josse, J., F. Laurent, and A. Diot, *Staphylococcal Adhesion and Host Cell Invasion: Fibronectin-Binding and Other Mechanisms.* Front Microbiol, 2017. **8**: p. 2433.
20. McCrea, K.W., et al., *The serine-aspartate repeat (Sdr) protein family in Staphylococcus epidermidis.* Microbiology, 2000. **146**(7): p. 1535-46.
21. Siboo, I.R., et al., *Clumping factor A mediates binding of Staphylococcus aureus to human platelets.* Infect Immun, 2001. **69**(5): p. 3120-7.
22. Chavakis, T., et al., *Staphylococcus aureus interactions with the endothelium: the role of bacterial "secretable expanded repertoire adhesive molecules" (SERAM) in disturbing host defense systems.* Thromb Haemost, 2005. **94**(2): p. 278-85.
23. Cheng, A.G., D. Missiakas, and O. Schneewind, *The giant protein Ebh is a determinant of Staphylococcus aureus cell size and complement resistance.* J Bacteriol, 2014. **196**(5): p. 971-81.
24. Geraci, J., et al., *The Staphylococcus aureus extracellular matrix protein (Emp) has a fibrous structure and binds to different extracellular matrices.* Sci Rep, 2017. **7**(1): p. 13665.

25. Hammel, M., et al., *The Staphylococcus aureus extracellular adherence protein (Eap) adopts an elongated but structured conformation in solution.* Protein Sci, 2007. **16**(12): p. 2605-17.
26. O'Toole, G.A., H.B. Kaplan, and R. Kolter, *Biofilm formation as microbial development.* Annu Rev Microbiol, 2000. **54**: p. 49-79.
27. Resch, A., et al., *Differential gene expression profiling of Staphylococcus aureus cultivated under biofilm and planktonic conditions.* Appl Environ Microbiol, 2005. **71**(5): p. 2663-76.
28. Fuchs, S., et al., *Anaerobic gene expression in Staphylococcus aureus.* J Bacteriol, 2007. **189**(11): p. 4275-89.
29. Resch, A., et al., *Comparative proteome analysis of Staphylococcus aureus biofilm and planktonic cells and correlation with transcriptome profiling.* Proteomics, 2006. **6**(6): p. 1867-77.
30. Mootz, J.M., et al., *Staphopains modulate Staphylococcus aureus biofilm integrity.* Infect Immun, 2013. **81**(9): p. 3227-38.
31. Periasamy, S., et al., *How Staphylococcus aureus biofilms develop their characteristic structure.* Proc Natl Acad Sci U S A, 2012. **109**(4): p. 1281-6.
32. Kiedrowski, M.R., et al., *Nuclease modulates biofilm formation in community-associated methicillin-resistant Staphylococcus aureus.* PLoS One, 2011. **6**(11): p. e26714.
33. Mann, E.E., et al., *Modulation of eDNA release and degradation affects Staphylococcus aureus biofilm maturation.* PLoS One, 2009. **4**(6): p. e5822.
34. Peschel, A. and M. Otto, *Phenol-soluble modulins and staphylococcal infection.* Nat Rev Microbiol, 2013. **11**(10): p. 667-73.
35. Cheung, G.Y., et al., *Phenol-soluble modulins--critical determinants of staphylococcal virulence.* FEMS Microbiol Rev, 2014. **38**(4): p. 698-719.
36. Shaw, L., et al., *The role and regulation of the extracellular proteases of Staphylococcus aureus.* Microbiology, 2004. **150**(Pt 1): p. 217-28.
37. Tang, J., et al., *Two thermostable nucleases coexisted in Staphylococcus aureus: evidence from mutagenesis and in vitro expression.* FEMS Microbiol Lett, 2008. **284**(2): p. 176-83.
38. Chao, Y., et al., *Streptococcus pneumoniae biofilm formation and dispersion during colonization and disease.* Front Cell Infect Microbiol, 2014. **4**: p. 194.
39. Roizman, D., et al., *In vitro evaluation of biofilm dispersal as a therapeutic strategy to restore antimicrobial efficacy.* Antimicrob Agents Chemother, 2017. **61**(10): p. e01088-17.
40. Moormeier, D.E. and K.W. Bayles, *Staphylococcus aureus biofilm: a complex developmental organism.* Mol Microbiol, 2017. **104**(3): p. 365-376.
41. Moormeier, D.E., et al., *Temporal and stochastic control of Staphylococcus aureus biofilm development.* MBio, 2014. **5**(5): p. e01341-14.
42. Olson, M.E., et al., *Staphylococcus aureus nuclease is an SaeRS-dependent virulence factor.* Infect Immun, 2013. **81**(4): p. 1316-24.
43. Peng, H.L., et al., *Cloning, characterization, and sequencing of an accessory gene regulator (agr) in Staphylococcus aureus.* J Bacteriol, 1988. **170**(9): p. 4365-72.
44. Dunman, P.M., et al., *Transcription profiling-based identification of Staphylococcus aureus genes regulated by the agr and/or sarA loci.* J Bacteriol, 2001. **183**(24): p. 7341-53.
45. Wang, R., et al., *Identification of novel cytolytic peptides as key virulence determinants for community-associated MRSA.* Nat Med, 2007. **13**(12): p. 1510-4.
46. Shang, Y., et al., *Regulation of saeRS, agrA and sarA on sasX Expression in Staphylococcus aureus.* Jundishapur Journal of Microbiology, 2018. **11**(6).
47. Cheung, A.L., et al., *The SarA protein family of Staphylococcus aureus.* Int J Biochem Cell Biol., 2009. **40**(3): p. 355-61.
48. Tsang, L.H., et al., *Factors contributing to the biofilm-deficient phenotype of Staphylococcus aureus sarA mutants.* PLoS One, 2008. **3**(10): p. e3361.
49. Liu, Y., et al., *Structural and function analyses of the global regulatory protein SarA from Staphylococcus aureus.* Proc Natl Acad Sci U S A, 2006. **103**(7): p. 2392-7.
50. Pane-Farre, J., et al., *The sigmaB regulon in Staphylococcus aureus and its regulation.* Int J Med Microbiol, 2006. **296**(4-5): p. 237-58.

51. Kavanaugh, J.S. and A.R. Horswill, *Impact of Environmental Cues on Staphylococcal Quorum Sensing and Biofilm Development.* J Biol Chem, 2016. **291**(24): p. 12556-64.
52. Kim, B.-R., Y.-M. Bae, and S.-Y. Lee, *Effect of Environmental Conditions on Biofilm Formation and Related Characteristics ofStaphylococcus Aureus.* Journal of Food Safety, 2016. **36**(3): p. 412-422.
53. Nair, R., et al., *Antimicrobial resistance and molecular epidemiology of Staphylococcus aureus from Ulaanbaatar, Mongolia.* PeerJ, 2013. **1**: p. e176.
54. McCarthy, H., et al., *Methicillin resistance and the biofilm phenotype in Staphylococcus aureus.* Front Cell Infect Microbiol, 2015. **5**: p. 1.
55. Mack, D., et al., *The intercellular adhesin involved in biofilm accumulation of Staphylococcus epidermidis is a linear beta-1,6-linked glucosaminoglycan: purification and structural analysis.* J Bacteriol, 1996. **178**(1): p. 175-183.
56. Rohde, H., et al., *Structure, function and contribution of polysaccharide intercellular adhesin (PIA) to Staphylococcus epidermidis biofilm formation and pathogenesis of biomaterial-associated infections.* Eur J Cell Biol, 2010. **89**(1): p. 103-11.
57. Conlon, K.M., H. Humphreys, and J.P. O'Gara, *icaR Encodes a Transcriptional Repressor Involved in Environmental Regulation of ica Operon Expression and Biofilm Formation in Staphylococcus epidermidis.* Journal of Bacteriology, 2002. **184**(16): p. 4400-4408.
58. Gerke, C., et al., *Characterization of the N-acetylglucosaminyltransferase activity involved in the biosynthesis of the Staphylococcus epidermidis polysaccharide intercellular adhesin.* J Biol Chem, 1998. **273**(29): p. 18586-93.
59. Cue, D., M.G. Lei, and C.Y. Lee, *Genetic regulation of the intercellular adhesion locus in staphylococci.* Front Cell Infect Microbiol, 2012. **2**: p. 38.
60. Tormo, M.A., et al., *SarA is an essential positive regulator of Staphylococcus epidermidis biofilm development.* J Bacteriol, 2005. **187**(7): p. 2348-56.
61. Valle, J., et al., *SarA and not SigB is essential for biofilm development by Staphylococcus aureus.* Mol Microbiol, 2003. **48**(4): p. 1075-1087.
62. Cerca, N., J.L. Brooks, and K.K. Jefferson, *Regulation of the intercellular adhesin locus regulator (icaR) by SarA, sigmaB, and IcaR in Staphylococcus aureus.* J Bacteriol, 2008. **190**(19): p. 6530-3.
63. Valle, J., et al., *SarA and not SigmaB is essential for biofilm development by Staphylococcus aureus.* Mol Microbiol, 2003. **48**(4): p. 1075-87.
64. Jefferson, K.K., et al., *The Teicoplanin-Associated Locus Regulator (TcaR) and the Intercellular Adhesin Locus Regulator (IcaR) Are Transcriptional Inhibitors of the ica Locus in Staphylococcus aureus.* Journal of Bacteriology, 2004. **186**(8): p. 2449-2456.
65. Pamp, S.J., et al., *Spx is a global effector impacting stress tolerance and biofilm formation in Staphylococcus aureus.* J Bacteriol, 2006. **188**(13): p. 4861-70.
66. Cue, D., et al., *Rbf promotes biofilm formation by Staphylococcus aureus via repression of icaR, a negative regulator of icaADBC.* J Bacteriol, 2009. **191**(20): p. 6363-73.
67. Fitzpatrick, F., H. Humphreys, and J.P. O'Gara, *Evidence for icaADBC-independent biofilm development mechanism in methicillin-resistant Staphylococcus aureus clinical isolates.* J Clin Microbiol, 2005. **43**(4): p. 1973-6.
68. Ulrich, M., et al., *The staphylococcal respiratory response regulator SrrAB induces ica gene transcription and polysaccharide intercellular adhesin expression, protecting Staphylococcus aureus from neutrophil killing under anaerobic growth conditions.* Mol Microbiol, 2007. **65**(5): p. 1276-87.
69. O'Neill, E., et al., *Association between methicillin susceptibility and biofilm regulation in Staphylococcus aureus isolates from device-related infections.* J Clin Microbiol, 2007. **45**(5): p. 1379-88.
70. O'Neill, E., et al., *A novel Staphylococcus aureus biofilm phenotype mediated by the fibronectin-binding proteins, FnBPA and FnBPB.* J Bacteriol, 2008. **190**(11): p. 3835-50.
71. Merino, N., et al., *Protein A-mediated multicellular behavior in Staphylococcus aureus.* J Bacteriol, 2009. **191**(3): p. 832-43.

72. Conrady, D.G., et al., *A zinc-dependent adhesion module is responsible for intercellular adhesion in staphylococcal biofilms.* Proc Natl Acad Sci U S A, 2008. **105**(49): p. 19456-61.
73. Corrigan, R.M., H. Miajlovic, and T.J. Foster, *Surface proteins that promote adherence of Staphylococcus aureus to human desquamated nasal epithelial cells.* BMC Microbiol, 2009. **9**: p. 22.
74. Trotonda, M.P., et al., *MgrA represses biofilm formation in Staphylococcus aureus.* Infect Immun, 2008. **76**(12): p. 5645-54.
75. Ebner, P., et al., *Excretion of cytoplasmic proteins (ECP) in Staphylococcus aureus.* Mol Microbiol, 2015. **97**(4): p. 775-89.
76. Foulston, L., et al., *The extracellular matrix of Staphylococcus aureus biofilms comprises cytoplasmic proteins that associate with the cell surface in response to decreasing pH.* MBio, 2014. **5**(5): p. e01667-14.
77. Schwartz, K., et al., *Extracellular DNA facilitates the formation of functional amyloids in Staphylococcus aureus biofilms.* Mol Microbiol, 2016. **99**(1): p. 123-34.
78. Schwartz, K., et al., *Functional amyloids composed of phenol soluble modulins stabilize Staphylococcus aureus biofilms.* PLoS Pathog, 2012. **8**(6): p. e1002744.
79. Taglialegna, A., et al., *Staphylococcal Bap Proteins Build Amyloid Scaffold Biofilm Matrices in Response to Environmental Signals.* PLoS Pathog, 2016. **12**(6): p. e1005711.
80. Dengler, V., et al., *An Electrostatic Net Model for the Role of Extracellular DNA in Biofilm Formation by Staphylococcus aureus.* J Bacteriol, 2015. **197**(24): p. 3779-87.
81. Qin, Z., et al., *Role of autolysin-mediated DNA release in biofilm formation of Staphylococcus epidermidis.* Microbiology, 2007. **153**(Pt 7): p. 2083-92.
82. Dubrac, S., et al., *New insights into the WalK/WalR (YycG/YycF) essential signal transduction pathway reveal a major role in controlling cell wall metabolism and biofilm formation in Staphylococcus aureus.* J Bacteriol, 2007. **189**(22): p. 8257-69.
83. Payne, D.E. and B.R. Boles, *Emerging interactions between matrix components during biofilm development.* Curr Genet, 2016. **62**(1): p. 137-41.
84. Huseby, M.J., et al., *Beta toxin catalyzes formation of nucleoprotein matrix in staphylococcal biofilms.* Proc Natl Acad Sci U S A, 2010. **107**(32): p. 14407-12.
85. Wang, S., et al., *The exopolysaccharide Psl-eDNA interaction enables the formation of a biofilm skeleton in Pseudomonas aeruginosa.* Environ Microbiol Rep, 2015. **7**(2): p. 330-40.
86. Ingavale, S., et al., *Rat/MgrA, a regulator of autolysis, is a regulator of virulence genes in Staphylococcus aureus.* Infect Immun, 2005. **73**(3): p. 1423-31.
87. Liang, X., et al., *Global regulation of gene expression by ArlRS, a two-component signal transduction regulatory system of Staphylococcus aureus.* J Bacteriol, 2005. **187**(15): p. 5486-92.
88. Groicher, K.H., et al., *The Staphylococcus aureus lrgAB operon modulates murein hydrolase activity and penicillin tolerance.* J Bacteriol, 2000. **182**(7): p. 1794-801.
89. Yang, S.J., et al., *A LysR-type regulator, CidR, is required for induction of the Staphylococcus aureus cidABC operon.* J Bacteriol, 2005. **187**(17): p. 5893-900.
90. Rolo, J., et al., *Evolutionary Origin of the Staphylococcal Cassette Chromosome mec (SCCmec).* Antimicrob Agents Chemother, 2017. **61**(6).
91. Pozzi, C., et al., *Methicillin resistance alters the biofilm phenotype and attenuates virulence in Staphylococcus aureus device-associated infections.* PLoS Pathog, 2012. **8**(4): p. e1002626.
92. O'Gara, J.P., *Into the storm: Chasing the opportunistic pathogen Staphylococcus aureus from skin colonisation to life-threatening infections.* Environ Microbiol, 2017. **19**(10): p. 3823-3833.
93. Ghasemian, A., et al., *Comparison of biofilm formation between methicillin-resistant and methicillin-susceptible isolates of Staphylococcus aureus.* Iran Biomed J, 2016. **20**(3): p. 175-81.
94. Loughran, A.J., et al., *Impact of individual extracellular proteases on Staphylococcus aureus biofilm formation in diverse clinical isolates and their isogenic sarA mutants.* Microbiologyopen, 2014. **3**(6): p. 897-909.

95. Vergara-Irigaray, M., et al., *Relevant role of fibronectin-binding proteins in Staphylococcus aureus biofilm-associated foreign-body infections.* Infect Immun, 2009. **77**(9): p. 3978-91.
96. Tsang, S.T.J., et al., *Underestimation of Staphylococcus aureus (MRSA and MSSA) carriage associated with standard culturing techniques: One third of carriers missed.* Bone Joint Res, 2018. **7**(1): p. 79-84.
97. Rudkin, J.K., et al., *Methicillin resistance reduces the virulence of healthcare-associated methicillin-resistant Staphylococcus aureus by interfering with the agr quorum sensing system.* J Infect Dis, 2012. **205**(5): p. 798-806.
98. Abraham, J., et al., *Staphylococcus aureus bacteremia and endocarditis: the Grady Memorial Hospital experience with methicillin-sensitive S aureus and methicillin-resistant S aureus bacteremia.* Am Heart J, 2004. **147**(3): p. 536-9.
99. Vanhommerig, E., et al., *Comparison of biofilm formation between major clonal lineages of methicillin-resistant Staphylococcus aureus.* PLoS One, 2014. **9**(8): p. e104561.
100. Amaral, M.M., et al., *The predominant variant of the Brazilian epidemic clonal complex of methicillin resistant Staphylococcus aureus has an enhanced ability to produce biofilm and to adhere to and invade airway epithelial cells.* J Infect Dis, 2005. **192**: p. 801-810.
101. Otto, M., *Staphylococcus aureus toxins.* Curr Opin Microbiol, 2014. **17**: p. 32-7.
102. Berube, B. and J. Wardenburg, *Staphylococcus aureus α-Toxin: Nearly a Century of Intrigue.* Toxins, 2013. **5**(6): p. 1140-1166.
103. Nygaard, T.K., et al., *Alpha-toxin induces programmed cell death of human T cells, B cells, and monocytes during USA300 infection.* PLoS One, 2012. **7**(5): p. e36532.
104. Foster, T.J., *The Staphylococcus aureus "superbug".* J Clin Invest, 2004. **114**(12): p. 1693-1696.
105. Tabor, D.E., et al., *Staphylococcus aureus Alpha-Toxin Is Conserved among Diverse Hospital Respiratory Isolates Collected from a Global Surveillance Study and Is Neutralized by Monoclonal Antibody MEDI4893.* Antimicrob Agents Chemother, 2016. **60**(9): p. 5312-21.
106. Caiazza, N.C. and G.A. O'Toole, *Alpha-Toxin Is Required for Biofilm Formation by Staphylococcus aureus.* Journal of Bacteriology, 2003. **185**(10): p. 3214-3217.
107. den Reijer, P.M., et al., *Detection of Alpha-Toxin and Other Virulence Factors in Biofilms of Staphylococcus aureus on Polystyrene and a Human Epidermal Model.* PLoS One, 2016. **11**(1): p. e0145722.
108. Anderson, M.J., et al., *Alpha-toxin promotes Staphylococcus aureus mucosal biofilm formation.* Front Cell Infect Microbiol, 2012. **2**: p. 64.
109. Anderson, M.J., et al., *Alpha-Toxin Contributes to Biofilm Formation among Staphylococcus aureus Wound Isolates.* Toxins (Basel), 2018. **10**(4).
110. Holden, M.T., et al., *Genome sequence of a recently emerged, highly transmissible, multi-antibiotic- and antiseptic-resistant variant of methicillin-resistant Staphylococcus aureus, sequence type 239 (TW).* J Bacteriol, 2010. **192**(3): p. 888-92.
111. De Backer, S., et al., *Remarkable geographical variations between India and Europe in carriage of the staphylococcal surface protein-encoding sasX/sesI and in the population structure of methicillin-resistant Staphylococcus aureus belonging to clonal complex 8.* Clin Microbiol Infect, 2018.
112. Soderquist, B., et al., *Staphylococcus epidermidis surface protein I (SesI): a marker of the invasive capacity of S. epidermidis?* J Med Microbiol, 2009. **58**(Pt 10): p. 1395-7.
113. Li, M., et al., *MRSA epidemic linked to a quickly spreading colonization and virulence determinant.* Nat Med, 2012. **18**(5): p. 816-9.
114. Otto, M., *How colonization factors are linked to outbreaks of methicillin-resistant Staphylococcus aureus: the roles of SasX and ACME.* Biomol Concepts, 2013. **4**(5): p. 533-7.
115. Queck, S.Y., et al., *Mobile genetic element-encoded cytolysin connects virulence to methicillin resistance in MRSA.* PLoS Pathog, 2009. **5**(7): p. e1000533.
116. Monecke, S., et al., *Distribution of SCCmec-associated phenol-soluble modulin in staphylococci.* Mol Cell Probes, 2012. **26**(2): p. 99-103.
117. Qin, L., et al., *PSM-Mec-A Virulence Determinant that Connects Transcriptional Regulation, Virulence, and Antibiotic Resistance in Staphylococci.* Front Microbiol, 2016. **7**: p. 1293.

118. Yang, Y., et al., *SCCmec-associated psm-mec mRNA promotes Staphylococcus epidermidis biofilm formation.* Antonie Van Leeuwenhoek, 2016. **109**(10): p. 1403-15.
119. Diep, B.A., et al., *Complete genome sequence of USA300, an epidemic clone of community-acquired meticillin-resistant Staphylococcus aureus.* Lancet, 2006. **367**(9512): p. 731-739.
120. Takano, T., et al., *A new local variant (ST764) of the globally disseminated ST5 lineage of hospital-associated methicillin-resistant Staphylococcus aureus (MRSA) carrying the virulence determinants of community-associated MRSA.* Antimicrob Agents Chemother, 2013. **57**(4): p. 1589-1595.
121. Diep, B.A., et al., *The arginine catabolic mobile element and staphylococcal chromosomal cassette mec linkage: convergence of virulence and resistance in the USA300 clone of methicillin-resistant Staphylococcus aureus.* J Infect Dis, 2008. **197**(11): p. 1523-30.
122. Thurlow, L.R., et al., *Functional modularity of the arginine catabolic mobile element contributes to the success of USA300 methicillin-resistant Staphylococcus aureus.* Cell Host Microbe, 2013. **13**(1): p. 100-7.
123. Planet, P.J., et al., *Emergence of the epidemic methicillin-resistant Staphylococcus aureus strain USA300 coincides with horizontal transfer of the arginine catabolic mobile element and speG-mediated adaptations for survival on skin.* MBio, 2013. **4**(6): p. e00889-13.
124. Otto, M., *Molecular insight into how MRSA is becoming increasingly dangerous.* Virulence, 2012. **3**: p. 521-523.

Chapter 2: Scope of the thesis

"MRSA – drug resistant staph – may be the most frightening epidemic since AIDS."

- Maryn McKenna

2.1. Research hypothesis

Staphylococci, with the lead species *Staphylococcus aureus*, are the most frequent causes of infections on indwelling medical devices [1]. These include endocarditis and prosthetic joint infections, and may even lead to life-threatening conditions, such as sepsis. The biofilm phenotype that the bacteria frequently adopt during these infections facilitates increased resistance to antibiotics and host immune defences. Many definitions have been used for biofilms. Most define a biofilm as a microbial community of cells that is embedded in a matrix of self-produced extracellular polymeric substances [2]. Cells in a biofilm characteristically show a phenotype - with respect to metabolism, gene transcription, and protein production - that is different from the planktonic phenotype [3], explaining the difficulty to eradicate this life form. Furthermore, research performed in many biofilm-forming organisms has revealed that the development of a biofilm is a 3-step process involving an initial attachment, subsequent maturation and final detachment phase. Here, each stage is physiologically different from each other and requires phase-specific factors [4]. For example, exopolysaccharides represent the matrix components that are most specifically implicated in biofilm formation. *S. aureus* produces one main biofilm exopolysaccharide, which is called polysaccharide intercellular adhesin (PIA), or according to its chemical composition, poly-N-acetylglucosamine (PNAG), which is produced by-products of the intercellular adhesion *icaADBC* gene locus [5]. However, biofilm formation can be accomplished by *S. aureus* isolates that do not harbour the *ica* locus. Here, biofilm formation appears to be predominantly protein-dependent, together with teichoic acids and eDNA [6]. Additionally, biofilm formation appears to be linked with antibiotic resistance; as methicillin-sensitive *S. aureus* (MSSA) strains frequently form PIA/PNAG-dependent biofilms and methicillin-resistant *S. aureus* (MRSA) strains adopt a protein/eDNA-dependent biofilm [7].

The mechanisms involved in biofilms are multifactorial and not yet fully understood. It has become clear that the molecules aiding biofilm formation by a specific strain might not be the same for all *S. aureus* strains, although general mechanisms are likely to exist. As such, biofilm-associated factors may contribute to prolonged infection and colonization, and the spread of specific MRSA clones.

As the majority of human infections (60-80%) are biofilm-associated [8], this mode of growth in staphylococci remains a serious clinical problem due to the enormous and continued difficulties in treating staphylococcal biofilm-associated infections. This work expands our knowledge of genetic factors controlling biofilm formation and may provide potential targets for therapeutic intervention. Moreover, it is an important task of current *S. aureus* pathogenesis research to delineate factors that define virulence of

the entire range of infectious MRSA strains, to generate drugs with as broad and long-lasting anti-staphylococcal potential as possible.

2.2. Aims

This thesis investigates the fundamental aspects of biofilm formation that partially underlie the pathogenic success of MRSA. We aim to do so by investigating particularly prolific biofilm forming MRSA clones. Our laboratory had previously screened a large collection of important MRSA clones and found that MRSA isolates UAS391, H-EMRSA-15 and EU_ST239_16 belonging to USA300, EMRSA-15 and Hungarian/Brazilian ST239 clonal lineages, respectively, formed abundant biofilms in both static and shear flow assays [9]. The globally successful USA300 lineage was initially the primary cause of nosocomial and community MRSA infections in the US, whereas the Hungarian/Brazilian clone ST239 has been predominant in mainly Asian countries. EMRSA-15 is also a well-established global lineage, being the major cause of MRSA infections in the UK and in some parts of continental Europe.

The main goal of this thesis is to further identify key genetic determinants contributing to biofilm formation in MRSA through genotypic and phenotypic analyses utilizing important pandemic clones such as USA300 UAS391, EMRSA-15 H-EMRSA-15, and ST239-SCC*mec*III EU_ST239_16 as models to identify specific mechanisms as well as commonalities in the formation of biofilms. A comparative transcriptome analysis was carried out to determine which genes were up-regulated in MRSA biofilm cells. Single gene changes then formed an elegant way of teasing apart the gene essentiality in overall expression (top-down approach). In parallel, a whole genome mutant library was used for high-throughput screening of gene targets involved in biofilm formation (down-top approach).

Thus, specific objectives of this thesis are:

- To identify transcriptional signatures exhibited by MRSA clones during *in vitro* planktonic and biofilm growth (**Chapter 3, part 3.1**.) (top-down approach)
- To perform a genome-wide screening for biofilm-associated target genes using a *bursa aurealis* transposon library in MRSA (**Chapter 3, part 3.2.**) (down-top approach)
- To identify biofilm-associated candidate genes using *in vitro* biofilm models of staphylococcal infection and comparative genomics (**Chapter 3, part 3.3.**).
- To characterize biofilm-associated candidate genes as a critical determinant of MRSA pathogenic success (**Chapter 3, part 3.4.**).

As such, this thesis investigates the fundamental aspects underlying the pathogenic success of a very important human infectious disease pathogen, and results from this thesis are to have the potential for diagnostic and therapeutic applications.

2.3. References

1. Otto, M., *Staphylococcal infections: mechanisms of biofilm maturation and detachment as critical determinants of pathogenicity.* Annu Rev Med, 2013. **64**: p. 175-88.
2. Donlan, R.M., *Biofilms: microbial life on surfaces.* Emerg Infect Dis, 2002. **8**(9): p. 881-90.
3. Beenken, K.E., et al., *Global gene expression in Staphylococcus aureus biofilms.* J Bacteriol, 2004. **186**(14): p. 4665-84.
4. Archer, N.K., et al., *Staphylococcus aureus biofilms: properties, regulation, and roles in human disease.* Virulence, 2011. **2**(5): p. 445-59.
5. Mack, D., et al., *The intercellular adhesin involved in biofilm accumulation of Staphylococcus epidermidis is a linear beta-1,6-linked glucosaminoglycan: purification and structural analysis.* J Bacteriol, 1996. **178**(1): p. 175-83.
6. Speziale, P., et al., *Protein-based biofilm matrices in Staphylococci.* Front Cell Infect Microbiol, 2014. **4**: p. 171.
7. McCarthy, H., et al., *Methicillin resistance and the biofilm phenotype in Staphylococcus aureus.* Front Cell Infect Microbiol, 2015. **5**: p. 1.
8. Hoiby, N., et al., *ESCMID guideline for the diagnosis and treatment of biofilm infections 2014.* Clin Microbiol Infect, 2015. Suppl **1**: S1-S25.
9. Vanhommerig, E., et al., *Comparison of biofilm formation between major clonal lineages of methicillin resistant Staphylococcus aureus.* PLoS One, 2014. **9**(8): p. e104561.

<u>Chapter 3</u>: Experimental work

"You run in the lab, you open your incubator, your experiment makes no sense, you think, 'I hate this job.' Then ten minutes later you think, 'Well, now, maybe I'll try this or I'll try that"

- Bonnie Bassler

3.1. Differential gene expression analysis to identify MRSA transcriptional signatures associated with the planktonic and biofilm phenotypes

3.1.1. Transcriptome sequencing analysis investigates global changes in Staphylococcus aureus biofilm gene expression and reveals a key role of arginine biosynthesis across pandemic methicillin-resistant USA300, EMRSA-15 and ST239-SCCmecIII clones

Unpublished.

3.1.1.1. Abstract

Methicillin-resistant *S. aureus* (MRSA) is a leading cause of severe and chronic infections with a strong biofilm component. Here, we identified key genetic determinants contributing to the development of ageing biofilms in MRSA belonging to USA300 (UAS391), EMRSA-15 (H-EMRSA-15), and ST239-SCC*mecIII* (EU_ST239_16), utilizing the transcriptomic profile of these important pandemic clones. RNA was extracted from biofilm and planktonic cells of UAS391, H-EMRSA-15, and EU_ST239_16 after 24h, 48 and 72h of growth to perform RNA-sequencing, differentially expressed gene identification and annotation. A total of 94, 209, and 89 differentially expressed genes (DEGs) for UAS391, H-EMRSA-15 and EU_ST239_16 biofilms, respectively, with 54, 94, 74 and 40, 115, 15 showing up- and down-regulation, respectively, were obtained. Our results suggest the existence of species-specific pathways contributing to biofilm formation, by the up-expression of cell wall-associated binding factors (*clfA*, *sasF*, normalized fold-change: 2.35; *p.adj*<0.001) in USA300, factors associated with cell lysis and genomic DNA release (*atl*, *lytM*, *sarA*; normalized fold-change: 8.08; *p.adj*<0.001) in EMRSA-15, as well as phenol-soluble modulins (PSMs) (*hld*, *psmβ1*; normalized fold-change: 2.22; *p.adj*<0.001) in ST239-*SCCmecIII*, during early biofilm formation. Our results also confirm that biofilms upon ageing represent a unique growth state by comparison to planktonic cultures in response to oxidative stress, exemplified by the up-expression of stress modulating factors (*cspA*, *cspB*, *cspC*, *rsbW*, *asp23*; normalized fold-change: 8.43, 7.59, 1.65; *p.adj*<0.001, for USA300, EMRSA-15 and ST239-*SCCmecIII*, respectively) in addition to arginine biosynthesis (*arcABCDR*; normalized fold-change: 1.94, 6.54, 2.26; *p.adj*<0.001) and ammonium production (*ureABCDEFG*, normalized fold-change: 3.63, 0.18, -1.12, *p.adj*<0.001*; narGHIJ*, normalized fold-change: -0.72, -0.23, -0.07, *p.adj*=0.002; *nirBDR*, normalized fold-change: 1.11, 1.29, -1.03 *p.adj*<0.001; *kdpABCDE,* normalized fold-change: 3.26, 4.66, -0.60, *p.adj*<0.001). The arginine deiminase (ADI)-pathway, and carbamoyl phosphate (*arcC*_2; normalized fold-change: 1.22, 10.62, 3.87, *p.adj*<0.001) which converts arginine to ATP and is also involved in pH homeostasis, were shown to be central for general biofilm formation by all MRSA tested and might be an interesting target to achieve biofilm eradication. The additional ACME-

encoded ADI pathway (*arcABCD* and *argR*, normalized fold-change: 0.81, *p.adj*<0.001) and oligopeptide permease transport system (*opp-3ABCDE*; normalized fold-change: 1.27, *p.adj*=0.36) might confer a survival advantage to USA300 biofilms.

3.1.1.2. Introduction

Microbial biofilms represent an important determinant of human chronic infections. Bacterial biofilms involve a genetically coordinated sequence of events, including initial surface attachment, microcolony formation, and community expansion. This leads to a complex and structured architecture protecting bacteria from host-defence mechanisms and killing by antimicrobials. Among the most clinically significant bacterial pathogens is *Staphylococcus aureus*, a leading cause of nosocomial and community-acquired infections [1]. A considerable amount of research has been directed at understanding the mechanisms of staphylococcal biofilm formation. Much of this research has focused on the bacterial mediators of biofilm formation [2], the environmental effectors of biofilm formation [3, 4], and, more recently, the global changes that occur during biofilm development [5-7]. The consensus from transcriptional profiling studies of *S. aureus* biofilms is that bacteria are growing microaerobically or anaerobically relative to planktonic cultures [5, 7]. This is exemplified by a switch from aerobic energy production to fermentative processes such as acetoin metabolism, a general down-regulation of active cell processes, such as protein, DNA and cell wall biosynthesis, and increased expression of genes involved in the arginine deiminase and urease pathways. Here, cells can gain energy in the form of ATP from the conversion of arginine to citrulline [8]. Also, the products of the proteins encoded by this gene cluster can be fed into the urea cycle and thereby lead to the generation of ammonia and/or urea to counteract low pH values caused by the production of lactic acid, acetic acid, and formic acid under anaerobic conditions. The switch from aerobic respiration to anaerobic fermentation has been reported to be relevant for antibiotic resistance [9], the transcription of virulence genes [10], as well as the expression of extracellular polysaccharides involved in cell-to-cell adhesion and biofilm formation [11].

Despite high incidence and significant morbidity, the molecular pathogenesis of chronic staphylococcal infections and contribution of biofilm production remain largely unknown and there is very little consensus about the metabolic requirements of *S. aureus* during biofilm growth. Hence, more knowledge about cell physiology and molecular processes involved in biofilm-associated infections is urgently needed to understand staphylococcal pathogenicity, which is a central point for the development of novel tools for diagnosis and successful treatment of *S. aureus* infections in the future.

To enhance our understanding of the metabolic requirements of *S. aureus* biofilm development, three *S. aureus* strains (UAS391, H-EMRSA-15, and EU_ST239_16) were grown in microtiter plates and the cultures were collected for whole transcriptome analysis. These strains were chosen because they represent MRSA phenotypes from distinct genetic backgrounds (USA300, EMRSA-15, ST239-SCC*mec*III) that form prolific biofilms and might serve as a model for a variety of biofilm-forming staphylococci.

3.1.1.3. Materials and methods

3.1.1.3.1. Bacterial strains and growth conditions

Earlier identified prolific biofilm-forming MRSA strain UAS391, H-EMRSA-15 and EU_ST239_16 belonging to pandemic clonal lineages USA300, EMRSA-15 and ST239-SCC*mec*III, respectively [12], were collected from abscess/wound infections [13-15]. *Bursa aurealis* transposon mutants in *S. aureus* USA300-JE2 (**Table 1**) were provided by the Network on Antimicrobial Resistance in *Staphylococcus Aureus* (NARSA) for distribution by BEI Resources (Nebraska Transposon Mutant Library (NTML), www.beiresources.org) [16]. All strains were routinely grown on either 5% horse blood Columbia agar plates (Becton, Dickinson & Company, USA) or in brain-heart infusion (BHI) broth supplemented with 0.1% D(+)-glucose monohydrate (Becton, Dickinson & Company, USA).

Table 1: *bursa aurealis* transposon insertion mutants in USA300-JE2 and other *S. aureus* knockout isolates used in this study. The NARSA repository is described by Fey et al. [16], and freely available at NARSA repository (www.beiresources.org/).

Name	Description	Reference
ΔACME	ACME element (31 kb) deletion in strain USA300 UAS391	[24]
ΔSCCmec	*SCCmec*-IV element (24 kb) deletion in strain USA300 UAS391	[24]
ΔACME/*ΔSCCmec*	ACME and *SCCmec*–IV element deletion in strain USA300 UAS391	[24]
*ΔspeG (*NR-48388*)*	JE2 Tn mutant (insertion position: 63351) in spermidine N(1)-acetyltransferase (*speG*, SAUSA300_0053; 63100..63597)	NARSA repository
ΔarcA ACME (NR-48136)	JE2 Tn mutant (insertion position: 73785) in arginine deiminase (*arcA*, SAUSA300_0065; 73113..74348)	NARSA repository
ΔarcB ACME (NR-47590)	JE2 Tn mutant (insertion position: 70528) in ornithine carbamoyltransferase (*arcR*, SAUSA300_0062; 69839..70837)	NARSA repository
ΔarcC ACME (NR-47054)	JE2 Tn mutant (insertion position: 69656) in carbamate kinase (*arcC*, SAUSA300_0061; 68890..69819)	NARSA repository
ΔarcD ACME (NR-47668)	JE2 Tn mutant (insertion position: 72892) in arginine/ornithine antiporter (*arcD*, SAUSA300_0064; 71606..73027)	NARSA repository
ΔargR ACME (NR-47776)	JE2 Tn mutant (insertion position: 74980) in arginine repressor (*argR*, SAUSA300_0066; 74617..75063)	NARSA repository
ΔSAUSA300_0063 (NR-46840)	JE2 Tn mutant (insertion position: 71563) in cyclic nucleotide-binding domain protein (SAUSA300_0063; 70875..71564)	NARSA repository

Δopp3A (NR-46770)	JE2 Tn mutant (insertion position: 80584) in peptide ABC transporter, peptide-binding protein (*opp3A*, SAUSA300_0073; 80394..81947)	NARSA repository
Δopp3B (NR-48041)	JE2 Tn mutant (insertion position: 82421) in oligopeptide permease, channel-forming protein (*opp3B*, SAUSA300_0074; 81950..82906)	NARSA repository
Δopp3C (NR-47413)	JE2 Tn mutant (insertion position: 83147) in oligopeptide permease, channel-forming protein (*opp3C*, SAUSA300_0075; 82906..83673)	NARSA repository
Δopp3D (NR-48172)	JE2 Tn mutant (insertion position: 83911) in ABC transporter ATP-binding protein (*opp3D*, SAUSA300_0076; 83640..84407)	NARSA repository
Δopp3E (NR-48145)	JE2 Tn mutant (insertion position: 84977) in ABC transporter ATP-binding protein (*opp3E*, SAUSA300_0077; 84400..85035)	NARSA repository
ΔcopA (NR-47133)	JE2 Tn mutant (insertion position: 86401) in ATPase copper transport (*copA*, SAUSA300_0078; 86094..88118)	NARSA repository
ΔarcA (NR-47166)	JE2 Tn mutant (insertion position: 2782592) in arginine deiminase (*arcA*, SAUSA300_2570; 2781714..2782949)	NARSA repository
ΔarcB (NR-48009)	JE2 Tn mutant (insertion position: 2781207) in ornithine carbamoyltransferase (*arcB*, SAUSA300_2569; 2780671..2781681)	NARSA repository
ΔarcC_1 (NR-48261)	JE2 Tn mutant (insertion position: 1163307) in carbamate kinase (*arcC*, SAUSA300_1063;1162602..1163534)	NARSA repository
ΔarcC_2 (NR-48206)	JE2 Tn mutant (insertion position: 2778632) in carbamate kinase (*arcC*, SAUSA300_2567; 2778192..2779133)	NARSA repository
ΔarcD (NR-46645)	JE2 Tn mutant (insertion position: 2780356) in arginine/ornithine antiporter (*arcD*, SAUSA300_2568: 2779150..2780580)	NARSA repository
ΔarcR (NR-46997)	JE2 Tn mutant (insertion position: 2778015) in transcriptional regulator, Crp/Fnr family (*arcR*, SAUSA300_2566; 2777389..2778093)	NARSA repository

3.1.1.3.2. Quantification of biofilm mass and growth

Growth rates of UAS391, H-EMRSA-15, and EU_ST239_16 cultures were determined as previously described [17]. At each time point, average optical densities were calculated from quadruplicates. Additionally, biofilms of pandemic USA300, EMRSA-15, and ST239-SCC*mec*III clones, as well as NARSA transposon mutants, were formed on pre-sterilized 96-well flat bottom polystyrene microtiter plates (CELLSTAR®, Greiner Bio-One, Austria) in triplicates as described elsewhere [17]. Flow biofilms were grown in the BioFlux™ system as previously described [17], stained with LIVE/DEAD™ (BacLight™ Bacterial Viability Kit) according to manufacturer's instructions, and images were captured after 17h growth employing ZEN 2012 software (Zeiss Efficient Navigation®, Göttingen, Germany) as 84 combined tile images consisting of one µm² horizontal tiles covering the entire microchannel.

3.1.1.3.3. Biofilm and planktonic sample collection (**Fig. 4**)

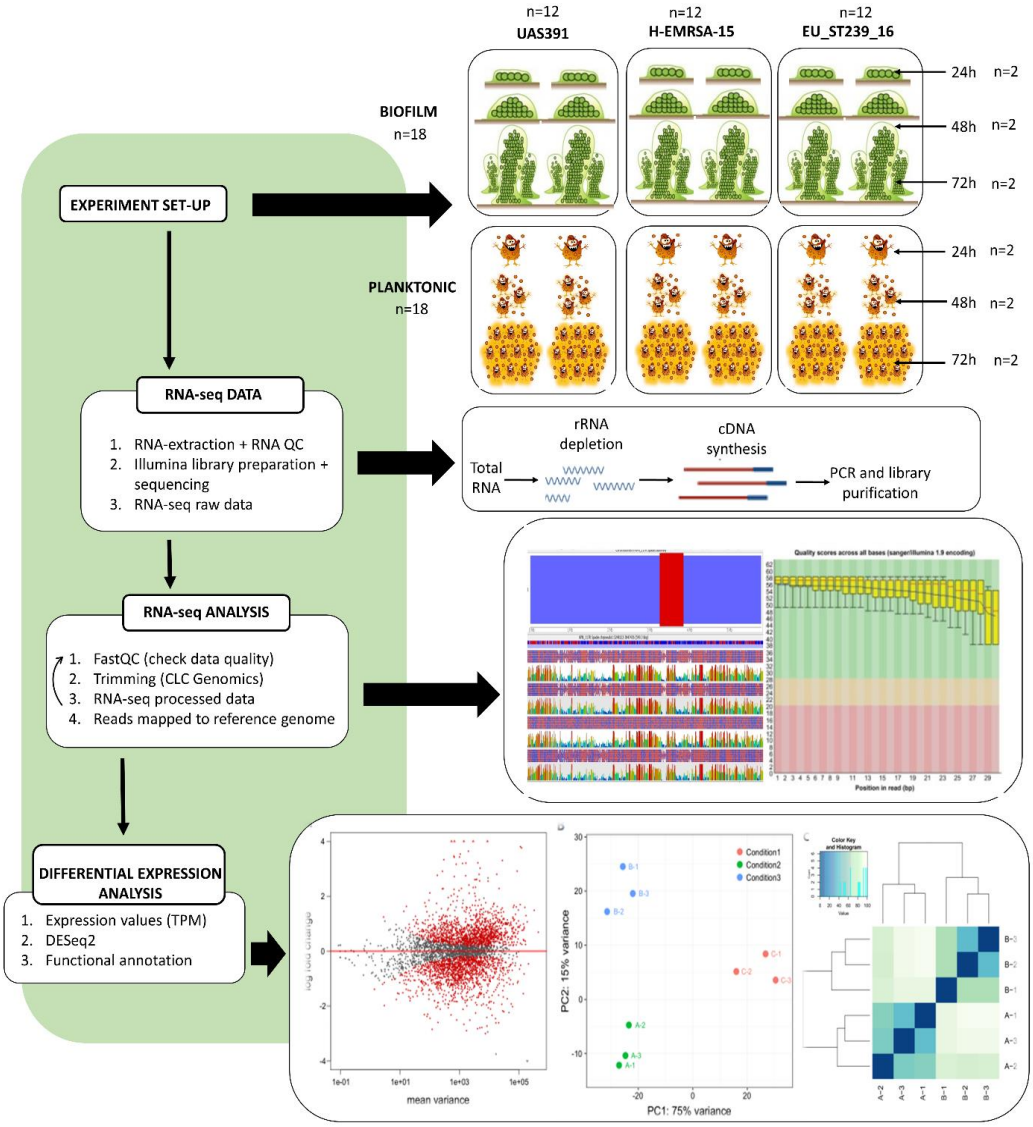

Figure 4: Experimental workflow for RNA-sequencing of biofilm and planktonic pandemic USA300, EMRSA-15 and ST239-SCC*mec*III MRSA phenotypes. Of each MRSA strain (UAS391, H-EMRSA-15, and EU_ST239_16), 2 biological replicates of both biofilm and planktonic phenotype were grown at a specific time point (24h, 48h or 72h). In total, 36 samples were sequenced.

0.05 McF of UAS391, H-EMRSA-15, and EU_ST239_16 in late exponential growth phase was inoculated in a 136 mm petri dish (Greiner Bio-One, Austria) during 24h, 48h or 72h under static conditions before rinsing (10xPBS, Thermo Fisher Scientific Inc., USA) and scraping off adherent cells. Simultaneously, one colony from overnight grown UAS391, H-EMRSA-15, and EU_ST239_16 cultures was re-suspended for 24h, 48h or 72h incubation whilst shaking (250 rpm, 37°C). The planktonic culture was refreshed every

24h, by spinning down the culture, removal of supernatant and addition of fresh medium. After incubation, cells were centrifuged at 4600xg for 20 min. Approximately, 0.200g of biofilm and planktonic cell suspensions was placed in RNAprotect™ Bacteria Reagent (Qiagen GmbH, Germany), incubated for 5 min at room temperature to stabilize the mRNA, and centrifuged at 5,000xg for 10 min at 4°C to harvest the cells. All samples per strain, phenotype and time point were collected, extracted, sequenced and analysed as two biological replicates.

3.1.1.3.4. RNA isolation, library construction, and sequencing (**Fig. 4**)

Total RNA was purified from the pellet using Masterpure™ Complete DNA and RNA Purification kit (Epicentre®, USA) according to the manufacturer's protocol with modifications. Briefly, cells were mechanically disrupted using lysing matrix B 0.1 mm silica sphere bead beating (FastPrep® 24 classic homogenization instrument, MP Biomedicals Inc., USA) before extraction. Each RNA sample was suspended in 30 µL of RNA storage solution and the quality of total RNA obtained was determined using Agilent 2100 Bioanalyzer (Agilent Technologies, Germany). Ribosomal RNA (rRNA) was depleted using the Ribo depletion kit (Thermo Fisher Scientific Inc., The Netherlands), a stranded TruSeq library was prepared and sequenced on NextSeq500, v2, 1x75bp (Illumina Inc., USA).

3.1.1.3.5. Differentially expressed genes identification and annotation (**Fig. 4**)

Prequality check, trimming, and mapping were performed using CLC Genomics Workbench v9.5.1 (CLCBio, Denmark). Total gene counts extracted from CLC Genomics Workbench were used for differential gene expression analysis using the DESeq2 package from Bioconductor in R (R v3.2.2.), as described [18]. Genes with an adjusted $|\log_2(\text{fold change})|>1$ and p-value<0.05 were identified as differentially expressed genes (DEG's) [19]. The top 50 DEGs (up- or down-expression) in the ageing biofilm phenotype (24h, 48h, and 72h) were mapped to the Kyoto encyclopaedia of genes and genomes (KEGG) pathway. DEG's were also assigned to TIGRFAMs protein families [20], which is based on TIGRFAM Hidden Markov Models (HMM) [21], by using the AureoWiki database repository of the *S. aureus* research and annotation community (http://aureowiki.med.uni-greifswald.de) [22]. Closely related *S. aureus* strains FPR3757 (#NC_007793.1), HO 5096 0412 (#HE681097), and TW20 (#NC_017331.1) were used as reference for gene functional assignment of UAS391, H-EMRSA-15 and EU_ST239_16, respectively [15].

3.1.1.3.6. RT-PCR validation

To validate the RNA-seq data, reverse transcription PCR (RT-PCR) was performed to validate expression levels using StepOne Plus (Life Technologies, USA) as described before [17]. For this, 12 DEG's were randomly selected (UAS391: *clfA*, *sodA*, *arcC*; H-EMRSA-15: *cspC*, *clpB*, *arcR*; EU_ST239_16: *arcR*, *spxA*, *pflA*). Transcript levels, in duplicate, were expressed as n-fold differences relative to levels obtained in planktonic vs. biofilm, and 24h vs. 48h vs. 72h, respectively by using the Comparative C_t method ($2^{-\Delta\Delta Ct}$). Gene-specific primers are listed in **Suppl. Table 1**.

3.1.1.3.7. Excision of ACME and/or SCCmec

ACME and/or SCC*mec* were artificially cured by electroporating (20°C, 100 Ω, 25 µF and 2.3 kV) pSR2, a thermosensitive plasmid containing the *ccrAB2* gene complex and a tetracycline-resistance marker, isolated from *Escherichia coli* SF8300 (ZymoPURE plasmid miniprep kit, Zymo Research, USA) into UAS391 using the method described by Katayama et al. and Diep et al. [23, 24]. Here, the pSR2 plasmid was first transferred into the restriction-deficient intermediate *S. aureus* cloning host RN4220 to adapt the plasmid DNA to *S. aureus* modifications. RN4220 and UAS391 transformants were grown for 3 consecutive days at 30°C in BHI broth supplemented with tetracycline. Single colonies were picked and grown for 24h at 42°C BHI broth to promote loss of pSR2. Excision of ACME, SCC*mec* or ACME/SCC*mec* was confirmed by usage of X1-X5, X2-X3 and X1-X3 PCR-primers designed by Diep et al. [24]. Additionally, transformants were screened for the presence of *arc* and *opp3* gene clusters by PCR—based assays, using the primer pairs AIPS.27 and AIPS.28 for *arc*A and AIPS.45 and AIPS.46 for *opp*3AB [25]. SCC*mec*-typing was based on *ccr* recombinase (*ccrmA1*, *ccrmA2*, *ccrα1*, *ccrα2*, *ccrα3*, *ccrβc*, *ccrα4*.2, *ccrβ4*.2, *ccrγR*, *ccrγF*) and *mec* (*mecmI6*, *mecIS7*, *mecIS2iS2*, *mecmA7*) PCR [26].

3.1.1.3.8. Statistical analysis

Adjusted *p*-values were calculated using a model I two-way ANOVA with post-hoc Tukey HSD test in 'The R Project for Statistical Computing' (R v3.2.2.) and considered significant if <0.05.

3.1.1.4. Results

3.1.1.4.1. Biofilm-forming capacity under no flow conditions

For this study, 3 pandemic MRSA clones were used to compare gene expression under biofilm and planktonic growth conditions. Hereof, UAS391 has been previously identified as a prolific biofilm former [12]. Interestingly, the 96-microtiter well plate biofilm assay under no flow conditions revealed that both H-EMRSA-15 and EU_ST239_16 (OD_{492}=0.856; 116% and OD_{492}=1.366; 183%, respectively) formed even

more biomass compared to UAS391 (OD_{492}=0.746; 100%; *p*=0.03) (**Fig. 5** & **Suppl. Fig. 1A**). To correlate the overall growth with biofilm formation capacity, we measured the OD_{620} after 24h of growth at 37°C. High biomass-forming H-EMRSA-15 (0.149 min^{-1}, doubling time: 4.65 min) and EU_ST239_16 (0.160 min^{-1}, doubling time: 4.31 min) reached a lower growth rate than did UAS391 (0.164 min^{-1}, doubling time: 4.21 min; *p*=0.046) (**Suppl. Fig. 1B**).

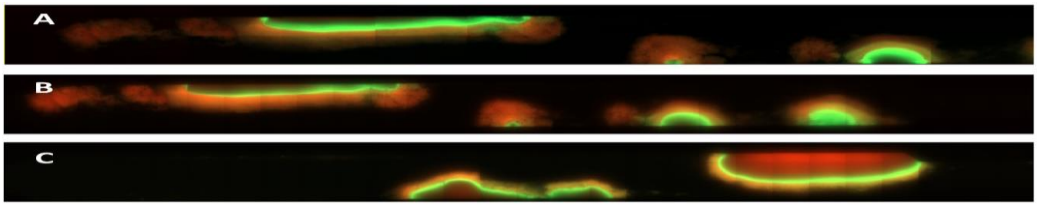

Figure 5: Biofilm formation of pandemic USA300, EMRSA-15, and ST239-SCC*mec*III MRSA clones under flow conditions. (**A**) UAS391, (**B**) H-EMRSA-15 and (**C**) EU_ST239_16 biofilms, visualized by SYTO 9 and propidium iodide staining (LIVE/DEAD™).

3.1.1.4.2. *Higher level expression of genes in biofilm cells*

By comparing gene expression under biofilm and planktonic growth conditions after 24, 48 and 72h of growth, several genes that were differentially expressed under the two growth conditions were identified and statistically validated (**Fig. 6** & **Suppl. Table 4-6**). In our 3 MRSA clones (UAS391, H-EMRSA-15, and EU_ST239_16, respectively), we identified 54, 94, and 74 genes in which expression was induced at least two-fold in biofilms compared to planktonic conditions ($|\log_2(\text{fold-change})|>1$ and *p*-value<0.05) (**Suppl. Fig. 2**). Similarly, we identified 40, 115, and 15 genes in which expression was repressed by a factor of at least 2 compared to planktonic cells (**Suppl. Fig. 2**). When we compared expression within the biofilm over time; we identified 1417, 111, and 174 differentially expressed genes in 48h biofilms compared to 24h biofilms (**Suppl. Fig. 4**). Similarly, we identified 130, 175, and 13 differentially expressed genes at 72h compared to 24h biofilm cells (**Suppl. Fig. 4**). As a control, $\log_2$(fold change) of housekeeping genes *gyrB*, *gmk*, *tpiA*, *aroE*, *glpF*, *pta,* and *yqiL* did not show any significant difference between the biofilm and planktonic phenotype (*p*=0.29, 0.67 and 0.79, respectively) (**Suppl. Table 2**). Furthermore, biofilm expression levels of randomly selected DEG's *clfA* (clumping factor A), *arcC_2* (carbamate kinase) and *sodA* (FE/Mn family superoxide dismutase) (in UAS391), *arcR* (Crp/FNR family transcriptional regulator), *cspC* (cold-shock protein) and *clpB* (chaperon ClpB) (in H-EMRSA-15) and *arcR*, *spxA* (transcriptional regulator Spx), and *pflA* (pyruvate formate-lyase activating enzyme) (in EU_ST239_16) were confirmed through RT-PCR analysis (**Suppl. Fig. 3A**). Log_2(fold change) of housekeeping genes *gyrB*, *gmk*, *tpiA*, *aroE*, *glpF*, *pta,* and *yqiL* also did not show any significant difference between different time points (*p*=0.85, 0.75 and

0.78, respectively) (**Suppl. Table 2**). Furthermore, aging biofilm expression levels of randomly selected DEG's *clfA*, *arcC_2* and *sodA* (in UAS391), *arcR*, *cspC* and *clpB* (in H-EMRSA-15) and *arcR*, *spxA*, and *pflA* (in EU_ST239_16) were also confirmed through RT-PCR analysis (**Suppl. Fig. 3B**).

3.1.1.4.3. *Expression of reported biofilm-associated genes in S. aureus*

Many cell wall-associated binding factors (*sdrE*, *clfA*, *isaB*, *sasF, eno*) were up-expressed in biofilm cells, suggesting that the cell envelope is a highly dynamic and active component of biofilms [27]. Interestingly, genes involved in murein synthesis and the synthesis of peptidoglycan as well as cell wall biosynthesis (*murQ*, *ftsL*, *mraZ*) were expressed in biofilms of UAS391 and H-EMRSA-15. Also collagen-like proteins (*clpC*, *clpL*) required for adhesion were up-expressed in EU_ST239_16 [28]. H-EMRSA-15 showed significant up-expression of factors associated with cell lysis and genomic DNA release during biofilm formation [29]. Examples are autolysin (*atl*), peptidoglycan hydrolase (*lytM*), as well as the staphylococcal accessory regulator A (*sarA*), which is an essential regulator controlling PIA/PNAG-producing *icaADBC* and surface protein *Bap* expression. Surprisingly, early biofilms of UAS391 showed high up-expression of cysteine proteases (*sspA*, *sspB*, *sspC*), whereas early EU_ST239 biofilms showed up-expression of δ-haemolysin (*hld*) and haemolytic protein *psmβ1* genes. These factors have been associated with biofilm dispersal rather than biofilm accumulation and maturation [30]. Other dispersal-inducing factors such as the serine proteases *splBEF* were down-expressed, as well as *icaC* of the PIA/PNAG-producing *icaADBC* operon. In H-EMRSA-15, no proteases were up-expressed upon ageing, but the *agrC* (accessory gene regulator protein C) gene of the *agr* operon, controlling quorum-sensing mediated dispersal of *S. aureus* biofilms [31], was. In both UAS391 and EU_ST239_16, *dltC* and *dltX* genes, which are responsible for the D-alanylation of teichoic acids, were down-expressed. Surprisingly, the net charge of teichoic acids has been reported to have a key role in *S. aureus* colonization of surfaces [32]. Interestingly, the native penicillin-binding protein 2 (*pbp2*) and the methicillin resistance regulatory *mecI* gene, which is involved in methicillin resistance-inducing production of PBP2A, were down-expressed in both strains. EU_ST239_16 demonstrated up-expression of transcriptional regulator Spx (*spxA*). SpxA activates the *icaR* repressor which regulates the *ica*-dependent pathway but also works as a global effector impacting stress tolerance [33]. Biofilm formation of all 3 MRSA was characterized by up-expression of cold-shock proteins A, B and C (*cspABC*). Csps have been shown to contribute to osmotic, oxidative, starvation, pH and ethanol stress tolerance [34]. ClpC and ClpL in EU_ST239_16 have also been associated with stress tolerance [28]. Additionally, serine-protein kinase RsbW (*rsbW*), which

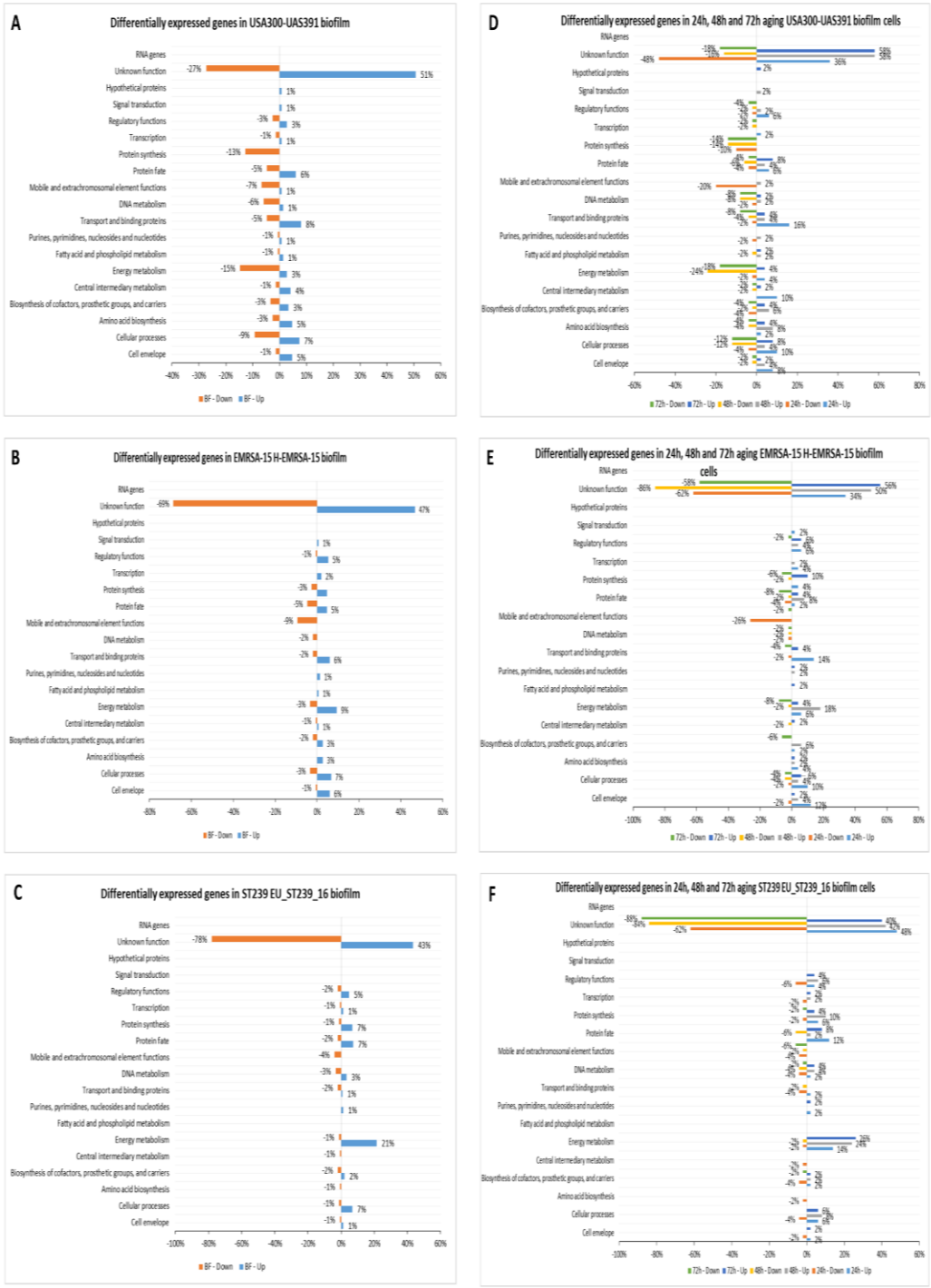

Figure 6: Metabolic functions of differentially up- and down-expressed genes (|$\log_2$(fold change)|>1) in pandemic USA300, EMRSA-15, and ST239-SCC*mec*III MRSA clones ageing biofilm cells. On average UAS391 (**A**), H-EMRSA-15 (**B**) and EU_ST239_16 (**C**) expression during 24h, 48h and 72h (**D, E, F**), respectively. Percentages represent X/50 genes belonging to TIGRFAM protein families.

activates the σ^B regulon, was up-expressed in 24h H-EMRSA-15 biofilms. σ^B is an essential regulator of *S. aureus* biofilm maturation induced by a variety of environmental stresses, including heat, alkaline, and high-salt conditions [35]. Of interest are the alkaline shock protein 23 (*asp23*) (expressed in UAS391, H-EMRSA-15 and EU_ST239_16) and hypothetical protein AmaP (*amaP*) (expressed in H-EMRSA-15 and EU_ST239_16), which is controlled by the essential biofilm regulator sigma factor B (σ^B), and solely in H-EMRSA-15: O-acetyltransferase OatA (*oatA*), glycosyltransferase group 2 family protein CsbB (*csbB*), and iron export ABC transporter permease subunit FetB (*fetB*), which are all under control of σ^B. In addition, H-EMRSA-15 demonstrated up-expression of hypothetical protein *saeP*, which is important for the functionality of the *sae* operon [15, 36]. *SaeRS* appears to be a central downstream regulator that controls the expression of major virulence genes such as *hla* (coding for α-haemolysin), *coa* (coding for coagulase), or *fnbA* (coding for fibronectin-binding protein A) [37]. Another important regulator in UAS391 appears to be transcriptional repressor CodY (*codY)* by controlling the up-expression of acetolactate synthase *ilvH*, glutamate synthase *gltD*, tryptophan synthase *trpB*, and capsular polysaccharide genes. CodY links changes in intracellular metabolite pools with the induction of numerous adaptive responses [38].

3.1.1.4.4. *Anaerobic conditions influence the expression of genes belonging to the central carbon metabolic and fermentation pathways*

Our data shows the higher-level expression of several genes belonging to the functional categories of glycolysis, fermentation and anaerobic respiration, which has been reported for planktonic cells under conditions of oxygen depletion [10]. Indeed, EU_ST239_16 biofilms showed up-expression of *eno* and *fbaA* genes involved in glycolysis/gluconeogenesis. Similarly, *ldh1* encoding lactate dehydrogenase and *butB* gene involved in butanediol synthesis for fermentation were also up-expressed. Interestingly, the other two UAS391 and H-EMRSA-15 clones did not show enhanced glycolytic activity or fermentation processes with significant down-expression of *fbaA*, *fdaB*, *gpmI*, *gapA*, *pykA, butA,* and *ldh1* genes. Other genes taking part in acetate and ethanol formation such as *pflB* and *pflA* genes had high levels of transcription as well in both EU_ST239_16 and H-EMRSA-15 but not in UAS391. Surprisingly, EU_ST239_16 biofilms showed up-expression of the *pdhABCD* operon genes encoding the pyruvate dehydrogenase (PDH) complex that converts pyruvate to acetyl-CoA under aerobic conditions. Also, *qoxABCD* genes associated with oxidative phosphorylation were up-expressed in EU_ST239_16 biofilms, while *qoxA* and *qoxB* were significantly down-expressed in UAS391 and H-EMRSA-15 biofilms.

Of interest, the transcription of several genes coding for virulence factors was found to be up-expressed as well in both EU_ST239_16 and UAS391; these are the genes

hld, *isaB*, *epiA,* and *epiF*. Moreover, genes involved in capsular polysaccharide synthesis were also up-expressed (*capA*, *capB*, *capC*, *capF*, *capG*, *capH*, *capI*, *capJ*, *capL*, *capM*, *capN*, *capO* and *capP*) in UAS391 and H-EMRSA-15. Additionally, the expression levels of genes encoding phage-associated factors were also significantly higher in 48h biofilms of UAS391, H-EMRSA-15, and EU_ST239_16. Up-expressed genes were mainly associated with phages 23MRA, phi2958PVL, phiN13, SA13, and SPβ-like. 47, 11 and 19 up-expressed genes in UAS391, H-EMRSA-15, and EU_ST239_16, respectively, code for hypothetical proteins. To obtain information on the possible function of the hypothetical proteins, BLAST analysis was carried out. Interestingly, some of these hypothetical proteins up-expressed in biofilms showed similarities to cell-envelope associated proteins.

3.1.1.4.4.1. The arginine biosynthesis pathway

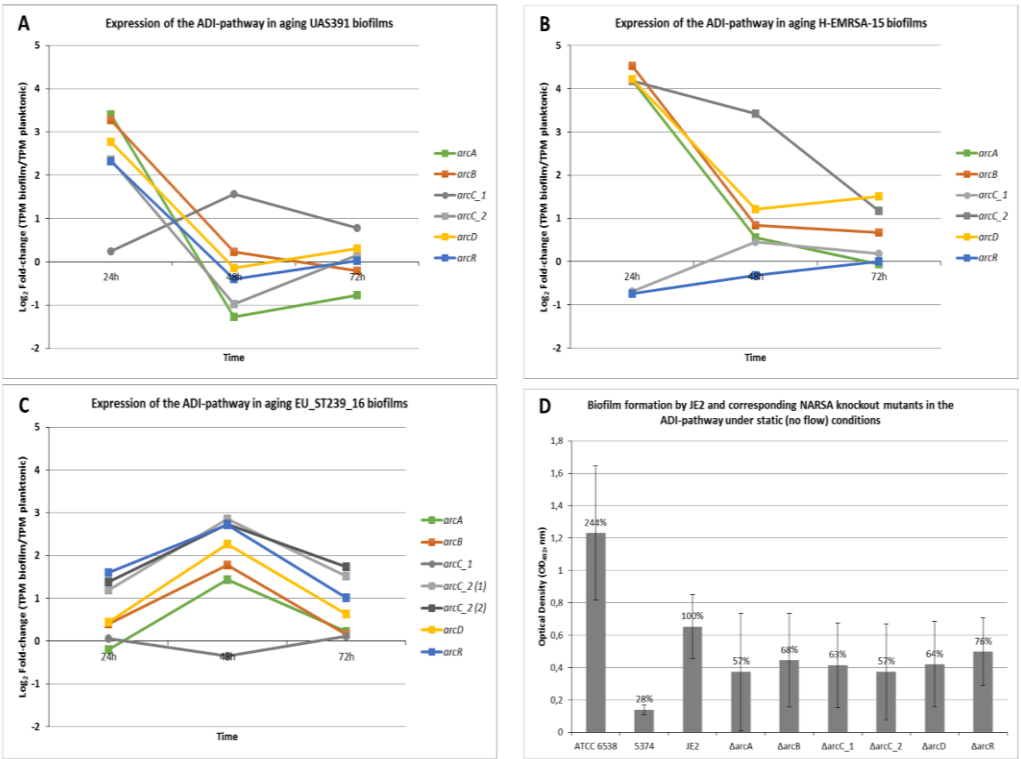

Figure 7: Expression of the ADI-pathway in ageing biofilm cultures of pandemic USA300, EMRSA-15 and ST239-SCC*mec*III MRSA clones. ADI-pathway associated genes: *arcA* (arginine deiminase), *arcB* (ornithine carbamoyltransferase), *arcC*_1 and _2 (carbamate kinase), *arcD* (arginine/ornithine antiporter) and *arcR* (positive transcriptional regulator). **(A)** Average fold-change of the ADI-pathway in 24h, 48h and 72h UAS391 biofilms; **(B)** Average fold-change of the ADI-pathway in 24h, 48h and 72h H-EMRSA-15 biofilms; **(C)** Average fold-change of the ADI-pathway in 24h, 48h and 72h EU_ST239_16 biofilms; **(D)** Formation of biofilms by

JE2, and corresponding transposon knockout mutants in ADI-pathway encoding genes (*arcA, arcB, arcC_1, arcC_2, arcD, arcR*) under static conditions. The total biomass was determined by crystal violet staining *in triplicate*. Error bars represent 95% confidence intervals.

Arginine either provides energy to the anoxic cell in the form of ATP through the conversion into citrulline or leads to the generation of ammonia by feeding products into the urea cycle. In UAS391, H-EMRSA-15 and EU_ST239_16 biofilms the arginine-producing ADI-pathway (*arcA*, *arcB*, *arcC_1* and *_2* (1) and (2) for EU_ST239_16), *arcD* and *arcR)* were 1.69, 2.64 and 2.17-fold up-expressed, respectively (**Suppl. Table 3**). Gene expression profiling revealed *arcB*, *arcC*_2 (1) and *arcC*_2 (2) to be most differentially expressed in UAS391, H-EMRSA-15 and EU_ST239_16 biofilms, respectively, as compared to planktonic cells. Arginine biosynthesis activity was highest in 24h biofilms of UAS391 and H-EMRSA-15, whilst EU_ST239_16 showed a peak at 48h (**Fig. 7A, B&C** & **Suppl. Table 3**). In line with these results, inactivation of *arcC_2* (OD_{492}=0.373, 57%; p<0.001) proved to have the most significant impact on biofilm formation in USA300-JE2 (OD_{492}=0.658; 100%) (**Fig. 7D**). Surprisingly, however, also *arcA* inactivation decreased the formed biofilm mass (OD_{492}=0.372, 57%; p<0.001).

Arginine is also synthesized by the pyrimidine nucleotide biosynthesis pathway (*pyrRPBC*, *carAB*, and *pyrFE*). This pathway was 1.6, 0.85, and 1-fold up-expressed in UAS391, H-EMRSA-15, and EU_ST239_16 biofilms, respectively (**Suppl. Table 3**). Gene expression profiling revealed *pyrB, pyrC, pyrP, carA* and *carB* to be most differentially expressed in UAS391, H-EMRSA-15 and EU_ST239_16 biofilms, respectively, as compared to planktonic cells. Pyrimidine nucleotide biosynthesis pathway associated genes showed a high up-expression at 48h for UAS391 (**Fig. 8A**). In contrast, biosynthesis was not highly up-expressed in H-EMRSA-15 and EU_ST239_16 biofilms throughout ageing (**Fig. 8B** & **C**).

In addition to arginine catabolism mediated ammonia production, the high-affinity K^+-specific transport system (*kdpABC* and *kdpDE*) also contributes to pH homeostasis through the exchange of K^+ for H^+. Here, UAS391, H-EMRSA-15, and EU_ST239_16 biofilms showed 1.7, 1.7, and 1.6-fold up-expression, respectively (**Suppl. Table 3**). Gene expression profiling revealed *kdpA, kdpC,* and *kdpD* to be most differentially expressed in UAS391, H-EMRSA-15 and EU_ST239_16 biofilms, respectively, as compared to planktonic cells. For both UAS391 and H-EMRSA-15 expression of the high-affinity K^+-specific transport system decreased after 24h (**Fig. 8D** & **E**). EU_ST239_16 did not show a significant up-expression, except for *kdpC* at 48h (**Fig. 8F**).

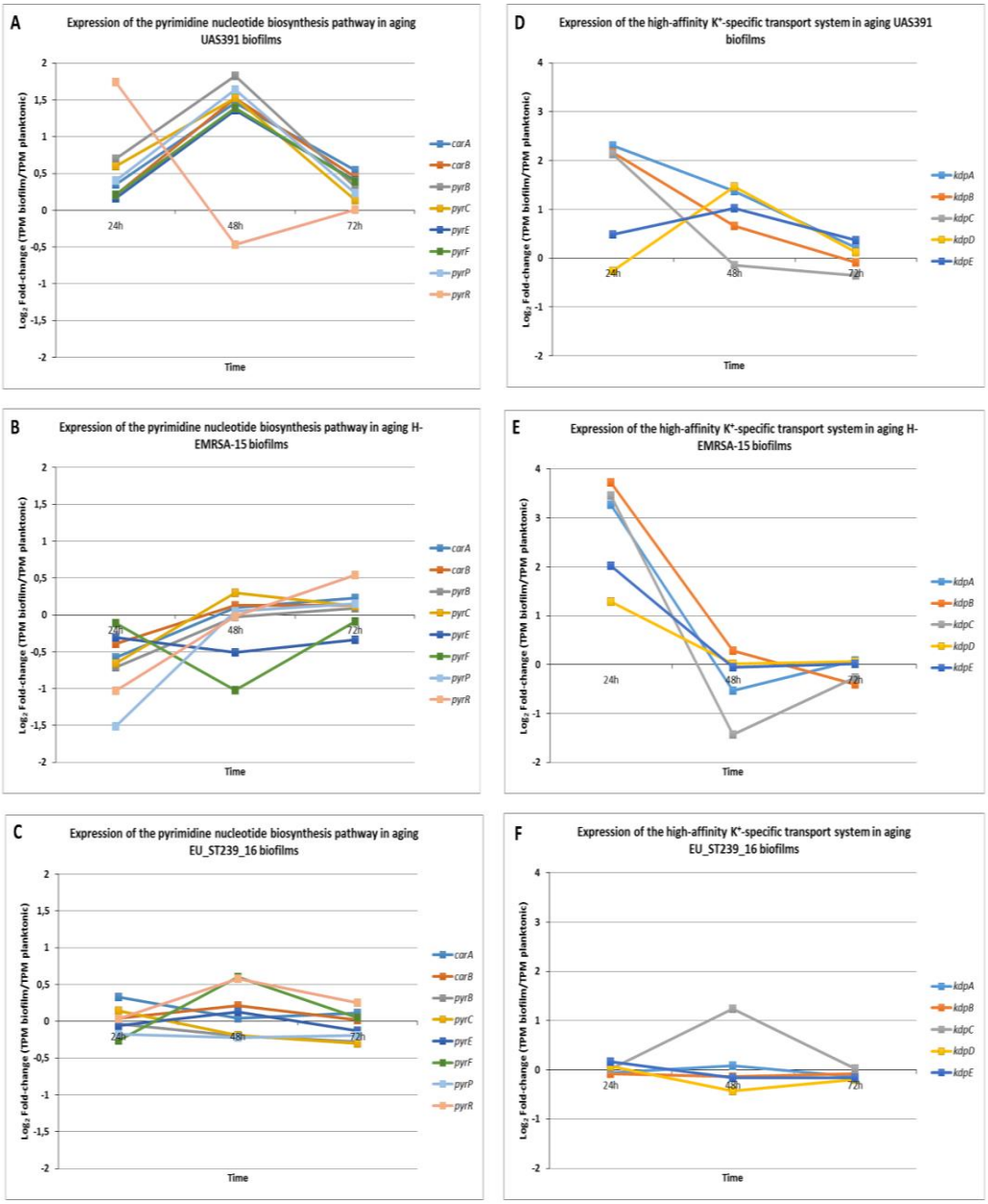

Figure 8: Expression of the pyrimidine nucleotide biosynthesis pathway and the high-affinity K^+-specific transport system in ageing biofilm cultures of pandemic USA300, EMRSA-15 and ST239-SCC*mec*III MRSA clones. Pyrimidine nucleotide biosynthesis pathway associated genes: *carA* (carbamoyl-phosphate synthase, small subunit), *carB* (carbamoyl-phosphate synthase, large subunit), *pyrB* (aspartate carbamoyltransferase), *pyrC* (dihydroorotase), *pyrE* (orotate), *pyrF* (orotine 5'-phosphate decarboxylase), *pyrP* (uracil permease), and *pyrR* (tetrapyrrole methylase family protein). **(A)** Average fold-change of the pyrimidine nucleotide biosynthesis pathway in 24h, 48h, and 72h UAS391 biofilms; **(B)** Average fold-change of the pyrimidine nucleotide biosynthesis pathway in 24h, 48h and 72h H-EMRSA-15 biofilms; **(C)** Average fold-change of the pyrimidine nucleotide biosynthesis pathway in 24h, 48h and 72h EU_ST239_16 biofilms. High-affinity K^+-specific transport system associated genes: *kdpA* (K^+-transporting ATPase, A subunit), *kdpB* (K^+-transporting

ATPase, B subunit), *kdpC* (K^+-transporting ATPase, C subunit), *kdpD* (sensor histidine kinase), and *kdpE* (DNA-binding response regulator). **(D)** Average fold-change of the high-affinity K^+-specific transport system in 24h, 48h, and 72h UAS391 biofilms; **(E)** Average fold-change of the high-affinity K^+-specific transport system in 24h, 48h and 72h H-EMRSA-15 biofilms; **(F)** Average fold-change of the high-affinity K^+-specific transport system in 24h, 48h and 72h EU_ST239_16 biofilms.

3.1.1.4.4.2. Carriage of an additional ADI-cluster on the ACME-element

As an additional ADI gene cluster is carried on the arginine catabolic mobile element (ACME)-element, which is uniquely carried by USA300, we determined up-expression of *speG*, *arcA*, *arcB*, *arcC*, *arcD*, *argR*, SAUSA3000_0063, *opp*-3A, *opp*-3B, *opp*-3C, *opp*-3D, and *copA* genes in UAS391 biofilms. Here, the ADI-pathway was on average 1.36-fold up-expressed, with its largest contribution to 48h old biofilms (**Fig 9A & Suppl. Table 3**).

Surprisingly, excision of the complete ACME-element did not result in any biofilm-deficiencies (OD_{492}=0.619, 83%), as compared to wild type UAS391 (OD_{492}=0.746, 100%; p=0.13) (**Fig. 9B**). ACME is closely associated with *SCCmec*, and when ACME was excised with the adjacent *SCCmec* element, there was a 42% decrease in biofilm formation capacity (OD_{492}=0.614, 58%; p<0.001) while *SCCmec* excision alone only resulted in an 18% decrease (OD_{492}=0.429, 82%; p=0.22). On average, *arcD* and *opp*-3D genes showed the most significant up-expression under biofilm conditions as compared to planktonic cells. Knocking-out each particular gene carried on the element revealed an effect of the *opp*-genes (*opp*-3A, *opp*-3B and *opp*-3C; OD_{492}=0.372-0.596; 57-91%, p≤0.03) rather than of the *arc*-genes (*arcD*, OD_{492}=0.556, 85%, p=0.06; *speG*, *arcA*, *arcB*, *arcC*, *argR*, SAUSA300_0063, *opp*-3C, *opp*-3E, *copA*, OD_{492}=0.571-0.677; 88-104%, p=0.10-0.41) on JE2 biofilm formation (OD_{492}=0.658; 100%) (**Fig. 9C**).

3.1.1.4.4.3. PH homeostasis

As ADI-pathway activity seems crucial for the *S. aureus* biofilm, its role might be attributed to the production of ammonia and/or urea. Therefore, we determined that the complete urea cycle (*argH*, *argG*, *argJ*, *rocF*, *ureA*, *ureB*, *ureC*, *ureE*, *ureF*, *ureG*, *ureD*) was 1.75, 0.97, 0.87-fold up-expressed in UAS391, H-EMRSA-15 and EU_ST239_16 biofilms, respectively (**Suppl. Table 3**). Gene expression profiling revealed *argH, argG*, and *ureA*, to be most differentially expressed in UAS391, H-EMRSA-15 and EU_ST239_16 biofilms, respectively, as compared to planktonic cells. In UAS391 biofilms, the *arg* genes were highest up-expressed at 48h, whilst the *ure* genes were highest at 24h (**Fig. 10A**). H-EMRSA-15 showed a comparable pattern with less significant up-expression (**Fig. 10B**), and up-expression of both *arg* and *ure* genes in the urea cycle remained relatively stable over time in EU_ST239_16 biofilms (**Fig. 10C**). Another source of ammonia production is the reduction of nitrate to nitrite. In UAS391, we saw a significant up-expression of respiratory nitrate reductase *(narGHIJ)* and nitrite reductase (*nirBDR)* associated genes

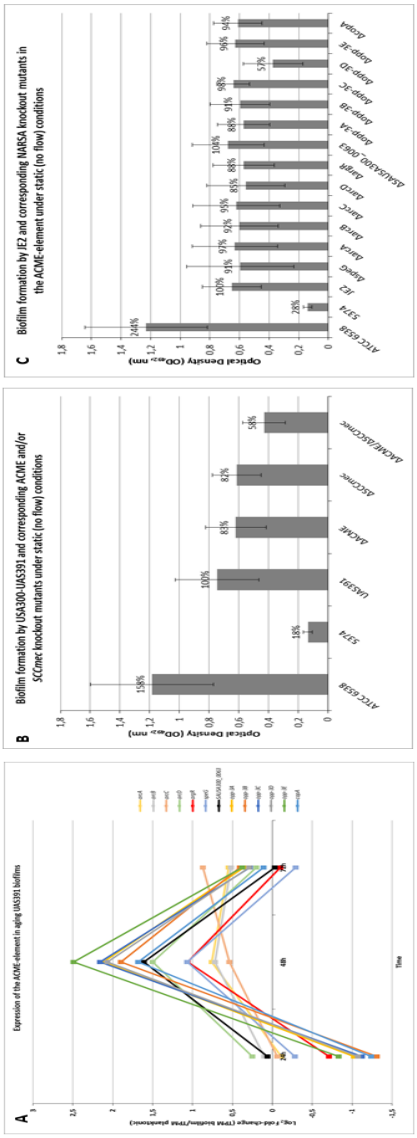

Figure 9: Expression of ACME-element associated genes and biofilm formation of corresponding knockout mutants in USA300. **(A)** ACME-element associated genes: *speG* (spermidine N(1)-acetyltransferase), *arcA*, *arcB*, *arcC*, *arcD*, *arcR*, SAUSA300_0063 (cyclic nucleotide binding domain protein), *opp*-3A (oligopeptide ABC transporter, substrate-binding protein), *opp*-3B (oligopeptide permease, channel-forming protein), *opp*-3C (oligopeptide permease, channel-forming protein), *opp*-3E (ABC transporter, ATP-binding protein), *copA* (ATPase copper transport), in aging biofilm cultures of USA300-UAS391; **(B)** Formation of biofilms by UAS391, and corresponding *ccr*-excision mediated mutants in ACME, SCC*mec* or ACME/SCC*mec* under static conditions; **(C)** Formation of biofilms by JE2 and corresponding transposon knockout mutants in ACME-element encoding genes (*speG*, *arcA*, *arcB*, *arcC*, *arcD*, *arcR*, SAUSA300_0063, *opp*-3A, *opp*-3B, *opp*-3C, *opp*-3E) under static conditions. The total biomass (B and C) was determined by crystal violet staining *in triplicate*. Error bars represent 95% confidence intervals.

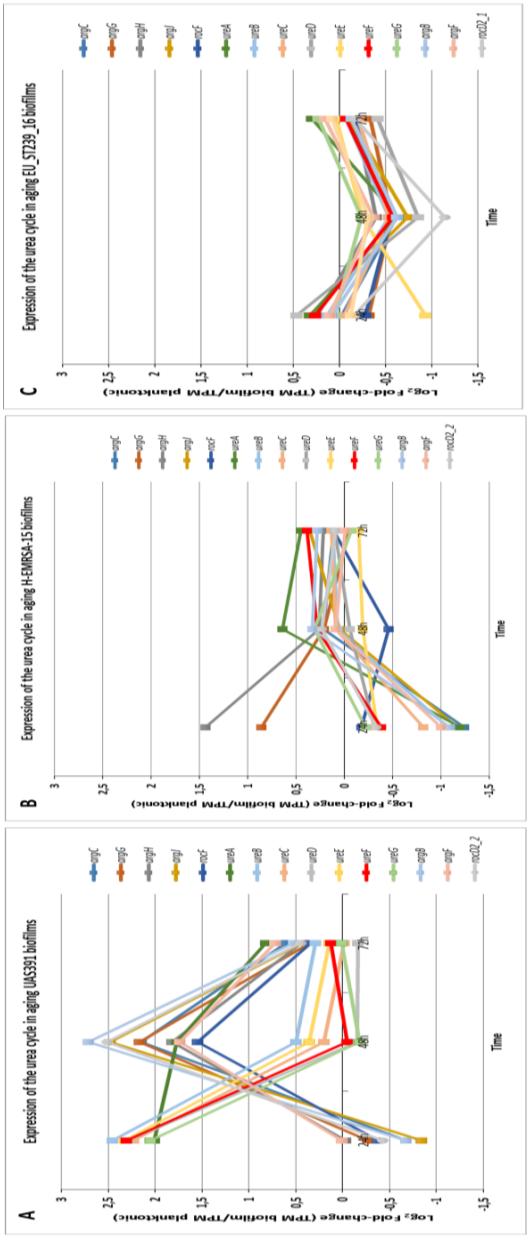

Figure 10: Expression of the urea cycle in ageing biofilm cultures of pandemic USA300, EMRSA-15 and ST239-SCC*mec*III MRSA clones. Urea cycle associated genes: *argB* (acetylglutamate kinase), *argC* (N-acetyl-gamma-glutamyl-phosphate reductase), *argF* (ornithine carbamoyltransferase), *argG* (argininosuccinate synthase), *argH* (argininosuccinate lyase), *argJ* (arginine biosynthesis bifunctional protein ArgJ), *rocD* (ornithine--oxo-acid transaminase), *rocF* (arginase), *ureA* (urea amidolyase-related protein), *ureB* (urease beta subunit), *ureC* (urease alpha subunit), *ureD* (urease accessory protein UreD), *ureE* (urease accessory protein UreE), *ureF* (urease accessory protein UreF), and *ureG* (urease accessory protein UreG), in aging biofilm cultures of UAS391, H-EMRSA-15 and EU_ST239_16. **(A)** Average fold-change of the urea cycle in 24h, 48h, and 72h UAS391 biofilms; **(B)** Average fold-change of the urea cycle in 24h, 48h and 72h H-EMRSA-15 biofilms; **(C)** Average fold-change of the urea cycle in 24h, 48h and 72h EU_ST239_16 biofilms.

at 48h. However, in both H-EMRSA-15 and EU_ST239_16, we did not see particularly elevated transcripts of these operons (**Suppl. Table 3)**.

3.1.1.5. Discussion

Here, we report a comparative transcriptome analysis of the global gene expression of *S. aureus* cells grown as an ageing biofilm and of planktonic cells grown to the stationary growth phase. Our analysis indicates spectacularly different mechanisms of biofilm formation compared between 3 pandemic clonal lineages of MRSA. We also demonstrated that distinct metabolic activity due to pH homeostasis under oxygen limitation can be considered as a general paradigm amongst biofilms formed by different lineages. Moreover, while we saw that early biofilms (24h) are mainly characterized by up-expression of genes associated with surface adhesion and matrix production, older biofilms (48h and 72h) show a shift in gene expression towards stress modulation, energy metabolism and pH homeostasis as nutrients and oxygen become more limited.

3.1.1.5.1. Changes in matrix composition of the biofilm

The expression of the *ica* genes and thereby the synthesis of PIA/PNAG have been reported to be important for adhesion and formation of staphylococcal biofilms [5, 7]. Our data did not show up-expression of *icaADBC* and points to a fundamentally different biofilm formation mechanism for MRSA. All 3 clonal lineages showed a high up-expression of numerous LPXTG-anchored cell wall-associated MSCRAMMs, which are commonly used during the first step of biofilm formation, called surface adhesion [39]. Here, also eDNA released following cell lysis can also act as component of the biofilm matrix [40, 41], which we indeed noted for H-EMRSA-15. Interestingly, both USA300 and ST239-SCC*mec*III lineages showed up-expression of proteases and PSMs, even during the early stages of biofilm formation. Recently, it has been reported that PSMs, besides their surfactant qualities, can also aggregate into amyloid structures that enhance biofilm formation [42, 43]. Surprisingly, we noted the up-expression of genes associated with capsular polysaccharide production in both USA300 and H-EMRSA-15. Boyle-Vavra et al. postulated that 4 conserved mutations (in the *cap5* promotor, *cap5D* nucleotide 994, *cap5E* nucleotide 223 and *cap5E*75 Asp) ablated capsule production in USA300 [44]. While the role of capsular polysaccharides in biofilm formation by *Klebsiella pneumoniae* [45], *Vibrio vulnificus* [46] and *Pasteurella multocida* [47] has been demonstrated, our results urge for a re-evaluation of the role of capsular polysaccharides in *S. aureus* biofilm formation.

We also found several prophage-related genes to be up-expressed in, especially 48h old, biofilm cells of USA300, EMRSA-15 and ST239-SCC*mec*III. Prophages play an

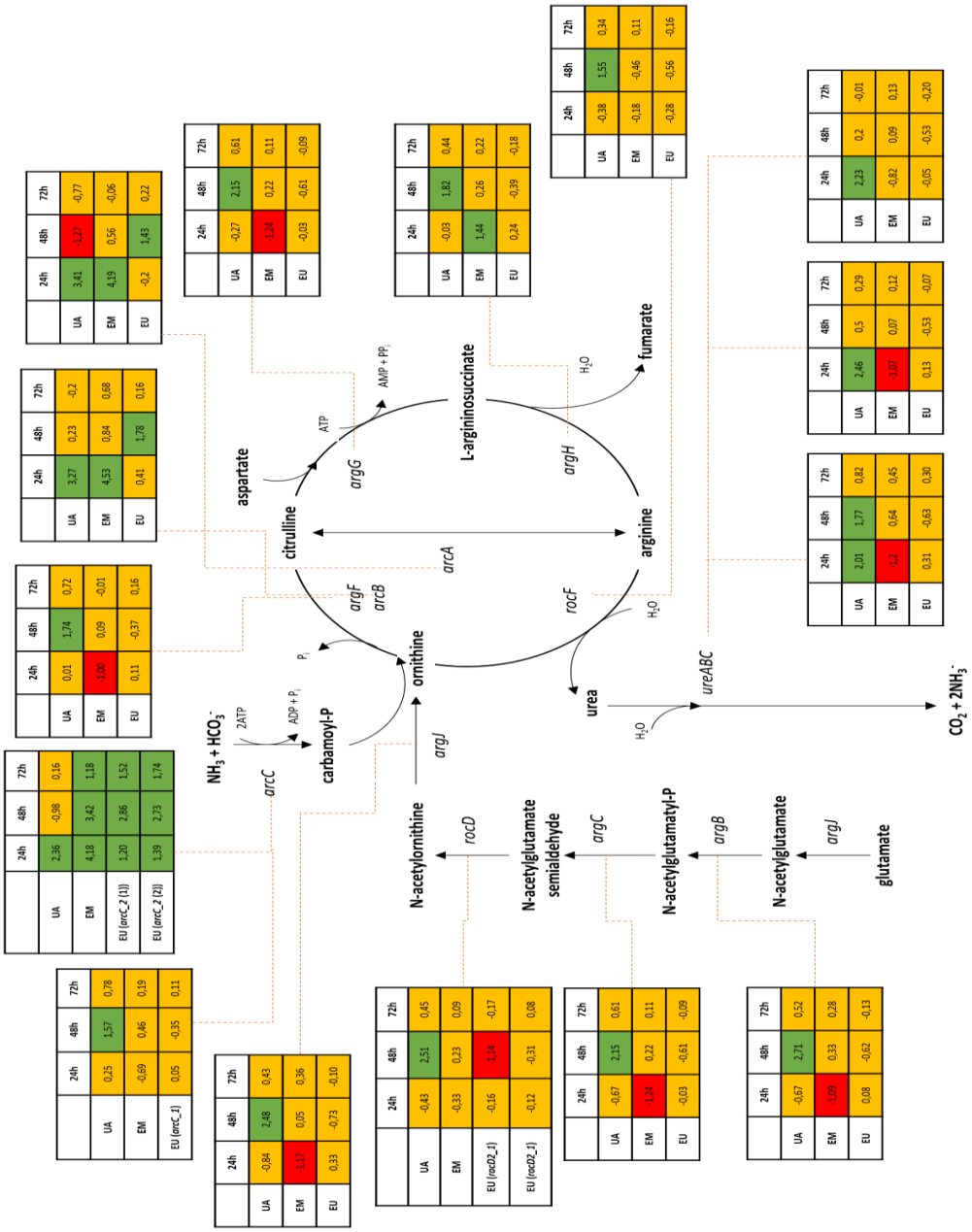

Figure 11: Log_2(fold change) of genes involved in arginine biosynthesis and the urea cycle under biofilm conditions for pandemic USA300, EMRSA-15 and ST239-SCC*mec*III MRSA clones. UAS391 (UA), H-EMRSA-15 (EM) and EU_ST239_16 (EU). Green boxes denote time points when the gene was significantly up-expressed ($|log_2$(fold- change)$|$>1), red boxes denote time points when the respective gene was significantly down-expressed ($|log_2$(fold- change)$|$>1) and yellow boxes indicate that there were no significant changes.

important role in the evolution of virulence of many pathogens by encoding numerous virulence or fitness factors [48]. In addition, phages are important vehicles for horizontal gene exchange between different bacterial species and account for a good share of the strain-to-strain differences within the same bacterial species [49]. The high amount of up-expressed phage genes strongly points at the crucial role of these mobile genetic elements (MGEs) in biofilm formation and hints at the competitive edge conferred by these MGEs to our highly successful MRSA clones.

Our results also identified many hypothetical proteins to be up-expressed during increased ageing of the biofilm in USA300, EMRSA-15 and ST239-SCC*mec*III. Some of these hypothetical proteins (e.g. EX97_07255, ER16_01245 and L_00729) were highly expressed at various times in biofilm cells and should therefore be characterized.

Cold-shock proteins and multiple stress factors under the regulatory control of the alternative sigma factor B (SigB, σ^B) were also highly up-expressed in our data. SigB is responsible for the transcription of genes that can confer resistance to heat, antibiotic and oxidative stresses [50]. This suggests that biofilm formation was strongly regulated by a variety of environmental and physiological cues [51].

3.1.1.5.2. Changes in metabolism of the biofilm

As such, our transcriptome data showed a change in expression of genes mainly associated with the central metabolic and fermentation pathways (**Fig. 8**), suggesting a shift to anaerobic conditions in the biofilm [23]. Under anaerobic conditions, some bacteria are able to generate ATP as an energy source through catabolism of arginine via the ADI pathway [8]. Indeed, our data show a strong up-expression of the *arcABDCR* operon in 24h old UAS391, 24h old H-EMRSA-15 and 48h old EU_ST239_16 biofilms, with a critical role for carbamate kinase *arcC_2*, which was up-expressed at all time points. Collectively, the *arc* genes convert arginine into ornithine, ammonia, and carbon dioxide, yielding 1 mol of ATP per mol of arginine. ArcC, in particular, transfers phosphate from carbamoylphosphate to ADP [8]. Carbamoylphosphate is also used in the pyrimidine biosynthetic pathway, which is encoded by the *carAB* and *pyrRPBC* and *pyrFE* genes. These genes were significantly up-expressed in our data, suggesting a crucial role for carbamoylphosphate in several pathways during fermentative growth. In addition, the ADI-pathway can also function as an ammonia-generating pathway, by the deiminiation of arginine, which is usually used by oral biofilm-forming bacteria such *Streptococcus salivarius* to maintain pH homeostasis [52]. However, Zhu et al. demonstrated that the ammonia generated by the ADI-pathway is insufficient to counteract the drop in pH due to the accumulation of organic acids [53]. As a second ammonia-producing pathway, urea cycle-associated genes (*ureABCEFGD*) were induced in USA300 biofilms. Interestingly, this was not the case for EMRSA-15 and ST239-SCC*mec*III. In all 3 clones,

especially H-EMRSA-15, the high-affinity K^+-specific transport system (*kdpABCDE*) was also up-expressed, apparently contributing to pH homeostasis by cation transport [54]. USA300 switched to nitrate and nitrite reduction to produce ammonia after 48h growth. This was also associated with an up-expression of the *argBCFGHJ* operon, while the *ureABCDEFG* genes showed no differential expression compared to planktonic cells anymore. In terms of energetics, nitrate respiration has been suggested to be a more favorable pathway for NADH recycling than fermentation [55].

3.1.1.5.3. Effect of the ACME-element on the biofilm

These results suggest that EMRSA-15 and ST239-SCC*mec*III biofilms are likely not as anoxic as USA300 biofilms, and ammonia generation through the ADI-pathway suffices for these strains to buffer the growth environment, or that EMRSA-15 and ST239-SCC*mec*III biofilms mature more slowly, in concordance with their observed slower growth rate than USA300. Vanhommerig et al. already postulated that the 34-kb genomic ACME island probably underlies the higher propensity of USA300 to form biofilms [12]. Furthermore, Diep and colleagues have shown that deletion of the entire ACME I element decreased virulence and fitness in a rabbit bacteremia model [17]. Interestingly, this element carries an additional ADI gene cluster [25]. However, only *arcD* and *argR* were significantly up-expressed under biofilm conditions and knockout mutation of these genes did not result in any biofilm deficiency. Inactivation of the oligopeptide ABC superfamily ATP binding cassette transporter, ABC protein (*opp-3D)*, however, did result in decreased biofilm formation and the *opp-3* genes, encoding an oligopeptide permease system, were also up-expressed. Oligopeptide permease transporters play a key role in bacterial nutrition, signaling and virulence, and the Opp-3 system has been identified as being the only system able to provide oligopeptides for growth [56]. Here, *opp-3D* provides energy for peptide transport [56]. Further work is required to ascertain the mechanisms underlying the role of *opp-3*. Interestingly, we did not observe an effect of *speG* (polyamine-resistance enzyme)-inactivation on biofilm forming capacity despite previous reports [57]. This could be explained by the fact the function of SpeG lies in combatting excess host polyamines and adherence to fibrinogen/fibronectin, which are factors not addressed in the static microtiter biofilm assay.

Additionally, the linked *SCCmec* element seems to have a synergistic effect together with ACME on biofilm formation by USA300, since excision of each element alone did not significantly influence the amount of biomass formed and joined excision did. This warrants more extensive research, since we noted the down-expression of both *pbp2* and *mecI* in our biofilm cells. As such, this demonstrates that, in addition to up-expression of certain virulence-associated genes, either oxygen availability or the role of

ADI in acid resistance indeed have an important influence on not only physiology, but also on virulence factor production and methicillin resistance, as suggested by [9, 23].

3.1.1.6. Addendum

3.1.1.6.1. Acknowledgements

We thank the Network on Antimicrobial Resistance in *Staphylococcus aureus* (NARSA) Program for providing *bursa aurealis* transposon mutants and other *S. aureus* strains. BBX was supported by the University of Antwerp Research funds (BOF-DOCPRO 2012-27450). SDB is supported by funding from Research Foundation Flanders (FWO, applicant number 1128818N). The described research is part of IWT-SBO project (#140746) and FWO research project (#GOD3516N).

3.1.1.6.2. Contribution to authorship

In detail, quantification of biofilm mass and growth, biofilm and planktonic sample collection, RNA isolation, RT-qPCR validation, excision of ACME and/orSCCmec and identification of differentially expressed genes and statistical analysis were performed by SDB.

3.1.1.6.3. Supplementary figures

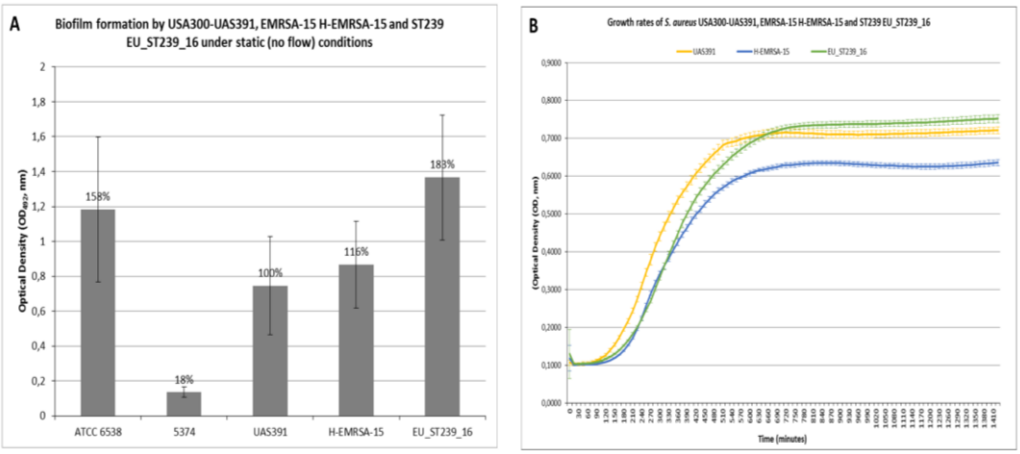

Supplementary figure 1: Phenotypic characterization of pandemic USA300, EMRSA-15, and ST239-SCC*mec*III MRSA clones. **(A)** Formation of biofilms by UAS391, H-EMRSA-15, and EU_ST239_16 under static conditions. The total biomass was determined by crystal violet staining *in triplicate*. Error bars represent 95% confidence intervals; **(B)** Background absorption-corrected 24h growth curves for UAS391, H-EMRSA-15 and EU_ST239_16. Error bars in corresponding colour represent the 95% confidence interval per strain.

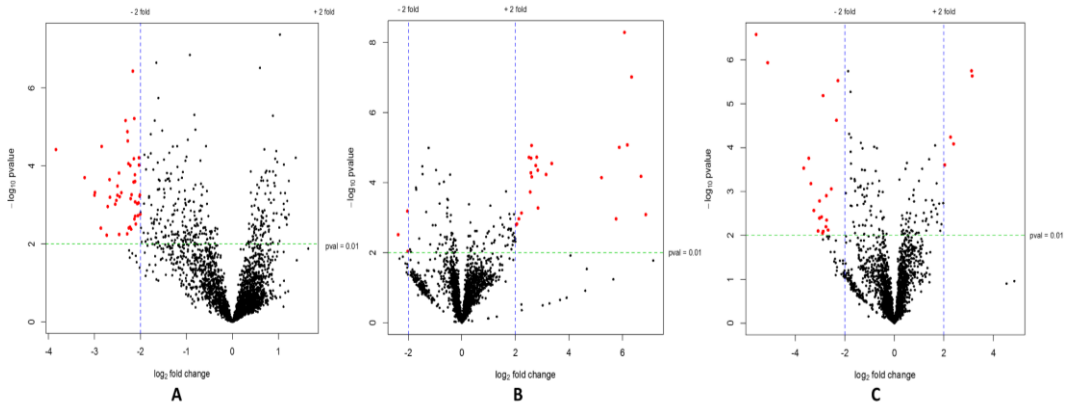

Supplementary figure 2: Volcano plot of pandemic USA300, EMRSA-15, and ST239-SCC*mec*III MRSA clones RNA-seq data. UAS391 (**A**), H-EMRSA-15 (**B**) and EU_ST239_16 (**C**). The $\log_2$ (FC) fold-change is plotted on the X-axis, and the negative $\log_{10}$ (FDR) (p-value) is plotted on the Y-axis. The black points show no differential gene expression with the absolute value of $\log_2$ (FC) less than 1 (FC = 2) and FDR no less than 0.05. The red points show differentially expressed genes with the absolute value of $\log_2$ (FC) no less than 1 (FC = 2) and FDR less than 0.05.

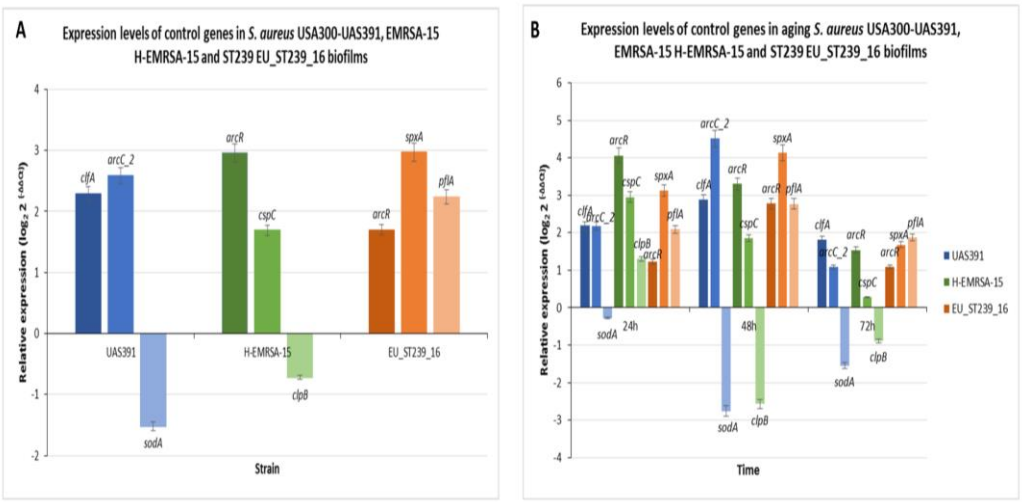

Supplementary figure 3: Quantification of relative gene expression in pandemic USA300, EMRSA-15, and ST239-SCC*mec*III MRSA clones. *ClfA* (clumping factor A), *arcC_2*, and *sodA* (superoxide dismutase (Mn/Fe family)), *arcR*, *cspC* (cold shock protein), and *clpB* (chaperone clpB), *arcR*, *spxA* (regulatory protein Spx), and *pflA* (pyruvate formate-lyase activating enzyme) relative gene expression in UAS391, H-EMRSA-15 and EU_ST239_16, respectively. **(A)** Average relative gene expression in planktonic cells of UAS391, H-EMRSA-15, and EU_ST239 was taken as baseline 0; **(B)** Relative gene expression in 24h, 48h and 72h planktonic cells UAS391, H-EMRSA-15, and EU_ST239 were taken as baseline 0.

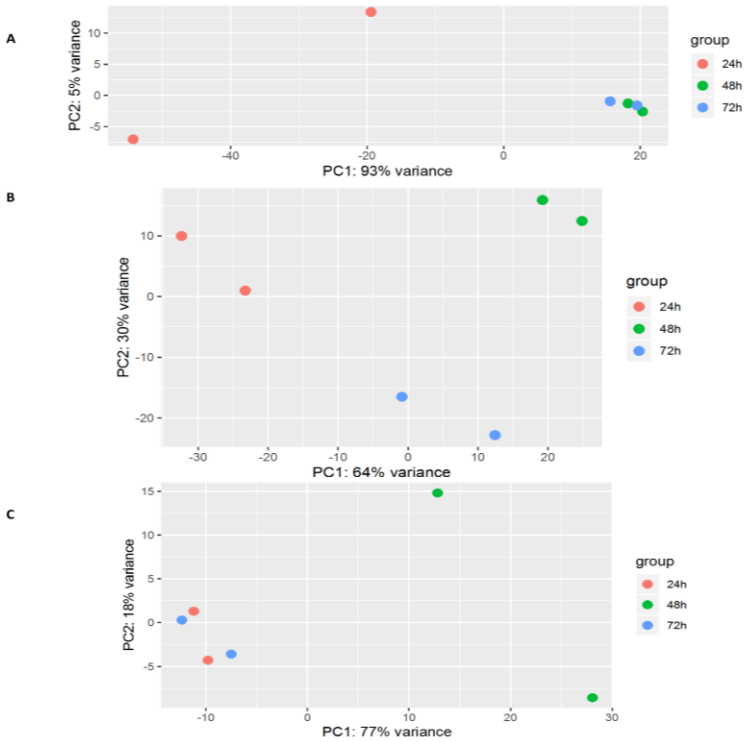

Supplementary figure 4: PCA plot of pandemic USA300, EMRSA-15 and ST239-SCC*mec*III MRSA clones. UAS391 (**A**), H-EMRSA-15 (**B**) and EU_ST239_16 (**C**) 24h, 48h and 72h biofilm RNA-seq data. Each dot indicates a sample.

3.1.1.6.3. Supplementary tables

Supplementary table 1: Gene-specific primers used for RT-PCR validation of RNA-Seq results. GyrB-primers were developed by Sihto et al. [57], while all other primers were developed in-house.

Gene	Forward primer	Sequence (5' 3')	Reverse primer	Sequence (5' 3')	Amplicon size (bp)
gyrB	GyrB-F	GTAACACGTCGTAAATCAGCG	GyrB-R	CGTAATGGTAAAATCGCCTGC	170
arcR	MOarcR-F	TTTTCGCCACAAGAAAGTAGCA	MOarcR-R	ACAATCGGTTAATGCTGTGC	180
	EMarcR-F	TTTCGCCACAAGAAAGTAGCA	EMarcR-R	AGGCCATCAATTCTCTAGGCA	213
spxA	MOspxA-F	TGAGGACGAGATTCGACGTTT	MOspxA-R	GTCAACCATACGTTGTGCTTCT	76
pflA	MOpflA-F	CCATGTCCTTGTGCCTGGTT	MOpflA-R	GGGCGCTTCGACATCTTCT	175
clfA	UAclfA-F	TGGCTTCAGTGCTTGTAGGT	UAclfA-R	TTTTGCGCCACACTCGTTTC	223
arcC	UAarcC-F	GTGGTGGCGGTATTCCAGTT	UAarcC-R	AACTTACCTTGTGCCGCGTA	229
sodA	UAsodA-F	GGTTCAGGTTGGGCTTGGTT	UAsodA-R	CCAATGTAGTCAGGGCGTTTG	167
cspC	EMcspC-F	CATCGAAAGAGAAGATGGTAGCG	EMcspC-R	CGATTGCTGAGAAGTGTACGA	50
clpB	EMclpB-F	GCAGCACTTCAATCTCGTGT	EMclpB-R	GTGCATCTTCCAACGCTTGT	103

Supplementary table 2: Expression of 7 housekeeping genes ($\log_2$ (fold-change)) under aging biofilm growth of pandemic USA300, EMRSA-15 and ST239-SCC*mec*III MRSA clones. *ArcC*_1: carbamate kinase; *aroE*:

shikimate 5-dehydrogenase; *glpF*: glycerol uptake facilitator; *gmk*: guanylate kinase; *ptoA*: phosphotransferase system, N-acetylglucosamine-specific IIBC component; *tpiA*: triosephosphate isomerase; *eutD*: phosphotransacetylase, respectively.

	UAS391			H-EMRSA-15			EU_ST239_16		
Gene	**24h**	**48h**	**72h**	**24h**	**48h**	**72h**	**24h**	**48h**	**72h**
arcC_1	0.02	1.14	0.39	-0.69	0.46	0.19	0.05	-0.35	0.11
aroE	-0.64	1.54	0.20	-0.07	0.12	0.21	-0.24	-0.35	-0.16
glpF	-0.29	1.62	0.31	1.39	0.38	0.24	0.58	-0.08	0.04
gmk	-0.86	0.55	0.06	-0.01	0.01	0.24	0.58	-0.08	0.04
ptaA	-0.58	-1.61	-0.29	-0.43	-0.21	0.11	0.23	1.05	0.07
tpiA	-0.90	-3.0	-1.79	0.13	-0.83	-0.69	0.13	1.33	0.08
eutD	0.06	2.33	0.55	-5.24	0.22	-0.30	-0.18	-0.54	-0.46

Supplementary Table 3: Differentially expressed genes ($\log_2$ (fold-change)) of urea cycle, arginine biosynthesis, pyrimidine biosynthesis, nitrite/nitrate respiration and cation transport as well as ACME-element associated genes (only in USA300) under ageing biofilm growth of pandemic USA300, EMRSA-15 and ST239-SCC*mec*III MRSA clones.

	UAS391			H-EMRSA-15			EU_ST239_16		
Gene	**24h**	**48h**	**72h**	**24h**	**48h**	**72h**	**24h**	**48h**	**72h**
ADI-pathway									
arcA	3.41	-1.27	-0.77	4.19	0.56	-0.06	-0.2	1.43	0.22
arcB	3.27	0.23	-0.2	4.53	0.84	0.68	0.41	1.78	0.16
arcC_1	0.25	1.57	0.78	-0.69	0.46	0.19	0.05	-0.35	0.11
arcC_2 (1)	2.36	-0.98	0.16	4.18	3.42	1.18	1.20	2.86	1.52
arcC_2 (2)							1.39	2.73	1.74
arcD	2.78	-0.14	0.31	4.22	1.21	1.51	0.44	2.27	0.63
arcR	2.33	-0.4	0.03	-0.74	-0.32	0.01	1.60	2.72	1.02
Urea cycle									
argB	-0.67	2.71	0.52	-1.09	0.33	0.28	0.08	-0.62	-0.13
argC	-0.67	2.15	0.61	-1.24	0.22	0.11	-0.03	-0.61	-0.09
argF	0.01	1.74	0.72	-1.00	0.09	-0.01	0.11	-0.37	0.16
argG	-0.27	2.17	0.35	0.86	0.21	-0.05	-0.32	-0.56	-0.33
argH	-0.03	1.82	0.44	1.44	0.26	0.22	0.24	-0.39	-0.18
argJ	-0.84	2.48	0.43	-1.17	0.05	0.36	0.33	-0.73	-0.10
rocD2_1							-0.16	-1.14	-0.17
rocD2_2	-0.43	2.51	0.45	-0.33	0.23	0.09	-0.12	-0.31	0.08
rocF	-0.38	1.55	0.34	-0.18	-0.46	0.11	-0.28	-0.56	-0.16
ureA	2.01	1.77	0.82	-1.2	0.64	0.45	0.31	-0.63	0.30
ureB	2.46	0.5	0.29	-1.07	0.07	0.12	0.13	-0.53	-0.07
ureC	2.23	0.2	-0.01	-0.82	0.09	0.13	-0.05	-0.53	-0.20
ureD	2.29	-0.15	-0.16	-0.31	-0.06	0.1	0.47	-0.85	-0.41
ureE	2.32	0.36	0.14	-0.34	-0.19	-0.15	-0.93	-0.25	0.03
ureF	2.31	-0.05	0.13	-0.38	0.28	0.39	0.26	-0.57	-0.07
ureG	2.05	-0.18	0.01	-0.22	0.31	-0.07	0.06	-0.24	0.23
Nitrate reductase									
narG	-1.60	2.12	0.52	-1.26	0.24	0.38	0.08	-0.04	-0.13
narH	-1.28	1.87	0.38	-0.75	0.26	0.12	0.05	0.08	0.01
narJ	-0.95	2.88	0.33	-0.29	0.92	-0.10	-0.01	-0.29	-0.18
narI	-0.91	1.77	0.45	-0.27	-0.19	-0.10	-0.01	-0.04	0.21
Nitrite reductase									
nirB	-0.84	1.86	0.36	-0.95	0.23	0.17	-0.03	-0.21	-0.20
nirD	-0.47	2.01	-0.15	-0.82	-0.23	0.18	-0.75	-1.81	-0.45
nirR	-0.95	1.86	0.38	-0.88	0.50	0.08	0.29	0.85	0.09
pyrimidine nucleotide biosynthesis pathway									

carA	0.35	1.46	0.54	-0.58	0.1	0.23	0.33	0.04	0.11
carB	0.21	1.52	0.45	-0.39	0.13	0.13	0.04	0.21	0.02
pyrB	0.7	1.83	0.32	-0.71	-0.03	0.09	-0.04	-0.20	-0.28
pyrC	0.6	1.52	0.14	-0.66	0.3	0.12	0.14	-0.19	-0.30
pyrE	0.16	1.36	0.4	-0.31	-0.51	-0.34	-0.06	0.13	-0.13
pyrF	0.21	1.39	0.39	-0.11	-1.02	-0.09	-0.26	0.60	0.05
pyrP	0.4	1.64	0.23	-1.51	0.05	0.15	-0.18	-0.22	-0.19
pyrR	1.74	-0.47	0.01	-1.03	-0.02	0.54	0.03	0.58	0.25
high-affinity K^+-specific transport system									
kdpA	2.31	1.37	0.22	3.27	-0.53	0.08	-0.06	0.08	-0.14
kdpB	2.17	0.66	-0.09	3.72	0.28	-0.4	-0.08	-0.14	-0.08
kdpC	2.13	-0.15	-0.36	3.46	-1.43	-0.26	0.01	1.24	0.03
kdpD	-0.26	1.47	0.12	1.29	0.02	0.06	0.07	-0.43	-0.20
kdpE	0.48	1.02	0.37	2.02	-0.05	0.01	0.17	-0.16	-0.16
ACME-element									
speG	-0.28	1.07	-0.29						
arcA	-0.11	0.76	0.55						
arcB	0.1	0.72	0.52						
arcC	-0.06	0.54	0.87						
arcD	0.25	1.5	0.2						
argR	-0.71	1.06	-0.10						
SAUSA300_0063	0.06	1.61	-0.03						
opp-3A	-1.02	2.12	0.36						
opp-3B	-1.31	1.9	0.41						
opp-3C	-1.12	2.16	0.28						
opp-3D	-1.07	2.07	0.29						
opp-3E	-0.83	2.49	0.38						
copA	-1.24	1.68	0.11						

Supplementary Table 4: Top differentially expressed genes with |fold-change>3| and FDR p-value correction<0.001 in biofilms of USA300 UAS391.

Feature ID	Gene name	Fold Change (normalized values)
EX97_09570	Chaperone protein DnaJ	-17,93
EX97_04250	Peptidase	-6,86
EX97_04255	Universal stress protein	-5,76
EX97_10030	Capsular polysaccharide biosynthesis protein Cap5A	-5,36
EX97_10130	Capsular polysaccharide biosynthesis protein Cap5B	-5,25
EX97_01160	Capsular polysaccharide biosynthesis protein Cap5C	-5,16
EX97_10135	Polysaccharide biosynthesis protein EpsC; disrupted	-5,11
EX97_13300	Capsular polysaccharide biosynthesis protein Cap5F	-5,04
EX97_10125	Capsular polysaccharide biosynthesis protein Cap5G	-4,94
EX97_10405	Capsular polysaccharide biosynthesis protein Cap5H	-4,77
EX97_12400	Capsular polysaccharide biosynthesis protein Cap5I	-4,76
EX97_10095	Glycosyl transferase family 1	-4,75
EX97_10115	Capsular polysaccharide biosynthesis protein Cap5M	-4,26
EX97_10060	UDP-glucose 4-epimerase	-4,24
EX97_10110	Hypothetical protein	-4,1
EX97_09475	Hypothetical protein	-4,05
EX97_10155	Hypothetical protein	-3,85
EX97_13170	Hypothetical protein	-3,84
groEL	5'-nucleotidase	-3,82
EX97_02700	Putative membrane protein	-3,74
EX97_11575	Xanthine phosphoribosyltransferase	-3,63
EX97_10120	Superantigen-like protein	-3,54
EX97_04265	Veg protein	-3,53

EX97_10040	tRNA-Val	-3,46
EX97_01585	50S ribosomal protein L11	-3,37
EX97_11580	Transcriptional regulator	-3,32
EX97_10280	Hypothetical protein	-3,31
EX97_11540	Hypothetical protein	-3,27
EX97_11545	Clumping factor A	-3,27
EX97_11570	Cold shock protein	-3,25
EX97_10295	Putative transcriptional regulator	-3,23
dnaK	Pathogenicity island protein	-3,22
EX97_02100	Hypothetical protein	-3,19
EX97_10105	CsbD-like superfamily	-3,19
EX97_01990	Chaperone clpB	-3,11
EX97_11535	Transcriptional regulator Spx	-3,08
EX97_11550	Cysteine protease	-3,05
EX97_11565	Cysteine protease	-3,01
rplB	V8 protease	-2,92
EX97_09300	Phosphoribosyl transferase	-2,9
EX97_04630	CSD family cold shock protein	-2,89
EX97_02545	Hypothetical protein	-2,85
EX97_09515	Hypothetical protein	-2,85
EX97_09530	tRNA-Gly	-2,57
EX97_09545	tRNA-Asp	-2,48
EX97_09305	tRNA-Met	-1,85
EX97_09285	tRNA-Gly	-1,51
EX97_10430	tRNA-Asp	2,7
EX97_04740	tRNA-Asp	2,78
EX97_01565	tRNA-Met	2,96
EX97_08795	tRNA-Gly	3,04
EX97_11005	Chemotaxis-inhibiting protein CHIPS	3,1
ureA	Staphylokinase	3,1
EX97_00360	PhiPVL ORF17-like protein	3,16
EX97_13130	Hypothetical protein	3,16
EX97_00160	Phi77 ORF-020-like protein, phage major tail protein	3,19
EX97_00860	Hypothetical protein	3,21
EX97_13135	Phi77 ORF029-like protein	3,28
EX97_04080	Hypothetical protein	3,3
EX97_00855	Phage head-tail adapter protein	3,32
EX97_06815	Phi77 ORF045-like protein	3,34
EX97_03525	Phi77 IRF006-like protein capsid protein	3,36
EX97_00850	Hypothetical protein	3,38
ureE	Hypothetical protein	3,41
EX97_13485	Phi77 ORF0104-like protein, phage anti-repressor protein	3,42
EX97_11765	Co-chaperonin GroES	3,45
EX97_00820	Delta-hemolysin	3,54
EX97_11780	Potassium-transporting ATPase subunit C	3,56
EX97_03150	Potassium-transporting ATPase subunit B	3,58
EX97_13465	Potassium-transporting ATPase subunit A	3,62
EX97_00830	Oxidoreductase	3,65
EX97_05745	Alkaline shock protein 23	3,66
EX97_00810	Membrane protein	3,7
EX97_12830	Hypothetical protein	3,77
EX97_00825	Hypothetical protein	3,78
EX97_11250	50S ribosomal protein L29	3,88
EX97_11775	50S ribosomal protein L16	3,9
EX97_04065	30S ribosomal protein S3	3,91
EX97_00835	50S ribosomal protein L22	3,96
EX97_11245	50S ribosomal protein L23	3,97

EX97_11355	50S ribosomal protein L4	4,1
EX97_11785	50S ribosomal protein L3	4,14
EX97_10670	30S ribosomal protein S10	4,17
ureB	Putative urea transporter	4,24
EX97_10665	Urease subunit alpha	4,35
EX97_04310	Urease accessory protein UreF	4,46
EX97_00800	Urease accessory protein UreG	4,73
EX97_11750	Urease accessory protein UreD	4,75
EX97_08800	IgG-binding protein SBI	4,79
EX97_01570	MerR family transcriptional regulator	4,85
EX97_10675	Hypothetical protein	5,02
EX97_01925	Hypothetical protein	5,32
EX97_12835	Secretory antigen precursor SsaA	5,37
EX97_11240	Hypothetical protein	5,41
EX97_00805	L-lactate dehydrogenase	5,56
EX97_01440	Ornithine carbamoyltransferase	5,71
EX97_00795	Immunodominant antigen B	5,95
EX97_02420	Cold shock protein	8,16
EX97_13820	Chaperonin GroEL	14,47
EX97_04995	50S ribosomal protein L2	14,51
EX97_05000	Urease subunit gamma	16,32
EX97_04105	Urease subunit beta	16,53
EX97_05005	Urease accessory protein UreE	19,18

Supplementary Table 5: Top differentially expressed genes with |fold-change>3| and FDR p-value correction<0.001 in biofilms of EMRSA-15 H-EMRSA-15.

Feature ID	Gene name	Fold Change (normalized values)
ER16_07055	Peptidase	-52,65
ER16_07050	Immunoglobulin G binding protein A precursor (protein A)	-40,47
ER16_07155	Transposase	-29,56
ER16_07180	Capsular polysaccharide synthesis enzyme CapA	-28,9
ER16_07120	Capsular polysaccharide synthesis enzyme CapB	-24,71
ER16_07170	Capsular polysaccharide synthesis enzyme CapC	-23,37
ER16_07130	Capsular polysaccharide synthesis enzyme CapF	-22,85
ER16_07160	Capsular polysaccharide synthesis enzyme CapG	-21,69
ER16_07165	Capsular polysaccharide synthesis enzyme O-acetyl transferase CapH	-20,83
ER16_07140	Capsular polysaccharide biosynthesis protein glycosyltransferase CapL	-19,27
ER16_07150	Capsular polysaccharide biosynthesis protein capM	-18,7
ER16_07135	Capsular polysaccharide biosynthesis protein CapN	-18,11
ER16_07175	Capsular polysaccharide biosynthesis protein CapO	-14,24
ER16_07145	Capsular polysaccharide biosynthesis protein CapP	-12,67
ER16_07065	Membrane protein	-11,37
ER16_09960	Complement inhibitor	-11,36
ER16_07100	PTS glucose transporter subunit IIB	-11,15
ER16_07085	Peptidoglycan hydrolase	-10,98
ER16_09950	5'-nucleotidase	-10,77
ER16_07105	MarR family regulatory protein	-10,35
ER16_07370	Hypothetical protein	-10,19
ER16_02370	Toxin	-10
ER16_09955	Membrane protein	-9,46
ER16_07095	Beta-lactamase	-9,43
ER16_09925	Hypothetical protein	-9,39

ER16_07080	Hypothetical protein	-9,21
ER16_09890	Hypothetical protein	-9,16
ER16_09860	Signal peptide protein	-9,04
ER16_07115	5S ribosomal RNA	-8,86
ER16_02365	Hypothetical protein	-8,77
ER16_09935	5S ribosomal RNA	-8,64
ER16_07090	tRNA-Val	-7,95
ER16_00975	tRNA-Thr	-7,91
ER16_07075	23S ribosomal RNA	-7,9
ER16_07350	5S ribosomal RNA	-7,72
ER16_09945	23S ribosomal RNA	-7,53
ER16_00585	Amino acid permease	-7,48
ER16_09940	Accessory regulator A	-7,46
ER16_09915	Secretory antigen SsaA-like protein	-7,41
ER16_09880	MarR family regulatory protein	-7,38
ER16_09980	Hypothetical protein	-7,25
ER16_09965	Putative exported protein	-7,08
ER16_04525	Fructose operon transcriptional regulator	-6,98
ER16_07345	Fructose 1-phosphate kinase	-6,79
ER16_09870	Fructose specific permease	-6,78
ER16_09930	tRNA-Arg	-6,62
ER16_01640	Hypothetical protein	-6,55
ER16_09895	Clumping factor A	-6,37
ER16_09990	Hypothetical protein	-6,34
ER16_09875	Cold-shock protein CSD family protein	-6,25
ER16_10455	Hypothetical protein	-6,06
ER16_09975	D-alanine transfer protein DltB	-5,96
ER16_10170	Alanine-phosphoribitol ligase	-5,75
ER16_01670	D-alanyl-lipoteichoic acid biosynthesis protein	-5,72
ER16_09970	Ideal family protein	-5,55
ER16_09910	Integrase; disrupted	-5,46
ER16_10165	Bifunctional autolysin precursor	-5,42
ER16_09905	Hypothetical protein	-5,34
ER16_10135	Formyl peptide receptor-like 1 inhibitory protein	-5,33
ER16_02430	Integrase	-4,98
ER16_02415	tRNA-Arg	-4,89
ER16_13235	Hypothetical protein	-4,89
ER16_06325	50S ribosomal protein L28	-4,82
ER16_01910	ATP-dependent protease	-4,81
ER16_07305	Hypothetical protein	-4,77
ER16_07295	DNA repair protein	-4,75
ER16_00415	Major cold-shock protein CspA	-4,69
ER16_12285	Hypothetical protein	-4,66
ER16_07330	Riboflavin transporter RibU	-4,6
ER16_10150	Bcgl-like restriction enzyme subunit alpha	-4,52
ER16_10215	Phage membrane protein	-4,49
ER16_07280	Phage amidase	-4,4
ER16_09995	Holin	-4,4
ER16_03810	PhiSLT ORF99-like protein	-4,19
ER16_07320	SLT ORF129-like protein	-4,17
ER16_07225	SLT ORF488-like protein	-4,15
ER16_07325	SLT ORF636-like protein	-4,09
ER16_12190	Hypothetical protein	-4,01
ER16_07310	Peptidase	-3,95
ER16_10095	Phage tail family protein	-3,94
ER16_07285	Phage tail family protein	-3,93
ER16_09390	PhiSLT ORF116b-like protein	-3,9

ER16_10010	Tail protein	-3,87
ER16_07005	Tail protein	-3,8
ER16_01845	Phage protein	-3,73
ER16_07290	SLT ORF123-like protein	-3,71
ER16_07040	SLT ORF110-like protein	-3,7
ER16_11010	Phage gp6-like head-tail connector protein	-3,65
ER16_10145	Phage major capsid protein	-3,62
ER16_07315	ATP-dependent Clp protease ClpP	-3,61
ER16_06980	Phage portal protein	-3,59
ER16_10100	Terminase	-3,59
ER16_07710	Terminase	-3,54
ER16_07275	HNH endonuclease	-3,44
ER16_10105	Transcriptional regulator	-3,41
ER16_11000	Nuclease	-3,41
ER16_10450	Hypothetical protein	-3,36
ER16_10015	Transcriptional regulator	-3,32
ER16_10110	Hypothetical protein	-3,23
ER16_01955	Hypothetical protein	-3,22
ER16_09850	Hypothetical protein	-3,22
ER16_10210	dUTP pyrophosphatase	-3,22
ER16_07230	Hypothetical protein	-3,18
ER16_07475	Phage hypothetical protein	-3,16
ER16_12115	Hypothetical protein	-3,16
ER16_03175	DNA polymerase	-3,14
ER16_08875	Phage hypothetical protein	-3,12
ER16_07240	Hypothetical protein	-3,1
ER16_10270	Hypothetical protein	-3,01
ER16_07470	TrmB family transcriptional regulator	-2,96
ER16_07480	Hypothetical protein	-2,96
ER16_07335	Hypothetical phage protein	-2,9
ER16_07220	Hypothetical phage protein	-2,89
ER16_10065	Hypothetical phage protein	-2,89
ER16_09865	Hypothetical protein	-2,88
ER16_01950	Hypothetical phage protein	-2,86
ER16_12040	Uracil-DNA glycosylase	-2,83
ER16_07595	Hypothetical phage protein	-2,8
ER16_01920	DNA-binding protein	-2,79
ER16_05160	Phage membrane protein	-2,78
ER16_01045	Ribonuclease Z	-2,75
ER16_10025	Glucose-6-phosphate dehydrogenase	-2,75
ER16_01485	AraC family transcriptional regulator	-2,74
ER16_10060	Peptidase M24	-2,73
ER16_10000	Superoxide dismutase	-2,69
ER16_10125	Putative membrane protein	-2,68
ER16_00830	Hypothetical protein	-2,61
ER16_01355	Mannosyl-glycoprotein endo-beta-N-acetylglucosamide	-2,59
ER16_10120	S-adenosylmethionine synthetase	-2,59
ER16_07185	Hypothetical protein	-2,5
ER16_10090	Cro/CI family transcriptional regulator	-2,47
ER16_12195	tRNA-Ser	-2,45
ER16_07200	tRNA-Arg	-2,44
ER16_10070	tRNA-Ala	-2,39
ER16_07235	phospholipase	-2,33
ER16_10085	Chemotaxis-inhibiting protein CHIPS	-2,32
ER16_07245	Peptidoglycan hydrolase	-2,29
ER16_07270	Staphylokinase precursor	-2,28
ER16_10020	Phage amidase	-2,28

ER16_07250	Holin	-2,2
ER16_10005	PhiPVL ORF17-like protein	-2,17
ER16_07215	Hypothetical phage protein	-2,05
ER16_09330	Phage minor structural protein	1,78
ER16_03690	Phage tail fiber protein	2,06
ER16_02170	Phage tail tape measure protein	2,41
ER16_02420	Hypothetical phage protein	2,42
ER16_02360	Phage major tail protein	2,45
ER16_00165	Hypothetical phage protein	2,81
ER16_10295	Hypothetical phage protein	2,84
ER16_05525	Phage head-tail adapter protein	2,97
ER16_03710	Hypothetical phage protein	3,03
ER16_04680	Phi77 ORF045-like protein	3,06
ER16_05675	Phi77 ORF006-like protein capsid protein	3,2
ER16_02765	Phi77 ORF0105-like protein protease	3,28
ER16_00630	Phage portal protein	3,34
ER16_03795	Hypothetical phage protein	3,47
ER16_09175	Hypothetical phage protein	3,47
ER16_05345	HNH endonuclease	3,53
ER16_08590	Phage protein	3,69
ER16_00675	Hypothetical protein	3,74
ER16_10485	Transcriptional activator RinB	3,76
ER16_00680	Hypothetical phage protein	3,89
ER16_04045	Hypothetical protein	3,98
ER16_01690	Hypothetical protein	4,06
ER16_10900	dUTP pyrophosphatase	4,06
ER16_00640	Hypothetical protein	4,16
ER16_10565	Hypothetical protein	4,28
ER16_11225	Hypothetical protein	4,3
ER16_05855	Holliday junction resolvase	4,32
ER16_07045	Hypothetical protein	4,38
ER16_04055	Replication protein DnaD	4,39
ER16_08910	Phage single-strand DNA-binding protein	4,4
ER16_00605	MBL fold metallo-hydrolase	4,5
ER16_00635	Hypothetical protein	4,59
ER16_00670	Hypothetical protein	4,65
ER16_03240	Phi PVL ORF39-like protein	4,73
ER16_11235	Phage protein	4,73
ER16_05265	Hypothetical phage protein	4,75
ER16_00660	Phage anti repressor	4,77
ER16_03340	Hypothetical phage protein	4,94
ER16_10540	Phage DNA-binding protein	5,07
ER16_11095	Phosphodiesterase	5,07
ER16_11835	Gamma-hemolysin subunit B	5,1
ER16_00610	Molecular chaperone GroES	5,26
ER16_03350	Delta-hemolysin	5,36
ER16_10550	5S ribosomal RNA	5,36
ER16_12730	23S ribosomal RNA	5,42
ER16_11105	RNA polymerase sigma factor SigB	5,53
ER16_04050	Serine-protein kinase RsbW	5,54
ER16_08585	Potassium-transporting ATPase subunit C	5,56
ER16_02930	Potassium-transporting ATPase subunit B	5,67
ER16_11650	Potassium-transporting ATPase subunit A	5,72
ER16_10490	PhoB family transcriptional regulator	5,73
ER16_03345	Transglycosylase SceD	5,92
ER16_08795	Lytic regulatory protein	5,96
ER16_11100	tRNA-Val	6,39

ER16_10545	5S ribosomal RNA	6,46
ER16_03940	16S ribosomal RNA	6,75
ER16_08075	Alkaline shock protein 23	6,88
ER16_00615	Putative membrane protein	6,9
ER16_06610	Putative membrane protein	6,91
ER16_00665	Truncated MHC class II analog protein	7,17
ER16_02240	Acetolactate synthase	7,56
ER16_13395	Secretory antigen precursor SsaA	7,72
ER16_13045	Staphyloxanthin biosynthesis protein	8,25
ER16_04665	Putative membrane protein	8,27
ER16_03160	Membrane protein	8,49
ER16_13405	Nitrate transporter NarT	8,49
ER16_01215	Formate/nitrite transporter	10,3
ER16_13060	Putative membrane protein	10,4
ER16_13390	Gamma-hemolysin subunit B	10,62
ER16_13385	Hypothetical protein	11,35
ER16_12935	Secretory antigen SsaA-like protein	12,26
ER16_13400	Secretory antigen precursor SsaA-like protein	12,45
ER16_03820	Immunodominant antigen A	12,66
ER16_03330	Transposase	14,58
ER16_10640	Lactate dehydrogenase	19,43
ER16_13715	Transcriptional regulator	28,8
ER16_11670	Carbamate kinase	32,48
ER16_10985	Arginine/ornithine antiporter	42,84
ER16_13230	Ornithine carbamoyltransferase	79,4

Supplementary Table 6: Top differentially expressed genes with |fold-change>3| and FDR p-value correction<0.001 in biofilms of ST239-*SCCmecIII*.

Feature ID	Gene name	Fold Change (normalized values)
L_02799	tRNA Thr anticodon TGT	-33,27
L_01436	tRNA Thr anticodon TGT	-25,14
L_02714	tRNA Ala anticodon TGT	-3,69
L_02702	Bifunctional autolysin	-3,57
L_01850	PhiPVL ORF057-like protein, transcriptional activator RinB	-2,6
L_02492	Integrase/recombinase	-2,47
L_02781	TIGR01741 family protein	-2,42
L_00211	Hypothetical protein	-2,35
xerD_2	TIGR01741 family protein	-2,34
L_00213	Hypothetical protein	-2,34
L_01706	Hypothetical protein	-2,24
L_00205	Hypothetical protein	-2,21
L_01466	Universal stress protein A1	-2,21
L_00527	Transcriptional regulator	-2,08
L_02800	Carbamate kinase	-1,94
L_00697	Carbamate kinase	-1,9
L_02801	Hypothetical protein	-1,65
L_02787	tRNA Pro Anticodon TGG	-1,59
L_02025	Quinol oxidase subunit I	-1,34
L_00437	Branched-chain alpha-keto acid dehydrogenase subunit E2	-1,16
L_01710	3-methyl-2-oxobutanoate hydroxymethyltransferase	-1,05
L_00528	tRNA anticodon Asp GTC	-1,01
L_02797	Delta-hemolysin	1,19
L_02784	Complement inhibitor SCIN	2,73
arcR	Dihydrolipoamide dehydrogenase	3,41
L_01712	tRNA Phe anticodon GAA	3,42

arcC2_2	GlsB/Yea/YmgE family stress response membrane protein	3,53
pdhC_1	Elongation factor Tu	3,57
L_02806	tRNA Arg anticodon ACG	3,66
L_02807	Cytochrome C oxidase subunit III	3,73
qoxB	Quinol oxidase subunit IV	3,78
butA	ATP-dependent Clp protease ATP-binding subunit ClpC	3,96
pdhD	Cold-shock protein CspB	3,99
L_01594	Pyruvate formate-lyase-activating enzyme	4,06
clpL	tRNA His antidodon GTG	4,12
pflB	Cold-shock protein CspA	4,13
L_02048	Formate acetyltransferase	4,15
arcC2_1	Clumping factor A	4,21
tuf	tRNA Leu anticodon GAG	4,24
hld	Ideal domain family	4,45
scn_3	Hypothetical protein	4,47
clfA	Hypothetical protein	4,54
pflA	tRNA Arg anticodon ACG	4,83
L_00285	Hypothetical protein	5
qoxC	L-lactate dehydrogenase	5,02
L_01709	Hypothetical protein	5,04
qoxD	Alkaline shock protein 23	5,07
L_02024	DNA-binding protein HU	5,16
cspC	Replication initiation factor	5,2
cspA_2	tRNA Cys anticodon GCA	5,5
ldhA	DUF443 domain-containing protein	5,74
L_02798	Transcriptional regulator spx	5,82
L_00863	tRNA Val anticodon TAC	6,11
L_02430	CsbD family protein	6,13
L_02142	tRNA Thr anticodon TGT	6,23
L_00729	50S ribosomal protein L28	6,46
L_02490	tRNA Asn anticodon GTT	6,8
L_02140	tRNA Met anticodon CAT	6,87
L_02792	tRNA Gln anticodon TTG	7,03
hup	tRNA Met anticodon CAT	7,32
L_02803	tRNA Gly anticodon TCC	7,82
spxA	tRNA Gly anticodon TCC	8,59
L_02788	tRNA Gly anticodon TCC	8,94
L_01395	tRNA Gly anticodon GCC	8,98
L_00861	tRNA Arg anticodon CCG	9,15
L_00748	tRNA Asp anticodon GTC	10,01
L_00439	tRNA Ala anticodon TGC	10,41
L_02779	tRNA Trp anticodon CCA	10,76
rpmB	tRNA Arg anticodon TCT	11,74
L_01713	tRNA Met anticodon CAT	13,18
L_01862	Staphylococcus aureus paralogous family	17,35
L_00524	10Sa RNA (tmRNA)	17,46
L_01462	PhiPVL ORF050-like protein	21,63
L_01692	PhiPVL ORF41-like protein	28,74
ssrA	PhiPVL ORF057-like protein, transcriptional activator RinB	30,16
recT	Putative membrane protein	39,89
L_01873	DNA-directed RNA polymerase subunit beta	40,01
L_01857	Phage protein	52,16
L_01861	Type I restriction-modification system subunit S	55,6
L_00525	Hypothetical protein	79,56

3.1.1.6.4. References

1. Archer, N.K., et al., *Staphylococcus aureus biofilms: properties, regulation, and roles in human disease.* Virulence, 2011. **2**(5): p. 445-59.
2. Dunman, P.M., et al., *Transcription profiling-based identification of Staphylococcus aureus genes regulated by the agr and/or sarA loci.* J Bacteriol, 2001. **183**(24): p. 7341-53.
3. Kavanaugh, J.S. and A.R. Horswill, *Impact of Environmental Cues on Staphylococcal Quorum Sensing and Biofilm Development.* J Biol Chem, 2016. **291**(24): p. 12556-64.
4. Kim, B.-R., Y.-M. Bae, and S.-Y. Lee, *Effect of Environmental Conditions on Biofilm Formation and Related Characteristics ofStaphylococcus Aureus.* Journal of Food Safety, 2016. **36**(3): p. 412-422.
5. Beenken, K.E., et al., *Global gene expression in Staphylococcus aureus biofilms.* J Bacteriol, 2004. **186**(14): p. 4665-84.
6. Resch, A., et al., *Comparative proteome analysis of Staphylococcus aureus biofilm and planktonic cells and correlation with transcriptome profiling.* Proteomics, 2006. **6**(6): p. 1867-77.
7. Resch, A., et al., *Differential gene expression profiling of Staphylococcus aureus cultivated under biofilm and planktonic conditions.* Appl Environ Microbiol, 2005. **71**(5): p. 2663-76.
8. Cuning, R., et al., *Biosynthesis and metabolism of arginine in bacteria.* Microbial Rev, 1986. **50**(3): p. 314-352.
9. Martinez, J.L. and F. Rojo, *Metabolic regulation of antibiotic resistance.* FEMS Microbiol Rev, 2011. **35**(5): p. 768-89.
10. Fuchs, S., et al., *Anaerobic gene expression in Staphylococcus aureus.* J Bacteriol, 2007. **189**(11): p. 4275-89.
11. Cramton, S.E., et al., *Anaerobic conditions induce expression of polysaccharide intercellular adhesin in Staphylococcus aureus and Staphylococcus epidermidis.* Infect Immun, 2001. **69**(6): p. 4079-85.
12. Vanhommerig, E., et al., *Comparison of biofilm formation between major clonal lineages of methicillin-resistant Staphylococcus aureus.* PLoS One, 2014. **9**(8): p. e104561.
13. De Backer, S., et al., *Remarkable geographical variations between India and Europe in carriage of the staphylococcal surface protein-encoding sasX/sesI and in the population structure of methicillin-resistant Staphylococcus aureus belonging to clonal complex 8.* Clin Microbiol Infect, 2018.
14. Murchan, S., et al., *Harmonization of pulsed-field gel electrophoresis protocols for epidemiological typing of strains of methicillin-resistant Staphylococcus aureus: a single approach developed by consensus in 10 European laboratories and its application for tracing the spread of related strains.* J Clin Microbiol, 2003. **41**(4): p. 1574-85.
15. Sabirova, J.S., et al., *Complete genome sequences of two prolific biofilm-forming Staphylococcus aureus isolates belonging to USA300 and EMRSA-15 clonal lineages.* Genome Announc, 2014. **2**(3).
16. Fey, P.D., et al., *A genetic resource for rapid and comprehensive phenotype screening of nonessential Staphylococcus aureus genes.* MBio, 2013. **4**(1): p. e00537-12.
17. Diep, B.A., et al., *The arginine catabolic mobile element and staphylococcal chromosomal cassette mec linkage: convergence of virulence and resistance in the USA300 clone of methicillin-resistant Staphylococcus aureus.* J Infect Dis, 2008. **197**(11): p. 1523-30.
18. De Backer, S., et al., *Enzymes Catalyzing the TCA- and Urea Cycle Influence the Matrix Composition of Biofilms Formed by Methicillin-Resistant Staphylococcus aureus USA300.* Microorganisms, 2018. **6**(4).
19. Love, M.I., W. Huber, and S. Anders, *Moderated estimation of fold change and dispersion for RNA-Seq data with DESeq2.* bioRxiv, 2014.
20. Liu, J., et al., *Transcriptomics Study on Staphylococcus aureus Biofilm Under Low Concentration of Ampicillin.* Front Microbiol, 2018. **9**: p. 2413.
21. Haft, D.H., et al., *TIGRFAMs and Genome Properties in 2013.* Nucleic Acids Res, 2013. **41**(Database issue): p. D387-95.

22. Finn, R.D., J. Clements, and S.R. Eddy, *HMMER web server: interactive sequence similarity searching.* Nucleic Acids Res, 2011. **39**(Web Server issue): p. W29-37.
23. Fuchs, S., et al., *AureoWiki The repository of the Staphylococcus aureus research and annotation community.* Int J Med Microbiol, 2018. **308**(6): p. 558-568.
24. Katayama, Y., T. Ito, and K. Hiramatsu, *A new class of genetic element, Staphylococcus Cassette Chromosome mec, encodes methicillin resistance in Staphylococcus aureus.* Antimicrob Agents Chemother, 2000. **44**(6): p. 1549-1555.
25. Diep, B.A., et al., *Complete genome sequence of USA300, an epidemic clone of community-acquired meticillin-resistant Staphylococcus aureus.* Lancet, 2006. **367**(9512): p. 731-739.
26. Kondo, Y., et al., *Combination of multiplex PCRs for staphylococcal cassette chromosome mec type assignment: rapid identification system for mec, ccr, and major differences in junkyard regions.* Antimicrob Agents Chemother, 2007. **51**(1): p. 264-74.
27. Branda, S.S., et al., *Biofilms: the matrix revisited.* Trends Microbiol, 2005. **13**(1): p. 20-6.
28. Liu, T.Y., et al., *Genetic evidence that multiple proteases are involved in modulation of heat-induced activation of the sigma factor SigI in Bacillus subtilis.* FEMS Microbiol Lett, 2017. **364**(7).
29. Mann, E.E., et al., *Modulation of eDNA release and degradation affects Staphylococcus aureus biofilm maturation.* PLoS One, 2009. **4**(6): p. e5822.
30. Le, K.Y., et al., *Molecular determinants of staphylococcal biofilm dispersal and structuring.* Front Cell Infect Microbiol, 2014. **4**: p. 167.
31. Boles, B.R. and A.R. Horswill, *Agr-mediated dispersal of Staphylococcus aureus biofilms.* PLoS Pathog, 2008. **4**(4): p. e1000052.
32. Gross, M., et al., *Key role of teichoic acid net charge in Staphylococcus aureus colonization of artificial surfaces.* Infect Immun, 2001. **69**(5): p. 3423-6.
33. Pamp, S.J., et al., *Spx is a global effector impacting stress tolerance and biofilm formation in Staphylococcus aureus.* J Bacteriol, 2006. **188**(13): p. 4861-70.
34. Keto-Timonen, R., et al., *Cold Shock Proteins: A Minireview with Special Emphasis on Csp-family of Enteropathogenic Yersinia.* Front Microbiol, 2016. **7**: p. 1151.
35. Lauderdale, K.J., et al., *Interconnections between Sigma B, agr, and proteolytic activity in Staphylococcus aureus biofilm maturation.* Infect Immun, 2009. **77**(4): p. 1623-35.
36. Steinhuber, A., et al., *Molecular Architecture of the Regulatory Locus sae of Staphylococcus aureus and Its Impact on Expression of Virulence Factors.* Journal of Bacteriology, 2003. **185**(21): p. 6278-6286.
37. Novick, R.P. and D. Jiang, *The staphylococcal saeRS system coordinates environmental signals with agr quorum sensing.* Microbiology, 2003. **149**(Pt 10): p. 2709-17.
38. Majerczyk, C.D., et al., *Direct targets of CodY in Staphylococcus aureus.* J Bacteriol, 2010. **192**(11): p. 2861-77.
39. Foster, T.J., et al., *Adhesion, invasion and evasion: the many functions of the surface proteins of Staphylococcus aureus.* Nat Rev Microbiol, 2014. **12**(1): p. 49-62.
40. Heilmann, C., et al., *Evidence for autolysin-mediated primary attachment of Staphylococcus epidermidis to a polystyrene surface.* Mol Microbiol, 1997. **24**(5): p. 1013-24.
41. Houston, P., et al., *Essential role for the major autolysin in the fibronectin-binding protein-mediated Staphylococcus aureus biofilm phenotype.* Infect Immun, 2011. **79**(3): p. 1153-65.
42. Schwartz, K., et al., *Extracellular DNA facilitates the formation of functional amyloids in Staphylococcus aureus biofilms.* Mol Microbiol, 2016. **99**(1): p. 123-34.
43. Schwartz, K., et al., *Functional amyloids composed of phenol soluble modulins stabilize Staphylococcus aureus biofilms.* PLoS Pathog, 2012. **8**(6): p. e1002744.
44. Boyle-Vavra, S., et al., *USA300 and USA500 clonal lineages of Staphylococcus aureus do not produce a capsular polysaccharide due to conserved mutations in the cap5 locus.* MBio, 2015. **6**(2).
45. Ko, K.S., *The contribution of capsule polysaccharide genes to virulence of Klebsiella pneumoniae.* Virulence, 2017. **8**(5): p. 485-486.
46. Lee, K.J., et al., *Role of capsular polysaccharide (CPS) in biofilm formation and regulation of CPS production by quorum-sensing in Vibrio vulnificus.* Mol Microbiol, 2013. **90**(4): p. 841-57.

47. Petruzzi, B., et al., *Capsular polysaccharide interferes with biofilm formation by Pasteurella multocida serogroup.* MBio, 2017. **8**(6): p. 1843-17.
48. Xia, G. and C. Wolz, *Phages of Staphylococcus aureus and their impact on host evolution.* Infect Genet Evol, 2014. **21**: p. 593-601.
49. Canchaya, C., et al., *Phage as agents of lateral gene transfer.* Current Opinion in Microbiology, 2003. **6**(4): p. 417-424.
50. Bischoff, M., et al., *Microarray-based analysis of the Staphylococcus aureus sigmaB regulon.* J Bacteriol, 2004. **186**(13): p. 4085-99.
51. Landini, P., *Cross-talk mechanisms in biofilm formation and responses to environmental and physiological stress in Escherichia coli.* Res Microbiol, 2009. **160**(4): p. 259-66.
52. Li, Y., Y. Chen, and R. Burne, *Regulation of urease gene expression by Streptococcus salivarius growing in biofilms.* Environ Microbiol, 2000. **2**(2): p. 169-77.
53. Zhu, Y., et al., *Staphylococcus aureus biofilm metabolism and the influence of arginine on polysaccharide intercellular adhesin synthesis, biofilm formation, and pathogenesis.* Infect Immun, 2007. **75**(9): p. 4219-26.
54. Cotter, P.D. and C. Hill, *Surviving the Acid Test: Responses of Gram-Positive Bacteria to Low pH.* Microbiology and Molecular Biology Reviews, 2003. **67**(3): p. 429-453.
55. Luchi, S., et al., *Effects of nitrate respiration on expression of the Arc-controlled operons encoding succinate dehydrogenase and flavin-link L-lactate dehydrogenase.* J Bacteriol, 1994. **176**(6): p. 1695-701.
56. Hiron, A., et al., *Only one of four oligopeptide transport systems mediates nitrogen nutrition in Staphylococcus aureus.* J Bacteriol, 2007. **189**(14): p. 5119-29.
57. Planet, P.J., et al., *Emergence of the epidemic methicillin-resistant Staphylococcus aureus strain USA300 coincides with horizontal transfer of the arginine catabolic mobile element and speG-mediated adaptations for survival on skin.* MBio, 2013. **4**(6): p. e00889-13.
58. Sihto, H.M., et al., *Validation of reference genes for normalization of qPCR mRNA expression levels in Staphylococcus aureus exposed to osmotic and lactic acid stress conditions encountered during food production and preservation.* FEMS Microbiol Lett, 2014. **356**(1): p. 134-40.

3.2. A *bursa aurealis* transposon library to screen MRSA knockout mutants for biofilm-associated targets

3.2.1. Screening of a bursa aurealis transposon mutant library for genes involved in the PIA/PNAG-independent biofilm phenotype formed by methicillin-resistant Staphylococcus aureus USA300

Unpublished.

3.2.1.1. Abstract

Staphylococcus aureus is notorious for its ability to cause biofilm-associated infections. The biofilm phenotype expressed by clinical isolates of *S. aureus* is influenced by acquisition of the methicillin resistance gene *mecA*. In contrast to methicillin-sensitive *S. aureus* (MSSA), the *ica* locus is redundant for methicillin-resistant *S. aureus* (MRSA) biofilm formation. We developed a *mariner*-based transposon, *bursa aurealis*, library of 1920 mutants in an MRSA clinical isolate (UAS391) that generates a PIA/PNAG-independent, proteinaceous/extracellular DNA (eDNA)-based biofilm matrix. The library was screened for defects in biofilm formation capacity under static conditions and 206 isolates showed a decrease in biofilm formation capacity (average OD_{492}<75% of UAS391-Ery^S; 28-72%; p<0.001) while 149 showed an increase in biofilm formation capacity (average OD_{492}>125% of UAS391-Ery^S; 130-221%; p<0.001), as compared to the parental strain (average OD_{492} 0.701). Out of 355 transposon mutants with reproducible biofilm formation defects under static conditions, 324 (n=200, average integrated pixel density <75% of UAS391-Ery^S, 10-64%, p=0.004; n=124, average integrated pixel density >125% of UAS391-Ery^S; 125-249%; p=0.049) showed a consistent effect under flow conditions (average integrated pixel density UAS391-Ery^S = 2032). 91 mutants had a growth defect in log phase (R^2<0.95) as compared to UAS391-Ery^S (average growth rate: 0.020 units of $minutes^{-1}$; average lag time: 28.4 minutes), which were eliminated from further analysis. 8 mutants showed altered susceptibility to ciprofloxacin (S→I, n=7) or cefoxitin (R→S, n=1). Arbitrary PCR and sequencing revealed transposon insertions to be in 207 single, unique genes (biofilm increase: n=91; decrease: n=116). Collectively, our screen identified novel loci involved in MRSA PIA/PNAG-independent biofilm formation and underline the importance of surface adhesion, pH homeostasis, persister formation, and toxin production.

3.2.1.2. Introduction

Staphylococcus aureus is the etiological agents of a myriad of chronic and recalcitrant human infections thanks to a vast armamentarium of virulence factors and its capacity to form sessile matrix-encased microcolonies termed biofilms [1]. Biofilms

are notoriously difficult to eradicate, with sessile populations being up to 1000-fold more resistant than their planktonic counterparts [2]. The biofilm matrix composition commonly varies between strains, but can contain in general host factors, polysaccharide (polysaccharide intercellular adhesin, PIA or polymeric N-acetylglucosamine, PNAG), proteins and extracellular DNA (eDNA) [3]. PIA/PNAG biosynthesis is accomplished by the products of the intercellular adhesion *icaADBC* locus and a regulatory gene (*icaR*) [4]. Expression of the *ica* gene locus is regulated by a variety of environmental factors and regulatory proteins, such as the staphylococcal accessory regulator A (SarA) and the alternative sigma factor SigB [5]. However, biofilm formation can also occur in an *ica*-independent fashion. Expression of methicillin resistance in MRSA has been shown to be commonly associated with a shift from PIA/PNAG- to a biofilm phenotype involving the release of eDNA and surface expression of several sortase-anchored proteins [6]. The biofilm-associated protein (Bap) in bovine mastitis *S. aureus* isolates and the fibronectin-binding proteins (FnBPs) in human MRSA isolates were among the first PIA/PNAG-independent biofilm mechanisms to be described [7, 8]. Many other surface adhesins, such as surface protein A (Spa) and cell wall surface anchor family protein SasG have also been implicated in this divergent biofilm mechanism [9, 10]. Additionally, clinical MRSA strains that produce an *ica*-independent biofilm require the major autolysin Atl for primary attachment to polystyrene surfaces [11]. Atl mediates cell lysis and the release of eDNA for biofilm accumulation [12].

Despite the important role of MRSA biofilms in disease, our understanding of the molecular factors contributing to the development of the biofilm mode of growth is still incomplete. This study reports the generation and subsequent screening of a mariner transposon mutant library of 1920 mutants in a prolific *ica*-independent biofilm forming USA300 UAS391-Ery^{S} strain. This work expands our current understanding of genetic factors controlling biofilm formation in absence of PIA/PNAG and may provide potential new targets for therapeutic intervention.

3.2.1.3. Materials & methods

3.2.1.3.1. Bacterial strains and growth conditions

The *S. aureus* strains in this study were derived from a prolific biofilm forming USA300 UAS391 strain isolated from an abscess infection in a Belgian hospital [13]. The transposon library was constructed in its erythromycin sensitive plasmid-cured derivative, UAS391-Ery^{S}, to avoid plasmid incompatibility and insertion concerns [14]. *S. aureus* strains were grown in Brain-Heart Infusion (BHI;

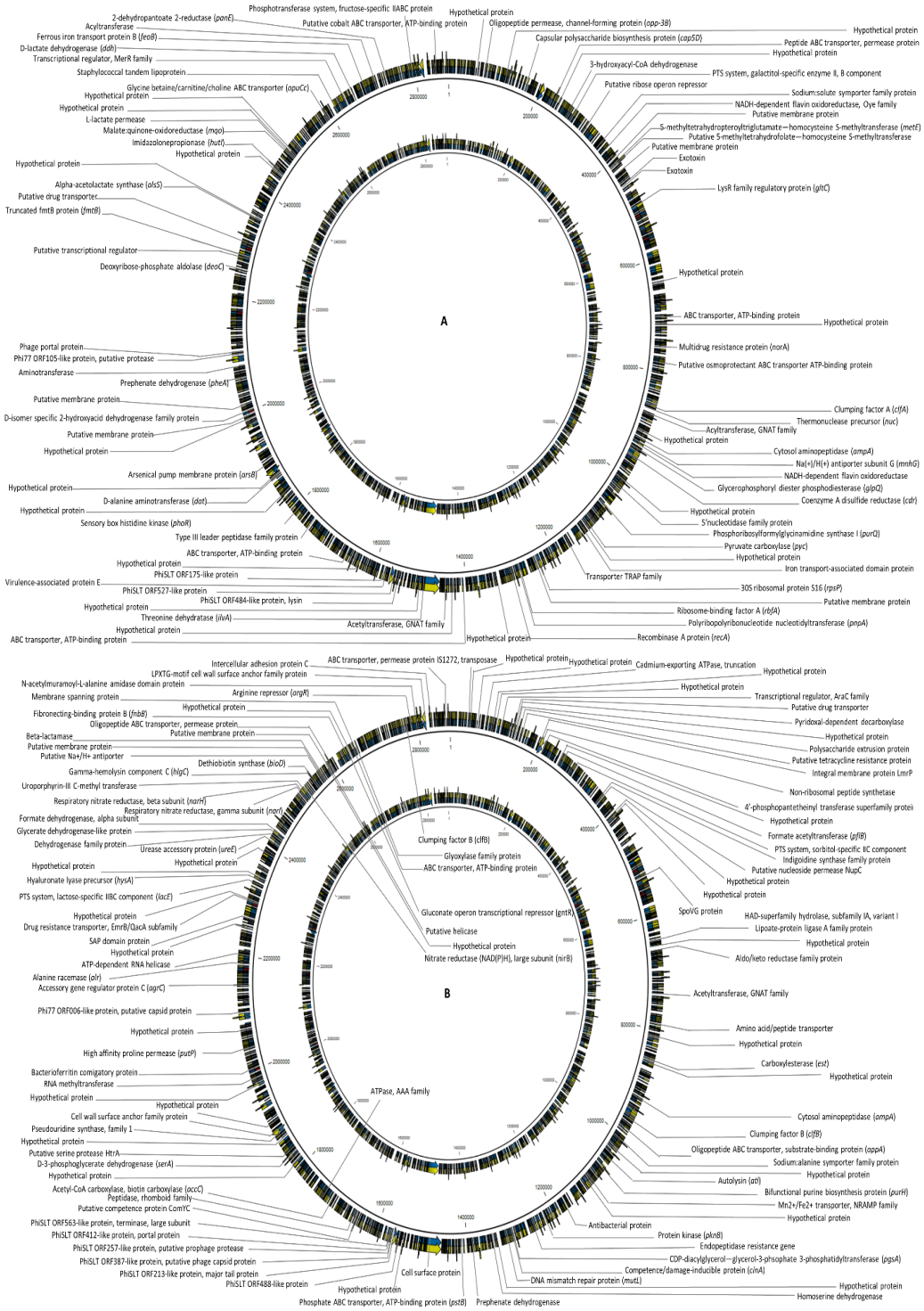

Figure 12: Visualization of the mapping of *bursa aurealis* transposon insertion UAS391-Ery^S mutants against *S. aureus* FPR3757 and USA300 UAS391. CLC Genomics Workbench 8 was used to create a circular

representation of the whole genome *S. aureus* FPR3757 (outer line) and UAS391 (inner line) GenBank sequence (accession numbers NC_007793.1 and CP007690.1, respectively). (**A**) mutants showing increased biofilm formation with transposon insertions in 91 single, unique genes. (**B**) mutants showing decreased biofilm formation with transposon insertions in 116 single, unique genes.

Becton, Dickinson and Company, USA) medium supplemented with 0.1% D(+)-glucose monohydrate (Merck Millipore, USA) for all assays and cultivated on BHI Bacto™ agar (Becton, Dickinson and Company, USA) containing 5 µg/ml erythromycin (Merck KGaA, USA).

3.2.1.3.2. Construction of the *bursa aurealis* transposon mutant library in UAS391

Transformation of *S. aureus* strain UAS391-Ery^S with plasmids pBursa and pFA545 was performed as essentially described [15, 16]. In short, the *Himar 1* (mariner) derived transposon *Bursa aurealis* was cloned into the pTS2 vector to generate the delivery vector pBursa, while the *Himar 1* transposase was encoded on a second plasmid pFA545, which is a derivative of vectors pSPT181 and pRN8103. *S. aureus* UAS391-Ery^S carrying pFA545 was transduced with phage ϕ11 that was propagated on pBursa-carrying UAS391-Ery^S. Due to the temperature sensitivity of both pBursa and pFA545, selection occurred on LB medium supplemented with chloramphenicol (10 µg/ml) (Merck KGaA, USA) and tetracycline (5 µg/ml) (Merck KGaA, USA) at 30°C for 48h to allow for transposition events. Individual resistant colonies were subsequently heat-shocked to cure pBursa and pFA545 plasmids and inoculated on LB plates containing erythromycin (25 µg/ml) at 43°C to detect the transposition event. Resulting colonies were screened for loss of both pBursa and pFA545 and retention of the *bursa aurealis* transposon carrying the erythromycin-resistance determinant *ermB* by patching these onto BHI plates with a different selection marker (erythromycin 25 µg/ml, chloramphenicol 10 µg/ml, and tetracycline 5 µg/ml). After growth at 43°C, colonies resistant to erythromycin but susceptible to chloramphenicol and tetracycline were selected for further analysis.

3.2.1.3.3. Screen for biofilm-defective mutants

24h or 17h-old biofilms of log phase transposon mutant and parental strains UAS391 and UAS391-Ery^S were grown in triplicate in either polystyrene microtiter plates (Greiner Bio-One, Austria) or microfluidic channels (Bioflux™, Fluxion Biosciences Inc.) under static or flow conditions, respectively, as described previously [13, 17]. *S. aureus* ATCC® 6538™ and 5374 functioned as a positive and negative control for biofilm formation under both conditions.

3.2.1.3.4. Screen for growth-defective mutants

The turbidity of UAS391-Ery^S transposon mutant log phase triplicate cultures was measured as described before [18]. The rate of change in the number of cells in a culture per unit time during the exponential phase was determined using the GrowthRates program [19] in order to exclude any possible pleiotropic growth deficiencies influencing the amount of formed biofilm mass.

3.2.1.3.5. Screen for mutants with a change in antibiotic susceptibility

To ensure loss of pBursa and pFA545 plasmids, the susceptibilities of transposon mutants, as well as control parental UAS391 and UAS391-Ery^S cultures to additional antibiotics (BBL™ SensiDisc™, Becton, Dickinson & Company, USA) ciprofloxacin (5µg), gentamycin (10µg), trimethoprim-sulfamethoxazole (1.25/23.75µg), chloramphenicol (30µg), clindamycin (5µg), erythromycin (15µg), cefoxitin (30µg), penicillin (10 units) and tetracycline (30µg) were evaluated in disk diffusion experiments according to CLSI-recommended guidelines [20]. *S. aureus* ATCC® 25923™ was used as quality control.

3.2.1.3.6. Inverse PCR

Genomic DNA of knockout mutants showing a change in biofilm formation, as compared to parental strains UAS391 and UAS391-Ery^S, was isolated using the Masterpure™ Complete DNA & RNA Purification kit (Epicentre®, USA), after lysis of the cells with TE buffer containing 12.5 µg/mL lyophilized lysostaphin powder from *Staphylococcus staphylolyticus* (Sigma-Aldrich®, USA). Briefly, isolated DNA was digested with 10U/µl *Aci*I (*Ssil*) restriction enzyme (Thermo Fisher Scientific, USA), after which 5U/L T4 DNA ligase (Thermo Fisher Scientific, USA) was aliquoted into the reaction. Last, the *bursa aurealis* genome junction was amplified and Sanger sequenced with outward-facing primers Buster and Martin-ermR (Sigma-Aldrich®, USA) that anneal to two different regions on the transposon [15] (**Suppl. Table 7**).

3.2.1.3.7. Identification of transposon insertion sites and disrupted genes

The flanking nucleotide sequences of the transposon were determined by local BLAST analysis (100-200 nucleotides downstream of the transposon end site CCTGTTA) against the *S. aureus* USA300 FPR3757 reference genome sequence (#NC_007793.1) and *S. aureus* USA300 UAS391 (CP007690) [21]. Genes were mapped to the Kyoto Encyclopaedia of Genes and Genomes (KEGG) pathway, annotated in GenBank, and also assigned to TIGRFAMs protein families [22], which is based on TIGRFAM Hidden Markov Models (HMM) [23], by using the AureoWiki database repository of the *S. aureus* research and annotation community (http://aureowiki.med.uni-greifswald.de) [24].

3.2.1.3.8. Relative gene expression of selected biofilm-defective mutants

To confirm complete gene knockout caused by the *bursa aurealis* insertion, RNA of 24h-old static biofilms of b*ursa aurealis*-bearing mutant strains and wild type strain UAS391-Ery^S was isolated, cDNA-converted and used for RT-qPCR in triplicate as described [18]. Gene-specific primers are mentioned in **Suppl. table 7**. Housekeeping gene *gyrB* (EX97_00025) was used as internal reference for data normalization [25]. The fold change in gene expression was calculated using the Comparative C_t method ($2^{-\Delta\Delta Ct}$).

3.2.1.3.9. Statistical analysis

Biomass quantification in the dynamic flow and static assays was performed using the R Project software (version 3.1.2.). A Welch Two-Sample T-Test or a Wilcoxon Rank Sum Test was used when data was either distributed normally or not, based on a Shapiro-Wilk Normality test. *P*-values <0.05 were considered significant.

3.2.1.4. Results & discussion

3.2.1.4.1. Identification of genes required for biofilm formation

Following transformation of MRSA UAS391-Ery^S with plasmid pBursa and pFA545, we produced 1920 mutants containing a random *bursa aurealis* transposon insertion in the genome. These mutants were tested for growth and antibiotic susceptibility as a control for the *bursa aurealis* transposon insertion and possible corresponding pleiotropic effects. 91 mutants had a growth defect in log phase under non-stressed conditions (R^2<0.95) as compared to UAS391-Ery^S (growth rate: 0.020 units of minutes^{-1}; lag time: 28.4 minutes). 9 isolates showed altered susceptibility to chloramphenicol (S→I, n=8) or tetracycline (S→R, n=1). These (n=100) were excluded from further analysis. Interestingly, 7 knockout mutants reverted from a sensitive phenotype for ciprofloxacin to intermediate susceptibility, and 1 mutant became sensitive to cefoxitin upon *bursa aurealis* insertion. These were not excluded from biofilm phenotype screening. The remaining mutants (n=1820) were screened for the inability to form a biofilm on the surface of a polystyrene microtiter plate and were also screened for the ability to form biofilm under shear force. Initial phenotype screening under static conditions revealed a total of 604 genes required for biofilm formation. Upon re-examination for reproducibility of the biofilm phenotype, 355 mutants again displayed biofilm formation defects. In detail, 206 isolates displayed a decrease in biofilm formation capacity (OD_{492}<75% of UAS391-Ery^S; 28-72%; p<0.001) and 149 showed an increase in biofilm formation capacity (OD_{492}>125% of UAS391-Ery^S; 130-221%; p<0.001) as compared to the parental strains (average OD_{492} UAS391 and UAS391-Ery^S = 0.712 and 0.701, respectively). Under flow conditions, 324 out of 355 isolates showed a similar phenotype. In detail, 200 showed a decrease in biofilm formation capacity (integrated pixel density <75% of UAS391-Ery^S; 10-64%; p=0.004) while 124 showed an increase in biofilm formation capacity (integrated pixel density >125% of UAS391-Ery^S; 125-249%;

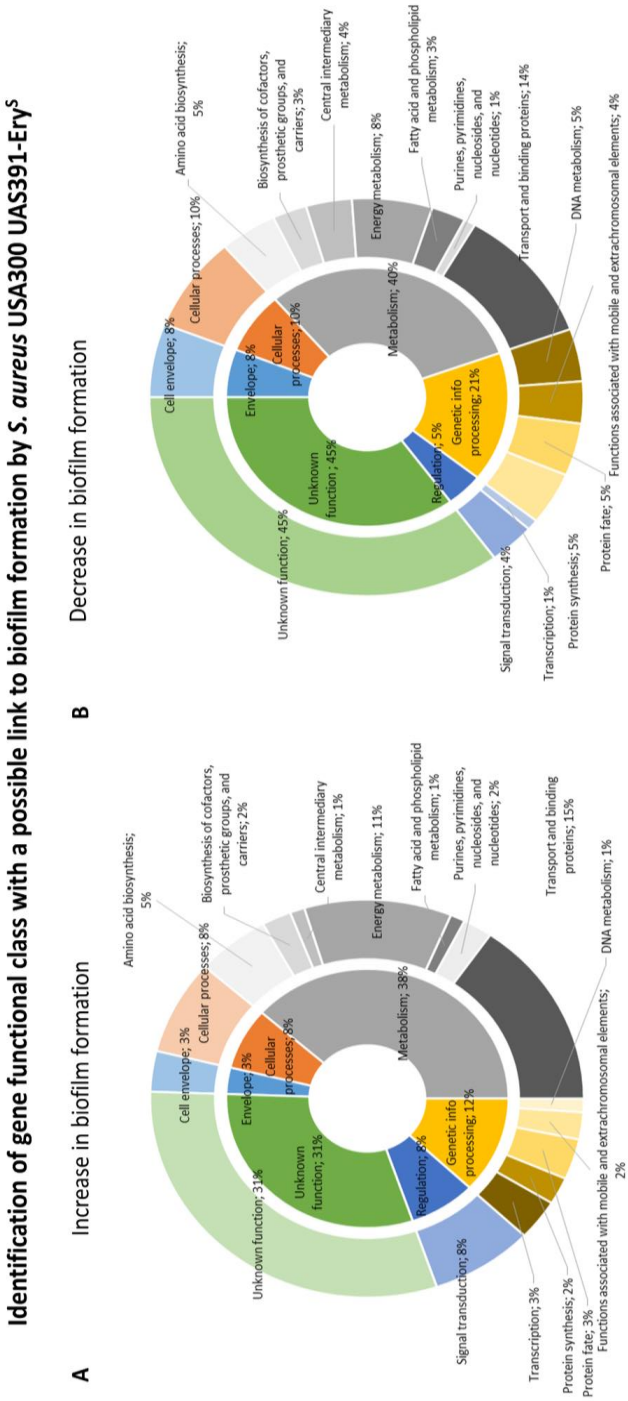

Figure 13: Gene functional assignment of *bursa aurealis* transposon UAS391-Ery^S mutants with a change in biofilm formation. Showing either ≥125% increase (**A**) or ≤75% decrease (**B**) in biofilm formation under static conditions as compared to USA300 UAS391-Ery^S. The gene functional assignment based on gene sequences

to TIGRFAMs protein families [22] based on TIGRFAM Hidden Markov Models (HMM) [23], was performed using the AureoWiki database repository of the *S. aureus* research and annotation community (http://aureowiki.med.uni-greifswald.de) [24]. Genes with unknown function encompass hypothetical proteins.

p=0.049), as compared to the parental strains (average integrated pixel density UAS391 and UAS391-Ery^S = 2133 and 2032, respectively).324 inverse PCR-identified *bursa aurealis* transpositions were mapped into the genome of *S. aureus* USA300 UAS391 (**Fig. 12 & Suppl. Table 8, 9**) and subsequently, mutants showing decreased or increased biofilm formation in 116 and 91 single, unique genes, respectively, could be identified. GenBank annotations and the KEGG database were used to identify putative gene functions based on sequence homology. The main functional categories that the 207 insertions fell into were: central metabolism, envelope, cellular processes, genetic info processing, regulation, and unknown function. The relative distribution of the 207 unique transposon insertions within these functional categories is shown in **Fig. 13**.

Here, we will discuss 8 UAS391-Ery^S knockout mutants with location of the transposon insertion in 1/3 of the gene length to avoid "leaky expression" (**Fig. 14 & Suppl. Fig 5**) and showing the largest defect in biofilm formation (n=4, increase in biofilm formation; n=4, decrease in biofilm formation) (**Fig. 15 & Suppl. Fig 6**). Additionally, 2 mutants knocked out in genes of already known function (Δ*nuc* and Δ*clfB*) were included as controls.

3.2.1.4.2. Genes involved in metabolism (energy and amino acid)

The largest fraction of transposon insertions (23%) was in the category of metabolism, specifically: energy and amino acid metabolism. Previous research has demonstrated that biofilms are physiologically different from planktonic cells [26, 27]. Metabolic changes include a switch to fermentative processes resulting from low oxygen concentration in biofilms [28, 29]. Up-regulation of pathways ultimately producing ammonia compounds has been explained to limit the deleterious effects of reduced pH associated with anaerobic growth conditions [26]. Indeed, inactivation of the beta subunit (*narH*) of respiratory nitrate reductase (formed by *narG*, *narH*, *narI,* and *narJ*) resulted in a 57% and even 82% decrease in formed biofilm mass under both static and flow conditions, respectively. NarH is commonly involved in energy/nitrogen metabolism where nitrate reductase is required to prevent toxic accumulation of nitric oxide and reduces nitrate to ammonia. A biofilm-specific role for *narH* has also already been elucidated in *Pseudomonas aeruginosa* [30], *Burkholderia pseudomallei* [31] and E*scherichia coli* [32]. We also found a similar ammonia-producing role for the large subunit (*nirB*) of nitrite reductase (formed by *nirB*, *nirD,* and *nasF*). Inactivation of this gene resulted in 32% and 87% decrease in formed biofilm mass, respectively. This

indicates that USA300 biofilms are characterized by unfavourable oxygen concentrations and acidification of the medium due to increased fermentation activity.

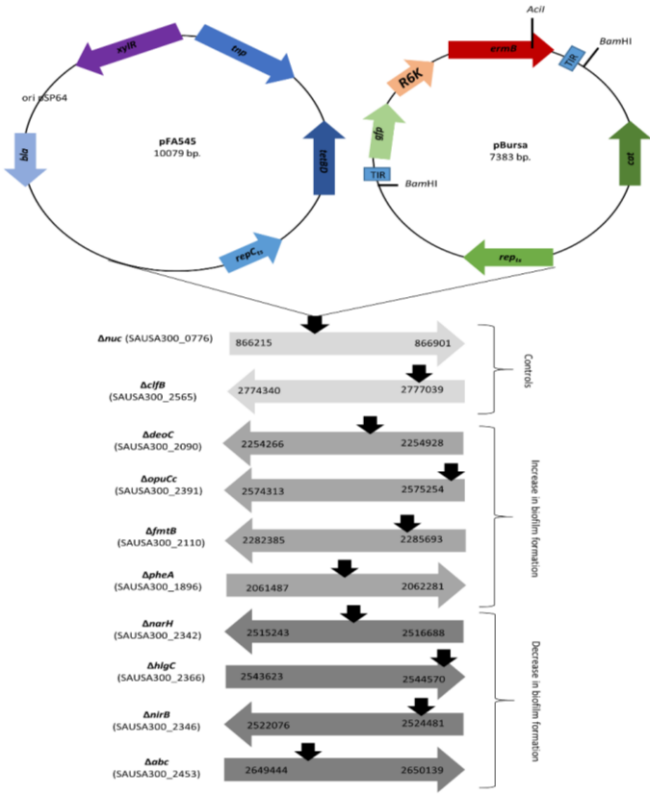

Figure 14: Schematic representation of pBursa plasmid with the *bursa aurealis* transposon and pFA545 plasmid carrying *bursa aurealis* transposase, and their insertion in ten selected *bursa aurealis* transposon UAS391-Ery^{S} mutants. (**Upper right part**) pBursa plasmid with the *bursa aurealis* transposon. This transposon consists out of the mariner terminal inverted repeats (TIR), a gene coding for the green fluorescent protein (*gfp*), the pir-dependent R6K origin of replication and the erythromycin resistance gene (*ermB*). The positions of the restriction enzyme recognition sites *AciI* and *BamHI* in *bursa aurealis* are marked by a black line. The pBursa plasmid also contains a temperature sensitive plasmid replicon (rep_{ts}) and the chloramphenicol resistance gene (*cat*) of the pTS2 vector. (**Upper left part**) pFA545 plasmid with the mariner transposase gene (*tnp*), the temperature sensitive origin of replication ($repC_{ts}$), the tetracycline resistance marker (*tetBD*) and the ampicillin resistance marker (*bla*) [16]. (**Lower part**) Location of the transposon insertion in the corresponding gene is shown by a black arrow. The orientation of the arrow displaying the gene of interest (grey) distinguishes whether the gene is located on the minus (left) or plus strand (right).

The limited nutrient and oxygen availability within the biofilm results in reduced metabolic activity and a lower energy state, forcing a subset of biofilm cells into stationary and persister-like states [33]. Prephenate dehydratase (*pheA*), involved in phenylalanine, tyrosine and tryptophan biosynthesis, has been shown to be involved in persister formation by *P. aeruginosa* [34]. Interestingly, our mutant screen revealed that

inactivation of *pheA* resulted in 61% and 40% increase, respectively. This suggests that the wild type UAS391 biofilm is enriched with adherent persister cells and these will contribute to biomass production if not dormant.

An important part of the formed biofilm mass is constituted by the accumulation of eDNA in the extracellular matrix (ECM) [35]. In this regard, several reports have demonstrated that deletion of the secreted nuclease (*nuc*) in *S. aureus* causes an increase in biofilm formation because of decreased eDNA degradation in the biofilm ECM [36, 37]. Nuc is known as a negative regulator of biofilm formation, and indeed, our screening results report a 99% and 56% increase in formed biomass under both static and flow conditions, respectively. Another regulator controlling biofilm dispersal has been shown to be deoxyribose-phosphate aldolase (*deoC*) in *Streptococcus mutans* [38]. DeoC is commonly involved in the phosphate pathway, and interestingly, other genes involved in this pathway, such as *zwf* and *rpiA*, have already been correlated with RNAIII transcription in *S. aureus* UAMS-1 [39] RNAIII is the effector molecule of the *agr* quorum-sensing system which induces dispersal and negatively regulates MSCRAMMs (microbial surface component recognizing adhesive matrix molecule) [40], thereby explaining the observed increase in biofilm (41% and 29%, respectively) observed in our screening.

3.2.1.4.3. Genes for environmental information processing (transport and binding proteins)

Twenty-seven transposon insertions (11% of total) resulting in a biofilm-deficient phenotype occurred in genes involved in transport. Genes EX97_12540 and EX97_12870 both encode ABC transporters. Gene EX97_12540 encodes a glycine betaine/carnitine/choline ABC transporter (*opuCc*) that is involved in the osmoprotectant transport system. Gene EX97_12870 encodes an ABC-2 type transport system ATP-binding protein. *OpuCc*-defective biofilm cells in *S. aureus* have been reported to show reduced phosphorylation of the second quorum-sensing system TRAP (Target of RNAIII Activating Protein) [41]. TRAP phosphorylation, which can be induced by the autoinducer RNAIII Activating Protein (RAP), was originally thought to lead to activating of the quorum sensing system *agr*, which modulates biofilm dispersal. However, contradictory results have been reported [42, 43]. Our results do seem to suggest a link between TRAP and *agr* since *ΔopuCc* had a stimulating effect on biofilm formation (63% and 62% increase, respectively). EX97_12870 was dramatically down-regulated in a *clpX* mutant of *S. aureus* 8325-4 [44]. *ClpX* seems to regulate the synthesis of surface-associated adhesion proteins, such as protein A, and of virulence factors, such as α–haemolysin, by controlling *agr*-activity. However, the mechanisms by which inactivation of EX97_12870 exactly influences the biofilm (63% and 80% decrease, respectively) remains unclear. Furthermore, transporters may also indirectly affect

biofilm formation by the transport of essential nutrient molecules, or they might have a more direct effect on biofilm formation by transporting autoinducer or other signaling molecules required for biofilm formation [45].

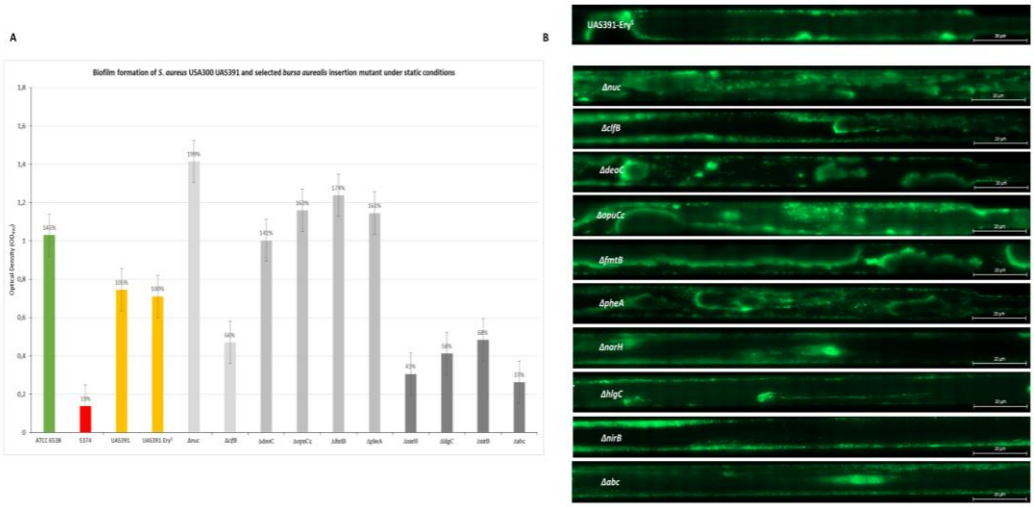

Figure 15: Identification and characterization of the ten *bursa aurealis* insertion UAS391-Ery^S mutant genes involved in biofilm formation. (**A**) Biofilm formation after 24h of parental strains UAS391, UAS391-Ery^S, and 8 selected *bursa aurealis* insertion mutants under no flow conditions. The total biomass was determined by crystal violet staining *in triplicate*. The biofilm-forming capacity of the strains was compared to the biofilm growth of positive control (ATCC 6538) and negative control (5374), while values were corrected for background absorption. Error bars represent the 95% confidence interval per strain. (**B**) Flow biofilm images of ten *bursa aurealis* insertion mutants and UAS391-Ery^S captured after 17 h growth employing ZEN 2012 software (Zeiss) as 84 combined tile images consisting of one µm² horizontal tiles covering the entire microchannel. The total biomass was determined by SYTO™ 9 staining *in duplicate*.

3.2.1.4.4. Genes for human diseases (*S. aureus* infection)

The influence of common *S. aureus* toxins, such as α–haemolysin (*hla* or α-toxin) and leukotoxin AB (LukAB), in biofilm formation through cell-cell and cell-surface interactions has already been demonstrated [46]. Based on our results, *hlgC*, encoding the gamma haemolysin component C, might have a similar in biofilm formation as knockout mutation resulted in 42% and 88% decrease, respectively. A STRING database search predicted interactions of *hlgC* with surface adhesins such as clumping factor B (*clfB)*, fibronectin-binding protein A (*fnbA)*, *spA* and *sarA* in *S. aureus* Mu50. ClfB was used as a control in the assays since it is another important virulence factor of *S. aureus* promoting nasal colonization in humans [47]. Additionally, the role of *clfB* in staphylococcal biofilm formation has been demonstrated already [48]. ClfB is a 150 kDa protein with a C-terminal LPXTG sorting motif, which is used to covalently anchor the MSCRAMM to the cell wall peptidoglycan [49]. Indeed, our results confirm these reports

by showing a 34% and 62% decrease, respectively, in formed biomass.

EX97_11070 codes for a protein of a deduced molecular mass of 263 kDa that contains 17 tandem repeats of 75 amino acids and a C-terminal LPXTG cell wall-sorting motif. Interestingly, Tn551-mediated insertional activation of the *fmtB* gene abolished methicillin resistance in *S. aureus* [50]. Indeed, our own *bursa aurealis* transposon insertion also resulted in cefoxitin sensitivity. Additionally, other factors besides *mecA* or *mecC* are also involved in methicillin resistance, such as the series of *fem* and *aux* factors, *llm*, and *sigB* [51]. Some of these have been demonstrated to be involved in peptidoglycan metabolism [52]. As such, the link between methicillin resistance expression and biofilm formation was suggested to be caused by changes in the cell wall architecture that block the export of PIA/PNAG to the cell surface [6]. Since we saw an increase in formed biofilm (74% and 83%, respectively) and protein-dependent biofilms are commonly less robust than those containing PIA/PNAG [53], it is tempting to speculate that inactivation of *fmtB* resulted in the loss of methicillin resistance together with reversion to the PIA/PNAG biofilm phenotype.

3.2.1.4.5. Other genes involved in biofilm formation

Of the numerous genes tested here, our screening also revealed genes that have been previously described as crucial for *S. aureus* biofilm formation in literature, providing a proof-of-concept of the applied methodology. Besides our two control genes, *nuc* and *clfB*, we also identified the giant surface protein Ebh [54], major autolysin Atl [12], fibronectin-binding protein FnBPB [8] and LPXTG-motif harbouring protein SasC [55] with a distinct decrease in biofilm formation (58% and 85%, 34% and 74%, 40% and 86%, 48%, and 49%, respectively).

3.2.1.5. Conclusion

This study identified 207 genes required for MRSA biofilm formation. Determinants with a decrease in biofilm formation could be promising targets for biofilm disruption, whilst determinants with an increase in biofilm formation might have therapeutic implications as stimulation of negative regulators of biofilm growth. Among these genes are several which have not previously been linked to biofilm formation, such as *hlgC*. Many genes, such as *deoC* and *pheA* are known to contribute to biofilm formation in other species such as *P. aeruginosa* and *S. mutans*, and this study has confirmed that they are also essential for biofilm formation in MRSA. The exact function of *fmtB* and EX97_12870 is unknown, and how these genes influence biofilm formation is a fascinating unresolved question. Collectively, our screen of *bursa aurealis* mutants identified novel genes involved in MRSA biofilm formation and underscored the importance of fermentative metabolism and pH homeostasis in biofilm formation. Our

research demonstrates that, despite recent advances, the genetic basis of biofilm formation by MRSA is still not yet fully elucidated and much remains to be discovered.

3.2.1.6. Addendum

3.2.1.6.1. Acknowledgements

We thank Liesbeth Bryssinck, Anouk Vanderstraeten and Merve Sezer, who contributed to this work by screening the library and identification of possible hits, which was an incredible amount of work.

3.2.1.6.2. Contribution to authorship

In detail, screening for biofilm- and growth-defective mutants, inverse PCR, identification of transposon insertion sites and relative gene expression of selected biofilm-defective mutants and statistical analysis were performed by SDB.

3.2.1.6.3. Supplementary figures

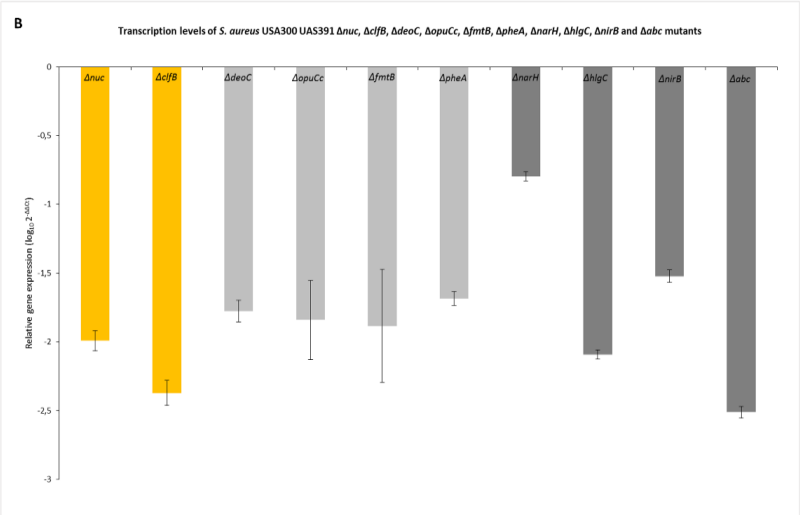

Supplementary figure 5: Relative quantification of gene expression in UAS391-Ery^S and the corresponding *bursa aurealis* insertion UAS391-Ery^S mutants. Genes: *nuc*: thermonuclease; *clfB*: clumping factor B; *deoC*: deoxyribose-phosphate aldolase; *opuCc*: glycine betaine/carnitine/choline ABC transporter; *fmtB*: truncated FmtB protein; *pheA*; prephenate dehydratase; *narH*: respiratory nitrate reductase, beta subunit; *hlgC*: gamma-haemolysin component C; *nirB*: nitrite reductase [AD(P)H], large subunit; and *abc*: ABC transporter ATP-binding protein. Values were normalized to *gyrB* expression and calculated using the Comparative C_t Method ($2^{-\Delta\Delta Ct}$). Gene expression in UAS391-Ery^S was taken as a baseline 0.

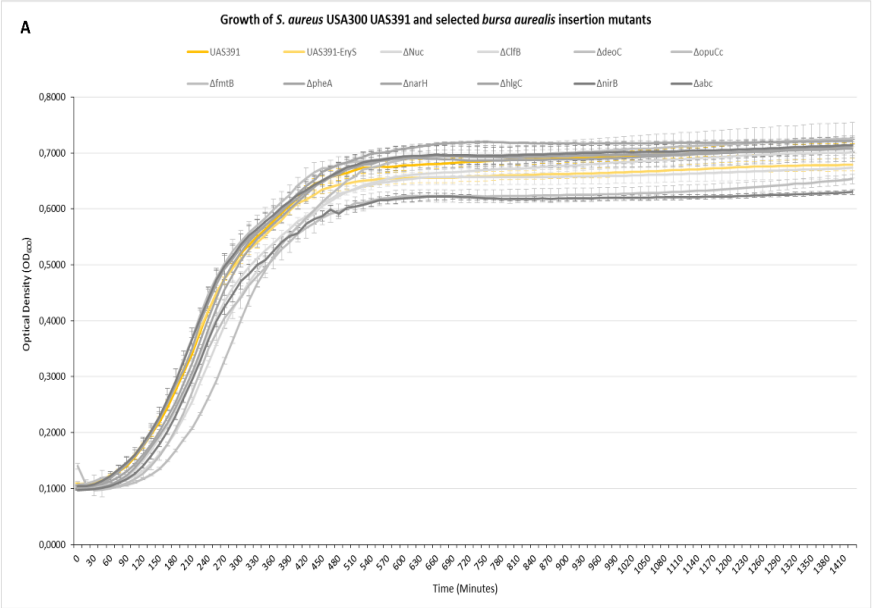

Supplementary figure 6: Background absorption-corrected 24h growth curves for UAS391, UAS391-Ery^S and ten selected *bursa aurealis* insertion mutants. Error bars in corresponding colour represent the 95% confidence interval per strain.

3.2.1.6.3. Supplementary tables

Supplementary Table 7: Primers used during the *bursa aurealis* transposon library study. Primers were designed against *S. aureus* strain USA300 UAS391 (#CP007690.1).

Gene name	ID	Sequence (5'→3')	Product size (bp)	Reference
Primers for inverse PCR				
	Buster	GCTTTTTCTAAATGTTTTTTAAGTAAATCAAGTACC		[16]
	Martin-ermR	AAACTGATTTTTAGTAAACAGTTGACGATATTC		[16]
Primers for RT-PCR				
gyrB	GyrB-F	GTAACACGTCGTAAATCAGCG	170	[25]
	GyrB-F	CGTAATGGTAAAATCGCCTGC		
Δ*nuc*	RTTn0724-F	ATGGACGTGGCTTAGCGTAT	181	This study
	RTTn0724-R	GCGTTGTCTTCGCTCCAAAT		
Δ*clfB*	RTTn1754-F	CTTGGTTCCGGTTCTGGGTC	103	
	RTTn1754-R	GTGGTGGAAGTGCTGATGGT		
Δ*deoC*	RTTn0299-F	CTTGCATAATTTGAACGCCTGC	51	
	RTTn0299-R	AAGCAGGTGCGACACGTATT		
Δ*opuCc*	RTTn0319-F	ACAGCACTCGCAGCATAAGG	211	
	RTTn0319-R	AAGGCGATGGCTATGAAGGA		
Δ*fmtB*	RTTn1219-F	GCATCAGGTGTAATGGCTGC	215	
	RTTn1219-R	GCAAAAGCGGAAATCGCTCA		
Δ*pheA*	RTTn0570-F	ACCTGGGTTGTTAGCAAGTGT	76	
	RTTn0570-R	AGGACGAGACTCAATCCAGG		
Δ*narH*	RTTn0012-F	GCTGGGAAAATCGCATCTGG	80	
	RTTn0012-R	TATTGCCCACCACTTAGCCC		
Δ*hlgC*	RTTn0038-F	TTATGGGGCGTCAAAGCGAA	211	
	RTTn0038-R	CGCTTGTATCGCTTGAACCT		
Δ*nirB*	RTTn0122-F	CCCAAGGTTCAGCTTCGACT	137	

	RTTn0122-R	TGCTGAAAGAACAGCGCCAT		
Δ*abc*	RTTn0778-F	CCAAAAGCTGTGCGAGATGT	232	
	RTTn0778-R	ATGCTTGGTCCTCCCTTTCT		

Supplementary Table 8: Overview of *bursa aurealis* transposon insertion mutants with an increase in biofilm formation capacity as compared to UAS391-Ery^S. Biofilm formation under static or flow conditions is mentioned as % compared to UAS391-Ery^S (100%). Insertion location of the transposon is given in function of the gene length (e.g. 1/3, 2/3 or 3/3 of the gene).

Increase in biofilm formation					
Name Tn	**Locus tag FPR3757**	**Gene name**	**Biofilm formation under static conditions**	**Biofilm formation under flow conditions**	**Insertion location of transposon**
Tn0622	SAUSA300_2274	Putative membrane protein	130%	181%	2/3
Tn0474	SAUSA300_0240	PTS system, galactitol-specific enzyme II, B component	131%	166%	1/3
Tn0560	SAUSA300_0351	Putative membrane protein	131%	125%	3/3
Tn0584	SAUSA300_2313	L-lactate permease	131%	133%	1/3
Tn0608	SAUSA300_2312	Malate:quinone-oxidoreductase (*mqo*)	131%	190%	1/3
Tn0644	SAUSA300_1178	Recombinase A protein (*recA*)	131%	145%	3/3
Tn1419	SAUSA300_2576	Phosphotransferase system, fructose-specific IIABC component	131%	128%	2/3
Tn1435	SAUSA300_0050	Conserved hypothetical protein	131%	130%	3/3
Tn0303	SAUSA300_0314	Sodium:solute symporter family protein	132%	142%	2/3
Tn0604	SAUSA300_0859	NADH-dependent flavin oxidoreductase	132%	169%	3/3
Tn0720	SAUSA300_0567	Conserved hypothetical protein	132%	142%	2/3
Tn0722	SAUSA300_1135	Putative membrane protein	132%	144%	2/3
Tn0056	SAUSA300_1638	Sensory box histidine kinase PhoR (*phoR*)	133%	146%	3/3
Tn0068	SAUSA300_0925	5' nucleotidase family protein	133%	141%	3/3
Tn0240	SAUSA300_1671	Conserved hypothetical protein	133%	159%	2/3
Tn0418	SAUSA300_0970	Phosphoribosylformylglycinamidine synthase I (*purQ*)	133%	134%	3/3
Tn0642	SAUSA300_0680	Multidrug resistance protein (*norA*)	133%	132%	1/3
Tn0835	SAUSA300_1696	D-alanine aminotransferase (*dat*)	133%	171%	1/3
Tn0072	SAUSA300_0111	Conserved hypothetical protein	134%	197%	2/3
Tn0073	SAUSA300_1940	Phage portal protein	134%	130%	1/3
Tn0086	SAUSA300_1851	Putative membrane protein	134%	200%	2/3
Tn0626	SAUSA300_2277	Imidazolonepropionase (*hutI*)	134%	148%	2/3

Tn1342	SAUSA300_1285	ABC transporter, ATP-binding protein	134%	166%	1/3
Tn0145	SAUSA300_2128	Putative drug transporter	135%	180%	1/3
Tn1126	SAUSA300_0830	Conserved hypothetical protein	135%	208%	3/3
Tn1432	SAUSA300_0862	Glycerophosphoryl diester phosphodiesterase (*glpQ*)	135%	126%	2/3
Tn0298	SAUSA300_1485	Conserved hypothetical protein	136%	179%	3/3
Tn0310	SAUSA300_1208	Conserved hypothetical protein	136%	176%	3/3
Tn0472	SAUSA300_2487	Ferrous iron transport protein B (*feoB*)	137%	178%	1/3
Tn0321	SAUSA300_1336	Conserved hypothetical protein	139%	167%	2/3
Tn0557	SAUSA300_0915	Conserved hypothetical protein	139%	147%	3/3
Tn0718	SAUSA300_1383	PhiSLT ORF484-like protein, lysin	139%	159%	2/3
Tn0776	SAUSA300_0772	Clumping factor A (*clfA*)	140%	128%	1/3
Tn0299	SAUSA300_2090	Deoxyribose-phosphate aldolase (*deoC*)	141%	129%	2/3
Tn0574	SAUSA300_2445	Transcriptional regulator, MerR family	142%	168%	2/3
Tn0041	SAUSA300_2463	D-lactate dehydrogenase (*ddh*)	143%	184%	1/3
Tn0571	SAUSA300_0374	Putative membrane protein	143%	195%	3/3
Tn1293	SAUSA300_2167	Conserved hypothetical protein	143%	199%	3/3
Tn1403	SAUSA300_0706	Putative osmoprotectant ABC transporter, ATP-binding protein	143%	134%	2/3
Tn0400	SAUSA300_0357	5-methyltetrahydroteroyltriglutamate--homocysteine S-methyltransferase (*metE*)	145%	136%	3/3
Tn0402	SAUSA300_1131	30S ribosomal protein S16	145%	132%	1/3
Tn0088	SAUSA300_0358	Putative 5-methyltetrahydrofolate--homocysteine methyltransferase	146%	136%	2/3
Tn0320	SAUSA300_1698	Conserved hypothetical protein	146%	182%	1/3
Tn0573	SAUSA300_1014	Pyruvate carboxylase (*pyc*)	146%	138%	3/3
Tn0777	SAUSA300_2166	Alpha-acetolactate synthase (*alsS*)	146%	127%	1/3
Tn0296	SAUSA300_0400	Exotoxin	147%	183%	1/3
Tn0414	SAUSA300_0401	Exotoxin	147%	198%	1/3
Tn0719	SAUSA300_0074	Oligopeptide permease, channel-forming protein (*opp-3B*)	147%	182%	1/3
Tn0070	SAUSA300_0226	3-hydroxyacyl-CoA dehydrogenase	148%	129%	1/3
Tn0394	SAUSA300_1417	PhiSLT ORF175-like protein	148%	168%	2/3

Tn0741	SAUSA300_2320	Conserved hypothetical protein	148%	161%	1/3
Tn0469	SAUSA300_1939	Phi77 ORF015-like protein, putative protease	149%	136%	3/3
Tn0395	SAUSA300_1516	ABC transporter, ATP-binding protein	150%	206%	3/3
Tn0547	SAUSA300_1809	Putative membrane protein	150%	210%	2/3
Tn0733	SAUSA300_1804	Conserved hypothetical protein	151%	177%	1/3
Tn0396	SAUSA300_2314	Conserved hypothetical protein	152%	196%	3/3
Tn0413	SAUSA300_1718	Arsenical pump membrane protein (*arsB*)	152%	132%	3/3
Tn0470	SAUSA300_2617	Putative cobalt ABC transporter, ATP-binding protein	152%	203%	1/3
Tn0572	SAUSA300_0444	LysR family regulatory protein (*gltC*)	152%	136%	2/3
Tn0069	SAUSA300_1843	D-isomer specific 2-hydroxyacid dehydrogenase family protein	153%	152%	3/3
Tn1337	SAUSA300_1609	Type III leader peptidase family protein	153%	195%	1/3
Tn0043	SAUSA300_1019	Conserved hypothetical protein	155%	141%	1/3
Tn0468	SAUSA300_0155	Capsular polysaccharide biosynthesis protein Cap5D (*cap5D*)	156%	160%	3/3
Tn1452	SAUSA300_1167	Polyribopolyribonucleotide nucleotidyltransferase (*pnpA*)	156%	142%	1/3
Tn0053	SAUSA300_0639	Conserved hypothetical protein	158%	151%	3/3
Tn0057	SAUSA300_1916	Aminotransferase	158%	143%	3/3
Tn1338	SAUSA300_1163	Ribosome-binding factor A (*rbfA*)	160%	144%	3/3
Tn0051	SAUSA300_2504	Acyltransferase	161%	149%	3/3
Tn0317	SAUSA300_0207	Conserved hypothetical protein	161%	180%	2/3
Tn0398	SAUSA300_1312	Acetyltransferase, GNAT family	161%	190%	1/3
Tn0570	SAUSA300_1896	Prephenate dehydratase (*pheA*)	161%	140%	2/3
Tn0318	SAUSA300_1030	Iron transport associated domain protein (*isdC*)	163%	136%	3/3
Tn0319	SAUSA300_2391	glycine betaine/carnitine/choline ABC transporter (*opuCc*)	163%	162%	1/3
Tn0392	SAUSA300_2429	Staphylococcal tandem lipoprotein	163%	134%	1/3
Tn0052	SAUSA300_0265	Putative ribose operon repressor	165%	145%	1/3
Tn0397	SAUSA300_0785	Acetyltransferase, GNAT family	165%	183%	3/3
Tn0050	SAUSA300_0322	NADH-dependent flavin oxidoreductase, Oye family	171%	170%	1/3
Tn0569	SAUSA300_1410	Virulence-associated protein E	173%	186%	1/3
Tn1219	SAUSA300_2110	Truncated FmtB protein (*fmtB*)	174%	183%	1/3

Tn0568	SAUSA300_2109	Truncated FmtB protein (*fmtB*)	175%	176%	3/3
Tn1217	SAUSA300_0202	Peptide ABC transporter, permease protein	176%	137%	2/3
Tn1031	SAUSA300_0630	ABC transporter, ATP-binding protein	178%	170%	3/3
Tn0567	SAUSA300_1064	Transporter, TRAP family	184%	157%	2/3
Tn0565	SAUSA300_0849	Na(+)/H(+) antiporter subunit G (*mnhG*)	190%	218%	3/3
Tn0566	SAUSA300_2535	2-dehydropantoate 2-reductase (*panE*)	193%	175%	3/3
Tn1122	SAUSA300_1391	PhiSLT ORF527-like protein	194%	195%	2/3
Tn0049	SAUSA300_1330	Threonine dehydratase (*ilvA*)	195%	147%	3/3
Tn1218	SAUSA300_1296	Conserved hypothetical protein (*msaA*)	196%	167%	1/3
Tn1029	SAUSA300_2106	Putative transcriptional regulator	198%	140%	1/3
Tn0724	SAUSA300_0776	Thermonuclease precursor (*nuc*)	199%	156%	2/3
Tn1028	SAUSA300_0873	Coenzyme A disulfide reductase (*cdr*)	208%	187%	3/3

Supplementary Table 9: Overview of *bursa aurealis* transposon insertion mutants with a decrease in biofilm formation capacity as compared to UAS391-Ery^S. Biofilm formation under static or flow conditions is mentioned as % compared to UAS391-Ery^S (100%). Insertion location of the transposon is given in function of the gene length (e.g. 1/3, 2/3 or 3/3 of the gene).

Decrease in biofilm formation					
Name Tn	**Locus tag FPR3757**	**Gene name**	**Biofilm formation under static conditions**	**Biofilm formation under flow conditions**	**Insertion location of transposon**
Tn0831	SAUSA300_0241	PTS system, sorbitol-specific IIC component	26%	17%	2/3
Tn1730	SAUSA300_1938	Phi77 ORF006-like protein, putative capsid protein	30%	18%	3/3
Tn0006	SAUSA300_2251	Dehydrogenase family protein	33%	14%	2/3
Tn0004	SAUSA300_0877	Chaperone clpB (*clpB*)	35%	13%	3/3
Tn0427	SAUSA300_2386	Beta-lactamase	36%	14%	2/3
Tn0019	SAUSA300_2410	Oligopeptide ABC transporter, permease protein	37%	15%	3/3
Tn0444	SAUSA300_1210	Conserved hypothetical protein	37%	13%	3/3
Tn0778	SAUSA300_2453	ABC transporter, ATP-binding protein	37%	20%	2/3
Tn0021	SAUSA300_0034	IS1272 transposase	38%	10%	3/3
Tn0013	SAUSA300_2101	SAP domain protein	39%	12%	3/3
Tn0002	SAUSA300_0540	HAD-superfamily hydrolase, subfamily IA, variant 1	40%	14%	3/3

Tn0014	SAUSA300_2446	Conserved hypothetical protein	41%	16%	2/3
Tn0426	SAUSA300_1141	Endopeptidase resistance gene	41%	19%	3/3
Tn1321	SAUSA300_0182	4-phosphopantetheinyl transferase superfamily protein	41%	11%	2/3
Tn0015	SAUSA300_1404	PhiSLT ORF563-like protein, terminase, large subunit	42%	18%	1/3
Tn0028	SAUSA300_1327	Cell surface protein (*ebh*)	42%	15%	3/3
Tn0012	SAUSA300_2342	Respiratory nitrate reductase, beta subunit (*narH*)	43%	16%	1/3
Tn0018	SAUSA300_0121	Putative drug transporter	44%	15%	1/3
Tn0979	SAUSA300_2579	N-acetylmuramoyl-L-alanine amidase domain protein	44%	15%	1/3
Tn0008	SAUSA300_0134	Polysaccharide extrusion protein	45%	16%	1/3
Tn0447	SAUSA300_0583	Conserved hypothetical protein	46%	13%	1/3
Tn0009	SAUSA300_0068	Cadmium-exporting ATPase, function	48%	11%	1/3
Tn1562	SAUSA300_2126	Drug resistance transporter, EmrB/QacA subfamily	48%	14%	3/3
Tn0448	SAUSA300_1792	Conserved hypothetical protein	49%	14%	3/3
Tn1113	SAUSA300_2431	Putative helicase	49%	10%	1/3
Tn0192	SAUSA300_1883	High affinity proline permease (*putP*)	50%	13%	2/3
Tn0985	SAUSA300_1113	Protein kinase (*pknB*)	51%	15%	3/3
Tn1310	SAUSA300_2454	Membrane spanning protein	51%	23%	1/3
Tn0602	SAUSA300_1189	DNA mismatch repair protein mutL (*mutL*)	52%	64%	1/3
Tn1619	SAUSA300_1702	Cell wall surface anchor family protein (*sasC*)	52%	41%	3/3
Tn0231	SAUSA300_2085	Conserved hypothetical protein	53%	11%	3/3
Tn1229	SAUSA300_1670	D-3-phosphoglycerate dehydrogenase (*serA*)	53%	47%	3/3
Tn1235	SAUSA300_0845	Cytosol aminopeptidase (*ampA*)	53%	17%	1/3
Tn0443	SAUSA300_0975	Bifunctional purine biosynthesis protein (*purH*)	54%	14%	1/3
Tn0445	SAUSA300_1991	Accessory gene regulator protein C (*agrC*)	54%	19%	1/3
Tn0025	SAUSA300_1674	Putative serine protease HtrA	55%	11%	3/3
Tn0219	SAUSA300_1012	Conserved hypothetical protein	55%	18%	2/3
Tn1094	SAUSA300_0181	Non-ribosomal peptide synthetase	55%	10%	1/3
Tn1231	SAUSA300_1260	Prephenate dehydrogenase	55%	49%	3/3
Tn1554	SAUSA300_2385	Putative membrane protein	55%	59%	1/3

Tn1735	SAUSA300_1176	CDP-diacylglycerol--glycerol-3-phosphate 3-phosphatidyltransferase (*pgsA*)	55%	11%	3/3
Tn1831	SAUSA300_0220	Formate acetyltransferase (*pflB*)	55%	18%	3/3
Tn0022	SAUSA300_1177	Competence/damage-inducible protein cinA (*cinA*)	56%	38%	1/3
Tn1005	SAUSA300_2602	Intercellular adhesion protein C (*icaC*)	56%	10%	3/3
Tn1862	SAUSA300_1716	Conserved hypothetical protein	56%	47%	1/3
Tn0173	SAUSA300_2589	LPXTG-motif cell wall surface anchor family protein	57%	17%	2/3
Tn0327	SAUSA300_2461	Glyoxalase family protein	57%	12%	1/3
Tn1307	SAUSA300_0092	Conserved hypothetical protein	57%	43%	3/3
Tn0038	SAUSA300_2366	Gamma-hemolysin component C (*hlgC*)	58%	12%	3/3
Tn0161	SAUSA300_2241	Urease accessory protein UreE (*ureE*)	58%	12%	3/3
Tn0964	SAUSA300_0104	Transcriptional regulator, AraC family	58%	19%	3/3
Tn1309	SAUSA300_2127	Conserved hypothetical protein	58%	14%	3/3
Tn1277	SAUSA300_0935	Conserved hypothetical protein	59%	19%	3/3
Tn1351	SAUSA300_1402	PhiSLT ORF257-like protein, putative prophage protease	59%	11%	1/3
Tn1618	SAUSA300_1844	Bacterioferritin comigratory protein	59%	14%	3/3
Tn0023	SAUSA300_1509	Peptidase, rhomboid family	60%	19%	2/3
Tn0442	SAUSA300_0914	Sodium:alanine symporter family protein	60%	10%	3/3
Tn0502	SAUSA300_2258	Formate dehydrogenase, alpha subunit	60%	16%	3/3
Tn1177	SAUSA300_2440	Fibronectin binding protein B (*fnbB*)	60%	14%	3/3
Tn0332	SAUSA300_0085	Conserved hypothetical protein	61%	13%	3/3
Tn0505	SAUSA300_1905	Conserved hypothetical protein	61%	11%	2/3
Tn0679	SAUSA300_0356	Conserved hypothetical protein	61%	18%	2/3
Tn0986	SAUSA300_1584	ATPase, AAA family	61%	18%	3/3
Tn1849	SAUSA300_0125	Pyridoxal-dependent decarboxylase	61%	16%	1/3
Tn0428	SAUSA300_0891	Oligopeptide ABC transporter, substrate-binding protein (*oppA*)	62%	12%	3/3
Tn0504	SAUSA300_2384	Putative Na+/H+ antiporter	62%	36%	2/3
Tn0523	SAUSA300_0763	Carboxylesterase (*est*)	62%	14%	2/3
Tn1150	SAUSA300_2150	PTS system, lactose-specific IIBC component (*lacE*)	62%	17%	2/3

Tn1558	SAUSA300_1403	PhiSLT ORF412-like protein, portal protein	62%	26%	3/3
Tn1677	SAUSA300_1005	Mn2+/Fe2+ transporter, NRAMP family	62%	16%	2/3
Tn0424	SAUSA300_0180	Integral membrane protein LmrP	63%	16%	3/3
Tn0578	SAUSA300_2027	Alanine racemase (*alr*)	63%	13%	3/3
Tn1191	SAUSA300_1280	Phosphate ABC transporter, ATP-binding protein (*pstB*)	63%	17%	1/3
Tn1209	SAUSA300_2405	Putative membrane protein	63%	18%	1/3
Tn1572	SAUSA300_2404	Conserved hypothetical protein	63%	15%	1/3
Tn1882	SAUSA300_0126	Conserved hypothetical protein	63%	17%	1/3
Tn0460	SAUSA300_1401	PhiSLT ORF387-like protein, putative phage capsid protein	64%	52%	3/3
Tn0483	SAUSA300_0036	Conserved hypothetical protein	64%	20%	1/3
Tn0506	SAUSA300_2161	Hyaluronate lyase precursor (*hysA*)	64%	16%	1/3
Tn0583	SAUSA300_1652	Conserved hypothetical protein	64%	15%	1/3
Tn1100	SAUSA300_1226	Homoserine dehydrogenase	64%	14%	1/3
Tn0984	SAUSA300_2163	Conserved hypothetical protein	65%	18%	2/3
Tn1176	SAUSA300_0353	Conserved hypothetical protein	65%	11%	3/3
Tn1326	SAUSA300_0475	SpoVG protein	65%	17%	1/3
Tn1747	SAUSA300_0662	Acetyltransferase, GNAT family	65%	13%	3/3
Tn1847	SAUSA300_2037	ATP-dependent RNA helicase	65%	12%	3/3
Tn1848	SAUSA300_1068	Antibacterial protein	65%	13%	3/3
Tn0034	SAUSA300_1693	Conserved hypothetical protein	66%	19%	3/3
Tn0543	SAUSA300_0767	Conserved hypothetical protein	66%	21%	3/3
Tn0962	SAUSA300_0955	Autolysin (*atl*)	66%	26%	3/3
Tn1263	SAUSA300_0732	Conserved hypothetical protein	66%	13%	1/3
Tn1708	SAUSA300_2444	Gluconate operon transcriptional repressor (*gntR*)	66%	16%	1/3
Tn1754	SAUSA300_2565	Clumping factor B (*clfB*)	66%	38%	1/3
Tn1786	SAUSA300_0589	Aldo/keto reductase family protein	66%	21%	3/3
Tn0135	SAUSA300_2571	Arginine repressor (*argR*)	67%	12%	3/3
Tn0501	SAUSA300_1699	Pseudouridine synthase, family 1	67%	21%	3/3
Tn0122	SAUSA300_2346	Nitrite reductase (NAD(P)H), large subunit (*nirB*)	68%	13%	1/3

Tn0217	SAUSA300_1805	RNA methyltransferase	68%	17%	1/3
Tn0423	SAUSA300_2215	Conserved hypothetical protein	68%	13%	1/3
Tn0697	SAUSA300_2344	Uroporphyrin-III C-methyl transferase	68%	15%	3/3
Tn0983	SAUSA300_0312	Indigoidine synthase family protein	68%	12%	3/3
Tn1099	SAUSA300_2634	ABC transporter, permease protein	68%	15%	2/3
Tn1175	SAUSA300_0047	Conserved hypothetical protein	68%	24%	1/3
Tn0104	SAUSA300_1388	PhiSLT ORF488-like protein	69%	14%	1/3
Tn0116	SAUSA300_0313	Putative nucleoside permease NupC	69%	16%	1/3
Tn0218	SAUSA300_1500	Putative competence protein ComYC	69%	21%	2/3
Tn0345	SAUSA300_1563	Acetyl-CoA carboxylase, biotin carboxylase (*accC*)	69%	24%	1/3
Tn0582	SAUSA300_2340	Respiratory nitrate reductase, gamma subunit (*narI*)	69%	23%	3/3
Tn0678	SAUSA300_1397	PhiSLT ORF213-like protein, major tail protein	69%	17%	3/3
Tn0973	SAUSA300_1374	Conserved hypothetical protein	69%	17%	2/3
Tn1093	SAUSA300_0571	Lipoate-protein ligase A family protein	69%	15%	3/3
Tn1860	SAUSA300_0214	Conserved hypothetical protein	69%	19%	1/3
Tn0191	SAUSA300_0139	Putative tetracycline resistance protein	70%	15%	3/3
Tn1171	SAUSA300_2373	Dethiobiotin synthase (*bioD*)	70%	14%	1/3
Tn1239	SAUSA300_0712	Amino acid/peptide transporter (Peptide: H+ symporter)	70%	10%	2/3
Tn1857	SAUSA300_2254	Glycerate dehydrogenase-like protein	70%	16%	2/3

3.2.1.6.4. References

1. Donlan, R.M., *Biofilms: microbial life on surfaces.* Emerg Infect Dis, 2002. **8**(9): p. 881-90.
2. Gilbert, P., J. Das, and I. Foley, *Biofilm susceptibility to antimicrobials.* Adv Dent Res, 1997. **11**(1): p. 160-7.
3. Zapotoczna, M., E. O'Neill, and J.P. O'Gara, *Untangling the Diverse and Redundant Mechanisms of Staphylococcus aureus Biofilm Formation.* PLoS Pathog, 2016. **12**(7): p. e1005671.
4. Vuong, C., et al., *Polysaccharide intercellular adhesin (PIA) protects Staphylococcus epidermidis against major components of the human innate immune system.* Cell Microbiol, 2004. **6**(3): p. 269-75.
5. Knobloch, J.K., et al., *Biofilm formation by Staphylococcus epidermidis depends on functional RsbU, an activator of the sigB operon: differential activation mechanisms due to ethanol and salt stress.* J Bacteriol, 2001. **183**(8): p. 2624-33.
6. Pozzi, C., et al., *Methicillin resistance alters the biofilm phenotype and attenuates virulence in Staphylococcus aureus device-associated infections.* PLoS Pathog, 2012. **8**(4): p. e1002626.
7. Cucarella, C., et al., *Bap, a Staphylococcus aureus surface protein involved in biofilm formation.* J Bacteriol, 2001. **183**(9): p. 2888-96.

8. O'Neill, E., et al., *A novel Staphylococcus aureus biofilm phenotype mediated by the fibronectin-binding proteins, FnBPA and FnBPB.* J Bacteriol, 2008. **190**(11): p. 3835-50.
9. Corrigan, R.M., H. Miajlovic, and T.J. Foster, *Surface proteins that promote adherence of Staphylococcus aureus to human desquamated nasal epithelial cells.* BMC Microbiol, 2009. **9**: p. 22.
10. Merino, N., et al., *Protein A-mediated multicellular behavior in Staphylococcus aureus.* J Bacteriol, 2009. **191**(3): p. 832-43.
11. Houston, P., et al., *Essential role for the major autolysin in the fibronectin-binding protein-mediated Staphylococcus aureus biofilm phenotype.* Infect Immun, 2011. **79**(3): p. 1153-65.
12. Bose, J.L., et al., *Contribution of the Staphylococcus aureus Atl AM and GL murein hydrolase activities in cell division, autolysis, and biofilm formation.* PLoS One, 2012. **7**(7): p. e42244.
13. Vanhommerig, E., et al., *Comparison of biofilm formation between major clonal lineages of methicillin-resistant Staphylococcus aureus.* PLoS One, 2014. **9**(8): p. e104561.
14. Fey, P.D., et al., *A genetic resource for rapid and comprehensive phenotype screening of nonessential Staphylococcus aureus genes.* MBio, 2013. **4**(1): p. e00537-12.
15. Bae, T., et al., *Generating a collection of insertion mutations in the Staphylococcus aureus genome using bursa aurealis.* Methods Mol Biol, 2008. **416**: p. 103-16.
16. Yajjala, V.K., et al., *Generation of a Transposon Mutant Library in Staphylococcus aureus and Staphylococcus epidermidis Using bursa aurealis.* Methods Mol Biol, 2016. **1373**: p. 103-10.
17. Sabirova, J.S., et al., *Fatty acid kinase A is an important determinant of biofilm formation in Staphylococcus aureus USA300.* BMC Genomics, 2015. **16**(1): p. 861.
18. De Backer, S., et al., *Enzymes Catalyzing the TCA- and Urea Cycle Influence the Matrix Composition of Biofilms Formed by Methicillin-Resistant Staphylococcus aureus USA300.* Microorganisms, 2018. **6**(4).
19. Hall, B.G., et al., *Growth rates made easy.* Mol Biol Evol, 2014. **31**(1): p. 232-8.
20. Institute, C.a.L.S., *Performance Standards for Antimicrobial Susceptibility Testing; Twenty-eight Informational Supplement*. CLSI document M100-S25. 2018, 950 West Valley Road, Suite 2500, Pennsylvania 19087 USA: Clinical and Laboratory Standards Institute.
21. Sabirova, J.S., et al., *Complete genome sequences of two prolific biofilm-forming Staphylococcus aureus isolates belonging to USA300 and EMRSA-15 clonal lineages.* Genome Announc, 2014. **2**(3).
22. Haft, D.H., et al., *TIGRFAMs and Genome Properties in 2013.* Nucleic Acids Res, 2013. **41**(Database issue): p. D387-95.
23. Finn, R.D., J. Clements, and S.R. Eddy, *HMMER web server: interactive sequence similarity searching.* Nucleic Acids Res, 2011. **39**(Web Server issue): p. W29-37.
24. Fuchs, S., et al., *AureoWiki The repository of the Staphylococcus aureus research and annotation community.* Int J Med Microbiol, 2018. **308**(6): p. 558-568.
25. Sihto, H.M., et al., *Validation of reference genes for normalization of qPCR mRNA expression levels in Staphylococcus aureus exposed to osmotic and lactic acid stress conditions encountered during food production and preservation.* FEMS Microbiol Lett, 2014. **356**(1): p. 134-40.
26. Beenken, K.E., et al., *Global gene expression in Staphylococcus aureus biofilms.* J Bacteriol, 2004. **186**(14): p. 4665-84.
27. Resch, A., et al., *Differential gene expression profiling of Staphylococcus aureus cultivated under biofilm and planktonic conditions.* Appl Environ Microbiol, 2005. **71**(5): p. 2663-76.
28. Fuchs, S., et al., *Anaerobic gene expression in Staphylococcus aureus.* J Bacteriol, 2007. **189**(11): p. 4275-89.
29. Mashruwala, A.A., A.V. Guchte, and J.M. Boyd, *Impaired respiration elicits SrrAB-dependent programmed cell lysis and biofilm formation in Staphylococcus aureus.* Elife, 2017. **6**.
30. Sauer, K., et al., *Characterization of nutrient-induced dispersion in Pseudomonas aeruginosa PAO1 biofilm.* J Bacteriol, 2004. **186**(21): p. 7312-26.
31. Mangalea, M.R., B.A. Plumley, and B.R. Borlee, *Nitrate Sensing and Metabolism Inhibit Biofilm Formation in the Opportunistic Pathogen Burkholderia pseudomallei by Reducing the Intracellular Concentration of c-di-GMP.* Front Microbiol, 2017. **8**: p. 1353.

32. Ren, D., et al., *Differential gene expression for investigation of Escherichia coli biofilm inhibition by plant extract ursolic acid.* Appl Environ Microbiol, 2005. **71**(7): p. 4022-34.
33. Waters, E.M., et al., *Convergence of Staphylococcus aureus Persister and Biofilm Research: Can Biofilms Be Defined as Communities of Adherent Persister Cells?* PLoS Pathog, 2016. **12**(12): p. e1006012.
34. De Groote, V.N., et al., *Novel persistence genes in Pseudomonas aeruginosa identified by high-throughput screening.* FEMS Microbiol Lett, 2009. **297**(1): p. 73-9.
35. DeFrancesco, A.S., et al., *Genome-wide screen for genes involved in eDNA release during biofilm formation by Staphylococcus aureus.* Proc Natl Acad Sci U S A, 2017. **114**(29): p. E5969-E5978.
36. Kiedrowski, M.R., et al., *Nuclease modulates biofilm formation in community-associated methicillin-resistant Staphylococcus aureus.* PLoS One, 2011. **6**(11): p. e26714.
37. Mann, E.E., et al., *Modulation of eDNA release and degradation affects Staphylococcus aureus biofilm maturation.* PLoS One, 2009. **4**(6): p. e5822.
38. Liu, J., et al., *A Nuclease from Streptococcus mutans Facilitates Biofilm Dispersal and Escape from Killing by Neutrophil Extracellular Traps.* Front Cell Infect Microbiol, 2017. **7**: p. 97.
39. Zhu, Y., et al., *RpiR homologues may link Staphylococcus aureus RNAIII synthesis and pentose phosphate pathway regulation.* J Bacteriol, 2011. **193**(22): p. 6187-96.
40. Foster, T.J., et al., *Adhesion, invasion and evasion: the many functions of the surface proteins of Staphylococcus aureus.* Nat Rev Microbiol, 2014. **12**(1): p. 49-62.
41. Kiran, M.D., et al., *OpuC – an ABC Transporter that is Associated with Staphylococcus Aureus Pathogenesis.* The International Journal of Artificial Organs, 2018. **32**(9): p. 600-610.
42. Shaw, L.N., et al., *Inactivation of traP has no effect on the agr quorum-sensing system or virulence of Staphylococcus aureus.* Infect Immun, 2007. **75**(9): p. 4519-27.
43. Tsang, L.H., et al., *Mutation of traP in Staphylococcus aureus has no impact on expression of agr or biofilm formation.* Infect Immun, 2007. **75**(9): p. 4528-33.
44. Frees, D., et al., *Clp ATPases are required for stress tolerance, intracellular replication and biofilm formation in Staphylococcus aureus.* Mol Microbiol, 2004. **54**(5): p. 1445-62.
45. Herzberg, M., et al., *YdgG (TqsA) controls biofilm formation in Escherichia coli K-12 through autoinducer 2 transport.* J Bacteriol, 2006. **188**(2): p. 587-98.
46. Scherr, T.D., et al., *Staphylococcus aureus Biofilms Induce Macrophage Dysfunction Through Leukocidin AB and Alpha-Toxin.* MBio, 2015. **6**(4).
47. Wertheim, H.F., et al., *Key role for clumping factor B in Staphylococcus aureus nasal colonization of humans.* PLoS Med, 2008. **5**(1): p. e17.
48. Abraham, N.M. and K.K. Jefferson, *Staphylococcus aureus clumping factor B mediates biofilm formation in the absence of calcium.* Microbiology, 2012. **158**(Pt 6): p. 1504-12.
49. Schneewind, O. and D. Missiakas, *Sortases, Surface Proteins, and Their Roles in Staphylococcus aureus Disease and Vaccine Development.* Microbiol Spectr, 2019. **7**(1).
50. Komatsuzawa, H., et al., *Tn551-mediated insertional inactivation of the fmtB gene encoding a cell wall-associated protein abolishes methicillin resistance in Staphylococcus aureus.* J Antimicrob Chemother, 2000. **45**(4): p. 421-31.
51. Stapleton, P. and P. Taylor, *Methicillin resistance in Staphylococcus aureus.* Sci Prog, 2002. **85**(Pt 1): p. 57-72.
52. de Jonge, B., et al., *Peptidoglycan composition of a highly methicillin-resistant Staphylococcus aureus strain.* J Biol Chem, 1992. **267**(16): p. 11248-54.
53. Fey, P.D., *Modality of bacterial growth presents unique targets: how do we treat biofilm-mediated infections?* Curr Opin Microbiol, 2010. **13**(5): p. 610-5.
54. Cheng, A.G., D. Missiakas, and O. Schneewind, *The giant protein Ebh is a determinant of Staphylococcus aureus cell size and complement resistance.* J Bacteriol, 2014. **196**(5): p. 971-81.
55. Schroeder, K., et al., *Molecular characterization of a novel Staphylococcus aureus surface protein (SasC) involved in cell aggregation and biofilm accumulation.* PLoS One, 2009. **4**(10): p. e7567.

3.3. Identification of biofilm-associated candidate genes using *in vitro* biofilm models of staphylococcal infection and comparative genomics

3.3.1. Enzymes catalysing the TCA- and urea cycles influence the matrix composition of biofilms formed by methicillin-resistant Staphylococcus aureus USA300

Sarah De Backer [1], Julia Sabirova [1], Ines De Pauw [1], Henri De Greve [2, 3], Jean-Pierre Hernalsteens [4], Herman Goossens [1] and Surbhi Malhotra-Kumar [1, *]

[1] Department of Medical Microbiology, Vaccine & Infectious Diseases Institute, University of Antwerp, 2610 Wilrijk, Belgium. [2] Structural & Molecular Microbiology, VIB-VUB Centre for Structural Biology, 1050 Brussels, Belgium. [3] Structural Biology Brussels, Vrije Universiteit Brussel, 1050 Brussels, Belgium. [4] Viral Genetics Laboratory, Vrije Universiteit Brussel, 1050 Brussels, Belgium.

* Corresponding author mailing address: Department of Medical Microbiology, Campus Drie Eiken, University of Antwerp, S6, Universiteitsplein 1, 2610 Wilrijk, Belgium. Phone: 32-3-265-27-52. Fax: 32-3-265-26-63. E-mail: surbhi.malhotra@uantwerpen.be

Published in: Microorganisms. 2018 Oct 29;6(4). pii: E113. doi: 10.3390/microorganisms6040113.

3.3.1.1. Abstract

In methicillin-sensitive *Staphylococcus aureus* (MSSA), the tricarboxylic acid (TCA) cycle is known to negatively regulate the production of the major biofilm-matrix exopolysaccharide, PIA/PNAG. However, methicillin-resistant *S. aureus* (MRSA) produce a primarily proteinaceous biofilm matrix, and contribution of the TCA-cycle therein remains unclear. Utilizing USA300-JE2 Tn-mutants (NARSA) in genes encoding TCA- and urea cycle enzymes for transduction into a prolific biofilm-forming USA300 strain (UAS391-Ery^{s}), we studied the contribution of the TCA- and urea cycle and of proteins, eDNA and PIA/PNAG, to the matrix. Genes targeted in the urea cycle encoded argininosuccinate lyase and arginase (*argH*::Tn and *rocF*::Tn), and in the TCA-cycle encoded succinyl-CoA synthetase, succinate dehydrogenase, aconitase, isocitrate dehydrogenase, fumarate hydratase class II, and citrate synthase II (*sucC*::Tn, *sdhA/B*::Tn, *acnA*::Tn, *icd*::Tn, *fumC*::Tn and *gltA*::Tn). Biofilm formation was significantly decreased under no flow and flow conditions by *argH::*Tn, *fumC::*Tn, and *sdhA/B::*Tn (range OD_{492} 0.374−0.667; integrated densities 2.065−4.875) compared to UAS391-Ery^{S} (OD_{492} 0.814; integrated density 10.676) ($p \leq 0.008$). Cellular and matrix stains, enzymatic treatment (Proteinase K,

DNaseI), and reverse-transcriptase PCR-based gene-expression analysis of fibronectin-binding proteins *(fnbA/B)* and the staphylococcal accessory regulator *(sarA)* on pre-formed UAS391-Ery^{s} and Tn-mutant biofilms showed: (i) < 1% PIA/PNAG in the proteinaceous/eDNA matrix; (ii) increased proteins under no flow and flow in the matrix of Tn mutant biofilms (on average 50 and 51 (±11)%) compared to UAS391-Ery^{s} (on average 22 and 25 (±4)%) (p<0.001); and (iii) down- and up-regulation of *fnbA/B* and *sarA*, respectively, in Tn-mutants compared to UAS391-Ery^{S} (0.62-, 0.57-, and 2.23-fold on average). In conclusion, we show that the biofilm matrix of MRSA-USA300 and the corresponding Tn mutants is PIA/PNAG-independent and are mainly composed of proteins and eDNA. The primary impact of TCA-cycle inactivation was on the protein component of the biofilm matrix of MRSA-USA300.

3.3.1.2. Introduction

Nosocomial and community-acquired infections caused by *Staphylococcus aureus* range from superficial to life-threatening [1]. The pathogenic ability of *S. aureus* is greatly facilitated by its capacity to form biofilms, sessile microbial communities that remain embedded in an extracellular polymeric glycocalyx (matrix) or slime layer [2]. Interestingly, recent studies have highlighted differences in biofilm formation between methicillin-sensitive *S. aureus* (MSSA) and their (multi-) drug-resistant counterpart, methicillin-resistant *S. aureus* (MRSA) [3,4]. In MSSA, the primary polysaccharide that forms the biofilm matrix is encoded by the *icaADBC* operon and is known as polysaccharide intercellular adhesin PIA or poly-*N*-acetylglucosamine PNAG [5]. On the other hand, MRSA exhibits a primarily proteinaceous biofilm matrix, with very little contribution of PIA/PNAG [6], that is mediated by adhesins such as the fibronectin binding proteins FnBPA/B [7]. In addition, recent reports also show an important contribution of extracellular DNA (eDNA) to the MRSA biofilm matrix [8]. eDNA in *S. aureus* is released by cell lysis, which has been shown to be dependent on autolysins such as the major autolysin *atl* [9,10], and on the holin/antiholin system *cidA/lrgA* [10,11].

The tricarboxylic acid (TCA) cycle is a central metabolic pathway that generates energy (ATP) and precursors for biosynthesis of macromolecules like 2-oxoglutarate [12]. Its role in regulating PIA/PNAG production in staphylococcal species has been well-studied. In *S. epidermidis*, environmental changes that inhibited TCA-cycle activity also resulted in a massive derepression of PIA biosynthetic genes and increased PIA production [13,14]. This inverse correlation was also confirmed for MSSA in a rabbit catheter model of biofilm infection [15]. However, the contribution of the TCA-cycle, if any, to biofilm formation by MRSA

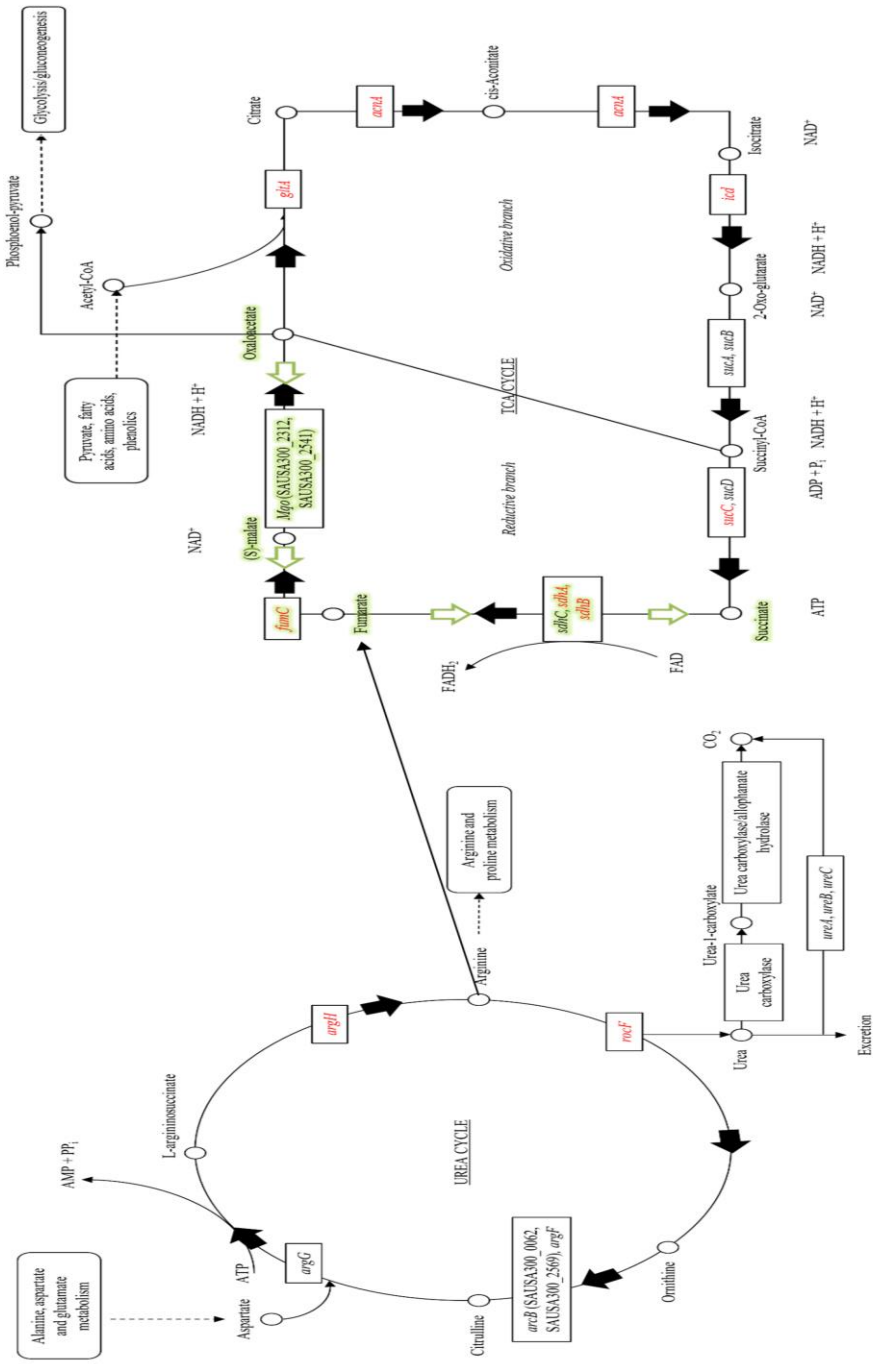

Figure 16: Schematic representation of the urea and tricarboxylic acid (TCA) cycles. Arginine is synthesized via the urea cycle. Carbamoyl phosphate reacts with ornithine to generate citrulline. An aspartate molecule adds to create argininosuccinate. ATP is cleaved to AMP and pyrophosphate to drive this reaction forward. Arginine is cleaved off argininosuccinate by the enzyme encoded by *argH* and can be used for protein synthesis. Hydrolysis of arginine generates ornithine and urea. Fumarate is the other product of the ArgH-

catalysed reaction and can be used in the TCA-cycle. Acetyl-CoA derived from pyruvate and other catabolic pathways enter the TCA-cycle. The acetyl group condenses with four-carbon oxaloacetate to produce citrate. Citrate rearranges to isocitrate, which is decarboxylated and forms NADH + H^+ by transferring $2H^+$ + $2e^-$. 2-Oxoglutarate is decarboxylated and transfers $2H^+$ + $2e^-$ to form NADH + H^+, while incorporating CoA to form succinyl-CoA. Succinate forms fumarate by transferring $2H^+$ + $2e^-$ resulting in $FADH_2$. Water is incorporated, and oxaloacetate is formed when $2H^+$ + $2e^-$ are transferred to form NADH + H^+. The pathway marked in green highlights the proposed model for NADH reoxidation (Arnon-Buchanan cycle).

In this study, utilizing Tn mutants, biofilm models, and various stains and enzymes, we studied the importance of the TCA- and urea cycle for biofilm formation by MRSA-USA300 and the net contribution of proteins, eDNA and PIA/PNAG, to the matrix.

3.3.1.3. Materials and methods

3.3.1.3.1. Bacterial strains and growth conditions

The strains used in this study are shown in **Table 2**. *Bursa aurealis* transposon (Tn) insertion mutations encoding functionally non-redundant TCA- and urea cycle enzymes (**Fig. 16**) in USA300-JE2 were obtained from the Nebraska Transposon Mutant Library (NTML, www.beiresources.org) [16]. Parental strains UAS391, UAS391-Ery^S (erythromycin resistance cured UAS391), and JE2 are all MRSA belonging to the highly virulent and widespread clonal lineage, USA300. These, as well as Tn insertion mutants, were routinely grown on Brain-Heart infusion (BHI; Becton, Dickinson and Company, USA) supplemented with 0.1% D(+)-glucose monohydrate (Merck Millipore, USA) and BHI Bacto™ agar (Becton, Dickinson and Company, USA) for biofilm, transduction and complementation experiments. Lysogeny broth (LB; Becton, Dickinson and Company, USA) was used for *Escherichia coli*. For the Tn-carrying *S. aureus* transductants with the erythromycin resistance marker *ermB*, 5 or 10 µg/mL erythromycin (Sigma-Aldrich®, USA) was supplemented to the growth medium.

Table 2: Bacterial strains and plasmids used during the TCA- and urea cycle study.

Name	Description	Source
	Strains	
UAS391	Prolific biofilm forming MRSA USA300 strain isolated from a patient with an abscess in a Belgian hospital.	[16, 17]
UAS391-Ery^S	Erythromycin-sensitive variant (loss of *ermC* gene) of *S. aureus* UAS391 obtained by plasmid curing through growth at 44°C during more than 48h.	[18]
JE2	Plasmid-cured (p01, a 3.1-kb cryptic plasmid, and p03, a 27-kb plasmid conferring resistance to erythromycin) derivative of MRSA USA300 LAC, isolated from skin and soft tissue infections in a detainee from the Los Angeles County jail.	[15]
RN0450 (NRS135)	MSSA strain derived from successive cycles of UV treatment of *S. aureus* strain NCTC8325 (NRS77), curing it of phages Φ11, Φ12, and Φ13.	NARSA repository
RN0451 (NRS136)	MSSA strain derived from *S. aureus* strain RN0450, lysogenic for phage Φ11.	NARSA repository

RN4220	Generated through UV and chemical mutagenesis of *S. aureus* strain NCTC 8325-4 and selected for transformability with DNA from *E. coli* (restriction deficient through mutation in *sau1 hsdR*).	NARSA repository
DH5α	Cloning strain with multiple mutations (*fhuA2 lac(del)U169 phoA glnV44 Φ80' lacZ(del)M15 gyrA96 recA1 relA1 endA1 thi-1 hsdR17*) that enable high-efficient transformations.	Thermo Fisher Scientific, Inc., USA
ATCC® 6538™	Positive quality control for biofilm formation of *S. aureus* under no flow conditions.	[19]
5374	Negative quality control for biofilm formation of *S. aureus* under no flow conditions.	[17]
ATCC® 25923™	PIA/PNAG-dependent biofilm producing strain used as positive quality control during fluorescent staining and enzymatic treatment of biofilm matrix.	[20]
NE106 (NR-46649)	Transposon mutant in JE2 with *bursa aurealis* disruption (insertion position: 943092) in argininosuccinate lyase (*argH*, EX97_04560; 943451..942071).	NARSA repository
NE134 (NR-46677)	Transposon mutant in JE2 with *bursa aurealis* disruption (insertion position: 2290057) in arginase (*rocF*, EX97_11090; 2290192..2289283).	NARSA repository
NE427 (NR-46970)	Transposon mutant in JE2 with *bursa aurealis* disruption (insertion position: 1985575) in fumarate hydratase, class II (*fumC*, EX97_09410; 1985597..1984211).	NARSA repository
NE491 (NR-47034)	Transposon mutant in JE2 with *bursa aurealis* disruption (insertion position: 1799416) in isocitrate dehydrogenase, NADP-dependent (*icd*, EX97_08575; 1799559..1798290).	NARSA repository
NE569	Transposon mutant in JE2 with *bursa aurealis* disruption (insertion position: 1247122) in succinyl-CoA synthetase, beta subunit (*sucC*, EX97_05980; 1260778..1261944).	NARSA repository
NE594 (NR-47137)	Transposon mutant in JE2 with *bursa aurealis* disruption (insertion position: 1800430) in citrate synthase II (*gltA*, EX97_08580; 1800729..1799607).	NARSA repository
NE626 (NR-47169)	Transposon mutant in JE2 with *bursa aurealis* disruption (insertion position: 1145819) in succinate dehydrogenase, flavoprotein subunit (*sdhA*, EX97_05490; 1145459..1147226).	NARSA repository
NE808 (NR-47351)	Transposon mutant in JE2 with *bursa aurealis* disruption (insertion position: 1147490) in succinate dehydrogenase iron-sulfur subunit (*sdhB*, EX97_05495; 1147225..1148041).	NARSA repository
NE861 (NR-47404)	Transposon mutant in JE2 with *bursa aurealis* disruption (insertion position: 1367722) in aconitate hydratase (*acnA*, EX97_06555; 1367131..1369837).	NARSA repository
Plasmids		
pALC2073	Contains the pSK236 vector, with the *tetR*-gene and the *xyl*/*tetO* promotor, originating from pWH35.	[21]
pGV5990	*argH* gene amplified with primers ArgH-1 and ArgH-2 and cloned in the *EcoRI* site of pALC2073 via Gibson cloning.	This study
pGV5992	*gltA* gene amplified with primers GltA-1 and GltA-2 and cloned in the *EcoRI* site of pALC2073 via Gibson cloning.	
pGV5994	*icd* gene amplified with primers Icd-1 and Icd-2 and cloned in the *EcoRI* site of pALC2073 via Gibson cloning.	
pGV5996	*sdhB* gene amplified with primers SdhB-1 and SdhB-2 and cloned in the *EcoRI* site of pALC2073 via Gibson cloning.	
pGV5998	*sucC* gene amplified with primers SucC-1 and SucC-2 and cloned in the *EcoRI* site of pALC2073 via Gibson cloning.	
pGV5999	*gltA* & *icd* genes (operon of two genes; 1st gene *gltA* & 2nd gene *icd*) amplified with primers GltA-1 and Icd-2 and cloned in the *EcoRI* site of pALC2073 via Gibson cloning.	
pGV6000	*sucC* genes (operon of two genes) amplified with primers SucC-1 and SucC-3 and cloned in the *EcoRI* site of pALC2073 via Gibson cloning.	
pGV6001	*sdhA* gene amplified with primer SdhA-1 and SdhA-2 and cloned in the *EcoRI* site of pALC2073 via Gibson cloning.	
pGV6002	*sdhA* (2nd gene in an operon of 3 genes) & *sdhB* (3rd gene in an operon of 3 genes) genes amplified with primers SdhA-1 and SdhB-2 and cloned in the *EcoRI* site of pALC2073 via Gibson cloning.	

pGV6003	*rocF* gene amplified with primers RocF-1 and RocF-2 and cloned in the *EcoRI* site of pALC2073 via Gibson cloning.	
pGV6005	*fumC* gene amplified with primers FumC-1 and FumC-2 and cloned in the *EcoRI* site of pALC2073 via Gibson cloning.	
pGV6007	*acnA* gene amplified with primers AcnA-1 and AcnA-2 and cloned in the *EcoRI* site of pALC2073 via Gibson cloning.	

3.3.1.3.2. Transduction experiments

Nine *bursa aurealis* Tn mutations in candidate genes of the TCA- and urea cycles were transduced with phage Φ11 from USA300-JE2 to UAS391-Ery^S. Gene knockouts in UAS391-Ery^S (*argH*::Tn, *icd*::Tn, *acnA*::Tn, *gltA*::Tn, *rocF*::Tn, *fumC*::Tn, *sdhA*::Tn, *sdhB*::Tn, and *sucC*::Tn) were constructed through phage Φ11-mediated homologous recombination of the chromosomal UAS391-Ery^S genes with mutated alleles carried by NTML USA300-JE2 Tn insertion mutants, as described in **Table 2** [17].

3.3.1.3.3. Growth rate analysis

To exclude the possibility of changes in biofilm mass due to a pleiotropic effect on the bacterial growth rate, an overnight grown culture of the Tn mutants or UAS391-Ery^S was diluted until a concentration of 0.5 McFarland and 20 µL was added to 180 µL fresh BHI-medium in a 96-well microtiter plate (CELLSTAR®96 Well Plate Flat Bottom (polystyrene), Greiner Bio-One, Austria). The optical density of each well was measured with a spectrophotometer (MultiSkan™ GO Microplate Spectrophotometer, Thermo Fisher Scientific Inc., USA) using SkanIt™ software during a course of 24 h at 37 °C (measurements were taken every 15 min, at 600 nm with shaking at 5 Hz and an amplitude of 15 mm). Growth rates were calculated based on the exponential portion of the curve, the maximum culture density, and the duration of the growth lag phase using GrowthRates software [23]. In total, 96 measurements were made and the growth pattern of each mutant or UAS391-Ery^S was measured in 8 different wells.

3.3.1.3.4. Quantitative biofilm assay under static (no flow) conditions

UAS391-Ery^S, Tn and complemented mutants were studied as 24h old biofilms under flow or no flow conditions as described [18] with one modification; washing to remove planktonic bacteria was performed by gently submerging the plate in a tub of 1× PBS (Thermo Fisher Scientific Inc., USA). OD values were measured at 492 nm (Multiskan FC photometer, Thermo Fisher Scientific Inc., USA), normalized to the blank and compared to simultaneously run ATCC reference strains 6538 and 5374 (positive and negative control, respectively), as well as UAS391-Ery^S. The assay was performed on three distinct days, each time on three different plates and control

strains, UAS391-Ery^S, as well as Tn and complementation mutants, were added in 6 different wells on the same plate.

3.3.1.3.5. Quantitative biofilm assay under flow (dynamic) conditions

All Tn and complemented mutants, as well as UAS391-EryS, were also tested for biofilm formation under dynamic conditions in the Bioflux™ system using glass 48-well plates (Fluxion Biosciences Inc., USA), as described by reference [17]. Imaging was performed with a high-end fluorescence Carl Zeiss™ microscope (Axio Observer® with Cell Observer SD, ApoTome.2, LSM710, Germany) using ZEN pro 2012 software (Zeiss Efficient Navigation®, Germany). Actual fluorescence quantification of the obtained images was performed using the program ImageJ (Image Processing and Analysis in Java), which measured integrated density (http://imagej.nih.gov/). The assay was performed on two distinct days. Control strains, UAS391-Ery^S, as well as Tn and complemented mutants on the same plate were added in duplicate.

3.3.1.3.6. Analysis of biofilm matrix composition

Additionally, UAS391-Ery^S, Tn and complemented mutants grown under flow and no flow conditions were studied for differences in cell densities and viability, as well as matrix composition using LIVE/DEAD™ (BacLight™ Bacterial Viability Kit), SYPRO®Ruby (FilmTracer™ SYPRO® Ruby Biofilm Matrix Stain), or wheat germ agglutinin (WGA) (Wheat Germ Agglutinin, Texas Red™-X Conjugate) fluorescent stains (Thermo Fisher Scientific Inc., USA). LIVE/DEAD™ stain consists of SYTO™ 9 which stains the entire cell mass green followed by propidium iodide which will only stain the dead or dying cells with a compromised membrane (red). WGA Texas Red™-X Conjugate binds to sialic acid and *N*-acetylglucosaminyl residues of PIA/PNAG, and FilmTracer™ SYPRO® Ruby Biofilm Matrix Stain labels most classes of proteins, such as glycoproteins, phosphoproteins, lipoproteins, calcium binding proteins, and fibrillar proteins. Briefly, after 24 (no flow) or 17 h (flow) growth and rinsing with either 1× PBS (no flow) or 0.9% sodium chloride (flow) to remove planktonic cells, biofilms were stained and microscopically visualized using the ImageJ program for data measurements, as explained before. Under no flow conditions (used for quantification), the assay was performed on three distinct days, each time on three different plates and control strains, UAS391-Ery^S, as well as mutants, were added in 6 different wells on the same plate. Under flow conditions (used for visualization), the assay was performed on two distinct days, with control strains, UAS391-Ery^S as well as Tn and complemented mutants added *in duplo* on the same plate. Percentages compared to UAS391-Ery^S were calculated as µm² area covered. In order to quantify the proportion of protein and eDNA in the biofilm matrix, pre-formed biofilms, grown

under flow or no flow conditions, were rinsed once with either 1X PBS (no flow) or 0.9% sodium chloride (flow) incubated for 2 (no flow) or 5h (flow) at 37 °C with Proteinase K (Sigma-Aldrich®, USA) (100 µg/mL in culture medium with 10 mM Tris-HCl, pH 7.5) or DNaseI (100 U/mL in culture medium) (Sigma-Aldrich®, USA). Control wells were treated with the appropriate buffer. Afterwards, the wells were washed and stained, as described before. Under no flow conditions (used for quantification), the assay was performed on three distinct days, each time on three different plates and control strains, UAS391-Ery^S, as well as mutants, were added in 6 different wells on the same plate. Under flow conditions (used for visualization), the assay was performed on two distinct days, with control strains, UAS391-Ery^S as well as Tn, and complemented mutants added *in duplo* on the same plate.

3.3.1.3.7. Relative gene expression analysis

To measure the impact of the Tn insertion in the target gene on the expression of the global regulator *sarA* and on the fibronectin-binding proteins encoded by *fnbA/B*, 24h-old no flow biofilms of Tn mutants and of UAS391-Ery^S were mechanically disrupted using bead beating (FastPrep®-24 classic homogenization instrument, MP Biomedicals, USA). Total RNA was isolated (Masterpure™ Complete DNA and RNA Purification kit, Epicentre®, USA), 1 µg RNA was purified (Turbo DNA-free™, Ambion®, Thermo Fisher Scientific Inc., USA) and first-strand cDNA was synthesized using random primers (Reverse Transcription System, Promega Corporation, USA). Reverse transcriptase-PCR (RT-PCR) was performed (StepOnePlus™ system, Applied Biosystems®, Thermo Fisher Scientific Inc., USA) with *Power* SYBR™ Green PCR Master Mix (Thermo Fisher Scientific Inc., USA). Gene-specific primers are listed in **Suppl. Table 10**. For data normalization, housekeeping gene *gyrB* (SAUSA300_0005) was used as an internal reference and the fold change in gene expression was calculated using the comparative C_t method ($2^{-\Delta\Delta Ct}$).

3.3.1.3.8. Complementation experiments

To confirm that the changed biofilm phenotype of the Tn mutants was caused by inactivation of the target gene and not because of secondary mutations in the genome, complementation by a cloned wild type copy of the target genes was performed. Briefly, total genomic DNA of UAS391-Ery^S was purified and the *argH*, *acnA*, *icd*, *gltA*, *fumC*, *sucC*, *sdhA*, *sdhB,* and *rocF* genes with a 25–26 bp overlap corresponding to the nucleotide sequences flanking the EcoRI site of the shuttle vector pALC2073, were amplified, as described in reference [17]. For genes in an operon, the distal genes were also included in the PCR fragments that were used for complementation. Primers are listed in **Suppl. Table 10**. PCR-fragments were

cloned (2× Gibson Assembly® Master Mix, New England BioLabs® Inc., USA) in the EcoRI-linearized (New England BioLabs® Inc., USA) pALC2073 vector, transformed into recombination-impaired $CaCl_2$-competent *E. coli* DH5α and transformants were selected on LB supplemented with carbenicillin (100 µg/mL). Transformants were checked by Sanger sequencing using pALC2073 vector primers TetR2, pALC-2, and internal gene sequence primers of interest (**Suppl. Table 10**). Constructs were first introduced by electroporation into the restriction-deficient *S. aureus* host RN4220 to adapt plasmid DNA from *E. coli* to *S. aureus* modifications. Transformants were selected on LB agar plates supplemented with 10 µg/mL chloramphenicol (Sigma-Aldrich®, USA). Subsequently, plasmid DNAs isolated from this strain were introduced by electroporation into the corresponding UAS391-Ery^S Tn mutants and the transformants were again selected on LB medium supplemented with 10 µg/mL chloramphenicol. The expression of the cloned genes was induced by adding 0.1 µg/mL anhydrotetracycline (Sigma-Aldrich®, USA) to the growth media.

3.3.1.3.9. Statistical analysis

Biomass quantification in the dynamic flow and no flow assays, as well as growth rate analysis, was performed using the R Project software (version 3.1.2.) (R Foundation, Austria). A Welch two-sample *t*-test or a Wilcoxon Rank Sum test was used when data was either distributed normally or not, based on a Shapiro-Wilk Normality test. *p*-values <0.05 were considered significant.

3.3.1.4. Results

3.3.1.4.1. Urea cycle mutant *argH*::Tn, but not *rocF*::Tn, demonstrates a significantly decreased capacity for biofilm formation

Comparison of average growth rates of *argH*::Tn and *rocF*::Tn mutants with UAS391-Ery^S showed no decrease in growth rates (p=0.158 and P=0.207, respectively) (**Table 3** and **Suppl. Fig. 7**). Next, no flow and flow biofilms formed by the *argH*::Tn and *rocF*::Tn mutants were quantified compared to UAS391-Ery^S. The *argH*::Tn mutant showed a significant decrease in biofilm formation both in the no flow (p<0.001) and in the flow model (p=0.008), compared to UAS391-Ery^S (**Table 3 and Fig. 17**). However, a similarly significant decrease was not observed with the *rocF::Tn* mutant (p≥0.103) (**Table 2** and **Fig. 17**). The biomass under flow and no flow conditions increased for *argH::*Tn upon complementation with pGV5990 to quantities comparable to UAS391-

Table 3: Overview of relative gene expression, formed biofilm mass, growth rate and staining results in the TCA- and urea cycle study. Quantification of relative gene expression (RT-qPCR), formed biofilm mass (optical density, static assay; integrated density, dynamic assay), growth rate (growth curve assay), live cells

(Syto™ 9 Green Fluorescent Acid stain), proteins (Filmtracer™ SYPRO™ Ruby Biofilm Matrix stain), and PNAG (WGA Texas Red™-X Conjugate stain). 95% confidence interval is mentioned next to each value (±) and the percentage value compared to wild type UAS391-Ery^S is mentioned between brackets. NT refers to not tested.

Strain	Relative gene expression (log_{10} $2^{-(\Delta\Delta Ct)}$)	Optical Density (OD_{492})	Integrated density (fluorescence in pixels)	Growth rate (min^{-1})	Live cells (area in µm²)	Proteins (area in µm²)	PNAG (area in µm²)
UAS391-Ery^S		0.814 ± 0.14 (100%)	11.301 ± 0.61 (100%)	0.157 ± 0.01	52520 ± 1640 (100%)	67471 ± 2167 (100%)	10071 ± 604 (100%)
ATCC® 25923™	NT	NT	NT	NT	51082 ± 1021 (97%)	23174 ± 7879 (34%)	84091 ± 2118 (835%)
argH::Tn	-1.837 ± 0.01	0.504 ± 0.07 (62%)	3.653 ± 0.45 (32%)	0.161 ± 0.01	40277 ± 6734 (77%)	32488 ± 6681 (48%)	11088 ± 1510 (110%)
pGV5990	NT	0.828 ± 0.15 (102%)	9.389 ± 0.66 (83%)	NT	59118 ± 1035 (113%)	56097 ± 1309 (83%)	10701 ± 1611 (106%)
acnA::Tn	-1.578 ± 0.01	0.782 ± 0.11 (96%)	6.51 ± 0.36 (58%)	0.163 ± 0.01	56598 ± 8148 (108%)	43415 ± 1947 (64%)	5539 ± 402 (77%)
pGV6007	NT	0.805 ± 0.15 (99%)	7.73 ± 0.57 (68%)	NT	59148 ± 803 (113%)	62016 ± 10491 (92%)	10172 ± 1108 (101%)
icd::Tn	-2.499 ± 0.02	0.838 ± 0.13 (103%)	8.264 ± 0.01 (73%)	0.166 ± 0.01	48662 ± 5156 (93%)	44876 ± 2427 (67%)	11088 ± 1712 (110%)
pGV5994	NT	1.143 ± 0.12 (141%)	8.308 ± 1.63 (74%)	NT	59655 ± 6882 (114%)	61070 ± 1801 (91%)	10071 ± 2014 (100%)
pGV5999	NT	1.248 ± 0.17 (153%)	8.076 ± 1.33 (72%)	NT	53197 ± 7619 (101%)	64673 ± 14805 (96%)	10172 ± 906 (101%)
gltA::Tn	-2.156 ± 0.01	0.789 ± 0.11 (97%)	7.911 ± 0.11 (70%)	0.157 ± 0.01	56999 ± 10138 (109%)	41076 ± 6930 (61%)	9165 ± 504 (91%)
pGV5992	NT	1.102 ± 0.12 (135%)	9.616 ± 0.25 (85%)	NT	54239 ± 9704 (103%)	62730 ± 337 (93%)	10071 ± 1209 (100%)
pGV5999	NT	1.055 ± 0.10 (130%)	8.149 ± 0.27 (72%)	NT	53197 ± 7619 (101%)	60370 ± 5783 (89%)	10071 ± 201 (100%)
fumC::Tn	-2.729 ± 0.01	0.374 ± 0.07 (46%)	2.065 ± 0.04 (18%)	0.162 ± 0.01	51948 ± 3792 (99%)	33366 ± 226 (49%)	12287 ± 705 (122%)
pGV6005	NT	0.941 ± 0.14 (116%)	7.662 ± 1.88 (68%)	NT	60993 ± 323 (116%)	53774 ± 3206 (80%)	10071 ± 1309 (100%)
sucC::Tn	-2.991 ± 0.01	0.847 ± 0.17 (104%)	7.506 ± 0.58 (67%)	0.150 ± 0.01	58876 ± 5123 (112%)	36296 ± 1949 (54%)	10373 ± 1712 (103%)
pGV5998	NT	0.804 ± 0.11 (99%)	8.715 ± 0.01 (77%)	NT	42102 ± 9764 (80%)	64790 ± 5032 (96%)	10172 ± 1611 (101%)

pGV6000	NT	1.041 ± 0.13 (128%)	7.599 ± 1.59 (67%)	NT	60213 ± 7627 (115%)	55961 ± 1675 (83%)	10172 ± 504 (101%)
sdhA::Tn	-3.506 ± 0.01	0.537 ± 0.11 (66%)	3.835 ± 0.60 (34%)	0.162 ± 0.01	60286 ± 5671 (115%)	22429 ± 1844 (33%)	8963 ± 806 (89%)
pGV6001	NT	1.002 ± 0.10 (123%)	9.002 ± 0.11 (80%)	NT	58905 ± 2784 (112%)	52687 ± 5281 (78%)	10172 ± 604 (101%)
pGV6002	NT	1.071 ± 0.11 (132%)	7.252 ± 0.92 (64%)	NT	53337 ± 3119 (102%)	62249 ± 6797 (92%)	10071 ± 1108 (100%)
sdhB::Tn	-3.409 ± 0.01	0.667 ± 0.10 (82%)	4.875 ± 0.56 (43%)	0.159 ± 0.01	46046 ± 2205 (88%)	29535 ± 12228 (44%)	8460 ± 705 (84%)
pGV5996	NT	0.908 ± 0.12 (112%)	11.057 ± 1.29 (98%)	NT	60498 ± 2381 (115%)	71505 ± 14152 (106%)	10071 ± 1309 (100%)
pGV6002	NT	1.140 ± 0.09 (140%)	8.455 ± 0.65 (75%)	NT	59301 ± 2735 (113%)	62304 ± 2147 (92%)	10071 ± 1712 (100%)
rocF::Tn	-2.279 ± 0.05	0.765 ± 0.12 (94%)	7.586 ± 0.15 (67%)	0.163 ± 0.01	46919 ± 6132 (89%)	34318 ± 7591 (51%)	8963 ± 1914 (89%)
pGV6003	NT	0.878 ± 0.09 (108%)	8.342 ± 0.21 (74%)	NT	54287 ± 860 (103%)	56373 ± 1896 (84%)	10172 ± 806 (101%)

Ery^S ($p \leq 0.045$), while the complemented *rocF::*Tn (with pGV6003) showed no change in biofilm formation, as compared to *rocF*::Tn mutant or to UAS391-Ery^S ($p \geq 0.057$) (**Table 3**).

3.3.1.4.2. TCA-cycle mutants, *fumC*::Tn, *sdhA*::Tn and *sdhB*::Tn, but not *acnA*::Tn, *icd*::Tn, *gltA*::Tn and *sucC*::Tn, demonstrate a significantly decreased capacity for biofilm formation

None of the 7 mutants tested (*acnA*::Tn, *icd*::Tn, *gltA*::Tn, *fumC*::Tn, *sucC*::Tn, *sdhA*::Tn and *sdhB*::Tn) displayed impaired growth rates (p=0.554) (**Table 3** and **Suppl. Fig. 7**). Biofilm formation under no flow conditions decreased by 1.5- to 2.2-fold in *fumC*::Tn (p<0.001) and *sdhA*::Tn (p<0.001), as compared to UAS391-Ery^S. Biofilm decrease was only 1.2-fold in *sdhB*::Tn (p=0.048). However, no significant decrease in biofilm formation was detected in the *acnA*::Tn, *gltA*::Tn, *sucC*::Tn, and *icd*::Tn mutants ($p \geq 0.059$) (**Table 3**). Under flow conditions, the *fumC*::Tn, *sdhA*::Tn and *sdhB*::Tn mutants also showed the largest decrease in biomass, compared to UAS391-Ery^S ($p \leq 0.012$). *AcnA*::Tn formed less biofilm under flow conditions (p=0.041), despite not displaying any effect under no flow conditions while *gltA*::Tn, *sucC*::Tn, and *icd*::Tn mutants showed no significant changes in biofilm formation ($p \geq 0.101$) (**Table 3** and **Fig. 17**). Biofilm formation by Tn mutants complemented with the corresponding intact gene (**Table 3**), showed no differences

in biofilm formation, as compared to UAS391-Ery^S under no flow (p=0.423) or flow conditions (p=0.053) (**Table 3**).

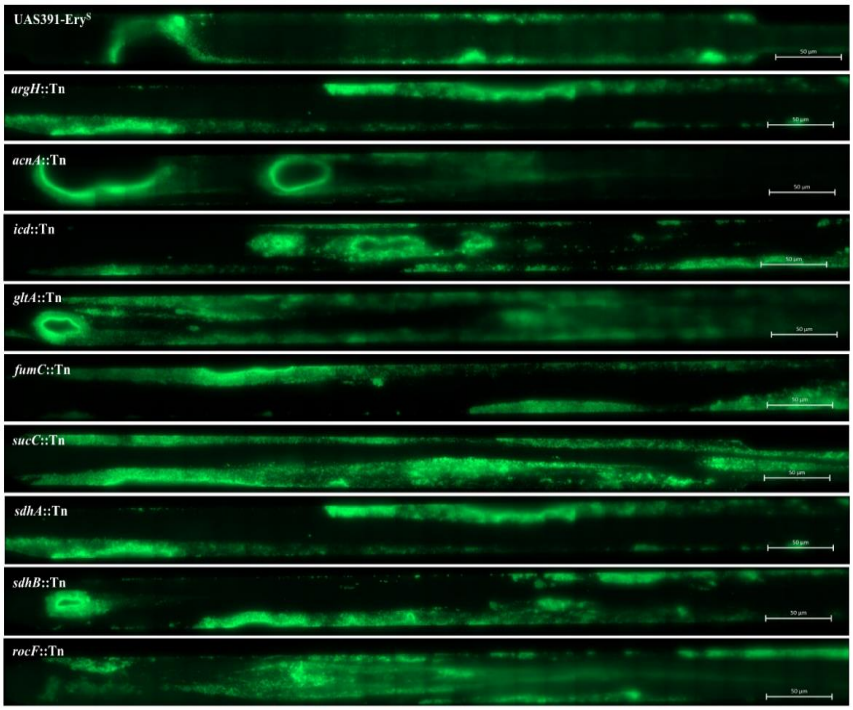

Figure 17: Effect of TCA- and urea cycle knockouts on the biofilm phenotype by USA300 UAS391-Ery^S. Argininosuccinate lyase (*argH*), aconitate hydratase A (*acnA*), isocitrate dehydrogenase (*icd*), citrate synthase II (*gltA*), fumarate hydratase class II (*fumC*), succinate—CoA ligase (subunit beta) (*sucC*), succinate dehydrogenase (flavoprotein subunit) (*sdhA*), succinate dehydrogenase iron-sulphur protein (*sdhB*), and arginase (*rocF*). Flow biofilm images were captured after 17 h growth employing ZEN 2012 software (Zeiss) as 84 combined tile images consisting of one µm² horizontal tiles covering the entire microchannel. The total biomass was determined by SYTO™ 9 staining *in duplicate*.

3.3.1.4.3. Fluorescent staining of the biofilm matrix reveals that the protein component is decreased in TCA- and urea cycle mutants

Under flow conditions, UAS391-Ery^S biofilms showed an average live:dead cell ratio of 61%:39% ± 8%, and a count of 606 ± 15 cells on the total imaged surface area. All 9 Tn mutants (*argH*::Tn, *acnA*::Tn, *icd*::Tn, *gltA*::Tn, *fumC*::Tn, *sucC*::Tn, *sdhA*::Tn, *sdhB*::Tn, and *rocF*::Tn, respectively) showed similar total cell numbers (609 ± 29, respectively) (p≥0.881). In contrast, the average live:dead cell ratio changed significantly for *argH*::Tn, *fumC*::Tn, *sucC*::Tn, *sdhA/*B::Tn, and *rocF*::Tn (46%:54% ± 3%) (p≤0.001), but not for *acnA*::Tn, *icd*::Tn, and *gltA*::Tn (59%:41% ± 2%) (p≥0.168) (**Table 3** and **Fig. 18**). Complemented strains showed no significant difference compared to the UAS391-Ery^S live:dead cell ratio (on average 59%:41% ± 9%) (p≥0.928). Staining with WGA Texas Red™-X conjugate showed < 1% total area

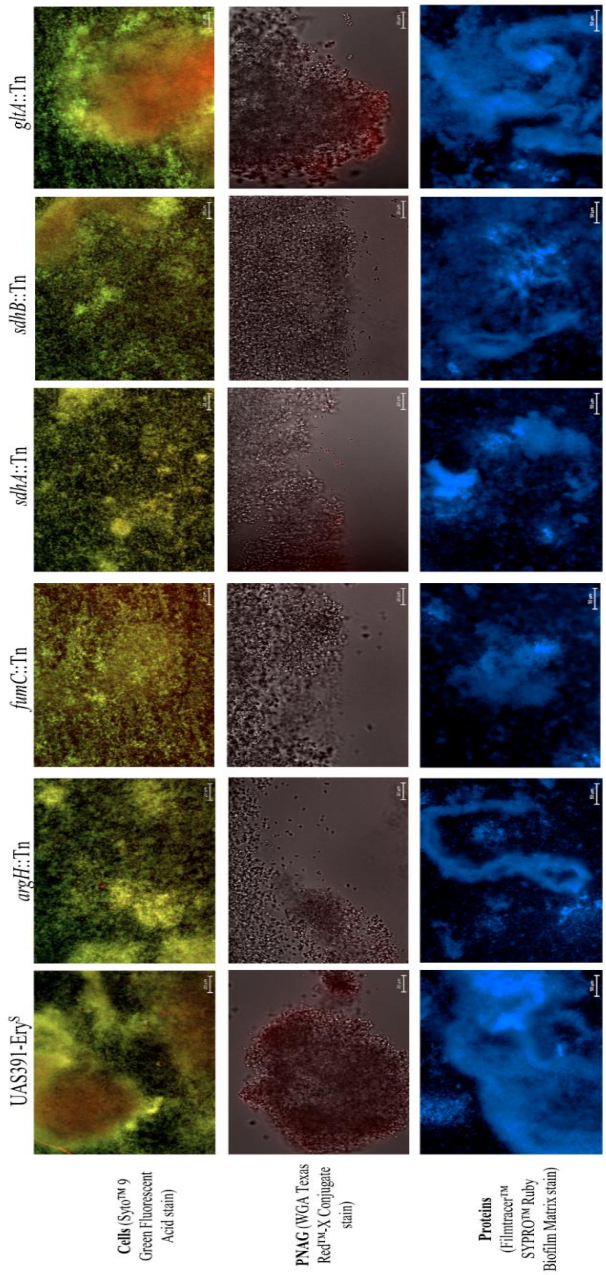

Figure 18: Static biofilm matrix structure obtained from fluorescent microscopy observations *of S. aureus* USA300 UAS391-Ery^S, and TCA- and urea cycle knockouts. Channel 1 shows total cells stained with SYTO™ 9 and PI. Channel 2 shows PNAG stained with WGA Texas Red™-X Conjugate and combined with Bright-field imaging. Channel 3 shows the protein component stained with FilmTracer™ SYPRO™ Ruby Biofilm Matrix.

coverage by PIA/PNAG for UAS391-Ery^S, as well as for all 9 Tn mutants and for their Corresponding complemented strains ($p \geq 0.943$) (**Table 3** and **Fig. 18**). In contrast, WGA staining of the PIA/PNAG producing MSSA control strain ATCC® 25923™ (image not shown) gave a total area coverage of 91% ± 2% (**Table 3**). Staining with FilmTracer™ SYPRO® Ruby Biofilm Matrix Stain showed an average area coverage decrease of 48% ± 19% compared to that of UAS391-Ery^S for *argH*::Tn, *acnA*::Tn, *icd*::Tn, *gltA*::Tn, *fumC*::Tn, *sucC*::Tn, *sdhA/B*::Tn, and *rocF*::Tn ($p \leq 0.001$) (**Table 3**). Complemented mutants showed similar average protein proportions of the biofilm matrix, as compared to UAS391-Ery^S (105% ± 7%) ($p \geq 0.194$).

3.3.1.4.4. Enzymatic digest correlates biofilm-defective transposon mutants with a protein- and eDNA-based matrix

Under no flow conditions, the 24h biomass of UAS391-Ery^S decreased by 22% ± 3% following proteinase K and 44% ± 5% following DNase I treatment (both $p<0.001$), while the biomass of ATCC® 25923™ *S. aureus* decreased by only 11% ± 3% and 6% ± 2%, respectively ($p \geq 0.134$) (**Fig. 19A, B**). Under flow conditions, the 17h biomass of UAS391-Ery^S decreased by 25% ± 7% following proteinase K and 53% ± 9% following DNase I treatment ($p \leq 0.028$), while that of ATCC® 25923™ *S. aureus* decreased by only 19% ± 8% and 12% ± 7%, respectively ($p \geq 0.145$) (**Fig. 19C, D**). After proteinase K treatment under no flow conditions, *argH*::Tn, *acnA*::Tn, *icd*::Tn, *gltA*::Tn, *fumC*::Tn, *sucC*::Tn, *sdhA/B*::Tn, and *rocF*::Tn showed on average 50% ± 12% reduction in biomass compared to the untreated biofilms of the corresponding mutants ($p \leq 0.001$) (**Fig. 19A**). Similarly, after proteinase K treatment under flow conditions, there was an average of 51% ± 8% ($p \leq 0.05$) (**Fig. 19C**). After DNase I treatment under no flow conditions, *argH*::Tn, *acnA*::Tn, *icd*::Tn, *gltA*::Tn, *fumC*::Tn, *sucC*::Tn, *sdhA/B*::Tn, and *rocF*::Tn showed an average 55% ± 10% reduction in biofilm mass as compared to the untreated biofilms of the corresponding mutants ($p \leq 0.005$) (**Fig. 19B**). Similarly, after DNase I treatment under flow conditions, there was a reduction of 52% ± 10% respectively ($p \leq 0.05$) (**Fig. 19D**). Complemented strains showed an average biomass decrease of 23% ± 6% and 48% ± 10% after both treatments under flow and no flow conditions ($p<0.001$), which is comparable to results obtained with UAS391-Ery^S. In all TCA- and urea cycle Tn mutants, *sarA* showed a distinct up-regulation (1.35 to 3.63-fold), except for *sucC*::Tn, which showed a 0.92-fold down-regulation (**Suppl. Fig. 8**). Overall, a knockout mutation in either the TCA- or urea cycle was associated with a decrease in *fnbA* and *fnbB* expression (0.53- to 0.78-fold and 0.51 to 0.77-fold, respectively) (**Suppl. Fig. 8**).

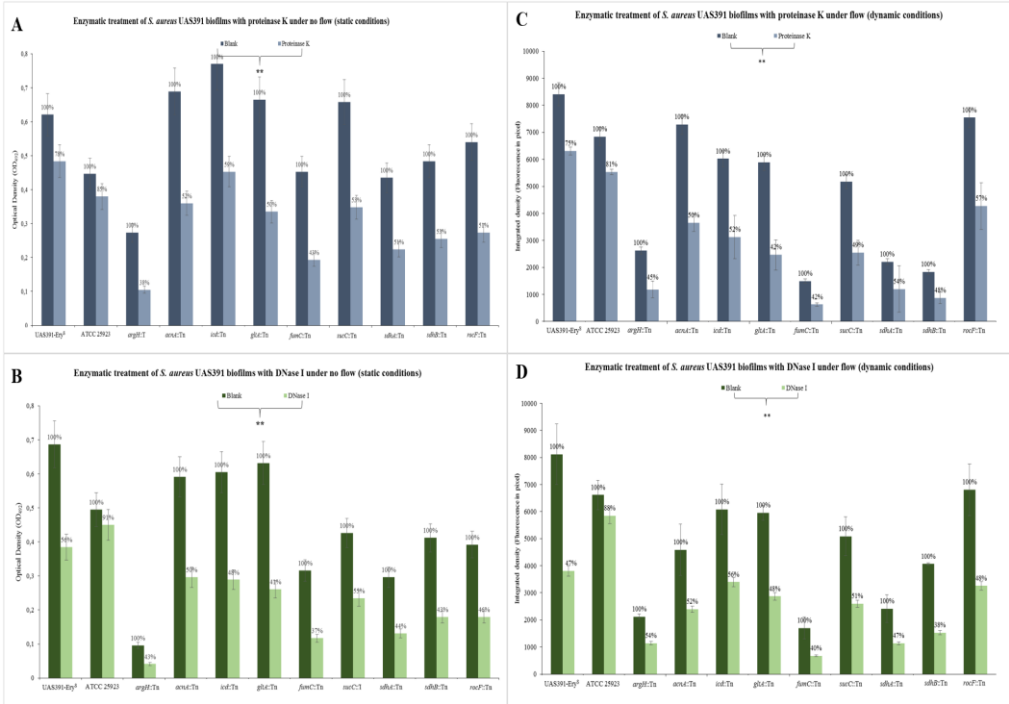

Figure 19: Enzymatic treatment of pre-formed 24h (no flow) or 17h (flow) old biofilms of UAS391-Ery^S, ATCC®25923™ and urea or TCA-cycle knockouts. 100 µg/mL proteinase K (**A,C**) or 100 U/mL DNase I (**B,D**) under no flow (no flow) (**A,B**) and dynamic (flow) (**C,D**) conditions. Blanks refer to incubation in either culture medium with 10 mM Tris-HCl for proteinase K treatment or culture medium for DNase I treatment. The total biomass was determined by crystal violet staining *in triplicate*. Error bars represent 95% confidence intervals. ** refers to p<0.001.

3.3.1.5. Discussion

3.3.1.5.1. The biofilm matrix of MRSA-USA300 and corresponding Tn mutants is PIA/PNAG-independent and mainly composed of proteins and eDNA.

Using enzymatic digest and biofilm-matrix staining experiments to assess the contribution of PIA/PNAG, protein, and eDNA to the biofilm matrix of MRSA-USA300, we first showed that the biofilm matrix of USA300 UAS391-Ery^S and Tn mutants was primarily composed of proteinaceous material and eDNA with < 1% contribution of PIA/PNAG. Interestingly, and in contrast to MSSA, inactivation of the TCA-cycle in MRSA Tn mutants did not result in any increase of PIA/PNAG in the biofilm matrix. In MSSA, decreased TCA-cycle activity was reported to shunt metabolites toward PIA/PNAG production [14]. We have previously whole genome sequenced the UAS391 strain and found an intact functional *icaADBC* operon [19]. These data fully support the results of Pozzi et al. that showed that high-level expression of PBP2a—the product of the methicillin resistance gene, *mecA*, harboured on the SCC*mec* element

that differentiates MRSA and MSSA—blocks *icaADBC*-dependent polysaccharide biofilm development and promotes the formation of proteinaceous biofilms [5]. Of note, *S. aureus* also produces a capsular polysaccharide (type 5 and 8), which has been implicated in biofilm formation [24]. The role of the TCA-cycle in capsular polysaccharide production was demonstrated by Sadykov et al. who showed that in the absence of glucose, the capsular sugar precursor fructose 6-phosphate is synthesized by gluconeogenesis from the TCA-cycle intermediate oxaloacetate [25]. However, the USA300 clonal lineage, including the UAS391 strain, harbours conserved mutations in the *cap5* locus and does not produce a capsular polysaccharide [26], which also made it easier to exclude the contribution of PIA/PNAG to the biofilm matrix of UAS391 and its Tn mutants.

3.3.1.5.2. TCA-cycle inactivation impacts the protein component of the biofilm matrix of MRSA-USA300

Upon comparison of the net protein contribution to the matrix under no flow and flow conditions, it was clear that the net contribution of proteins to the entire Tn mutant biomass (on average 50% and 51%, respectively) was significantly higher than for UAS391-Ery^{S} (on average 22% and 25%, respectively).

Several studies have reported a role for proteins and eDNA in the *ica*-independent MRSA biofilm phenotype [8,9,27]. Houston et al. demonstrated an important role for eDNA during the primary attachment and early stages of MRSA biofilm formation by employing a Δ*atl* knockout mutant in MRSA isolate BH1CC [9]. These authors also reported that DNaseI impaired biofilm development by MRSA isolates from clonal complex 5 (CC5), CC22 and sequence type 239 (ST239). Moreover, treatment of USA300 biofilms after 6 h and 22 h of growth demonstrated both a significant impact of DNaseI and proteinase K, with the latter having the largest impact on the total biofilm mass [27]. Our results also indicate the possibility of the USA300 biofilm matrix containing other components, as protein and eDNA only accounted for on average 23.5% and 48.5% of the biomass. These might have been teichoic acids associated with the cell wall (cell wall teichoic acid, WTA) or cell membrane (lipoteichoic acid, LTA) [28].

A prior study on an *ica*-knockout MSSA strain RN6390 has shown that, in the presence of citrate, the fibronectin-binding proteins, FnBPA and FnBPB, stimulate biofilm formation by promoting both cell-to-surface and cell-to-cell interactions, which is part of a larger network of virulence factors that are controlled by the staphylococcal accessory regulator, SarA [29]. All urea and TCA-cycle Tn mutants in our study showed a significant down-regulation in *fnbA* and *fnbB* gene expression

compared to UAS391-Ery^S, whereas *sarA* was up-regulated for all Tn mutants except *sucC*::Tn. SarA has been reported to work synergistically with the two-component *saeRS* system to repress extracellular proteases that would otherwise reduce the accumulation of critical proteins that contribute to the biofilm matrix [30]. Down-regulation of *fnbA/*B would potentially lead to a decreased protein biofilm matrix, but up-regulation of sarA might neutralize and counteract this effect in the Tn mutants.

3.3.1.5.2. Inactivation of specific TCA-cycle genes is associated with a high metabolic fitness cost

Using live-dead staining on flow biofilms, we found a significantly higher number of dead cells in the biofilms formed by *argH*::Tn, *fumC*::Tn, *sdhA*::Tn, *sdhB*::Tn, *sucC*::Tn, and *rocF*::Tn mutants. However, these mutants neither demonstrated attenuated or slower growth on growth curve assays nor were the total number of cells in their respective biofilms significantly different from those in UAS391-Ery^s biofilms. However, Halsey et al. have shown that Tn mutants with mutations in TCA-cycle genes past the 2-oxoglutarate node (*fumC*, *sdhA*, and *sucC*) did not grow at all in their planktonic *S. aureus* growth assay [31]. The fact that these defects were not detected in our corresponding TCA-cycle Tn mutants might be due to differences in growth media.

A higher number of dead cells found in the biofilms of Tn mutants might be indicative of a high metabolic cost for the bacterium. It is important to note that propidium iodide does not only stain cells with a compromised membrane, but also eDNA. However, the proportion of eDNA in the biofilm matrix, observed by DNase I digestion, did not differ significantly between the Tn mutants (on average 52% and 55% under flow and no flow conditions, respectively) and UAS391-Ery^S (on average 44% and 53% under flow and no flow conditions, respectively). Thus, based on our data, inactivation of the TCA-cycle is likely not associated with any change in eDNA biofilm matrix composition.

In conclusion, we identified an important role of the TCA-cycle in mediating biofilm formation, specifically by influencing the matrix composition, in MRSA USA300 biofilms. These metabolic pathway hits require further screening of MRSA of different clonal lineages to confirm commonality of the target mechanisms and eventually yield interesting therapeutic targets.

3.3.1.6. Addendum

3.3.1.6.1. Acknowledgements

We thank Francine Deboeck for excellent technical assistance during the complementation experiments. SDB is supported by funding from Research Foundation Flanders (FWO, applicant number 1128818N). The described research is part of IWT-SBO project (#140746) and FWO research project (#GOD3516N).

3.2.1.6.2. Contribution to authorship

JS, HDG, J-PH, HG and SMK conceived the study. SDB carried out the experimental work. The methodology was designed by JS and IDP. SDB drafted the manuscript, review and editing of the manuscript was performed by SDB and SMK. All authors read, gave input and approved the final manuscript. In detail, growth rate analysis, biofilm assays under flow and dynamic conditions, analysis of the biofilm matrix composition, relative gene expression analysis and statistical analysis were performed by SDB.

3.2.1.6.3. Supplementary figures

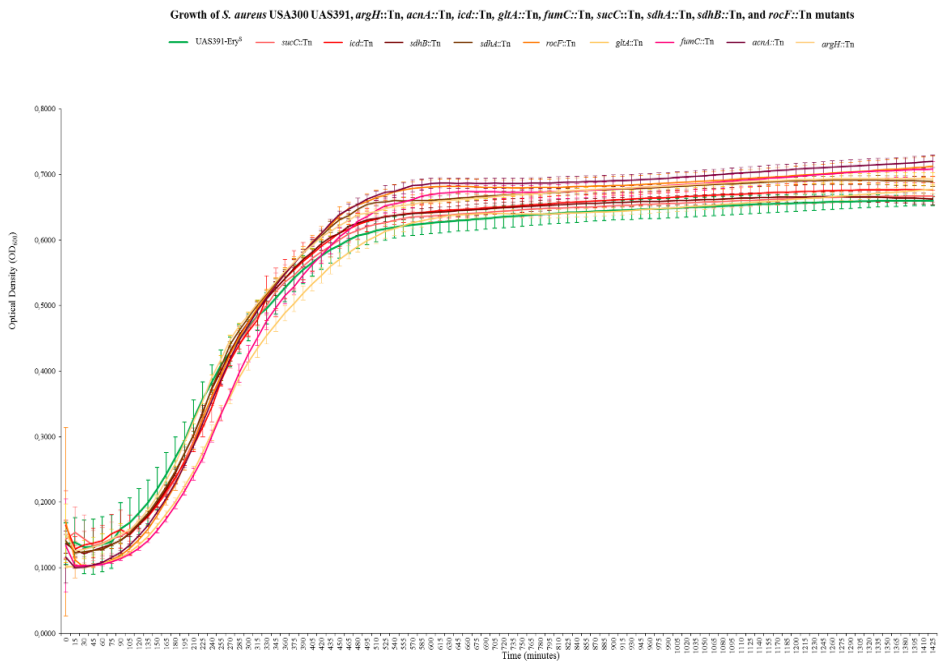

Supplementary figure 7: Background absorption-corrected 24h growth curves for UAS391-Ery^S as well as TCA- and urea cycle knockouts. Error bars in corresponding colour represent the 95% confidence interval per strain.

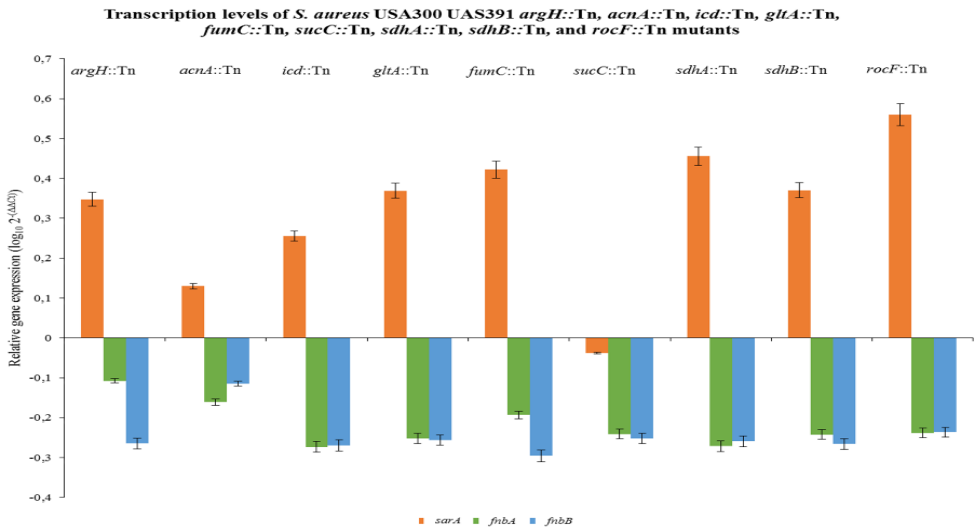

Supplementary figure 8: Quantification relative gene expression in UAS391-Ery^S and the corresponding TCA- and urea cycle knockout mutants. *fnbA:* fibronectin-binding protein A; *fnbB:* fibronectin-binding protein B; and *sarA:* staphylococcal accessory regulator A. Normalized to *gyrB* expression and calculated using the Comparative C_t Method ($2^{-\Delta\Delta Ct}$). Gene expression in UAS391-Ery^S was taken as baseline 0.

3.3.1.6.4. Supplementary tables

Supplementary Table 10: Primers used during the TCA- and urea cycle study. Primers were designed against *S. aureus* strain USA300-UAS391 (#CP007690.1).

Gene name	ID	Sequence (5'→3')	Product size (bp)	Reference
Primers for RT-PCR				
gyrB	GyrB-F	GTAACACGTCGTAAATCAGCG	170	[31]
	GyrB-R	CGTAATGGTAAAATCGCCTGC		
fnbB	RTFnbB-F	AGGTGCAGAAGGTCATGCAG	222	**This study**
	RTFnbB-R	TGATCGCTAACAGCACCAGT		
fnbA	RTFnbA-F	CCAGTACCACCTGCCAAAGA	195	
	RTFnbA-R	TCCGCCGAACAACATACCTT		
sarA	RTSarA-F	GCTGTATTGACATACATCAGCGA	250	
	RTSarA-R	CGTTGTTTGCTTCAGTGATTCG		
Primers for complementation				
pALC2073 plasmid	TetR-2	CAATGTAGGCTGCTCTACACCTAG	547	[18]
	pALC-2	GATCGGTGCGGGCCTCTTCGCTAT		
argH	ArgH-1	AGCTTGATGGTACCGAGCTCGAATTTGGAGGCT ATAGCAATGAGCAATA	1807	This study
	ArgH-2	GTTGTAAAACGACGGCCAGTGAATTCTTATTGTG ATAGTAATTGTTTAGCAAC		
acnA	AcnA-1	AGCTTGATGGTACCGAGCTCGAATTATGTATCAA GGGGGATCATTAAATGGCTGCAAATTTTAAAGA GCAATC	3141	
	AcnA-2	GTTGTAAAACGACGGCCAGTGAATTCTTATTGCG CTAATTTATTTCTTAAAACCATTTG		

gtlA	GltA-1	AGCTTGATGGTACCGAGCTCGAATTTAAAGGGG AAATTTATCATGGCAGAATTACAAAGAG	GltA-1 + GltA-2: 1522 GltA-1 + Icd-2: 2869	
	GltA-2	GTTGTAAAACGACGGCCAGTGAATTCTTATTTTC TTTCTTCAAGCGGGATATA		
Icd	Icd-1	AGCTTGATGGTACCGAGCTCGAATTTTGGAGGT AAAATAACTATGACTGCAGAAAAAATTAC	Icd-1 + Icd-2: 1699 GltA-1 + Icd-2: 2869	
	Icd-2	GTTGTAAAACGACGGCCAGTGAATTCTTATTTTA AATTTTTAATCAATTCATC		
rocF	RocF-1	AGCTTGATGGTACCGAGCTCGAATTTAGAGCAA AGGGGGACGCTTATGACAAAGACAAAAG	1342	
	RocF-2	GTTGTAAAACGACGGCCAGTGAATTCTTATAATA AAGTTTCACCAAAAAATGTTCCAAC		
fumC	FumC-1	AGCTTGATGGTACCGAGCTCGAATTAACAGTGA TAAGGGGAGAAATTGAATGTCAGTAAGAATTGA AC	1823	
	FumC-2	GTTGTAAAACGACGGCCAGTGAATTCTTAATGA GGATCTACCATATCTTCTG		
sdhA	SdhA-1	AGCTTGATGGTACCGAGCTCGAATT AGGGGAGTGAAATTTTTATGGCAGAGAAACATC	SdhA-1 + SdhA-2: 2197 SdhA-1 + SdhB-2: 3012	
	SdhA-2	GTTGTAAAACGACGGCCAGTGAATTCTTATTTTT TACCCCCTTTAGACTTAC		
sdhB	SdhB-1	AGCTTGATGGTACCGAGCTCGAATTCTAAAGGG GGTAAAAAATAATGACTGAACAATCAGTG	SdhB-1 + SdhB-2: 1254 SdhA-1 + SdhB-2: 3012	
	SdhB-2	GTTGTAAAACGACGGCCAGTGAATTCTTATTCTA CTTCATGGTCTGAACCAAAG		
sucC	SucC-1	AGCTTGATGGTACCGAGCTCGAATTAACCTAAGT AACAGGAGGATGGAAGATGAATATCCACGAGTA TC	SucC-1 + SucC-2: 1605 SucC-1 + SucC-3: 2595	
	SucC-2	GTTGTAAAACGACGGCCAGTGAATTCTTATGCTT CTTTGACTAGTTTAAC		
	SucC-3	GTTGTAAAACGACGGCCAGTGAATTCTTATTTAT TAACAGTTAATAATGATTC		

3.3.1.6.5. References

1. Lee, A.S., et al., *Methicillin-resistant Staphylococcus aureus.* Nature Reviews Disease Primers, 2018. **4**: p. 18033.
2. Archer, N.K., et al., *Staphylococcus aureus biofilms: properties, regulation, and roles in human disease.* Virulence, 2011. **2**(5): p. 445-59.
3. Fitzpatrick, F., H. Humphreys, and J.P. O'Gara, *Evidence for icaADBC-independent biofilm development mechanism in methicillin-resistant Staphylococcus aureus clinical isolates.* J Clin Microbiol, 2005. **43**(4): p. 1973-6.
4. O'Neill, E., et al., *Association between methicillin susceptibility and biofilm regulation in Staphylococcus aureus isolates from device-related infections.* J Clin Microbiol, 2007. **45**(5): p. 1379-88.
5. O'Gara, J.P., *ica and beyond: biofilm mechanisms and regulation in Staphylococcus epidermidis and Staphylococcus aureus.* FEMS Microbiol Lett, 2007. **270**(2): p. 179-88.
6. Pozzi, C., et al., *Methicillin resistance alters the biofilm phenotype and attenuates virulence in Staphylococcus aureus device-associated infections.* PLoS Pathog, 2012. **8**(4): p. e1002626.
7. O'Neill, E., et al., *A novel Staphylococcus aureus biofilm phenotype mediated by the fibronectin-binding proteins, FnBPA and FnBPB.* J Bacteriol, 2008. **190**(11): p. 3835-50.
8. Izano, E.A., et al., *Differential roles of poly-N-acetylglucosamine surface polysaccharide and extracellular DNA in Staphylococcus aureus and Staphylococcus epidermidis biofilms.* Appl Environ Microbiol, 2008. **74**(2): p. 470-6.
9. Houston, P., et al., *Essential role for the major autolysin in the fibronectin-binding protein-mediated Staphylococcus aureus biofilm phenotype.* Infect Immun, 2011. **79**(3): p. 1153-65.

10. Mann, E.E., et al., *Modulation of eDNA release and degradation affects Staphylococcus aureus biofilm maturation.* PLoS One, 2009. **4**(6): p. e5822.
11. Rice, K.C., et al., *The cidA murein hydrolase regulator contributes to DNA release and biofilm development in Staphylococcus aureus.* Proc Natl Acad Sci U S A, 2007. **104**(19): p. 8113-8.
12. Sonenshein, A.L., *The Krebs citric acid cycle*, ed. A.L. Sonenshein. 2002, Washington, D.C., USA: ASM Press.
13. Sadykov, M.R., et al., *Tricarboxylic acid cycle-dependent regulation of Staphylococcus epidermidis polysaccharide intercellular adhesin synthesis.* J Bacteriol, 2008. **190**(23): p. 7621-32.
14. Vuong, C., et al., *Staphylococcus epidermidis polysaccharide intercellular adhesin production significantly increases during tricarboxylic acid cycle stress.* J Bacteriol, 2005. **187**(9): p. 2967-73.
15. Zhu, Y., et al., *Tricarboxylic acid cycle-dependent attenuation of Staphylococcus aureus in vivo virulence by selective inhibition of amino acid transport.* Infect Immun, 2009. **77**(10): p. 4256-64.
16. Fey, P.D., et al., *A genetic resource for rapid and comprehensive phenotype screening of nonessential Staphylococcus aureus genes.* MBio, 2013. **4**(1): p. e00537-12.
17. Sabirova, J.S., et al., *Fatty acid kinase A is an important determinant of biofilm formation in Staphylococcus aureus USA300.* BMC Genomics, 2015. **16**(1): p. 861.
18. Sabirova, J.S., et al., *Complete genome sequences of two prolific biofilm-forming Staphylococcus aureus isolates belonging to USA300 and EMRSA-15 clonal lineages.* Genome Announc, 2014. **2**(3).
19. Vanhommerig, E., et al., *Comparison of biofilm formation between major clonal lineages of methicillin-resistant Staphylococcus aureus.* PLoS One, 2014. **9**(8): p. e104561.
20. Luppens, S.B.I., et al., *Development of a standard test to assess the resistance of Staphylococcus aureus biofilm cells to disinfectants.* Appl Environ Microbiol, 2002. **68**(9): p. 4194-4200.
21. Somerville, G.A. and R.A. Proctor, *At the crossroads of bacterial metabolism and virulence factor synthesis in Staphylococci.* Microbiol Mol Biol Rev, 2009. **73**(2): p. 233-48.
22. Bateman, B.T., et al., *Evaluation of a tetracycline-inducible promoter in Staphylococcus aureus in vitro and in vivo and its application in demonstrating the role of sigB in microcolony formation.* Infect Immun, 2001. **69**(12): p. 7851-7.
23. Hall, B.G., et al., *Growth rates made easy.* Mol Biol Evol, 2014. **31**(1): p. 232-8.
24. O'Riordan, K. and J.C. Lee, *Staphylococcus aureus Capsular Polysaccharides.* Clinical Microbiology Reviews, 2004. **17**(1): p. 218-234.
25. Sadykov, M.R., et al., *Using NMR metabolomics to investigate tricarboxylic acid cycle-dependent signal transduction in Staphylococcus epidermidis.* J Biol Chem, 2010. **285**(47): p. 36616-24.
26. Boyle-Vavra, S., et al., *USA300 and USA500 clonal lineages of Staphylococcus aureus do not produce a capsular polysaccharide due to conserved mutations in the cap5 locus.* MBio, 2015. **6**(2).
27. Lauderdale, K.J., et al., *Biofilm dispersal of community-associated methicillin-resistant Staphylococcus aureus on orthopedic implant material.* J Orthop Res, 2010. **28**(1): p. 55-61.
28. Otto, M., *Staphylococcal biofilms.* Curr Top Microbiol Immunol, 2008. **322**: p. 207-228.
29. Shanks, R.M., et al., *Genetic evidence for an alternative citrate-dependent biofilm formation pathway in Staphylococcus aureus that is dependent on fibronectin binding proteins and the GraRS two-component regulatory system.* Infect Immun, 2008. **76**(6): p. 2469-77.
30. Mrak, L.N., et al., *saeRS and sarA act synergistically to repress protease production and promote biofilm formation in Staphylococcus aureus.* PLoS One, 2012. **7**(6): p. e38453.
31. Halsey, C.R., et al., *Amino acid catabolism in Staphylococcus aureus and the function of carbon catabolite repression.* MBio, 2017. **8**(1).
32. Sihto, H.M., et al., *Validation of reference genes for normalization of qPCR mRNA expression levels in Staphylococcus aureus exposed to osmotic and lactic acid stress conditions encountered during food production and preservation.* FEMS Microbiol Lett, 2014. **356**(1): p. 134-40.

3.3.2. Fatty acid kinase A is an important determinant of biofilm formation in methicillin-resistant Staphylococcus aureus USA300

Julia S. Sabirova[1#], Jean-Pierre Hernalsteens[2], Sarah De Backer[1], Basil B. Xavier[1], Pieter Moons[1], Agata Turlej-Rogacka[1], Henri De Greve[3,4], Herman Goossens[1], Surbhi Malhotra-Kumar[1*]

[1]Laboratory of Medical Microbiology, Vaccine & Infectious Disease Institute, University of Antwerp, Antwerp, Belgium, [2]Viral Genetics Research Group, Vrije Universiteit Brussel, Brussels, Belgium, [3] Structural Biology Brussels, Vrije Universiteit Brussel, Brussels, Belgium, [4]Structural and Molecular Microbiology, Structural Biology Research Centre, VIB, Brussels, Belgium.

[*]Corresponding author mailing address: Laboratory of Medical Microbiology, Campus Drie Eiken, University of Antwerp, S6, Universiteitsplein 1, B-2610 Wilrijk, Belgium. Phone: 32-3-265-27-52. Fax: 32-3-265-26-63. E-mail: surbhi.malhotra@uantwerpen.be

Published in: BMC Genomics. 2015 Oct 26;16:861. doi: 10.1186/s12864-015-1956-8.

3.3.2.1. Abstract

Methicillin-resistant *Staphylococcus aureus* (MRSA)-USA300 is notorious for its ability to cause community- and healthcare-acquired infections, which are even more difficult to treat when associated with a biofilm phenotype. We aimed to characterize the genetic determinants of biofilm formation in a USA300 skin abscess isolate (UAS391) that formed prolific biofilms. USA300 *S. aureus* strains, TCH1516, and FPR3757, were found to be closely related based on whole genome mapping (Argus™ Optical Mapping System, Opgen Inc, USA) to UAS391 (96.3-99.1 % similarity, p=0.0151), however differed markedly in biofilm formation (p=0.0001) on a dynamic assay (BioFlux 200, Fluxion Biosciences, USA). Comparison of whole genome sequences of these strains identified differences in a total of 18 genes. Corresponding Tn (*bursa aurealis*-bearing) knockout mutants in these target genes were obtained from a publicly available mutant library of the same clonal lineage (USA300-JE2) and were characterized phenotypically for biofilm formation. Tn mutants showing significant differences in biofilm formation were utilized for transduction into a plasmid-cured erythromycin-sensitive derivative of UAS391 and for complementation experiments. All strains were tested on the dynamic assay, and 17h-biofilms were stained (SYTO9, Life Technologies, USA) and fluorescence intensity quantified by microscopy (Zeiss, Germany; ImageJ, USA). Gene expression levels in Tn

and transduced mutants were studied by quantitative reverse transcriptase PCR (StepOnePlus™, Applied Biosystems®, USA). Comparison of the sequenced genomes of TCH1516, FPR3757 and UAS391 yielded a limited number of variant genes (n=18) that were hypothesized to account for the observed difference in biofilm-forming capacity. Screening of Tn mutants disrupted in these target genes identified one mutant (NE229) bearing a transposon insertion in SAUSA300_1119 (*fakA*), which exhibited increased biofilm formation like UAS391 (p=0.9320). Transduction experiments confirmed that *fakA*::Tn corresponded to 1.9- to 4.6-fold increase in biofilm formation depending on the USA300 strain background ($p \leq 0.0007$), while complementation of the TCH1516 wild type *fakA* allele in UAS391 resulted in a 4.3-fold reduction in biofilm formation ($p<0.0001$). This sequential approach, consisting of strain typing, genome comparison, and functional genomics, identified *fakA*, a recently described fatty acid kinase in *S. aureus* that is essential for phospholipid synthesis and impacts the transcription of numerous virulence factors, as a negative regulator of biofilm formation in *S. aureus* USA300.

3.3.2.2. Background

Staphylococcus aureus causes infections ranging from minor skin infections to life-threatening diseases, such as pneumonia, meningitis, osteomyelitis, endocarditis, and septicaemia. Since their emergence in the 1960s, methicillin-resistant *S. aureus* have become one of the major causes of hospital-acquired (HA) infections such as implant-associated and postsurgical wound infections, as well as of community-acquired (CA) infections such as pneumonia. The success of these hospital-acquired MRSA (HA-MRSA) clones can be partly attributed to virulence-specific factors, such as extracellular toxins, surface structures facilitating tissue colonization, immune evasion and tissue destruction [1], as well as to prolonged persistence of MRSA infections linked to the formation of biofilms *in vivo* [2].

It is generally accepted that biofilms, comprising conglomerations of cells attached to a solid support and embedded in a matrix of extracellular polymers, represent a major problem in clinical practice, due to their formation on implanted medical devices [3] and their intrinsic enhanced resistance to antibiotics that are otherwise efficacious against the bacterium's planktonic life forms [4]. These biofilm-associated complications have triggered the search for potential genes and/or metabolic pathways, interruption of which could represent new therapeutic or preventive interventions specifically targeting this bacterial lifestyle. Functional genomics approaches such as transcriptomics and proteomics, performed on biofilm versus planktonic cells, have shed some light on the complexity of the biofilm phenotype in *S. aureus*. Among genes found to be up-regulated in biofilm cells were those encoding proteins involved in the synthesis of polysaccharide intercellular adhesin (PIA)/

polymeric *N*-acetyl-glucosamine (PNAG) as well as proteins mediating transport, amino acid metabolism, and translation, with many other up-regulated genes encoding hypothetical proteins of still unknown function [5]. Subsequent proteomic studies performed by Resch et al. [6] showed still more stringently that biofilm-induced proteins are involved in cell attachment and peptidoglycan synthesis, in pyruvate and formate metabolism, as well as in regulatory processes those exerted by the staphylococcal accessory regulator A protein.

We recently screened a large collection of clinically important MRSA isolates for their ability to form biofilms and subsequently typed these isolates [7]. This work yielded several strong biofilm-forming strains, with three of them belonging to the USA300 clonal lineage, one of which was selected for genome sequencing. Subsequent comparison of the strain's genome with those of other USA300 sequenced isolates revealed a particularly interesting pair of closely related USA300 strains showing notably different capacities for biofilm formation (UAS391 and USA300_TCH516). This finding offered the opportunity to search in clinical isolates at genome level for mechanisms of biofilm formation. Thus, various USA300 *S. aureus* clones, which are closely related as per whole genome mapping, but markedly different in biofilm formation, were compared at genome level and consequently, genetic loci with different alleles were identified. Corresponding knockout mutants of these genes, obtained from a publicly available mutant library of the same clonal lineage (USA300-JE2), were then phenotypically characterized for their potential role in biofilm formation. Transposon-mediated interruption of one of the tested divergent genes, SAUSA300_1119, corresponding to the gene *fakA*, resulted in drastically increased levels of biofilms as compared to the parental control strain JE2, marking this gene as an important determinant of biofilm formation. These results shed more light on the genetic factors regulating biofilm formation in *S. aureus*.

3.3.2.3. Methods

3.3.2.3.1. Bacterial strains and growth conditions

USA300 strains used for clonal, genomic, and phenotypic analyses are listed in **Table 4**. Tn insertion mutants used for genotypic and phenotypic analysis of biofilm formation were obtained from a sequence-defined transposon mutant library consisting of 1,952 strains, each containing a single mutation within a nonessential gene in strain USA300 JE2 [8] obtained from the NARSA repository (www.beiresources.org/). *S. aureus* USA300 FPR3757 (FPR3757) and USA300 JE2 (JE2) were also obtained from the NARSA repository. Strains UAS391, TCH1516, FPR3757 and JE2 were routinely grown on brain heart infusion (BHI) and lysogeny broth (LB) (Becton, Dickinson and Company,

USA) medium for biofilm and transduction experiments, respectively. Transposon insertion mutants were grown on BHI medium containing 10 µg/ml of erythromycin (Sigma-Aldrich, USA).

Table 4: USA300 strains used for clonal, genomic, and phenotypic analyses during the fatty acid kinase A study.

Strains/Plasmids	Description	Source
Strains		
UAS391	*Staphylococcus aureus* strain USA300_UAS391_	[18]
JE2	*Staphylococcus aureus* USA300 parental strain for the NARSA transposon library	NARSA
FPR3757	*Staphylococcus aureus* subsp. aureus USA300_FPR3757	NARSA
TCH1516	*Staphylococcus aureus* subsp. aureus USA300_TCH1516	ATCC
UAS391-Ery^S	Heat-cured erythromycin-sensitive derivative of UAS391	This study
TCH1516-Ery^S	Heat-cured erythromycin-sensitive derivative of TCH1516	This study
UAS391-NE229	UAS391-Ery^S transductant with mutation in EX97_05885	This study
TCH1516-NE229	TCH1516-Ery^S transductant with mutation in USA300HOU_1162	This study
NE229- pHD954	*Staphylococcus aureus* strain NE229 complemented with pHD954	This study
NE229- pHD957	*Staphylococcus aureus* strain NE229 complemented with pHD957	This study
RN0451	Phage φ11 lysogenic *S. aureus* strain (NARSA strain NRS136)	NARSA
RN0450	*S. aureus* RN0450 (NARSA strain NRS135)	NARSA
RN4420	Restriction-deficient intermediate *S. aureus* cloning host RN4420	NARSA
NE1646	Transposon mutant with insertion in USA300HOU_0155 (SAUSA300_0145)	NARSA
NE229	Transposon mutant with insertion in USA300HOU_1162 (SAUSA300_1119)	NARSA
NE1081	Transposon mutant with insertion in USA300HOU_2626 (SAUSA300_2561)	NARSA
NE454	Transposon mutant with insertion in USA300HOU_2631 (SAUSA300_2566)	NARSA
NE1290	Transposon mutant with insertion in USA300HOU_264 (SAUSA300_2576)	NARSA
NE81	Transposon mutant with insertion in USA300HOU_2319 (SAUSA300_2285)	NARSA
NE1036	Transposon mutant with insertion in USA300HOU_2602 (SAUSA300_2542)	NARSA
NE1038	Transposon mutant with insertion in USA300HOU_2678 (SAUSA300_2610)	NARSA
NE33	Transposon mutant with insertion in USA300HOU_2654 (SAUSA300_2589)	NARSA
NE1262	Transposon mutant with insertion in USA300HOU_2026 (SAUSA300_1984)	NARSA
NE1875	Transposon mutant with insertion in USA300HOU_1943 (SAUSA300_1918)	NARSA
NE1	Transposon mutant with insertion in USA300HOU_1372 (SAUSA300_1327)	NARSA
NE334	Transposon mutant with insertion in USA300HOU_2197 (SAUSA300_2161)	NARSA
NE809	Transposon mutant with insertion in USA300HOU_1260 (SAUSA300_1214)	NARSA
NE1403	Transposon mutant with insertion in USA300HOU_1626 (SAUSA300_1585)	NARSA
NE1026	Transposon mutant with insertion in USA300HOU_1325 (SAUSA300_1298)	NARSA
NE1314	Transposon mutant with insertion in USA300HOU_0953 (SAUSA300_0896)	NARSA
Plasmids		
pALC2073	Shuttle vector pALC2073	[11]
pHD954	pALC2073 with cloned *fakA* gene amplified from UAS391	This study
pHD957	pALC2073 with cloned *fakA* gene amplified from TCH1516	This study

3.3.2.3.2. Transduction experiments

Transduction was performed essentially as described [9]. Transducing phage φ11 was obtained from the supernatant of a culture of the lysogenic *S. aureus* strain RN0451 (NARSA strain NRS136) and propagated on *S. aureus* RN0450 (NARSA strain NRS135) by standard techniques [10]. A transducing phage stock was prepared by infection at 37 °C of *S. aureus* containing the *bursa aurealis* transposon insertion. After infection of cultures of the recipient *S. aureus* strains (UAS391 and TCH1516) with this

stock, transductants were selected on LB plates with 0.05 % sodium citrate (Sigma-Aldrich, USA) containing 5 mg/L erythromycin at 37 °C. The resulting colonies were purified at least twice on the same medium to ensure loss of the transducing phage.

3.3.2.3.3. Complementation experiments

To complement the *S. aureus* mutant strain NE229, total genomic DNA of strains UAS391 and TCH1516 was purified with the Quick Pick™ SML gDNA kit (BN Products & Services, Finland) according to the manufacturer's recommendations. *S. aureus* strains were lysed by adding 5 µg lysostaphin (Sigma-Aldrich, USA). The genes corresponding to SAUSA300_1119 from the *S. aureus* strains UAS391 and TCH1516 were amplified using ExTaq DNA polymerase (Takara Bio Europe, France) with the primer pair Glyk-1 (5'-TACCGAGCTCGAATTCTAGGAGGACAACTTGAAATGATTAG-3') and Glyk-2 (5'-GACGGCCAGTGAATTCATTTTTATTCTACTGAAAAGAAATATTG-3'). Polymerase chain reactions (PCR) were carried out in an Applied Biosystems 2720 Thermal Cycler using Ex Taq DNA polymerase. Annealing and elongation temperatures were 55 °C and 68 °C respectively, with an elongation time of 1 min per 1000 bp during 30 cycles. PCR-fragments were purified using the Qiaquick PCR Purification Kit (Qiagen GmbH, Germany) and analysed by gel electrophoresis on 1.0 % agarose gels. The resulting 1753 bp PCR fragments were cloned by the InFusion technique (Clontech Laboratories, Inc, USA) in the *EcoRI* site of the shuttle vector pALC2073 [11] yielding the plasmids pHD954 (UAS391) and pHD957 (TCH1516). DNA sequencing was performed at the VIB core sequencing facility (VIB Genetics Department, University of Antwerp, Belgium) using the pALC2073 vector primers TetR2 (5'-CAATGTAGGCTGCTCTACACCTAG-3'), pALC-2 (5'-GATCGGTGCGGGCCTCTTCGCTAT-3'), and the internal gene sequence primers Glyk-3 (5'-GGAGTACATTATTGTAAAAGCCAATGAATC-3') and Glyk-4 (5'- CCACACATATCATTAGTGGTGGACA-3'). These plasmids were transferred into the restriction-deficient intermediate *S. aureus* cloning host RN4220 to adapt the plasmid DNA [12] to the *S. aureus* modifications. Transformants were selected on LB plates supplemented with 10 µg/ml chloramphenicol (Sigma-Aldrich, USA). The plasmids pHD954 and pHD957 were isolated from the RN4220 strain and used to transform strain NE229. UAS391 was also complemented with the wild type *fakA* allele carried on pHD957.

3.3.2.3.4. RNA extraction and RT-PCR

Mutant strain NE229 and wild type strains FPR3757 and JE2 were grown as overnight cultures in 10 ml of BHI medium at 37 °C with shaking. Total RNA of the three bacterial strains was extracted after 16 h growth using Express Amptec kit (Ambion® by Life Technologies™, The Netherlands). Two µg of RNA was treated with DNase using the Turbo DNA-free™ Kit (Ambion® by Life Technologies™, The Netherlands) and

subsequently used for reverse transcription reaction using the Reverse Transcription System (Promega) with random primers according to the manufacturer's instructions. Real-time PCR was performed using a StepOnePlus™ system (Applied Biosystems®, USA) in a 20 µl reaction mixture with Absolute Blue qPCR SYBR Green ROX mix (Thermo Scientific, Inc, USA). For RT-PCR analysis, the cDNA samples were amplified with gene-specific primers 1162 F (5'-ATGATGTGGACGCAACACTTG-3') and 1162Rev (5'-AATCAAGCCCATAAACGCGTC-3'), in duplicate. Cycling conditions were 95 °C for 10 min, and 40 cycles of 95 °C for 15 s and 60 °C for 60 s and 72 °C for 40 s. Amplification plot and melting curve were analysed for the dynamics of fluorescence and specificity of amplification, correspondingly. Resulting PCR products were checked by gel electrophoresis.

3.3.2.3.5. Whole genome mapping

For WGM, UAS391 and TCH1516 were grown on BHI plates, and high molecular weight DNA was extracted from the overnight colonies using Argus® HMW DNA extraction kit (Opgen, Inc, USA). Following DNA extraction as recommended by manufactures protocol, DNA molecules were loaded on a MapCard surface (Opgen, Inc, USA) where single DNA molecules were immobilized and linearized. The linearized DNAs were subjected to *in situ* digestion with *NcoI* (Opgen, Inc, USA). Following digestion, the DNA molecules were stained with the fluorescent intercalating agent JoJo-1 forming part of the staining kit (Opgen, Inc, USA). The digested and stained DNA fragments were imaged and assembled by in-built assembler of Map Manager to produce whole genome restriction maps, as described previously [13]. Finally, derived whole genome maps were analysed using BioNumerics v7.5. (Applied Maths, Belgium).

3.3.2.3.6. Genome sequencing

The complete genome sequence of UAS391 was generated by using the Illumina HiSeq2000 platform, as described previously [14]. Sequence data of UAS391 were *de novo* assembled using Velvet [15] and SPAdes [16]. Assembled contigs were ordered against the UAS391 whole genome map using MapSolver software (Opgen, Inc, USA). Validated scaffolds were ordered against published *S. aureus* genome TCH1516 (accession no. CP000730), and the generated pseudo chromosome was compared to the genomes of TCH1516 and FPR3757 (accession no. CP000255.1) using Mauve v2.3.1 [17]. Similarly, we also performed a reference assembly independently by using the genome sequences of TCH1516 and FPR3757 as references, and SNPs were extracted in CLC Genomics Workbench 7.5.1 (QIAGEN, Denmark). The assembled chromosome of UAS391 was annotated as described [18]. Multiple alignment and phylogenetic analysis were performed using MEGA6 [19].

3.3.2.3.7. Flow biofilm assay and quantification of biofilm mass

A medium-throughput continuous flow system BioFlux 200 (Fluxion Biosciences, USA) was used to study biofilm formation under shear flow conditions, which mimics flow conditions of physiological liquids in the human body [20]. BHI or 0.5xBHI with 0.1 % glucose (Sigma-Aldrich, USA) was used to feed into the flow cell. Bacterial cultures at 0.05 McFarland were then used to inoculate the output wells; bacteria were pushed through the flow cell from the output well up to the horizontal microfluidic channel by reversing the flow and could attach for one hour followed by 16 h of incubation at 37 °C in BHI or 0.5xBHI with 0.1 % glucose at a flow rate of 0.5 dyne/cm^2. Biomass in the microfluidic channels was stained with SYTO 9 fluorescent stain (Invitrogen, Life Technologies, USA). Biofilm images were captured employing ZEN 2012 software (Zeiss, Germany) as combined tile images consisting of 81 one µm^2 horizontal tiles covering the entire microchannel. Actual fluorescence quantification was recorded as integrated density on the entire combined tile image using Image J freeware (http://imagej.nih.gov/) using "integrated density", "mean value" and "area" as measurement settings. Presented values are averages of three independent combined tile images.

3.3.2.3.8. Statistical analysis

Statistical analysis of biomass formation in the dynamic flow assay was performed using the R Project software (version 3.1.2.) (R Foundation, Austria). The influence of a gene interruption on biofilm formation and the comparison of the space occupied by the cells within the dynamic biofilms were analysed using a pairwise one-way ANOVA, Shapiro-Wilk normality testing, Bartlett's test of variances, and Tukey's honest significance difference testing. Results from RT-PCR were analysed through a Wilcoxon signed-rank test. $p<0.05$ were significant.

3.3.2.4. Results

3.3.2.4.1. Typing and phenotypic analysis of USA300 isolates

Whole genome mapping (WGM) allowed typing and grouping of strain UAS391 with sepsis strain USA300_TCH1516 (TCH1516) isolated at Texas Children's Hospital in Houston [21] along with two other *S. aureus* USA300 strains, USA300-FPR3757 (FPR3757) and its plasmid-cured laboratory derivative USA300-JE2 (JE2), both belonging to the USA300 clonal lineage. According to the WGM similarity cut-off recently established for USA300 isolates [22], a WGM-based clonal cluster is defined as a set of isolates having a whole genome map similarity of >95%, which assigned all four isolates discussed here to the same WGM clonal cluster (**Fig. 20**). As UAS391 was previously

identified as a prolific biofilm former [7], we directly compared its biofilm forming capacity to the other clonally related strains in a dynamic biofilm assay. Comparison of UAS391 with the other USA300 isolates in this dynamic biofilm model consistently revealed clear differences in this strain's ability to form biofilms under these conditions, with UAS391 forming 1.6- to 3.6-fold more biofilm than the other three USA300 strains, as measured by readout of fluorescence (p<0.0001) (**Fig. 21**).

Figure 20: Whole-genome maps of USA300 strains. Green lines indicate the identity of restriction pattern among the maps and red horizontal marks represent the variations.

3.3.2.4.2. Identifying potential gene targets by comparative genomics

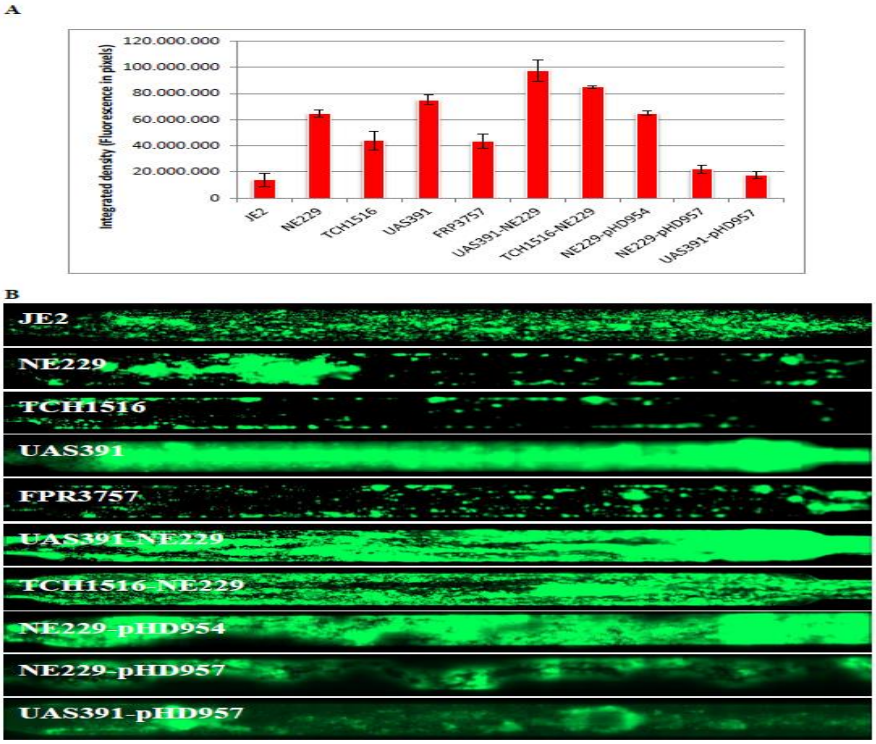

Figure 21: Biofilm formation of USA300 strains in the dynamic shear flow assay. The total biomass was determined by SYTO™ 9 staining *in triplicate*. Error bars in the graph represent the 95% confidence interval per strain. Quantification **(A)** and visualization **(B)** of biofilms formed by wild type USA300 strains and corresponding derivate strains.

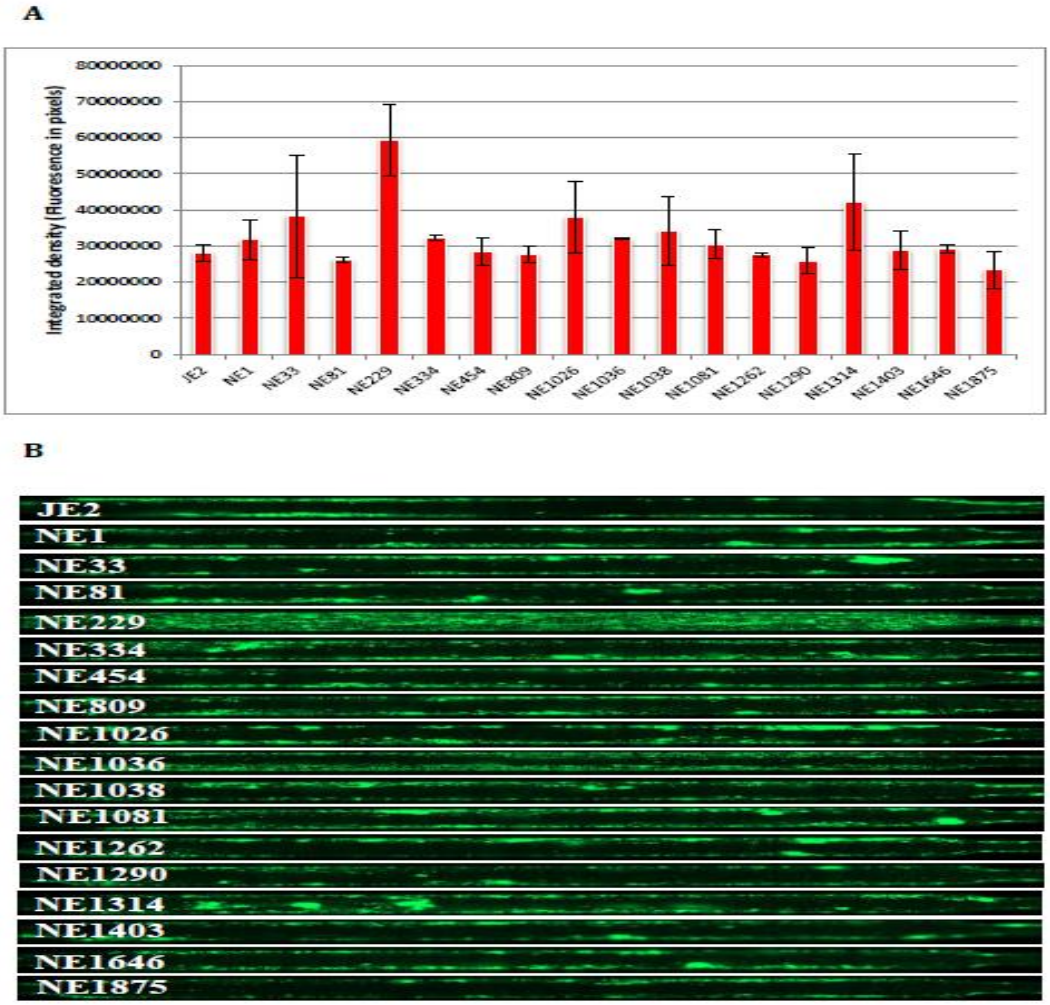

Figure 22: Biofilm formation of USA300 strains in the dynamic shear flow assay. The total biomass was determined by SYTO™ 9 staining *in triplicate*. Error bars in the graph represent the 95% confidence interval per strain. Quantification **(A)** and visualization **(B)** of biofilms formed by JE2 and its transposon mutants.

Genomic divergence between phenotypically diverse strains from the USA300 clonal lineage should be very limited [21, 23]. Since TCH1516 was closely related to UAS391 as per WGM and its total genome sequence is already available [21], we reasoned that comparing the whole genome sequences of UAS391 and TCH1516 would likely yield genetic differences that could account for the observed differences in the biofilm phenotype between these two USA300 strains. We thus sequenced the UAS391 genome by using the Illumina HiSeq2000 platform [18] and identified a total of 52 gene loci where UAS391 and TCH1516 exhibited single nucleotide polymorphisms (SNPs)

(**Suppl. Table 2**), of which 47 mapped within open reading frames (ORFs) and 5 within intergenic regions.

Based on genome sequence data and comparison of whole genome maps (**Fig. 20**), FPR3757 is closely related to TCH1516 [24], and thus also to UAS391, and forms less biofilms in the dynamic biofilm model, compared to UAS391 (p=0.0172) and like TCH1516 (**Fig. 21**) (p=1.0000). As the complete sequence for FPR3757 is also available, we then compared UAS391 and FPR3757 and identified a total of 91 gene loci where UAS391 and FPR3757 exhibited SNPs (**Suppl. Table 12**), of which 60 mapped within ORFs and 31 within intergenic regions. To further narrow down this initial list of deviating genes, we identified an overlap between the gene alleles of UAS391, TCH1516, and FPR3757 (**Suppl. Tables 11 & 12**). This reduced the initial list of genetic variations between strains UAS391 and TCH1516 to only those SNPs that were identical in the two weak biofilm forming strains TCH1516 and FPR3757 but different in UAS391, potentially identifying those SNPs primarily responsible for the increased biofilm formation in UAS391. This comparison yielded 18 SNPs as shown in **Table 5**. Of this, SNPs in transposases and phage-elements (USA300HOU_0286 and 1488) were excluded from further analysis (n = 2). Similarly, comparative genome alignment was performed for TCH1516, FPR3757 and UAS391 to confirm the data obtained by whole genome sequencing (**Suppl. Fig. 9**).

3.3.2.4.3. Identification of genes involved in biofilm formation using gene knockout mutants

To investigate the role of the corresponding genes in biofilm formation, we obtained 12 mutants from the Network on Antimicrobial Resistance in *S. aureus* (NARSA) library in which transposon insertions map in genes affected by SNPs, belonging to the above-identified group of 16 genes enumerated in **Table 5**. For the remaining four candidate genes, USA300HOU_0521, 1051, 1166, and 0502, corresponding knockout mutants were not present in the library and these were not studied further. We also randomly selected five genes affected by SNPs solely in either TCH1516 or FPR3757 in comparison to UAS391. In total, the 17 mutants obtained from the NARSA library (corresponding to USA300HOU_ 0953, 0155, 1162, 1260, 1372, 2197, 2626, 2631, 2641, 2319, 2602, 2678, 2654, 1626, 2026, 1338, 1943) were phenotypically tested in duplicate for their ability to form flow biofilms using the library parental strain JE2 as the corresponding control. Significant positive and negative variations of the degree of biofilm formation as compared to JE2 were found (p=0.0018). Out of the 17 mutants tested (**Fig. 22**), one mutant NE229 showed a 2-fold increase in biofilm formation compared to JE2 (p=0.0024). NE229 harbours the transposon insertion at position 393

in ORF SAUSA300_1119 encoding the fatty acid kinase *fakA* located in the genome from position 1223940 to 1225586 nt [25] (**Suppl. Fig. 10**).

Table 5: Single nucleotide polymorphisms (SNPs) between TCH1516/FPR3757 and UAS391. Consensus base representing TCH1516 and FPR3757, allele represents UAS391.

Consensus base (TCH1516/FPR3757)	Allele UAS391	Gene locus tag (in TCH1516/FPR3757)	Predicted amino acid change (TCH1516/FPR3757)	Gene and putative function
G	T	USA300HOU_0286/SAUSA300_0267	ABX28317.1:p.Leu1Phe/ ABD20793.1:p.Leu1Phe	IS1272 transposase
T	C	USA300HOU_0155/SAUSA300_0145		Phosphate-import protein PhnD/ABC Transporter, periplasmic binding protein
G	A	USA300HOU_0521/SAUSA300_0513	ABX28547.1:p.Met386Ile /ABD21711.1:p.Met386Ile	*gtlX*: glutamyl-tRNA synthetase
A	C	USA300HOU_1051/SAUSA300_1013	ABX29071.1:p.Asn267Thr /ABD22865.1:p.Asn263Thr	Bacterial cell division membrane protein FtsW
A	G	USA300HOU_1162/SAUSA300_1119	ABX29177.1:p.Glu524Gly /ABD22391.1:p.Glu524Gly	*fakA*: Fatty acid kinase
G	T	USA300HOU_1166/SAUSA300_1123	ABX29181.1:p.Gly169Val /ABD22842.1:p.Gly169Val	*fabD*: malonyl CoA-acyl carrier protein transacylase (Lipid metabolism)
A	G	USA300HOU_1372/SAUSA300_1327	ABX29382.1:p.Val1114Ala/ABD22444.1:p.Val1114Ala	Ebh: Cell Wall-Associated Fibronectin-Binding Protein
C	A	USA300HOU_2197/SAUSA300_2161		Hyaluronate lyase is a glycosaminoglycan (GAG) polysaccharide lyase family. This family consists of a group of secreted bacterial lyase enzymes capable of acting on glycosaminoglycans, such as hyaluronan and chondroitin, in the extracellular matrix of host tissues, contributing to the invasive capacity of the pathogen.
G	A	USA300HOU_2631/SAUSA300_2566	ABX30617.1:p.Pro27Ser/ ABD22163.1:p.Pro27Ser	HTH-type Transcriptional regulator ArcR, signal transduction system
C	T	USA300HOU_2641/SAUSA300_2576		PTS system, fructose-specific II ABC component, multi-protein system involved in regulation of metabolic and transcriptional processes
T	C	USA300HOU_2319/SAUSA300_2285		Aldose 1-epimerase
G	A	USA300HOU_2602/SAUSA300_2542	ABX30588.1:p.Arg517*/ABD21513.1:p.Arg517*	Acyl-coenzyme A synthetases/AMP-(fatty) acid ligases (Lipid metabolism)
A	C	USA300HOU_2654/SAUSA300_2589	ABX30640.1:p.Ser1782Ala/ABD21900.1:p.Ser1782Ala	Serine-rich adhesin for platelets, cell surface protein precursor; KxYKxGKxW signal peptide

C	T	USA300HOU_0502/SAUSA300_0486	ABX28528.1:p.Thr85Met/ABD20674.1:p.Thr85Met	Uncharacterized protein YabR
C	T	USA300HOU_1626/SAUSA300_1585	ABX29633.1:p.Ser35Leu/ABD21751.1:p.Ser35Leu	tRNA threonylcarbamoyladenosine dehydratase (Cells lacking this gene have a normal growth phenotype but are unable to survive in a competitive growth situation with the wild type strain. They display only the t6A but not the ct6A modification in tRNAs, and have lower decoding efficiency than wild type. They show no defects in motility or antibiotic sensitivity. In growth competition experiments, a tcdA mutant shows reduced fitness compared to wild type, but outcompetes a *csdA* mutant.)
A	G	USA300HOU_2026/SAUSA300_1984	ABX30023.1:p.Lys118Arg/ABD20720.1:p.Lys118Arg	Putative membrane peptidase YdiL
T	C	USA300HOU_1488/SAUSA300_1436		phage lipoprotein
T	-	USA300HOU_1338/SAUSA300_1298	ABX29349.1:p.Phe130fs/ABD22196.1:p.Phe132fs	5-bromo-4-chloroindolyl phosphate hydrolysis protein

Reverse transcription PCR (RT-PCR) was performed to determine whether the *bursa aurealis* insertion had affected transcription of SAUSA300_1119. Primers were designed downstream of the transposon mutation. Transcription of SAUSA300_1119 in NE229 showed a significant decrease compared to that in wild type strains FPR3757 and JE2 (Cts of 31.9, 26.2, and 26.0, respectively) (p<0.0001). A similar decrease in transcription was also observed for the TCH1516-EryS and the UAS391-Ery^S strain transduced with the SAUSA300_1119 mutated allele from NE229 (p<0.0001) (**Fig. 23**).

The SAUSA300_1119 in UAS391 harbours a non-synonymous SNP (Glu524Gly) as compared to strains TCH1516 and FPR3757 (**Table 5**). BLAST search identified it as a unique SNP and it can thus be considered as the mutant version of the corresponding gene present in TCH1516 and FPR3757, with similar wild type alleles being present among other sequenced *S. aureus* isolates (**Suppl. Fig. 10**).

3.3.2.4.4. Transductants mutated in *fakA* gene exhibit elevated biofilm formation

To further corroborate the negative role of *fakA* in biofilm formation by USA300, the knockout mutation in gene SAUSA300_1119 was transferred from NE229 into both UAS391-EryS and TCH1516-EryS employing phage-mediated transduction resulting in UAS391-NE229 and TCH1516-NE229, respectively. Knocking out SAUSA300_1119 in TCH1516 (locus tag USA300HOU_1162) resulted in a 1.7-fold increase in biofilm formation compared to the wild type TCH1516 (p=0.0007) and at levels like the wild type

UAS391 (*p*=0.9710) (**Fig. 21**). This effect was also observed in the UAS391 background where UAS391-NE229 exhibited even more abundant biofilm formation than the wild type UAS391 (*p*=0.0510) (**Fig. 21**).

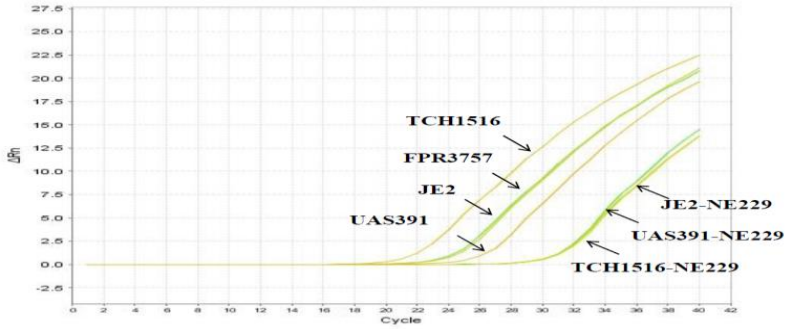

Strain	Ct (mean)	Ct (Std Dev)
JE2	26.0482	0.1228
FPR3757	26.229	0.0322
UAS391	27.8113	0.0867
TCH1516	23.6982	0.0541
JE2-NE229	31.8522	0.4254
TCH1516-NE229	31.5482	0.054
UAS391-NE229	32.2225	0.2792

Figure 23: Transcription levels of the *fakA* gene in UAS391, TCH1516, FPR3757, JE2 and in corresponding transductant strains. Transcription levels of *fakA* were measured *in duplicate* by real-time RT-PCR and expressed as an amplification plot and Ct mean values.

3.3.2.4.5. A plasmid-borne copy of the wild type *fakA* gene complements the mutant phenotype

To unambiguously prove that the enhanced biofilm phenotype observed in the NE229 strain is indeed due to the knockout mutation of the *fakA* gene, the mutant strain was complemented with a plasmid-borne intact *fakA* allele present in the TCH1516 strain or with the corresponding SNP-containing allele present in the UAS391 strain, yielding NE229-pHD957 and NE229-pHD954 strains, respectively. As shown in **Fig. 21**, the amount of biofilm produced by NE229-pHD957 was 2.9-fold lower as compared to NE229 (*p*=0.0003), and like the amount of biofilm produced by the parent JE2 strain (*p*=0.9831), whereas the amount of biofilm produced by NE229-pHD954, containing only mutant *fakA* allele was the same as in NE229 (*p*=1.0000). Additionally, complementing UAS391 with pHD957 resulted in a 4.3-fold decrease in biofilm mass as compared to the parent UAS391 (*p*<0.0001).

3.3.2.5. Discussion

By comparing the whole genome sequences of closely related USA300 strains that strongly differed in their capacity to form biofilms in a dynamic flow model, identified genetic differences (SNPs) were hypothesized to be responsible for this altered biofilm phenotype. Seventeen transposon mutants knocked out in these genes in the

USA300-JE2 background (NARSA strains) were evaluated for the degree of biofilm formation in comparison to the parent JE2. Transposon-mediated interruption of one of the tested divergent genes, *fakA* [25], previously known as *vfrB* [26], resulted in a 4.6-fold increase in biofilm formation as compared to the parental control strain JE2. In the other USA300 strains, UAS391 and TCH1516, the *fakA*::Tn mutations also led to increased biofilm formation, and further complementation experiments confirmed the role of *fakA* in the regulation of biofilm formation.

Running the protein sequence of SAUSA300_1119 in Simple Modular Architecture Research Tool (SMART) identified two domains within the protein sequence: Dak2 encoding the predicted phosphatase domain of the dihydroxyacetone kinase family (35 to 200 nt), and Dak1_2 encoding the kinase domain of the dihydroxyacetone kinase family (236 nt to 548 nt). The glutamic acid to glycine change is located at position 524 of the protein corresponding to its kinase domain. These proteins, collectively called Dak2 domain proteins have homologues in a wide variety of bacteria. Transposon insertions in *fakA* were first isolated in a large *S. aureus* transposon (*bursa aurealis*-bearing) insertion mutants library screen based on an increased resistance to an antimicrobial peptide [27]. Importantly, this *fakA* (then called *dak2*) mutant exhibited an altered membrane phospholipid composition compared to its wild type parent [27]. Recent studies have further delineated the multiple functions of *fakA* as an important regulator of virulence factors [26] and as a fatty acid kinase responsible for host fatty acid incorporation by *S. aureus* [25]. Interestingly, in the present study, complementation by the *fakA* allele of TCH1516, which is the consensus allele, in the *fakA*::Tn NE229 and in the UAS391 strains decreased the amount of biofilm formation by 2.7- and 4.3-fold, respectively, to the level observed in the JE2 wild type strain. However, similar complementation by the UAS391 *fakA* allele, which harbours the glutamic acid to glycine change, did not affect biofilm formation in *fakA*::Tn NE229. Taken together, these results imply that the mutation in the UAS391 *fakA* might have impacted the catalytic activity of the kinase and whether UAS391 exhibits an altered membrane phospholipid composition due to this amino acid change, which increased its biofilm forming ability, remains to be studied.

Interestingly, microarray-based gene expression data from a USA300 *fakA*::Tn mutant showed significant up-regulation of 26 and down-regulation of 19 genes [25]. The down-regulated genes included *saeP* and *saeQ* that are part of the *saeRS* two-component regulatory system and are known to regulate the activity of the *saeS*-encoded sensor histidine kinase [28]. The *saeRS* system was also recently shown to be a negative regulator of biofilm formation in *S. aureus* [29]. This study showed that an *S. aureus* Newman Δ*saeRS* strain exhibited an enhanced biofilm phenotype, like

the *fakA*::Tn JE2-NE229 mutant and the UAS391 wild type strains in our study. Taken together, these phenotypic and gene expression data strongly suggest a potential interaction between *fakA* and *saeRS* in negatively regulating biofilm formation in *S. aureus*. Finally, mice infected with *vfrB*::Tn (*fakA*::Tn) *S. aureus* have been shown to develop significantly larger abscess areas and dermonecrosis [26], which also reflects the increased biofilm abundance observed for the *fakA*::Tn mutant in our study.

Thus, utilizing a combination of functional assays and genomics, we identified *fakA*, a known virulence factor regulator and a fatty acid kinase, as an important negative regulator of biofilm formation in *S. aureus* USA300.

3.3.2.6. Conclusions

The sequential approach used here, starting from comparing clonally related (as per optical mapping) clinical isolates with different clinically relevant phenotypes, then comparing the respective total genome information allowed to pinpoint a gene locus, that is clearly of relevance for biofilm formation in *S. aureus*.

3.3.2.7. Addendum

3.2.2.7.1. Acknowledgements

We thank the Network on Antimicrobial Resistance in *Staphylococcus aureus* (NARSA) Program for providing *bursa aurealis* transposon mutants and other *S. aureus* strains. We also thank Olivier Denis (Université Libre de Bruxelles) for providing strains and Francine Deboeck for excellent technical assistance. This work is supported by funding from Research Foundation Flanders (FWO G.0983.10N and Research grant no. 1522412N). B.B.X. is supported by the University of Antwerp Research Funds (BOF-DOCPRO 2012-27450). SDB is supported by a research grant by the Institute for the Promotion of Innovation by Science and Technology (IWT) in Flanders, project number 140746.

3.3.2.7.2. Contribution to authorship

SMK, HG and JS conceived the study. JS, SDB, PM, JPH, HDG and ATR carried out the experimental work. SMK, HDG, JPH, HG, JS and SDB drafted the manuscript. BBX performed bioinformatic analysis. All authors read and approved the final manuscript. In detail, flow biofilm assay, quantification of biofilm mas and statistical analysis was performed by SDB.

3.3.2.7.3. Supplementary figures

Supplementary Figure 9: Comparative genome alignment of USA300, TCH1516, FPR3757 and UAS391. Pink regions show homology and the vertical lines shows conserved blocks. The UAS391 ~13 kb genomic region (from 680369 bp to 693620 bp) is translocated to (1630711 to 1642611bp) in FPR3757.

Supplementary Figure 10: Multiple alignments of *fakA* gene sequences in *S. aureus* and *S. epidermidis*. Unique nucleotide variation in SAUSA300_1119 of UAS391 encoding a fatty acid kinase *fakA* at position 1223940 nt, corresponding to nt 393 of the gene. The respective SAUSA300_1119 allele in UAS391 contains a non-synonymous SNP (Glu to Gly) as compared to strains TCH1516 and FPR3757. The Genbank accession numbers were indicated among these 50 strains. The first 45 strains represent *S. aureus*, the last 5 strains represent *S. epidermidis*.

3.3.2.7.4. Supplementary tables

Supplementary Table 11: Complete list of SNPs in genes representing divergent alleles in UAS391 and TCH1516 and their putative gene functions. TCH1516 was used as a reference for comparison with the allelic change in UAS391. Nucleotide changes in bold red represent the common SNPs in both FPR3757 and TCH1516 as compared to UAS391 (also in Table 5). [1] The symbol (*) refers to the predicted amino acid change as a stop codon caused by the corresponding SNP. [2] The abbreviation (fs) refers to 'frame shift mutation'.

Reference	Allele	Gene locus tag	Predicted amino acid change	Gene and putative function
T	C	USA300HOU_0026		Transposase for insertion sequence-like element IS431*mec*
A	G	USA300HOU_0026		Transposase for insertion sequence-like element IS431*mec*
G	A	USA300HOU_0026	Ala143Val	Transposase for insertion sequence-like element IS431*mec*

T	**C**	**USA300HOU_0155**		**Phosphate-import protein PhnD/ABC Transporter, periplasmic binding protein**
T	C	USA300HOU_0169		*cap5G*: Capsular protein
A	-	USA300HOU_0188	Leu1830Phe	The adenylation domain of nonribosomal peptide synthetases (NRPS)
C	T	USA300HOU_0192	Leu1830Phe	Tyrocidine synthase 3 (produced by *Bacillus brevis* ATCC 8185) act via the nonribosomal pathway)
G	**T**	**USA300HOU_0286**	**Leu1Phe**	**IS1272 transposase**
C	A	USA300HOU_0386	Glu33*[1]	uncharacterized protein
C	**T**	**USA300HOU_0502**	**Thr85Met**	**S1_RPS1_repeat_hs4 small ribosomal subunit thought to be involved in the recognition and binding of mRNA's during translation initiation**
C	**T**	**USA300HOU_0502**	**Thr85Met**	**Uncharacterized protein YabR**
G	**A**	**USA300HOU_0521**	**Met386Ile**	***gtlX*: glutamyl-tRNA synthetase**
A	G			Intergenic region
A	C	USA300HOU_0684	Tyr137His	Uncharacterized protein
T	C	USA300HOU_0684	Tyr137His	Phosphate transport regulator (distant homolog of PhoU)
A	G	USA300HOU_0858	Lys56Glu; Gln2Arg	uncharacterized protein
T	**A**	**USA300HOU_0953**	**Val209Glu**	***oppC3*: Oligopeptide ABC transporter, permease protein which generally binds type 2 PBPs.**
G	T			Intergenic region
G	A			Intergenic region
A	**C**	**USA300HOU_1051**	**Asn267Thr**	**Bacterial cell division membrane protein FtsW**
A	C	USA300HOU_1087	Asp88Ala	Non-canonical purine NTP pyrophosphatase
A	**G**	**USA300HOU_1162**	**Glu524Gly**	***fakA*- Fatty acid kinase**
G	**A**	**USA300HOU_1163**	**Gly644Asp**	***recG*: recG ATP-dependent DNA helicase**
G	**T**	**USA300HOU_1166**	**Gly169Val**	***fabD*: malonyl CoA-acyl carrier protein transacylase (Lipid metabolism)**
A	G	USA300HOU_1260		Low specificity L-threonine aldolase (Amino acid transport and metabolism)
T	**-**	**USA300HOU_1338**	**Phe130fs[2]**	***xpaC*: 5-bromo-4-chloroindolyl phosphate hydrolysis protein**
A	**G**	**USA300HOU_1372**	**Val1114Ala**	***ebh*: Cell Wall-Associated Fibronectin-Binding Protein**
T	A	USA300HOU_1386	Tyr34Phe	uncharacterized protein
T	**C**	**USA300HOU_1488**		**phage lipoprotein**
C	T	USA300HOU_1492		lipoprotein

| Fatty acid kinase A

G	**A**	**USA300HOU_1626**	**Ser35Leu**	**tRNA threonylcarbamoyladenosine dehydratase (Cells lacking this gene have a normal growth phenotype but are unable to survive in a competitive growth situation with the wild type strain. They display only the t6A but not the ct6A modification in tRNAs, and have lower decoding efficiency than wild type. They show no defects in motility or antibiotic sensitivity. In growth competition experiments, a tcdA mutant shows reduced fitness compared to wild type, but outcompetes a csdA mutant.)**
A	G	USA300HOU_1630	Ser63Pro	*lytH*: peptidoglycan aminohydrolase involved in cell envelope biogenesis, outer membrane
C	T	USA300HOU_1825	Gly234Glu	*hemE*: uroporphyrinogen decarboxylase is a dimeric cytosolic enzyme
C	T	USA300HOU_1844		*rluA2*: Ribosomal large subunit pseudouridine synthase
A	G	USA300HOU_1881		*vraS*: signal transduction histidine kinase
A	T	USA300HOU_1899		Uncharacterized protein
C	T	USA300HOU_1942		*mapW2*: Cell surface/membrane protein, superantigen-like protein 7
T	-	USA300HOU_1967	Lys73fs	Phage terminase small subunit
A	**G**	**USA300HOU_2026**	**Lys118Arg**	**Putative membrane peptidase YdiL**
A	G	USA300HOU_2118	Ile81Thr	Uncharacterized N-acetyltransferase YbbJ
C	**A**	**USA300HOU_2197**		***hysA*: Hyaluronate lyase is a glycosaminoglycan (GAG) polysaccharide lyase family. This family consists of a group of secreted bacterial lyase enzymes capable of acting on glycosaminoglycans, such as hyaluronan and chondroitin, in the extracellular matrix of host tissues, contributing to the invasive capacity of the pathogen.**
A	C	USA300HOU_2249	Tyr6Ser	uncharacterized protein
T	**C**	**USA300HOU_2319**		**Aldose 1-epimerase**
G	A			Intergenic region
A	C			Intergenic region
C	A	USA300HOU_2486		Pseudogene - frameshift of cell wall surface anchor protein
G	**A**	**USA300HOU_2602**	**Arg517***	***acsA2*: Acyl-coenzyme A synthetases/AMP-(fatty) acid ligases (Lipid metabolism)**
T	A	USA300HOU_2626	Ser355Thr	PhoA Alkaline phosphatase Inorganic ion transport and metabolism

G	**A**	**USA300HOU_2631**	**Pro27Ser**	**HTH-type Transcriptional regulator ArcR, signal transduction system**
C	**T**	**USA300HOU_2641**		**PTS system, fructose-specific II ABC component, multi-protein system involved in regulation of metabolic and transcriptional processes**
A	**C**	**USA300HOU_2654**	**Ser1782Ala**	**Serine-rich adhesin for platelets, cell surface protein precursor; KxYKxGKxW signal peptide**
C	T	USA300HOU_2678		*hisC2*: Histidinol-phosphate aminotransferase, biosynthesis of amino acids

Supplementary Table 12: Complete list of SNPs in genes representing divergent alleles in UAS391 and FPR3757 and their putative gene functions. FPR3757 was used as a reference for comparison with the allelic change in UAS391. Nucleotide changes in bold red represent the common SNPs in both FPR3757 and TCH1516 as compared to UAS391 (also in Table 5). [1] The symbol (*) refers to the predicted amino acid change as a stop codon caused by the corresponding SNP. [2] The abbreviation (fs) refers to 'frame shift mutation'.

Reference	Allele	Gene locus tag	Predicted amino acid change	Gene and putative function
A	G			Intergenic region
C	G	SAUSA300_0004	Pro358Ala	*recF*: DNA replication and repair protein RecF
T	C	SAUSA300_0005	Leu84Ser	*gyrA*: DNA gyrase subunit A
T	A	SAUSA300_0026 , Misc. feature: SCCmecIV		Ribosomal RNA large subunit metyhltransferase H
T	**C**	**SAUSA300_0145**		**Phosphonate ABC transporter, phosphonate binding protein**
T	**G**	**SAUSA300_0160**	**Leu235Val**	**Cap5I: Capsular polysaccharide biosynthesis protein**
T	A	SAUSA300_0203	Asn358Lys	putative lipoprotein
C	T			Intergenic region
T	C	SAUSA300_0226	Thr601Ala	3-hydroxylacyl-CoA dehydrogenase
A	C	SAUSA300_0242	Thr341Pro	*gutB*: sorbitol dehydrogenase
G	**T**	**SAUSA300_0267**	**Leu1Phe**	**Transposase**
C	T	SAUSA300_0322	Asp258Asn	NADH-dependent flavin oxidoreductase, Oye family
T	G	SAUSA300_0322	Ser200Arg	NADH-dependent flavin oxidoreductase, Oye family
C	A			Intergenic region
A	T	SAUSA300_0375	Glu106Asp	Histidine phosphatase superfamily
C	T	SAUSA300_0380	Gly108Asp	*ahpF*: Alkyl hydroperoxide reductase subunit F
A	T	SAUSA300_0414 , Misc. feature: vSAalpha	Glu209Asp	Tandem lipoprotein
T	-			Intergenic region
T	C			Intergenic region
G	A			Intergenic region

C	**T**	**SAUSA300_0486**	**Thr85Met**	**S1 RNA binding protein**
T	C			Intergenic region
G	**A**	**SAUSA300_0513**	**Met386Ile**	***gltX*: Glutamate-tRNA ligase**
T	-			Intergenic region
AA	TT			Intergenic region
G	T			Intergenic region
A	T			Intergenic region
T	A			Intergenic region
TTTTT	GAGCC			Intergenic region
T	G			Intergenic region
T	C	SAUSA300_0694		Uncharacterized protein
G	T	SAUSA300_0750	Glu17Asp	Uncharacterized protein
A	C			Intergenic region
A	T			Intergenic region
A	-			Intergenic region
T	**A**	**SAUSA300_0895**	**Val209Glu**	***oppC*: Oligopeptide ABC transporter permease**
G	T			Intergenic region
G	A			Intergenic region
G	A	SAUSA300_0980	Asp71Asn	Membrane protein
A	**C**	**SAUSA300_1013**	**Asn263Thr**	**Cell division protein FtsW/RodA/SpoVE family protein**
C	A	SAUSA300_1020	Ala95Ser	Glycerophosphoryl diester phosphodiesterase
T	C	SAUSA300_1073	Tyr306His	*Sun*: Ribosomal RNA small subunit methyltransferase B
A	**G**	**SAUSA300_1119**	**Glu524Gly**	***fakA*: fatty acid kinase**
G	**T**	**SAUSA300_1123**	**Gly169Val**	***fabD*: malonyl CoA-acyl carrier protein transacylase (Lipid metabolism)**
A	T	SAUSA300_1157		*polC*: DNA polymerase III polC-type
C	T			Intergenic region
A	G	SAUSA300_1169	Lys180Arg	*ftsK*: Cell division protein FtsW/RodA/SpoVE family protein
A	G	SAUSA300_1177		*cinA*: competence damage inducing protein A
C	T	SAUSA300_1236		Uncharacterized protein
T	A			Intergenic region
A	T	SAUSA300_1242	Ile761Phe	*sbcC*: exonuclease
A	C	SAUSA300_1251	Tyr80Ser	*parC*: DNA topoisomerase IV subunit A
T	**-**	**SAUSA300_1298**	**Phe132fs[1]**	**5-bromo-4-chloroindolyl phosphate hydrolysis protein**
A	**G**	**SAUSA300_1327**	**Val1114Ala**	***ebh*: Cell Wall-Associated Fibronectin-Binding Protein**
G	C			Intergenic region

T	A			Intergenic region
A	T			Intergenic region
T	-			Intergenic region
C	T	SAUSA300_1403 , Misc. feature: PhiSA2USA		Phage portal protein
T	**C**	**SAUSA300_1436 , Misc. feature: PhiSA2USA**		**Phage lipoprotein**
T	C	SAUSA300_1543	Thr145Ala	Coproporphyrinogen III oxidase
G	**A**	**SAUSA300_1585**	**Ser35Leu**	**ThiF family protein**
A	C	SAUSA300_1611		*valS*: signal transduction histidine kinase
T	C	SAUSA300_1725	Ile6Val	Transaldolase
C	G	SAUSA300_1753	Gly11Ala	*splF*: Serine protease
A	G			Intergenic region
C	T			Intergenic region
T	A			Intergenic region
C	T	SAUSA300_1779		
A	-	SAUSA300_1810	Glu438fs	IS1181 transposase
A	T			Intergenic region
-	A	SAUSA300_1918	Lys3fs	Phospholipase C domain protein
A	C	SAUSA300_1930 , Misc. feature: PhiSA3USA	Ile384Ser	Phage tail protein
A	-	SAUSA300_1968, Misc. feature: PhiSA3USA	Tyr38fs	Putative tail tape transcriptional regulator
A	**G**	**SAUSA300_1984**	**Lys118Arg**	**CAAX amino terminal protease self-immunity**
C	T	SAUSA300_2068		Uncharacterized protein
A	G	SAUSA300_2107	Glu56Gly	*mtlA*: Mannitol-specific phosphotransferase enzyme IIA component
T	C			
C	**A**	**SAUSA300_2161**		***hysA*: Hyaluronate lyase**
G	-			Intergenic region
T	**C**	**SAUSA300_2285**		***galM*: Aldose-1-epimerase**
T	-			Intergenic region
T	G	SAUSA300_2486	Ser249Ala	ATP-dependent Clp protease ATP-binding subunit ClpL
T	G	SAUSA300_2489	Lys795Gln	Antibiotic transport-associated protein like
T	G	SAUSA300_2503		Uncharacterized protein
G	**A**	**SAUSA300_2542**	**Arg517*[2]**	**Acyl-coenzyme A synthetases/AMP-(fatty) acid ligases (Lipid metabolism)**
T	A	SAUSA300_2559	Ser355Thr	*phoB*: Alkaline phosphatase
G	**A**	**SAUSA300_2566**	**Pro27Ser**	***arcR*: HTH-type transcriptional regulator ArcR**

C	**T**	**SAUSA300_2576**		**PTS System, fructose-specific IIABC component**
A	**C**	**SAUSA300_2589**	**Ser1782Ala**	**Serine-rich adhesin for platelets**
C	T	SAUSA300_2610		*hisC*: Histidinol-phosphate aminotransferase hisC

3.3.2.7.5. References

1. Stefani, S. and P.E. Varaldo, *Epidemiology of methicillin-resistant staphylococci in Europe.* Clin Microbiol Infect, 2003. **9**(12): p. 1179-1186.
2. Jones, S.M., et al., *Effect of vancomycin and rifampicin on meticillin-resistant Staphylococcus aureus biofilms.* Lancet, 2001. **357**(9249): p. 40-41.
3. Raad, I., A. Alrahwan, and K. Rolston, *Staphylococcus epidermidis: emerging resistance and need for alternative agents.* Clin Infect Dis, 1998. **26**(5): p. 1182-7.
4. Donlan, R.M. and J.W. Costerton, *Biofilms: Survival Mechanisms of Clinically Relevant Microorganisms.* Clin Microbiol Rev, 2002. **15**(2): p. 167-193.
5. Resch, A., et al., *Differential gene expression profiling of Staphylococcus aureus cultivated under biofilm and planktonic conditions.* Appl Environ Microbiol, 2005. **71**(5): p. 2663-76.
6. Resch, A., et al., *Comparative proteome analysis of Staphylococcus aureus biofilm and planktonic cells and correlation with transcriptome profiling.* Proteomics, 2006. **6**(6): p. 1867-77.
7. Vanhommerig, E., et al., *Comparison of biofilm formation between major clonal lineages of methicillin-resistant Staphylococcus aureus.* PLoS One, 2014. **9**(8): p. e104561.
8. Fey, P.D., et al., *A genetic resource for rapid and comprehensive phenotype screening of nonessential Staphylococcus aureus genes.* MBio, 2013. **4**(1): p. e00537-12.
9. Fitzgerald, J.R., *Methicillin-Resistant Staphylococcus aureus (MRSA) protocols*. Second Edition ed. 2007, Totoway, New Jersey, USA: Humana Press Inc.
10. Adams, M.H., *Bacteriophages*. 1959, New York, USA: Interscience Publishers, Inc. 1-620.
11. Bateman, B.T., et al., *Evaluation of a tetracycline-inducible promoter in Staphylococcus aureus in vitro and in vivo and its application in demonstrating the role of sigB in microcolony formation.* Infect Immun, 2001. **69**(12): p. 7851-7.
12. Kreiswirth, B.N., et al., *The toxic shock syndrome exotoxin structural gene is not detectably transmitted by a prophage.* Nature, 1983. **305**(20): p. 709-712.
13. Sabirova, J., et al., *Whole genome mapping as a fast-track tool to assess genomic stability of sequenced Staphylococcus aureus strains.* BMC Res Notes, 2014. **8**(7): p. 704.
14. Sabirova, J., et al., *Transcriptomics profile of biofilms produced by Staphylococcus aureus USA300.* Intersci Conf Antimicrob Agents Chemother, 2013. **Oral presentation**.
15. Zerbino, D.R. and E. Birney, *Velvet: algorithms for de novo short read assembly using de Bruijn graphs.* Genome Res, 2008. **18**(5): p. 821-9.
16. Bankevich, A., et al., *SPAdes: a new genome assembly algorithm and its applications to single-cell sequencing.* J Comput Biol, 2012. **19**(5): p. 455-77.
17. Darling, A.C., et al., *Mauve: multiple alignment of conserved genomic sequence with rearrangements.* Genome Res, 2004. **14**(7): p. 1394-403.
18. Sabirova, J.S., et al., *Complete genome sequences of two prolific biofilm-forming Staphylococcus aureus isolates belonging to USA300 and EMRSA-15 clonal lineages.* Genome Announc, 2014. **2**(3).
19. Tamura, K., et al., *MEGA6: Molecular Evolutionary Genetics Analysis version 6.0.* Mol Biol Evol, 2013. **30**(12): p. 2725-9.
20. Benoit, M.R., et al., *New device for high-throughput viability screening of flow biofilms.* Appl Environ Microbiol, 2010. **76**(13): p. 4136-42.
21. Highlander, S.K., et al., *Subtle genetic changes enhance virulence of methicillin resistant and sensitive Staphylococcus aureus.* BMC Microbiol, 2007. **7**: p. 99.
22. Shukla, S.K., et al., *Comparative whole-genome mapping to determine Staphylococcus aureus genome size, virulence motifs, and clonality.* J Clin Microbiol, 2012. **50**(11): p. 3526-33.

23. Tewhey, R., et al., *Genetic structure of community acquired methicillin-resistant Staphylococcus aureus USA300.* BMC Genomics, 2012. **13**: p. 508.
24. Diep, B.A., et al., *Complete genome sequence of USA300, an epidemic clone of community-acquired meticillin-resistant Staphylococcus aureus.* Lancet, 2006. **367**(9512): p. 731-739.
25. Parsons, J., et al., *Identification of a two-component fatty acid kinase responsible for host fatty acid incorporation by Staphylococcus aureus.* Proc Natl Acad Sci U S A, 2014. **111**(29): p. 10532-7.
26. Bose, J.L., et al., *Identification of the Staphylococcus aureus vfrAB operon, a novel virulence factor regulatory locus.* Infect Immun, 2014. **82**(5): p. 1813-22.
27. Li, M., et al., *Staphylococcus aureus mutant screen reveals interaction of the human antimicrobial peptide dermcidin with membrane phospholipids.* Antimicrob Agents Chemother, 2009. **53**(10): p. 4200-10.
28. Jeong, D.W., et al., *The auxiliary protein complex SaePQ activates the phosphatase activity of sensor kinase SaeS in the SaeRS two-component system of Staphylococcus aureus.* Mol Microbiol, 2012. **86**(2): p. 331-48.
29. Cue, D., et al., *SaeRS-dependent inhibition of biofilm formation in Staphylococcus aureus Newman.* PLoS One, 2015. **10**(4): p. e0123027.

3.4. Characterization of biofilm-associated candidate genes as a critical determinant of MRSA pathogenic success.

3.4.1. Remarkable geographical variations between India and Europe in carriage of the staphylococcal surface protein-encoding sasX/sesI and in the population structure of methicillin-resistant Staphylococcus aureus belonging to clonal complex 8

Sarah De Backer[1+], Basil B. Xavier[1+], Lavanya Vanjari[3], Jasmine Coppens[1], Christine Lammens[1], Lakshmi Vemu[3], Biljana Carevic[4], Waleria Hryniewicz[5], Philippe Jorens[6], Samir Kumar-Singh[2], Andie Lee [7#], Stephan Harbarth[7], Jacques Schrenzel[7], Evelina Tacconelli[8], Herman Goossens[1], Surbhi Malhotra-Kumar[1*]

[1] Laboratory of Medical Microbiology, [2] Molecular Pathology Group, Cell Biology and Histology, University of Antwerp, Wilrijk, Belgium, [3] Nizam's Institute of Medical Sciences, Hyderabad, India; [4] Clinical Centre of Serbia, Belgrade, Serbia; [5] National Institute of Public Health, Warsaw, Poland; [6] Intensive Care Unit, Antwerp University Hospital, University of Antwerp, Edegem, Belgium; [7] University of Geneva Hospitals and Medical Faculty, Geneva, Switzerland; [8] Department of Diagnostics and Public Health, G.B. Rossi University Hospital, University of Verona, Verona, Italy. These authors contributed equally to this article. #Current affiliation: Departments of Infectious Diseases and Microbiology, Royal Prince Alfred Hospital, Sydney, Australia; Faculty of Medicine, University of Sydney, Sydney, Australia.

[*]Corresponding author mailing address: Laboratory of Medical Microbiology, Campus Drie Eiken, University of Antwerp, S6, Universiteitsplein 1, B-2610 Wilrijk, Belgium. Phone: 32-3-265-27-52. Fax: 32-3-265-26-63. E-mail: surbhi.malhotra@uantwerpen.be

Published in: Clin Microbiol Infect. 2018 Aug 2. pii: S1198-743X(18)30542-1. doi: 10.1016/j.cmi.2018.07.024.

3.4.1.1. Abstract

SasX is a colonization-virulence factor that potentially underlies the success of methicillin-resistant *Staphylococcus aureus* (MRSA) sequence type (ST) 239 in Asia. We aimed to study the spread of *sasX* and the population structure of MRSA in two geographically distinct regions, Europe and India. MRSA (n=128) from screening and clinical samples from tertiary care patients in 12 European countries (n=119), and from India (n=9) were multilocus-sequence-typed and screened for *sasX* and its carrier ϕSPβ-like prophage by PCR. Whole genome sequencing was performed on *sasX*-harbouring

strains from India (n=5) and Europe (n=2) and on a selection non-harbouring *sasX* (n=36) (2x150bp, Miseq, Illumina, USA). Reads were mapped to the ST239 reference strain, TW20. *SasX* and *sesI*, a *sasX* homologue native to *Staphylococcus epidermidis*, were detected in five of the nine Indian MRSA belonging to ST239 and to other sequence types of CC8. In contrast, *sasX* was restricted to two ST239 strains in Europe. The intact *sasX* and *sesI* carrier ϕSPβ -like prophages were ~80 kb and ~118 kb and integrated into the *yeeE* gene. We identified 'novel' ST239 clades in India and Serbia that showed significant differences in base substitution frequencies (0.130 and 0.007, respectively, Tamura-Nei model) ($p<0.05$). Our data highlight the dissemination of *sasX* to non-ST239 sequence types of CC8. Detection of the *S. epidermidis*-associated *sesI* in MRSA provided unquestionable evidence of transfer between the two species. Stark differences in evolutionary rates between the novel Indian and Serbian ST239 clades identified here might be due to inherent clade characteristics or influenced by other environmental differences such as antibiotic use.

3.4.1.2. Introduction

Methicillin-resistant *Staphylococcus aureus* (MRSA) sequence type (ST) 239 is a highly prevalent clone in Asia, including India where hospital- and community-associated carriage of MRSA is high [1]. However, potential factors underlying the dissemination of ST239, such as the acquisition of antibiotic resistance and virulence-associated genes [2], remain largely elusive. For instance, an increased incidence of MRSA ST239 in clinical samples during 1998 in a Brazilian hospital was linked to the clone's remarkable capacity to adhere to epithelial cells and to form abundant biofilms [3], a tight assemblage of microbial cells enclosed by a protective polysaccharide matrix [4]. Furthermore, Li et al. [5] showed for the first time how an LPXTG motif-harbouring predicted surface protein SasX (SATW20_21850, herewith referred to as native SasX), contributed to the Chinese ST239 MRSA outbreak by enhancing nasal colonization, bacterial aggregation, lung disease, abscess formation, and immune evasion. *SasX*, carried on ϕSPβ-like prophage, was first identified in ST239 TW20 isolated in the UK [6-8]; however, its presence in other STs has also been recently reported [5,8,9]. *SasX* shows 95.79% homology at the nucleotide level to the *Staphylococcus epidermidis* surface protein *sesI*, which is also harboured on the ϕSPβ-like prophage [10,11], indicating a potential horizontal transfer between the closely related species. Acquisition of *sasX* by ST239 is believed to be the driving force underlying its successful dissemination in Asia [12]. On the other hand, *sasX* harbouring MRSA, including ST239, have remained rare in Europe [13]. We aimed to study and compare the occurrence and spread of *sasX* in ST239 and other STs isolated in Europe and India to understand the fundamental differences in the MRSA population structure in these two geographically distinct regions.

3.4.1.3. Methods

3.4.1.3.1. Bacterial strains and growth conditions

Among the 160 staphylococci studied, 128 were MRSA of different clonal types and 32 were coagulase-negative staphylococci. Of these, 95 were clonal complex (CC) 8 MRSA isolated from nasal/skin screening swabs from one Serbian (n=74), one Romanian (n=2) and one Italian (n=19) hospital within the SATURN project (2010-2015); 24 MRSA were isolated from wound, blood or sputum of hospitalized patients in Poland (n=9), Italy (n=2), Greece (n=1), Switzerland (n=1), Slovenia (n=2), Spain (n=1), Latvia (n=1), France (n=4), Germany (n=1), the United Kingdom (n=1) and Portugal (n=1) within the MOSAR project (2007-2011). Nine MRSA were isolated from infected wounds of patients admitted to a tertiary care hospital in India (2013-2014). Additionally, to study *sasX* in other staphylococci, *S. epidermidis* (n=22), *Staphylococcus capitis* (n=4) and *Staphylococcus hominis* (n=6), isolated from extubated endotracheal tubes at the University Hospital Antwerp, Belgium (2012-2013), were included. For all strains collected during the clinical trials, ethical approval at the corresponding hospital or clinical site was obtained. Informed consent was sought from each patient.

3.4.1.3.2. Molecular typing

Multilocus sequence typing (MLST) and CC groups (5/7 alleles shared) were performed as described previously (http://saureus.beta.mlst.net/) [14], and data were visualized using eBURST® v3 (Imperial College London, UK). All strains were screened for *sasX/sesI* by PCR/Sanger-sequencing as described previously [5], and similarly also for the presence of the ϕSPβ-like prophage (primers in **Suppl. Table 13**).

3.4.1.3.3. Quantitative biofilm assays

Log-phase cultures of all MRSA isolates harbouring *sasX/sesI* (n=7) and randomly selected isolates not harbouring these genes (n=35) were studied *in triplicate* for 24h -old or 17h -old biofilm formation under static (96-well microtiter plate) and continuous (Bioflux™; Fluxion Biosciences Inc., USA) flow conditions, respectively, as described previously [15,16].

3.4.1.3.4. Whole genome sequencing and comparative genome analysis

Genomic DNA was extracted from all seven MRSA harbouring *sasX/sesI* and a selection not harbouring *sasX* (n=36) (Master- Pure™ Complete DNA & RNA Purification Kit; Epicentre® Technologies Corp., USA) and whole genome sequencing was performed (2X150 bp paired-end sequencing, Nextera XT DNA Sample Preparation Kit, Miseq V2 kit; Illumina Inc., USA). Strain sequences were *de novo* assembled (SPADES v3.10.1) [17], and contigs were screened for virulence genes (https://cge.cbs.dtu.dk/services/VirulenceFinder/)

[18]. Contigs were mapped to the reference ST239 strain, TW20 (**Suppl. Table 14**), using MAUVE [19]. Also, the insertion site of the ϕSPβ-like prophages of corresponding study and reference strains was analysed using CLC Genomics Workbench V9.5.3 (QIAGEN, Denmark).

3.4.1.3.5. Phylogenetic analysis

Using PARSNP [20], 3064 core-genome single nucleotide polymorphisms (SNPs) were obtained from 43 randomly chosen clinical strains and 19 global representatives of ST239 from NCBI (**Suppl. Table 14**), in comparison with TW20. Phylogenetic reconstruction was performed using the maximum likelihood method (based on the Tamura-Nei model [21]) with MEGA7 [22]. Initial tree(s) for the heuristic search were obtained automatically by applying Neighbour-join and BIONJ algorithms to a matrix of pairwise distances estimated using the Maximum Composite Likelihood approach, and then selecting the topology with superior log-likelihood value. The tree with the highest log likelihood (-26677.11) was selected. A discrete Gamma distribution was used to model evolutionary rate differences among sites (five categories (+G, parameter ¼ 200.0000)). The rate variation model allowed for some sites to be evolutionarily invariable (+I, 0.35% sites). Phylogeny of *sasX/sesI* was studied using CLUSTALW multiple alignments of reference sequences of *sasX* (SATW20_21850, #NC_017331.1) and *sesI* (SERP1654, #NC_002976.3) with the genes isolated from the seven *sasX/sesI*-harbouring study strains [23].

3.4.1.3.6. Statistical analysis

A Welch two-sample T-test or a Wilcoxon rank sum test was used when data were either distributed normally or not, based on a Shapiro-Wilk normality test. Values of $p<0.05$ were considered significant (R Project software (version 3.1.2.); R foundation, Austria).

3.4.1.4. Results

3.4.1.4.1. Identification of *sesI* and *sasX* in hospital-associated Indian and European MRSA of different ST types

The 128 MRSA studied here belonged to 20 STs (**Suppl. Fig. 11**). Of note, 63/67 ST239 were isolated from a single Serbian hospital. Only two of the 119 European MRSA harboured *sasX* and both were ST239. These are strains (EU_ST239_7 and EU_ST239_16) isolated from an outbreak in the northeast/central Poland (**Suppl. Table 15**), identified by pulsed-field gel electrophoresis as common types prevalent in Poland during 1990-2001 [24]. On the other hand, in the very limited collection of Indian MRSA (n=9), *sasX* was detected in five strains belonging to different STs (ST239, ST161, and ST368). Of

note, all seven MRSA harbouring *sasX* identified in this study belonged to CC8 (**Suppl. Fig. 11**). Interestingly, in two (IN_ST368 and IN_ST239_2) of these seven MRSA, PCR-sequencing and BLAST analysis showed 100% homology to the *sesI* gene known to be harboured in *S. epidermidis* RP62A (**Fig. 24** and **Suppl. Table 15**). Sequence analysis showed 99.64%-100% homology of *sasX* detected in European (n=2) and Indian (n=3) strains to the native *sasX* found in TW20. Of the two European *sasX*-harbouring MRSA, the allele in EU_ST239_16 was 100% homologous and in EU_ST239_7 only 99.64% homologous at the nucleotide level to the native *sasX*. The latter, a novel variant that we named *sasX*-1, showed four SNPs, of which one was non-synonymous (Thr158Ala) compared with the native *sasX* (**Suppl. Fig. 12**). *SasX* or its variants could not be detected in the European coagulase-negative staphylococci studied here (n=32).

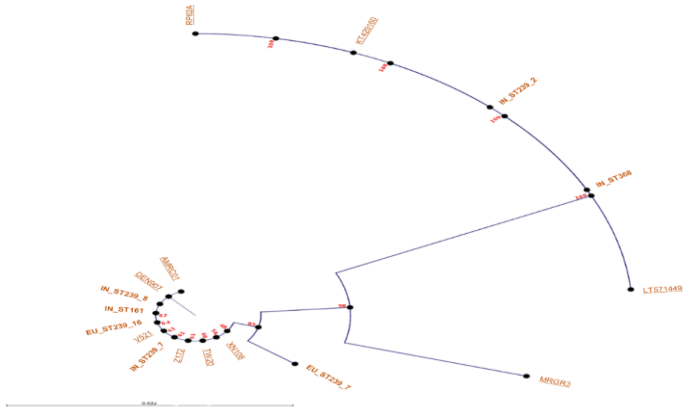

Figure 24: Circular phylogram reflecting evolutionary relationships between Indian and European clinical strains based on *sasX* homology and compared to ST239 reference sequences. XN108 (SAXN108_2287), TW20 (SATW20_21850), Z172 (SAZ172_2149), ARMC01, DEN907, V521, MRGR3, SPβ-like prophage carried by *S. epidermidis* (#KT429160.1), *S. epidermidis* isolate BHP0662 (#BN6763_RS09315) and RP62A (SERP1654) based on the maximum likelihood method showing bootstrap values for each tree branch. Reference strains are underlined; study strains are depicted in bold.

3.4.1.4.2. MRSA harbouring *sasX*, *sasX*-1 or *sesI* exhibit enhanced biofilm forming capacity

All MRSA carrying *sasX*, *sasX*-1 or *sesI* formed significantly more abundant biofilms under static conditions (optical density at 492 nm (OD_{492}) 0.240) (**Fig. 25A**) than those not harbouring the gene (OD_{492} 0.061; $p<0.001$). Interestingly, MRSA harbouring *sesI* (OD_{492} 0.330) formed even more abundant biofilms than those with *sasX* (OD_{492} 0.240) under static conditions ($p=0.037$). Indian MRSA carrying *sasX* or *sesI* formed significantly more abundant biofilms under both static and flow conditions (OD_{492} 0.245; $p=0.005$) (**Fig. 25A**) and continuous flow conditions (integrated pixel density 61 741 548; $p=0.011$) (**Fig. 25B&C**) than those not harbouring the gene (OD_{492} 0.055; integrated pixel

density 24 184 645). In contrast, *sasX*- and *sasX*-1-harbouring ST239 from Europe were also characterized by a strong biofilm formation capacity in the static assay (compared with other ST types: OD_{492} 0.062; p=0.022; compared with ST239: OD_{492} 0.048; p=0.0253), but these differences were less distinct in the continuous flow assay (integrated pixel densities of *sasX*- and *sasX*-1-harbouring ST239: 47, 447, 495, and of non-*sasX* harbouring ST types: 46, 124, 713; p=0.937).

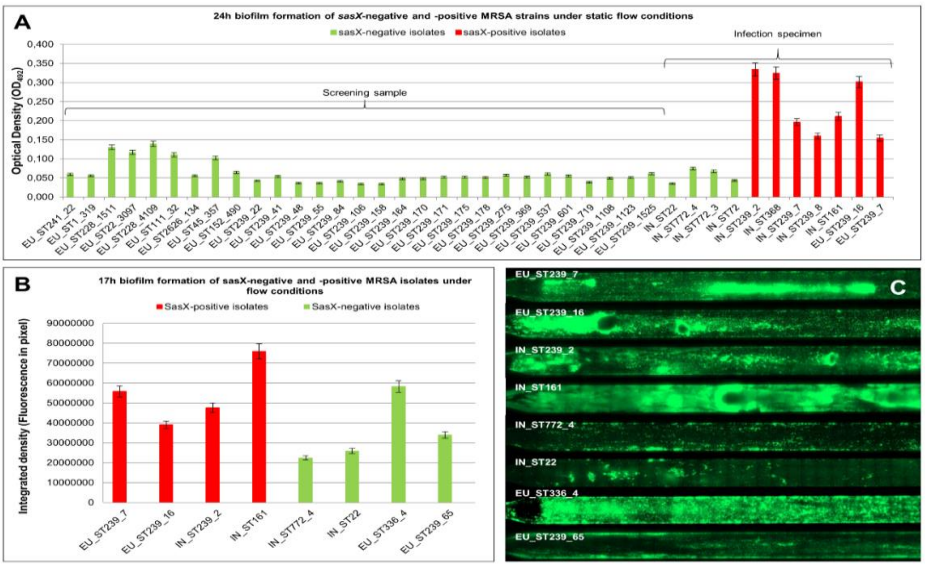

Figure 25: Formation of biofilms by 9 Indian and 33 European CC8 strains isolated from either hospital-associated infection specimens or nasal screening samples. **(A)** under static conditions, sasX, *sasX*-1 or *sesI*-harbouring strains are depicted in red, while non-*sasX*, -*sasX*-1 or –*sesI* harbouring strains are green. The total biomass was determined by crystal violet staining *in triplicate*. Represented are average OD_{492} values with error bars depicting 95% CIs; **(B)** Formation of flow biofilms by infection specimen strains EU_ST239_7, EU_ST239_16, IN_ST239_2, IN_ST161, IN_ST772_4, IN_ST22, EU_ST336_4, and EU_ST239_65; *sasX*, *sasX*-1 or *sesI*- harbouring strains are depicted in red, while non-*sasX*, -*sasX*-1 or –*sesI* harbouring strains are green. The total biomass was determined by SYTO™ 9 staining *in duplicate*. Error bars depict 95% CI; **(C)** Fluorescent microscopy images of infection specimen flow biofilms.

3.4.1.4.3. Variations in the ϕSPβ-like prophage among Indian and European MRSA

The *sesI*, *sasX,* and *sasX*-1 harbouring prophages in seven sequenced MRSA (two European, five Indian), as well as the *sesI*-carrying prophage of RP62A, were identified as the Bacillus ϕSPβc2 prophage, referred to as the ϕSPβ-like prophage. The prophage insertion was site-specific in all studied strains, as in TW20, and disrupted a 1080-bp putative inner membrane protein (*yeeE*, SATW20_20280) at nucleotide position 295, giving rise to two hypothetical proteins of 750 bp and 330 bp (**Fig. 26A**). The ϕSPβ-like prophage in RP62A was ~126 kb, whereas Indian strains harbouring *sesI* carried a ~116.7-120.8 kb ϕSPβ-like prophage. In TW20, ϕSPβ-like prophage is ~128.3 kb, whereas Indian

and European strains harbouring *sasX* carried a substantially shorter prophage of ~78-84.7 kb. *SasX*-1 in EU_ST239_7 was carried on a ~122-kb ϕSPβ-like prophage (**Fig. 26B**).

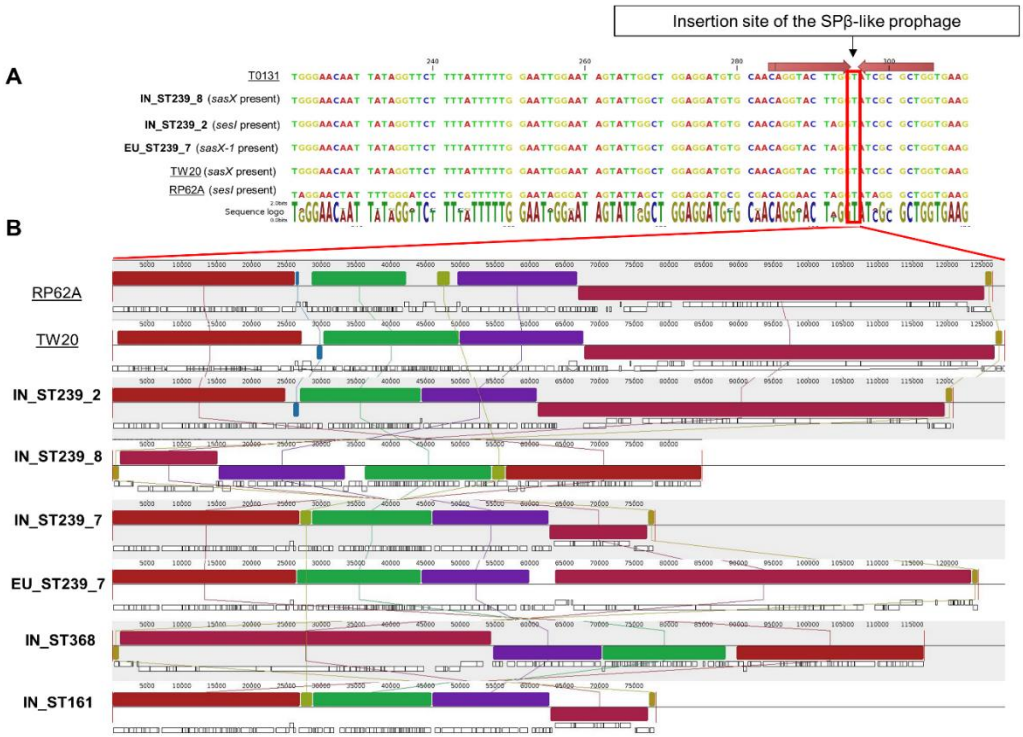

Figure 26: Characterization of the *sasX*, *sasX*-1 and *sesI*-carrying ϕSPβ-like prophage. (**A**) Likely insertion site of the ϕSPβ-like prophage in the genome of *S. aureus* T0131 and *sasX*-carrying TW20, IN_ST239_8, *sasX*-1 carrying EU_ST239_7, and *sesI*-carrying IN_ST239_2 and RP62A. The prophage element integrates within the *yeeE* gene recognizing the recombination site at the 295th nucleotide. References strains are underlined, study strains are depicted in bold. (**B**) Structure of the 127.2 kb SPβ-like prophage compared between RP62A, TW20, and Indian and European MRSA harbouring *sesI*, *sasX* or *sasX*-1. References strains are underlined, study strains are depicted in bold.

3.4.1.4.4. Phylogenetic analysis reveals the existence of novel clades

Based on the core genome of ST239, a maximum likelihood phylogeny was constructed and SNPs within the core genome were compared against TW20 (**Fig. 27A**). Both IN_ST368 and IN_ST161 were also included as these are single locus variants of ST239 with one SNP in the *tpi* gene (**Suppl. Fig. 11**). The tree showed a striking consistency with geographic origin and the 43 studied strains were assigned to four different clades based on previous findings [7]. Eight publicly available sequences clustered within the Asian clade (TW20, V605, DEN907, S2, Z172, V521, AMRC01, and XN108) [7,9], showing an average SNP difference of 161 compared with TW20 and 51 SNPs among each other. Strikingly, Indian strains harbouring *sasX* showed on average

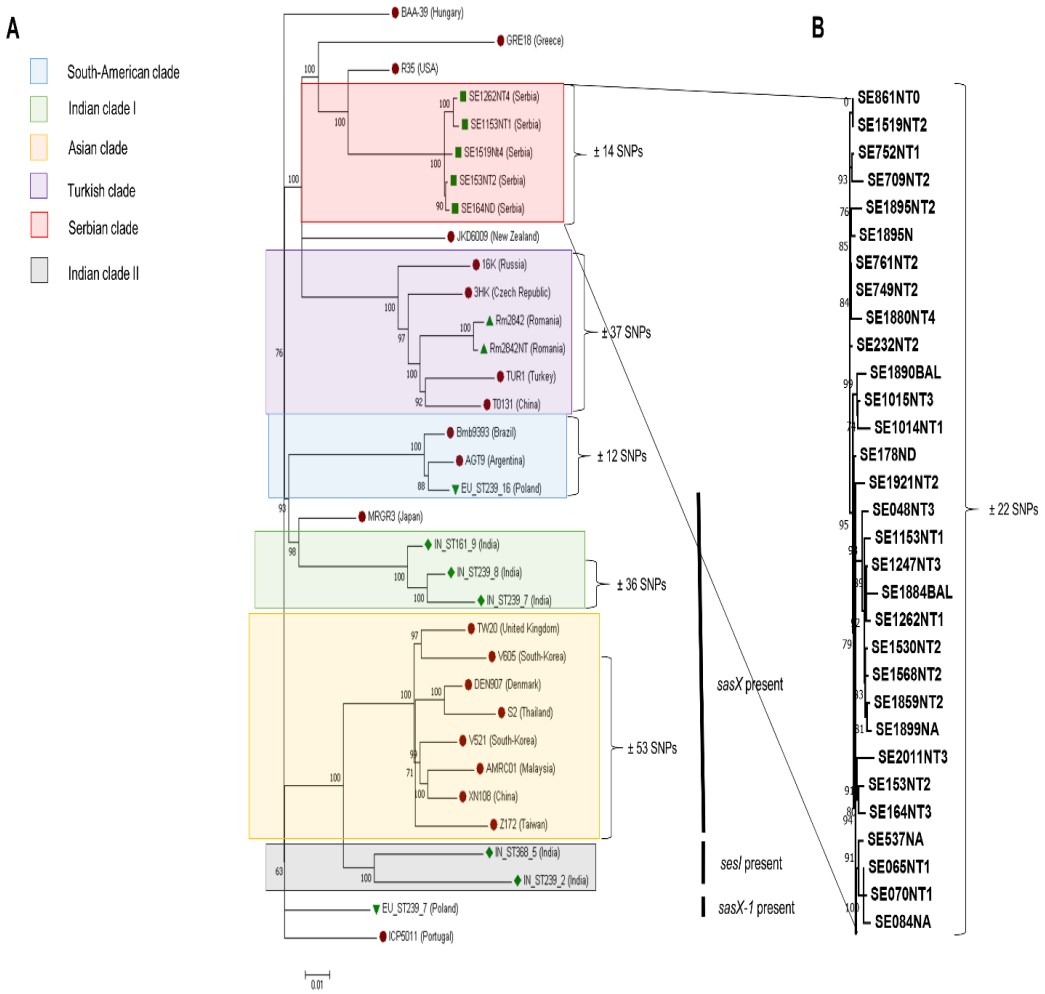

Figure 27: Maximum likelihood phylogenetic tree based on the core genome SNPs of CC8 strains from India and Europe. **(A)** Maximum likelihood phylogenetic tree based on core genome SNPs of CC8 strains, annotated with the country of origin. Bootstrap support values (1000 replicates) are shown above each branch. The percentage of trees in which the associated taxa clustered together is shown next to the branches. The tree is drawn to scale, with branch lengths measured in the number of substitutions per site. Reference strains (n=20) are indicated in green and randomly chosen study strains (n=13) in red colour, while shapes indicate origin from different countries. Strains with prefix 'SE' refer to clinical samples collected in Serbia, Europe. Strains with prefix 'Rm' refer to clinical samples collected in Romania, Europe. The Serbian clade is exemplified by 5 randomly chosen clinical strains. Numbers with each clade represent the number of SNP difference within each clade. **(B)** Maximum likelihood phylogenetic tree based on core genome SNPs of randomly chosen Serbian ST239 strains (n=31). Two strains (SE1153NT1 and SE153NT2) were also represented in figure A.

431 SNP differences with TW20. Therefore, these strains were assigned to a novel 'Indian' clade I. For within-clade SNP differences allowed, a cut-off value of ≤60 core genome SNPs was used based on the distribution of pairwise SNP differences (Hamming distance, **Suppl. Fig. 13**). Interestingly, this cut-off was also used by Tong et al. to assign

clades in a single hospital [25]. Differences in SNPs among the *sasX*-harbouring 'Indian' clade I were on average 36 SNPs for only ST239, and 64 SNPs when also including ST161. Similarly, Indian strains harbouring *sesI* also showed SNP differences of 345 (ST239) and 315 (ST368) with TW20 and did not cluster with the Asian clade (**Fig. 27a**). Base substitution frequency differed significantly between the Asian clade (0.043) and Indian ST239 (0.130) (p<0.001). *SesI*-harbouring IN_ST239_2 also differed by an average of 86 SNPs compared with the Indian clade I, and when single locus variant ST161 was included, by 71 SNPs. With a total difference of 30 SNPs between IN_ST239_2 and IN_ST368, we could hypothesize that IN_ST239_2 and IN_ST368 might have diverged from the Asian clade as 'Indian' clade II. EU_ST239_7 from Poland formed a distant singleton (**Fig. 27a**), showing a difference of 148 and 134 SNPs compared with TUR1 and T0131 references from Eastern Europe, whereas EU_ST239_16 clustered within the South American clade (12 SNPs). Serbian isolates only differed by, on average, 22 SNPs, among the 31 sequenced isolates (2011-2014) and formed a novel 'Serbian' clade (**Fig. 27b**) [25]. The Serbian clade is most closely related to the Turkish clade, however, the base substitution frequency (0.007 and 0.05, respectively) was found to be significantly different (p<0.05). Also, there was a significant difference in the base substitution frequency between the Serbian (0.007), Indian ST239 (0.130) and Indian non- ST239 (0.147), (p<0.05).

3.4.1.5. Discussion

We report here, for the first time, the occurrence of *sasX*, a key virulence determinant believed to have transferred from *S. epidermidis* [26], in Indian ST239 (100%, n=3) and its dissemination to other CC8 STs (12%, n=6) (overall prevalence in Indian strains: 55%, n=9). Other studies have shown a 5% and 11% prevalence of sasX in 150 and 450 Indian ST239 and ST368 strains of India [27]. In contrast, *sasX* and its variant *sasX*-1 were limited to ST239 and were present in a very small proportion of the European ST239 studied here (1.7%, n=119). Moreover, detection of the native *sesI* in Indian *S. aureus*, which is also found in *S. epidermidis* [10], and the recently reported *sasX* carriage in coagulase-negative staphylococci from India [28,29], provide unquestionable evidence of a horizontal transfer event between the staphylococcal species. Interestingly, MRSA isolated from hospital-associated infections and harbouring *sasX/sesI* exhibited a significantly higher biofilm formation capacity (393% increase), which was also shown in [5]. Of note, *sesI*-carrying *S. aureus* strains were even more abundant biofilm formers than *sasX*-carrying strains (137% increase). This might be because *sesI* is a known colonization factor in *S. epidermidis*, whereas *sasX* is a virulence factor promoting lung disease, abscess formation and mechanisms of immune evasion [3,5,12,30]. Recent data also show that SasX is an effector rather than a regulatory

protein, as biofilm formation by *sasX* knockout strains was significantly impaired compared with the wild type strains and again restored in *sasX*-complemented strains [5]. Interestingly, the same study showed that inactivation of *sasX* did not impact the expression of *icaA* (biofilm exopolysaccharide biosynthesis), RNAIII (biofilm and virulence regulator *agr*), or a series of cytolysins such as *psmα* and *hla*, and other adhesion genes such as *clfA*, *fnbA*, *sasA,* and *spa*. Nonetheless, the possibility that the ϕSPβ-like prophage might harbour regulators that affect the expression of RNAIII was raised because RNAIII and *psmα* expression and the percentage of invasive infection caused by *sasX*-harbouring ST239 MRSA appeared to be higher than those caused by ST239 MRSA not harbouring *sasX* [5,31,32].

We also show that the ϕSPβ-like prophage inserts site specifically in a hypothetical protein encoded by *yeeE* in MRSA, including TW20, and in *S. epidermidis* RP62A [8,11]. Our analysis showed that this prophage remained largely unchanged in the Indian *sesI*-harbouring strains with an average length of 118 kb, whereas *sasX*-harbouring strains IN_ST239_8, IN_ST239_7, IN_ST161, and EU_ST239_16 carried on average a 48 kb shorter ϕSPβ-like prophage, compared with the 128.3-kb TW20 ϕSPβ-like prophage. In contrast, *sasX*-1 in Europe was carried on a 122-kb ϕSPβ-like prophage that was homologous to the TW20 ϕSPβ-like prophage in size and gene content. The largely intact phage in EU_ST239_7, together with the presence of *sasX* in a very small number of isolates in our study, suggests either a lack of selection pressure or a rather recent transfer of the virulence gene into the European MRSA studied here. Corroborating evidence from Poland showed that ST239 isolates of the Asian lineage, clustering closely together with TW20, might have been repeatedly introduced into Eastern Europe or that native Polish strains might have acquired the *sasX* gene from imported Asian strains [13]. However, our finding of a yet unreported *sasX* variant (*sasX*-1) in Europe might indicate potential local variation within the gene. Another *sasX* variant with a three-amino acid loss that did not affect its function as an LPXTG motif surface-anchored protein was isolated previously in Geneva (MRGR, AHZL00000000.1) (**Suppl. Table 14**).

Phylogenetic analysis showed that the Indian *sasX*/*sesI*-carrying strains were clustered into two clades, Indian I and II, respectively, distinct from the Asian clade. The fact that we identified two clades in a mere five hospital-associated MRSA collected from one hospital in India in 1 year, contrasts starkly with the single clade identified from 34 hospital-associated MRSA collected from one Serbian hospital in 3 years and serves to underscore the wide differences in evolutionary timelines between these novel clades. Whether these differences are due to the inherent characteristics of the local clades or are influenced by differences in antibiotic-use patterns or other environmental factors remains to be studied.

3.4.1.6. Addendum

3.4.1.6.1. Acknowledgements

We thank Abe Kimihiro (Hosei University, Research Centre for Micro-Nano Technology, Tokyo, Japan) for giving us valuable insights that helped in locating the ϕSPβ-like prophage insertion site. All participants of MOSAR (EU-FP6 under proposal no. 037941, 'Mastering hOSpital Antimicrobial Resistance and its spread into the Community', 2007-2011, ClinicalTrials.gov Identifier: NCT00685867) and SATURN (EU-FP7 under grant agreement no. 241796, 'Impact on Specific Antibiotic Therapies on the prevalence of hUman host ResistaNt bacteria', 2010e2015, ClinicalTrials.gov Identifier: NCT01208519)WP4 study groups, and the intensive care unit at the University Hospital of Antwerp, Belgium (2012-2013, Clinical Trial Registration: 12/12/112) are thanked for making these studies possible. Preliminary results from this study were presented at the European Congress of Clinical Microbiology and Infectious Diseases (ECCMID) 2015 (25th edition), Copenhagen, Denmark (25-28 April 2015) and ECCMID 2016 (26th edition), Amsterdam, the Netherlands (9-12 April 2016). LVanjari was supported by a visiting post-doctoral grant from the Flemish Inter-university Council (VLIR-UOS). BBX was supported by the University of Antwerp Research funds (BOF-DOCPRO 2012-27450). SDB is supported by funding from Research Foundation Flanders (FWO, applicant number 1128818N). The described research is part of IWT-SBO project (#140746) and FWO research project (#GOD3516N).

3.4.1.6.2. Access to data

Whole genome sequences of IN_ST161, IN_ST239_8, IN_ST239_7, IN_ST368, and IN_ST239_2 have been submitted to NCBI BioProject as NMR09, NMR08, NMR07, NMR05 and NMR02, respectively, and were assigned GenBank accession numbers SAMN04621063, SAMN04621062, SAMN04621061, SAMN04621060 and SAMN04621059, respectively.

3.4.1.6.3. Contribution to authorship

SMK and HG conceived the study. SDB, LVanjari, JC and CL carried out the experimental work. ET, SH, AL, BC, JS, WH, SMK, CL and HG carried out the clinical trials and strain collections as part of EU projects MOSAR and SATURN. LVemu collected strains from India. BBX performed bioinformatics analysis. SMK, SKS, HG, SDB and BBX analysed the data and drafted the manuscript. All authors read and approved the final manuscript. In detail, molecular typing, quantitative biofilm assays and statistical analysis was performed by SDB.

3.4.1.6.4. Supplementary figures

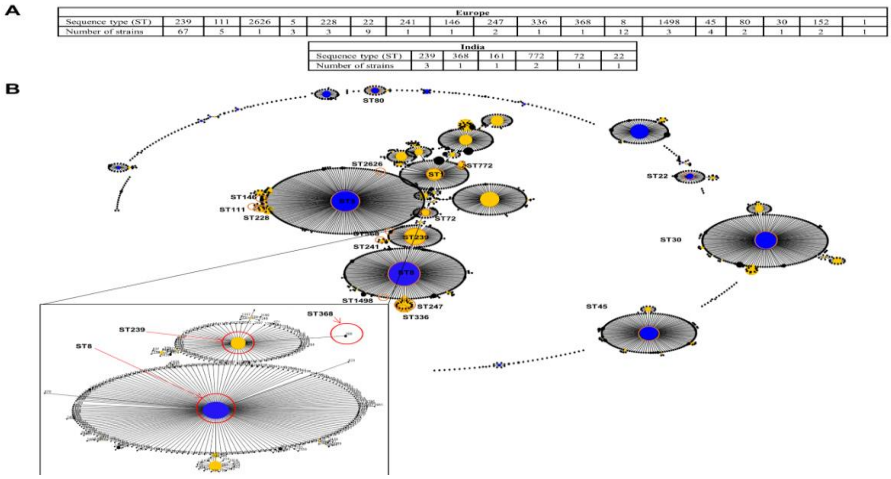

Supplementary figure 11: MLST typing of Indian and European MRSA. **(A)** ST distribution **(B)** Analysis of European and Indian *S. aureus* isolates with eBURST as a population snapshot based on all unique STs of the entire *S. aureus* MLST database. All members assigned to the same group or clonal complex share identical alleles at =5 of the 7 loci with at least one other member of the group. Primary founders are depicted in blue; secondary founders are depicted in yellow. Nodes carrying SLVs of interest were elongated and separated from other STs for clarity. Isolates within this study are highlighted in red, and their corresponding ST is indicated. Novel ST161 is not indicated within the eBURST diagram.

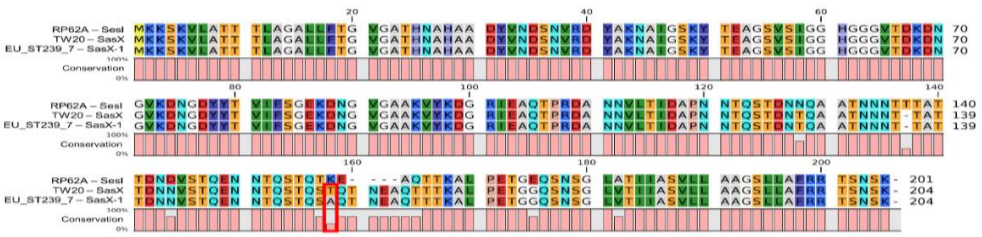

Supplementary figure 12: Alignment of SasX, SasX-1 and SesI protein of Indian (IN) and European (EU) isolates exemplified by TW20, EU_ST239_7 and RP62A, respectively. EU_ST239_7 shows an additional change within SasX-1, which is highlighted in red.

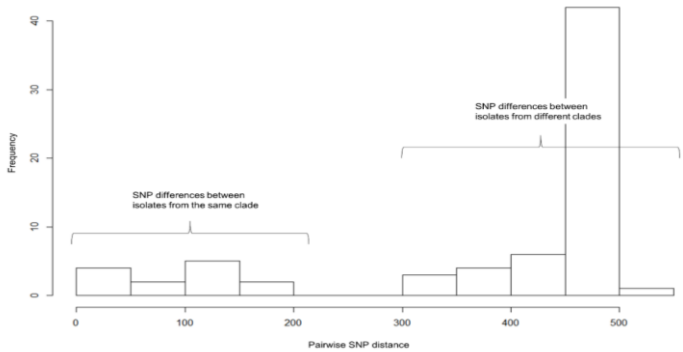

Supplementary figure 13: Histogram of pairwise SNP differences between 64 study strains (Hamming distance). Left: SNP differences between isolates from the same clade, right: SNP differences between isolates from different clades.

3.4.1.6.5. Supplementary tables

Supplementary Table 13: Primers used in the *S. aureus* surface protein *sasX/sesI* study.

Target name	ID	Sequence (5'→3')	Product size (bp)	Reference
sasX	SasX-f	agaattagaagtacgtctaaatgc	522	[5]
	SasX-r	gctgattatgtaaatgactcaaatg		
ϕSPβ-like prophage	sasXG1-f	gaactgatggccaagacgga	5397	This study
	sasXG2-f	aaagagccacagtgccgaaa	4105	
	sasXG3-f	caaaggatgtagctctggtct	687	
	sasXG-r	ccagaaacaggcggacaatc		

Supplementary table 14: Table of ST239 reference isolates used in the *S. aureus* surface protein *sasX/ses*I study with corresponding accession numbers.

Strain ID	Accession number	Site of isolation	ST type	*sasX/sesI*
TW20	FN433596	United Kingdom	ST239	yes
3HK	ERX042880	Czech Republic	ST239	no
XN108	CP007447	China	ST239	yes
V521	SAMN04219577	South-Korea	ST239	yes
V605	SAMN04219581	South-Korea	ST239	yes
AGT9	ERX042896	Argentina	ST239	no
T0131	CP002643	China	ST239	no
16K	BABZ00000000.1	Russia	ST239	no
Bmb9393	CP005288	Brazil	ST239	no
AMRC01	AMRC00000000.1	Malaysia	ST239	yes
BAA-39	AEEK00000000.1	Hungary	ST239	no
MRGR3	AHZL00000000.1	Japan [9]	ST239	yes
JKD6009	ABSA00000000.1	New Zealand	ST239	no
Z172	CP006838	Taiwan	ST239	yes
R35	ERX001254	United States of America	ST239	no
DEN907	ERX001218	Denmark	ST239	yes
ICP5011	ERX042906	Portugal	ST239	no
TUR1	PRJEB2173	Turkey	ST239	no
GRE18	ERX042875	Greece	ST239	no
S2	ERS049914	Thailand	ST239	yes

Supplementary Table 15: Characteristics of MRSA isolates carrying *sasX*, *sasX*-1 or *sesI* in the S. *aureus* surface protein *sasX/sesI* study. MRSA strains and *S. epidermidis* strains without the surface-anchored protein (not mentioned in the table) came from wound swabs, pus specimen, blood specimen, nasal screening, or skin screening belonging to CC22 (ST22), CC5 (ST111, ST2626, ST5, ST228), CC8 (ST72, ST241, ST247, ST336, ST368, ST8, ST1498, ST239, ST161), CC45 (ST45), CC2 (ST80), CC9 (ST146), CC30 (ST30, ST152), and CC1 (ST772, ST1), respectively.

Name	CC	Site of collection	*SasX* homology	*SesI* homology	Site of isolation
IN_ST239_2	8	NIMS	95.79%	100%	Wound swab
IN_ST368	8	Nizam's Institute of Medical Sciences (NIMS, Hyderabad, India)	95.79%	100%	Tissue specimen
IN_ST239_7	8	Nizam's Institute of Medical Sciences (NIMS, Hyderabad, India)	100%	95.79%	Tissue specimen
IN_ST239_8	8	Nizam's Institute of Medical Sciences (NIMS, Hyderabad, India)	100%	95.79%	Wound swab
IN_ST161	8	Nizam's Institute of Medical Sciences (NIMS, Hyderabad, India)	100%	95.79%	Pus specimen
EU_ST239_16	8	National Medicines Institute (Poland)	100%	95.79%	Wound specimen
EU_ST239_7	8	National Medicines Institute (Poland)	99.64%	95.15%	Sputum specimen

3.4.1.6.6. References

1. Bouchiat, C., et al., *Epidemiology of Staphylococcus aureus in Bangalore, India: emergence of the ST217 clone and high rate of resistance to erythromycin and ciprofloxacin in the community.* New Microbes New Infect, 2015. **7**: p. 15-20.
2. Otto, M., *Molecular insight into how MRSA is becoming increasingly dangerous.* Virulence, 2012. **3**(6): p. 521-3.
3. Amaral, M.M., et al., *The predominant variant of the Brazilian epidemic clonal complex of methicillin resistant Staphylococcus aureus has an enhanced ability to produce biofilm and to adhere to and invade airway epithelial cells.* J Infect Dis, 2005. **192**: p. 801-810.
4. Donlan, R., *Biofilms: microbial life on surfaces.* Emerg Infect Dis, 2002. **8**(9): p. 881-890.
5. Li, M., et al., *MRSA epidemic linked to a quickly spreading colonization and virulence determinant.* Nat Med, 2012. **18**(5): p. 816-9.
6. Baines, S.L., et al., *Convergent adaptation in the dominant global hospital clone ST239 of methicillin-resistant Staphylococcus aureus.* MBio, 2015. **6**(2): p. e00080.
7. Harris, S.R., et al., *Evolution of MRSA during hospital transmission and intercontinental spread.* Science, 2010. **327**: p. 469-474.
8. Holden, M.T., et al., *Genome sequence of a recently emerged, highly transmissible, multi-antibiotic- and antiseptic-resistant variant of methicillin-resistant Staphylococcus aureus, sequence type 239 (TW).* J Bacteriol, 2010. **192**(3): p. 888-92.
9. Wang, Z., et al., *Comparative genomics of methicillin resistant Staphylococcus aureus ST239: distinct geographical variants in Beijing and Hong Kong.* BMC Genomics, 2014. **15**: p. 529-539.
10. Soderquist, B., et al., *Staphylococcus epidermidis surface protein I (SesI): a marker of the invasive capacity of S. epidermidis?* J Med Microbiol, 2009. **58**(Pt 10): p. 1395-7.
11. Gill, S.R., et al., *Insights on evolution of virulence and resistance from the complete genome analysis of an early methicillin-resistant Staphylococcus aureus strain and a biofilm-producing methicillin-resistant Staphylococcus epidermidis strain.* J Bacteriol, 2005. **187**(7): p. 2426-38.
12. Otto, M., *How colonization factors are linked to outbreaks of methicillin-resistant Staphylococcus aureus: the roles of SasX and ACME.* Biomol Concepts, 2013. **4**(5): p. 533-7.

13. Aanensen, D.M., et al., *Whole-genome sequencing for routine pathogen surveillance in public health: a population snapshot of invasive Staphylococcus aureus in Europe.* MBio, 2016. **7**(3).
14. Enright, M.C., et al., *Multilocus sequence typing for characterization of methicillin resistant and methicillin susceptible clones of Staphylococcus aureus.* J Clin Microbiol, 2000. **38**: p. 1008-1015.
15. Sabirova, J.S., et al., *Fatty acid kinase A is an important determinant of biofilm formation in Staphylococcus aureus USA300.* BMC Genomics, 2015. **16**(1): p. 861.
16. Vanhommerig, E., et al., *Comparison of biofilm formation between major clonal lineages of methicillin-resistant Staphylococcus aureus.* PLoS One, 2014. **9**(8): p. e104561.
17. Bankevich, A., et al., *SPAdes: a new genome assembly algorithm and its applications to single-cell sequencing.* J Comput Biol, 2012. **19**(5): p. 455-77.
18. Kleinheinz, K.A., K.G. Joensen, and M.V. Larsen, *Applying the ResFinder and VirulenceFinder web-services for easy identification of acquired antibiotic resistance and E. coli virulence genes in bacteriophage and prophage nucleotide sequences.* Bacteriophage, 2014. **4**(1): p. e27943.
19. Darling, A.E., et al., *Mauve assembly metrics.* Bioinformatics, 2011. **27**(19): p. 2756-7.
20. Treangen, T.J., et al., *The Harvest suite for rapid core genome alignment and visualization of thousands of intraspecific microbial genomes.* Genome Biol 2014. **15**(11): p. 524-539.
21. Nei, M. and S. Kumar, *Molecular evolution and phylogenetics*. 1st edition ed. 2000, New York: Oxford University Press. 333.
22. Kumar, S., G. Stecher, and K. Tamura, *MEGA7: Molecular Evolutionary Genetics Analysis version 7.0 for bigger datasets.* Mol Biol Evol, 2016. **33**(7): p. 1870-4.
23. Thompson, J., D. Higgings, and T. Gibson, *CLUSTAL W: improving the sensitivity of progressive multiple sequence alignment through sequence weighting, position-specific gap penalties and weight matrix choice.* Nucleic Acids Res, 1994. **22**(22): p. 4673-4680.
24. Krzyszton-Russjan, J., et al., *Clonal structure of the methicillin resistant Staphylococcus aureus (MRSA) population in Poland: Revision and update.* Microb Drug Resist, 2005. **11**(2): p. 127-136.
25. Tong, S.Y., et al., *Genome sequencing defines phylogeny and spread of methicillin-resistant Staphylococcus aureus in a high transmission setting.* Genome Res, 2015. **25**(1): p. 111-8.
26. Otto, M., *Coagulase-negative staphylococci as reservoirs of genes facilitating MRSA infection: Staphylococcal commensal species such as Staphylococcus epidermidis are being recognized as important sources of genes promoting MRSA colonization and virulence.* Bioessays, 2013. **35**(1): p. 4-11.
27. Bakthavathchalam, Y. D., et al., *A distinct geographic variant of sasX in methicillin resistant Staphylococcus aureus ST239 and ST368 lineage from South India.* Microb Drug Resist, 2019. **25**(3): 413-420.
28. Soumya, K.R., et al., *Studies on prevalence of biofilm associated genes and primary observation on sasX gene in clinical isolates of coagulase negative staphylococci (CoNS).* APMIS, 2016.
29. Soumya, K.R., et al., *Studies on coexistence of mec gene, IS256 and novel sasX gene among human clinical coagulase-negative staphylococci.* 3 Biotech, 2016. **6**(2).
30. Eshaghi, M., et al., *Genotype diversity and evaluation of biofilm formation in sasX positive methicillin-resistant Staphylococcus aureus.* Avicenna J Clin Microb Infec, 2017. **In Press**(In Press): p. e46049.
31. Archer, N.K., et al., *Staphylococcus aureus biofilms: properties, regulation, and roles in human disease.* Virulence, 2011. **2**(5): p. 445-59.
32. Li, S., et al., *Comparative analysis of the virulence characteristics of epidemic methicillin-resistant Staphylococcus aureus (MRSA) strains isolated from Chinese children: ST59 MRSA highly expresses core gene-encoded toxin.* APMIS, 2014. **122**(2): p. 101-14.

Chapter 4: Concluding insights

"Science never solves a problem without creating ten more.'

- George Bernard Shaw

4.1. General discussion

S. aureus produces biofilm and this mode of growth facilitates infections that are often difficult to treat, thereby causing high morbidity as well as mortality. Despite the important role of *S. aureus* biofilms in disease, our understanding of the molecular basis contributing to biofilm formation is incomplete. This work aimed to comprehensively identify and characterize molecular factors involved in the production of biofilm matrix components and the regulatory network governing overall biofilm development in MRSA/*S. aureus*. Lessons from our transposon library screen and transcriptional profiling study revealed that cells in MRSA biofilms characteristically show a distinct phenotype and gene expression profiles in comparison to planktonic cells. Metabolic changes were due to a switch to fermentative processes resulting from the low oxygen availability in these biofilms. Additionally, the upexpression of urease and arginine deiminase pathways, which ultimately produce ammonia compounds, were potentially used to limit the deleterious effects of the reduced pH associated with anaerobic growth. MRSA were shown to employ different mechanisms to form biofilms, but this did not appear to impair their ability to colonize surfaces. Going further into detail, we provided a link between biofilm formation, central metabolism and external fatty acid utilization by the important contributions of *argH*, *fumC*, *sdhA*, *sdhB* and *fakA* that are part of the urea/TCA-cycles and exogenous fatty acid phosphorylation pathway. Our study on the *sasX* virulence factor and its close associated with clonal lineages like ST239 that are rather specific to geographic regions, demonstrated that each MRSA lineage is genetically distinct and evolves independently shaped by the environment, health-care practices, including antibiotic use, and social as well as geographic factors. We strongly believe that some of these 'hits' have potential to be explored as alternative therapeutic strategies or as adjuvants to antibiotic treatment. For instance, our SCC*mec*-associated hits in the transposon library (*fmtB*) and an in-depth analysis of the ACME-element which allows for genetic "hitchhiking" of SCC*mec* all open up the possibility of a single target affecting two key aspects of MRSA pathogenesis; β-lactam resistance and biofilm formation, and show that these are closely interconnected with each other as also suggested before [1]. Here, it would be interesting to construct single gene knockout mutants (Δ*mecA*, Δ*mecI*, Δ*mecR1,* Δ*psm-mec*) in the SCC*mec* element and asses their capacity for biofilm production in our *in vitro* assays.

S. aureus exhibits a remarkable capacity to adapt rapidly to environmental shifts. This impressive adaptability of *S. aureus* to radically different environments is dependent in part on biofilm formation. Multiple biofilm mechanisms have been described and control of these phenotypes by environmental conditions adds to the complexity [2]. Environmental triggers such as osmotic stress [3, 4], oxygen [5], acidity [6], temperature

and sub-inhibitory concentrations of antibiotics [7] have been shown to contribute to the regulation of biofilm production. We showed that altered respiration under oxygen-depleted conditions, and consequently an acidic pH, resulted in activation of the Atl (eDNA)- and FnBP-mediated biofilm mechanism. In this context, the TCA-cycle might act as a signal transduction pathway that translates external environmental cues into intracellular metabolic signals that modulate the activity of transcriptional regulators. TCA-cycle activity has been shown to influence PIA synthesis as well as Atl (eDNA)- and FnBP-mediated biofilm formation by an unknown mechanism [8, 9]. Additionally, the central metabolism, biofilm formation, and external conditions can be linked by FakA, which is involved in host fatty acid utilization [10, 11]. FakA is important for the activation of the SaeRS two-component system and production of secreted virulence factors like α–hemolysin, which have all been implicated in *S. aureus* biofilm formation.

In response to changing environments, *S. aureus* can also undergo rapid phenotypic switches by means of small regulatory RNAs (sRNAs). Here, these sRNA's act by base pairing with their target mRNA as well as by modulating protein activity by mimicking secondary structures of other nucleic acids [12]. More than 250 sRNA's were discovered and detected as expressed transcripts in various *S. aureus* strains and experimental conditions [13]. Recent evidence suggests that regulatory networks directing the decision whether to attach and form biofilms or remain as planktonic cells are further prone to regulation by sRNAs [14]. RNAIII, for example, is the largest and best-studied sRNA implicated in biofilm formation of *S. aureus* [15]. Several studies only deduced the role of sRNAs in biofilm formation based on their effect on constituents of major regulatory networks previously described to either enhance or impair attachment and biofilm formation. There is a great need for determining sRNA function in relation to biofilm developmental aspects, since biofilm formation requires regulatory cascades that control the temporal and spatial expression of genes.

These examples illustrate that *S. aureus* has evolved a very complex but coordinated set of responses to exploit the infection milieu and accumulate into a self-protective biofilm. Furthermore, the numerous mechanisms and multidimensional regulation of *S. aureus* biofilm underpin the importance of this mode of growth to the pathogen. Indeed, lessons from transcriptional profiling show that biofilms represent a unique, physiologically different, growth state from planktonic cultures, directly contributing to the bacterial fitness within specific settings. But these studies also suggest the existence of strain-specific pathways contributing to biofilm formation. For example, specific clonal types of MRSA tend to be successful in hospitals with high antibiotic usage whilst other clones spread in the healthy community [16]. This multi-environment adaptiveness is made possible by a sophisticated regulation of gene expression and a capacity to undertake genome remodelling through horizontal gene

transfer events. Many virulence factors and antibiotic resistance genes aiding in the spread of MRSA are carried on mobile genetic elements (MGE's). The acquisition of ACME, which produces ammonia by the additionally carried ADI-pathway to counter the acidic skin environment, demonstrates that genome-remodelling events happen often in response to more specific environmental conditions. Carriage of ACME has shown to give the USA300 lineage a major selective advantage during skin infection and colonization [17]. In similarity to ACME, the SasX protein is responsible for the spread of the ST239-SCC*mec*III MRSA clonal lineage in China and India due to increased colonization capacity [18, 19]. Additionally, while MGE's tend to be lineage-associated, due to restriction barriers [20], our study proved that these boundaries that once contained MRSA are now slowly fading. In the future, MRSA will likely be capable of creating highly fit and hardly treatable "superbugs' that can both proliferate in hospitals and cause disease in healthy humans.

4.2. Future perspectives

In the medical domain, numerous difficulties to treat *S. aureus* biofilm-associated infections are described: resistance to antibiotics and to the immune system, the spread of infection, septic shock and even surgical risks to remove infected implant or tissue [21]. Consequently, the development of new therapeutic and prevention strategies, through a more pronounced focus on the in-depth evaluation of biofilm formation, is necessary and imperative.

Our transcriptome analysis, screening of the *bursa aurealis* transposon library, TCA-cycle and *sasX* studies demonstrated that staphylococcal surface proteins fulfil key functions during the infectious biofilm process, and antibody-based strategies (vaccines) targeting surface proteins may provide protection against *S. aureus*. In fact, several surface proteins are currently being used for vaccine development that are under different phases of development; MedImmune developed monoclonal antibody 11H10, with inhibitory activity for ClfA binding to fibrinogen [22], that is being targeted against surgical site infections. This IgG1 is also being developed in conjunction with monoclonal antibodies against α-toxin to improve the outcome of patients with ventilator-associated pneumonia (VAP) [23]. Additionally, α-toxin was recently shown to promote biofilm formation on epithelial surfaces [24], and a recently concluded phase II trial with the anti-α toxin antibody (MedImmune) in mechanically ventilated patients colonized with *S. aureus* showed a signiciant decrease of VAP incidence in this population (COMBACTE consortium, unpublished results). Further, a multicomponent vaccine composed of ClfA, capsular polysaccharide type 5 and 8 conjugates, and manganese transporter C (Pfizer Inc., SA4Ag), rapidly induced high levels of antibodies in healthy adults [25]. However, aphase 2B efficacy trial in patients undergoing elective spinal fusion o prevent

postoperative invasive surgical site infection and bloodstream infection caused by *S. aureus* was recently discontinued. IsdB antibodies, blocking heme iron scavenging, provided partial protection against *S. aureus* bacteraemia in preclinical models [26]. However, IsdB immunization or V710 did not protect patients from *S. aureus* surgical site infections and even increased the risk for *S. aureus* associated bacteraemia [27]. SpA-neutralizing antibodies have been engineered but have not been subjected to clinical testing [28]. Alternatively, general anchoring of surface proteins to the cell wall envelope of *S. aureus* can be abolished by small-molecular inhibitors of sortase [29, 30]. There has been some preclinical success with anti-PIA antibodies in an *S. aureus* periprosthetic osteomyelitis rat model and using the encoding *ica* genes as qPCR-based biomarkers for infection [31]. However, the *ica* operon is not present in all *S. aureus* strains and therefore, it cannot be used as a general biomarker. The SasX protein also presents promising potential as a vaccine component and was evaluated in a mouse infection model for passive and active immunization [32]. However, the use of any drug targeting SasX would of course be limited to *sasX*-positive clones. Furthermore, the discovery of SasX-1 indicated that an effective vaccine will need to contain the full spectrum of variant types of these surface proteins. Probably, all such virulence or colonization-targeted approaches to find anti-MRSA therapeutics will require a mixture of drugs or antibodies targeting different bacterial virulence or colonization determinants. Additionally, it is necessary to find either a universal biomarker that defines all biofilm species or at least, since the previous factor likely does not exist, a biomarker species-specific detectable in the case of biofilm presence. Unfortunately, attempts at vaccine or diagnostic marker development for MRSA have been disappointing to date.

Our study of the MRSA matrix composition within context of the TCA-cycle revealed that the usage of various enzymes to degrade the extracellular polymeric matrix of the biofilm to make it more accessible to traditional antibiotic treatment holds great promise. For example, dispersin B is a PIAase produced by *Actinobacillus actinomycetemcomitans* [33]. It has been shown to degrade staphylococcal PIA/PNAG-dependent biofilms *in vitro* [34, 35]. Lysostaphin, a lysin produced by *Staphylococcus staphylolyticus*, is used in the laboratory to digest staphylococcal cells and has been investigated intensely as an antistaphylococcal agent [36]. Notably, lysostaphin eradicated *S. aureus* in a catheter-associated infection model in mice [37]. Other matrix-degrading enzymes, such as proteases, have also been proposed to treat biofilm infections [38]. However, this might induce biofilm dispersal, which is believed to cause severe and life-threatening conditions, such as bloodstream infections. For instance, several studies in *Streptococcus pneumoniae* reported dispersed cells (not planktonic or biofilm cells) to be responsible for the transition to invasive disease [39, 40]. Additionally, recent RNA-seq analysis of dispersed *Pseudomonas aeruginosa* at the Lab. Med. Micro

at UA has confirmed that a large dissimilarity exists between the dispersed and planktonic state of cells (Rohit et al., in preparation). The same problem is true for quorum-sensing blockers [41].

Our results demonstrate that antimicrobials targeting the fatty acid synthesis (FASII) pathway might also have potential for biofilm-associated staphylococcal infections [42]. However, resistance to FASII inhibitors has emerged due to mutations in the FASII target genes [43], as exemplified by our data. Surprisingly, the FASII inhibitor enoyl-acyl carrier protein (ACP) reductase therapeutic AFN-1252 was effective against *S. aureus*, even when extracellular fatty acids were abundant and FASII is normally bypassed [44]. This holds promise that it might prove possible to "trap" *S. aureus* that bypasses FASII inhibitors with a second synergistic antimicrobial that targets "FASII bypass essential" functions.

Since our transcriptome data indicated that MRSA biofilms highly invest in combatting the acidic microenvironment of the biofilm, local physiologically compatible alkalinisation could be considered as another alternative approach to improve the antibiotic efficiency of certain antimicrobials. Acidification has been shown to compromise the activity of aminoglycosides, macrolides, and tetracyclines [45, 46]. The alkaline amino acid L-arginine or EDTA, a cation chelator that destabilizes the biofilm matrix, and pH-mediated potentiation of aminoglycosides such as gentamicin were shown to be effective with 99% biofilm mortality in an *in vivo* model of catheter-related infection [47, 48].

Other therapeutic strategies for staphylococcal biofilm-associated infections include antimicrobial peptides (AMPs) that form pores in the bacterial membrane [49], material alterations to lower adhesive features or coating of the device surface with antibacterial compounds, such as silver, copper, antibiotics or AMPs [50]. However, device surfaces are frequently also covered with human matrix proteins to which the bacteria attach independently of the device surface. Another reservoir leading to infection and spread of MRSA is the colonization of human skin and nares [51, 52]. Colonized patients are not only at higher risk of infection [53], but they are the reservoir of transmissible isolates. MRSA spread from patient to patient via direct contact, equipment, staff, visitors or the environment. Transmission is also likely to be enhanced by prescribing of antibiotics that select for the colonization of resistant MRSA (β-lactams and fluoroquinolones) [54]. Here, decolonization may reduce the risk of MRSA infection in individual carriers and prevent transmission to other patients [55].

Bacteriophages could be an effective therapy in the setting of a deficient (mutant) or disrupted biofilm structure where cell surface-located bacteriophage receptor molecules are easily accessible [56]. Bacteriophages ϕIPLA-RODI, ϕIPLA-C1C

and K reduced *in vitro* staphylococcal biofilms [57, 58]. Additionally, bacteriophage lysin CF-301 has shown potential to disrupt *S. aureus* biofilms in a manner similar to enzymatic treatment [59]. Bacteriophages may also come to the rescue by enhancing the effectiveness of antibiotic doses [60].

Most studies of biofilms involve a single species; however, in many natural environments, biofilms grow in structured multispecies communities. Examples of such diseases include periodontal disease, otitis media, rhinosinusitis, ventilator-associated pneumonia, wound infections and cystic fibrosis lung infection [61]. Importantly, these adjunct microbial species can influence both the behaviour of the pathogen and the efficacy of treatment by influencing the local microenvironment (excretion of molecules, depletion of certain nutrients, interference with signalling pathways, etc.) and alter gene expression patterns of the primary pathogen [62].

This urges all in all for a multi-targeted approach towards MRSA infections. Therefore, successful treatment of biofilm infections will require multidisciplinary collaborations between clinical microbiology, surgery, infectious diseases, pharmacology, and basic science.

4.3. Summary

This dissertation aims at understanding the fundamental processes and genetic regulation underlying biofilm development by *S. aureus*. The present thesis is constructed around 4 chapters, which are intended to be self-explanatory and contain enough information to be read independently of each other. The first chapter is an introductory review that is meant to bring non-expert readers as well as expert readers to the state-of-the-art of the topic. The following chapter briefly outlines a logical order of experimental questions and correlates different methodological approaches used to study biofilm-associated signatures of *S. aureus*/MRSA. Chapter 3 describes new research performed in the context of this thesis, going from basic gene identification to the contribution of those factors in the spread of MRSA, whilst the last chapter summarizes the work and sets new questions as well as experimental perspectives. Altogether the four chapters present a coherent development of scientific questions, hypotheses, and perspectives about as yet only partially solved questions regarding biofilm formation by *S. aureus*.

Chapter 1 describes how microbial biofilms represent an important determinant of human chronic infections. The formation of bacterial biofilms involves a genetically coordinated sequence of events including initial surface attachment, microcolony formation, and community expansion. This leads to a complex and structured architecture protecting bacteria from host-defence mechanisms and killing by antimicrobials. Among the most clinically significant bacterial pathogens is *S. aureus*, a

leading cause of bone and foreign body infections. Despite high incidence and significant morbidity, the molecular pathogenesis of chronic staphylococcal infections and contribution of biofilm production remain largely unknown.

C**hapter 2** exhibits our research focus, where we aim to study crucial molecular mechanisms involved in biofilm formation by three major MRSA clones that underlie their pathogenic success and high biological fitness to survive in diverse environments such as hospitals, the community and, of course, the human host.

Chapter 3 contains the experimental work performed. Briefly, we used either targeted knockout mutation of candidate genes based on transcriptional profiling of *S. aureus* associated with the planktonic and biofilm phenotypes, (top-down approach) or a blind genome-wide genetic screening of a random insertional inactivation library that has been recently implemented in our laboratory (down-top approach). By performing a morphological analysis of biofilm development as well as genetically validating the most promising targets by standard inactivation and complementation strategies, we aimed to correlate morphologic stages with defined patterns of gene expression. Furthermore, we also aimed to delineate which of these factors define the virulence of infectious MRSA strains.

Differential gene expression analysis of *S. aureus* transcriptional signatures associated with *in vitro* planktonic and biofilm phenotypes is presented in **part 3.1. of chapter 3**. Transcriptomic analysis of highly prolific MRSA strains (USA300 UAS391, EMRSA-15 H-EMRSA-15, and ST239-SCC*mec*III EU_ST239_16) **(article 1, chapter 3)** with biofilm growth at different time points (24h, 48h, 72h) has shown that biofilms represent a unique growth state by comparison to planktonic cultures, and they also suggest the existence of species-specific pathways that contribute to biofilm formation. In detail, genes associated with the arginine deiminase (ADI)-pathway and urea cycle were highly up-regulated, pointing to a crucial role for the deamination of arginine by the ADI-pathway resulting in the extracellular accumulation of ammonia to facilitate bacterial pH homeostasis. Furthermore, the additional ACME-encoded ADI-pathway was also up-regulated and could thus confer a survival advantage to USA300 biofilms. **Article 2 of chapter 3 (part 3.2.)** encompasses research findings based on the genetic screening of a random insertional inactivation library. Here, we utilized a *mariner*-based transposon, *bursa aurealis*, to generate a random library of approximately 1920 mutants in a clinical isolate (USA300 UAS391) to query the USA300 genome for nonessential genetic pathways involved in biofilm formation. Initial screening for biofilm formation in microtiter plates yielded 206 isolates with a decrease in biofilm formation capacity (OD_{492}<70% of UAS391-Ery^S) while 149 showed an increase in biofilm formation capacity

(OD_{492}>125% of UAS391-Ery^S), as compared to the parental strains. Mutants with severe growth defects were eliminated from further analysis and the remaining potential biofilm mutants were re-examined for reproducibility in the microtiter plate assay (decrease in biofilm, n=200; increase in biofilm, n=124). Arbitrary PCR and sequencing were used to map the insertion location of the transposon. Eight mutants (Δ*deoC*, Δ*opuCc*, Δ*fmtB*, Δ*pheA*, Δ*narH*, Δ*hlgC*, Δ*nirB*, and Δ*abc*) with the largest defect in biofilm formation (decrease: OD_{492} 37-68% of UAS391-Ery^S; increase: OD_{492} 141-174% of UAS391-Ery^S) were involved in surface adhesion, persister formation, pH homeostasis and toxin production.

Part 3.3. of chapter 3 encompasses research findings based on the targeted knockout mutation of candidate genes that might be essential for biofilm formation. First, as 'hits' identified during the previous transcriptome analysis, revealed a key role of *argH*, we studied its importance for biofilm formation by MRSA-USA300 utilizing transposon mutants, specialized biofilm models and various stains/enzymes **(article 3, chapter 3)**. The transductant mutant disrupted in *argH* gene encoding argininosuccinate lyase was found to produce 1.6-fold less biofilm mass than control strains UAS391 and UAS391-Ery^S. According to KEGG, argininosuccinate lyase (*argH*) plays a central role in arginine metabolism by converting L-arginino-succinate to arginine and fumarate. As fumarate feeds into the TCA cycle, we further explored the role of the TCA cycle in biofilm formation employing transductants harbouring mutations in succinyl-CoA synthetase, beta subunit (*sucC*::Tn), succinate dehydrogenase flavoprotein and iron-sulfur subunits (*sdhA*::Tn and *sdhB*::Tn), aconitase (*acnA*::Tn), isocitrate dehydrogenase (*icd*::Tn), fumarate hydratase class II (*fumC*::Tn), and citrate synthase II (*gtlA*::Tn) genes. Biofilm formation was found to be affected in *sdhA::Tn*, *sdhB::Tn*, and *fumC::Tn*, with the strongest TCA-cycle dysfunction occurring in *fumC::Tn* mutant strain. No defect in biofilm formation was detected in *sucC::Tn, acnA::Tn* and *icd::Tn* mutants. Moreover, the second product of argininosuccinate lyase, arginine, is not only an essential amino acid during biofilm growth but its catabolic by-product, ammonia, is required for pH homeostasis and thus the role of the urea cycle was explored through knockout mutation of arginase (*rocF*::Tn). However, there was no effect of the knockout mutation on formed biofilm mass. Pleiotropic effects caused by the transposon insertion were determined by the construction of growth curves, RT-qPCR, and complementation. Furthermore, the primary impact of TCA-cycle inactivation was on the proteinaceous component of the biofilm matrix of MRSA-USA300. The search for mechanisms of biofilm formation at genome level was expanded by the identification of potential gene targets of biofilm formation in *S. aureus* utilizing comparative genomics **(article 4, chapter 3).** Strain USA300 UAS391 was selected for whole-genome sequencing and subsequent comparison of the strain's genome with those of other sequenced USA300 isolates

(TCH1516 and FPR3757) yielded a limited number of variant genes (n=18) that were hypothesized to account for an observed difference in biofilm forming capacity. Screening of Tn mutants disrupted in these target genes identified one mutant (NE229) bearing a transposon insertion in SAUSA300_1119 (*fakA*), which exhibited increased biofilm formation like UAS391. Transduction experiments confirmed that *fakA*::Tn corresponded to 1.9- to 4.6-fold increase in biofilm formation depending on the USA300 strain background, while complementation of the TCH1516 wild type *fakA* allele in UAS391 resulted in a 4.3-fold reduction in biofilm formation. This sequential approach, consisting of strain typing, genome comparison, and functional genomics, identified *fakA*, a recently described fatty acid kinase in *S. aureus* that is essential for phospholipid synthesis and impacts the transcription of numerous virulence factors, as a negative regulator of biofilm formation in *S. aureus* USA300.

Part 3.4. of chapter 3 focuses on the question of whether biofilm-associated candidate genes may function as critical determinants of MRSA pathogenic success and widespread prevalence **(article 5, chapter 3).** This is exemplified by *sasX* (SATW20_21850), a novel surface-anchored virulence factor identified by genome sequencing of a London ST239 strain (TW20) and promoting colonization as well as biofilm formation**.** Our research confirmed *sasX* as a colonization-virulence factor that potentially underlies the endemic success of MRSA-ST239 in parts of Asia. We studied its distribution in MRSA from India and Europe, and report, for the first time, the occurrence of *sasX* and its variants, including the *S. epidermidis*-harboured *sesI,* in Indian ST239 and in other MRSA of the CC8 lineage (5/9). In contrast, *sasX* was restricted to a few ST239 in Europe (2/121). Among ST239 MRSA, we identified a novel 'Indian' and a 'Serbian' clade. The intact ϕSPβ-like prophage that carries *sasX* was~80 kb in size while *sesI* was carried on a~118 kb ϕSPβ-like prophage. Integration site of this ϕSPβ-like prophage in *S. aureus* was identified as the *yeeE* gene. Our data highlight the dissemination and diversification of *sasX* and its variants beyond ST239 in India and the presence of novel prevalent ST239 clades in Indian and European hospitals.

Finally, **chapter 4** reflects on the research findings made and discusses how improved knowledge of the genetic basis of staphylococcal biofilms should lead to the usage of novel screening assays, identification of new drug targets and development of advanced biomedical devices to prevent biofilm formation.

4.4. Nederlandstalige samenvatting

Deze doctoraatsthesis richt zich op het begrijpen van de genetische regulatie die aan de basis ligt van biofilmvorming in *S. aureus*. De huidige thesis werd opgebouwd rond vier duidelijke en overzichtelijke hoofdstukken, die genoeg informatie bevatten om

onafhankelijk van elkaar te kunnen worden gelezen. Het eerste hoofdstuk is een introductieve literatuurstudie die zowel gespecialiseerde als niet-gespecialiseerde lezers laat kennis maken met de huidige state-of-the-art rond het onderwerp. Het volgende hoofdstuk lijnt kort de experimentele vraagstelling uit en correleert de verschillende methodologische benaderingen die werden gebruikt om de biofilm-geassocieerde kenmerken van *S. aureus*/MRSA te onderzoeken. Hoofdstuk 3 beschrijft het experimentele onderzoek dat werd uitgevoerd in context van deze thesis, gaande van gen identificatie tot de bijdrage van deze genetische factoren aan de verspreiding van MRSA, terwijl het laatste hoofdstuk een overzicht biedt op het uitgevoerde werk en nieuwe vragen alsook experimentele perspectieven aanhaalt. Samen vormen deze vier hoofdstukken een samenhangende ontwikkeling van wetenschappelijke vraagstellingen, hypotheses en perspectieven over slechts gedeeltelijk opgeloste vragen betreffende de fundamentele mechanismen van biofilmvorming in *S. aureus*.

Hoofdstuk 1 beschrijft hoe microbiële biofilms een belangrijk kenmerk vormen van chronische infecties bij de mens. De vorming van bacteriële biofilms omvat een genetisch gecoördineerde opeenvolging van gebeurtenissen, zoals onder andere: initiële vasthechting aan een oppervlak, de vorming van microkolonies en gemeenschapsuitbreiding. Dit leidt tot een complexe en gestructureerde architectuur die de bacteriën beschermt tegen het immuunsysteem van de gastheer alsook tegen de werking van antimicrobiële geneesmiddelen. *S. aureus* vormt één van de meest klinisch significante bacteriële pathogenen en is de voornaamste oorzaak van bot- en medische apparatuur geassocieerde infecties. Ondanks hoge incidentie en significante morbiditeit, blijft de moleculaire pathogenese van chronische infecties en de bijdrage van biofilmproductie tot op heden voor het grootste deel onbekend.

Hoofdstuk 2 beschrijft de focus van ons onderzoek, waarbij we cruciale moleculaire mechanismen beogen te bestuderen die betrokken zijn in biofilmvorming door drie belangrijke MRSA klonen en aan de basis liggen van zowel hun pathogeen succes alsook hun hoge biologische fitness die ervoor zorgt dat deze klonen kunnen overleven in een wijde variëteit aan omgevingen zoals het ziekenhuis, de gemeenschap, en natuurlijk de menselijke gastheer.

Hieropvolgend legt **hoofdstuk 3** uit hoe ons onderzoek focust op de genetische regulatie van biofilmontwikkeling door gebruik te maken van ofwel doelgerichte inactiverende mutatie van een selectie kandidaat-genen die mogelijk essentieel zouden kunnen zijn voor het proces van biofilmvorming en gebaseerd zijn op de transcriptionele profilering van het planktonische en biofilm fenotype in *S. aureus* (top-down benadering), ofwel een blinde genoom-wijde genetische screening van een random insertionele inactivatie bibliotheek die recentelijk in het bezit van ons laboratorium is gekomen (down-top benadering). Door het uitvoeren van zowel morfologische analyse

van biofilm ontwikkeling als het genetisch valideren van de meest veelbelovende factoren door middel van standaard inactivatie en complementatie strategieën, beogen we om de morfologische stadia in de biofilm te combineren met gedefinieerde patronen van genexpressie. Bovendien beogen we om af te bakenen welke van deze factoren specifiek bijdragen tot virulentie in infectieuze MRSA stammen.

Differentiële genexpressie-analyse van *S. aureus* transcriptionele kenmerken geassocieerd met *in vitro* planktonische en biofilm fenotypes wordt gepresenteerd in **deel 3.1. van hoofdstuk 3**. Uit transcriptoom analyse van sterk biofilmvormende MRSA stammen (USA300 UAS391, EMRSA-15 H-EMRSA-15, en ST239 EU_ST239_16) (**artikel 1, hoofdstuk 3**) met biofilmgroei op verschillende tijdspunten (24u, 48u en 72u) en RNA-seq op planktonische en biofilm culturen bleek dat biofilms een unieke groeistatus vertonen in vergelijking met planktonische culturen, en onze data suggereert ook het bestaan van stam-specifieke regulatorische cascades die bijdragen tot biofilmvorming. De sterkst opgereguleerde genen waren geassocieerd met de arginine deiminase (ADI)- en urea cycli. Dit verwijst naar een cruciale rol voor de deaminatie van arginine wat resulteert in een accumulatie van de extracellulaire ammonium-concentratie nodig om bacteriële pH homeostase te handhaven. Tegelijkertijd was ook de ACME-element geëncodeerde ADI-cyclus opgeëxpreseerd waardoor het element mogelijk een overlevingsvoordeel biedt aan USA300 biofilms. **Artikel 2 van hoofdstuk 3** (**deel 3.2.**) omvat de onderzoeksresultaten die bekomen werden gebaseerd op de genetische screening van een random insertionele inactivatie bibliotheek. Hierbij maakten we gebruik van een mariner-gebaseerde transposon, genaamd *bursa aurealis*, om een random bibliotheek van ongeveer 1920 mutanten te construeren in een klinisch isolaat (USA300 UAS391). Zodoende onderzochten we het USA300 genoom voor niet-essentiële genetische regulatorische cascades die betrokken zijn bij biofilmvorming. Aanvankelijk resulteerde microtiterplaat screening voor biofilmvorming in een totaal van 206 isolaten die een afname vertoonde in gevormde biofilm biomassa (OD_{492}<70% of UAS391-Ery^S), terwijl 149 isolaten een toename vertoonden in gevormde biofilm biomassa (OD_{492}>125% of UAS391-Ery^S) in vergelijking met de ouderlijke stammen. Mutanten met ernstige defecten in groei werden geëlimineerd uit verdere analyse en de overblijvende potentiële biofilmmutanten werden verder onderzocht op reproduceerbaarheid in het microtiterplaat experiment (afname in biofilm, n=200; toename in biofilm, n=124). PCR en daaropvolgende sequenering werden gebruikt om de insertie locatie van het transposon te lokaliseren. Acht mutanten (Δ*deoC*, Δ*opuCc*, Δ*fmtB*, Δ*pheA*, Δ*narH*, Δ*hlgC*, Δ*nirB*, and Δ*abc*) met het grootste defect in biofilmvorming (afname: OD_{492} 37-68% of UAS391-Ery^S; toename: OD_{492} 141-174% of UAS391-Ery^S) waren betrokken in vasthechting aan oppervlakte, persister vorming, pH homeostase en toxineproductie.

Deel 3.3. van hoofdstuk 3 omvat de onderzoeksresultaten die bekomen werden gebaseerd op de doelgerichte inactiverende mutatie van kandidaatgenen die mogelijk

essentieel zijn voor biofilmvorming. 'Hits' die werden bekomen uit de voorgaande transcriptionele studie onthulden een belangrijke rol voor *argH.* De impact van dit gen op USA300 biofilmvorming werd bestudeerd door gebruik te maken van transposon mutanten, gespecialiseerde biofilmmodellen en talrijke kleuringen alsook enzymen (**artikel 3, hoofdstuk 3**). De transductie mutant met het geïnactiveerde argH gen, wat codeert voor argininosuccinaat lyase, produceerde 1.6-maal minder biofilm dan de controle stammen UAS391 en UAS391-EryS. Volgens KEGG speelt argininosuccinaat lyase (*argH*) een centrale rol in arginine metabolisme door het converteren van L-arginosuccinaat naar arginine en fumaraat. Omdat fumaraat deel uitmaakt van de TCA-cyclus, onderzochten we de rol van de TCA-cyclus in biofilmvorming door gebruik te maken van transductanten met mutaties in succinyl-CoA synthetase, beta subunit (*sucC*::Tn), succinaat dehydrogenase flavoprotein en ijzer-zwavel subunits (*sdhA*::Tn en *sdhB*::Tn), aconitase (*acnA*::Tn), isocitraat dehydrogenase (*icd*::Tn), fumaraat hydratase klasse II (*fumC*::Tn), en citraat synthase II (*gtlA*::Tn) genen. Inactiverende mutaties in *sdhA*, *sdhB* en *fumC* hadden een impact op biofilmvorming, waarbij de *fumC*::Tn mutant stam de grootste TCA-cyclus disfunctie vertoonde. Er werd geen defect in biofilmvorming gedetecteerd voor de *sucC*::Tn, *acnA*::Tn en *icd*::Tn mutanten. Bovendien is het tweede product van argininosuccinaat lyase, arginine, niet enkel een essentieel aminozuur gedurende biofilmgroei, maar is het katabolische bijproduct van arginine, ammonium, vereist voor pH homeostase. Daarom werd de rol van de urea cyclus onderzocht door middel van een inactiverende mutatie in arginase (*rocF*::Tn). Er was echter geen effect op de hoeveelheid gevormde biofilm biomassa. Pleiotropische effecten die mogelijks veroorzaakt werden door de transposon insertie werden nagekeken door middel van groeicurven, kwantitatieve reverse transcriptase PCR en complementatie. Er werd aangetoond dat de primaire impact van de TCA-cyclus zich situeert ter hoogte van de eiwit component die de biofilm matrix opbouwt in MRSA-USA300. De queeste voor biofilmvormingsmechanismen op het genoomniveau werd ook uitgebreid door de identificatie van potentieel betrokken genen in *S. aureus* biofilmvorming, door gebruik te maken van comparatieve genetische analyse (**artikel 4, hoofdstuk 3**). De stam USA300 UAS391 werd geselecteerd voor complete genoomsequenering en de daaropvolgende vergelijking van het UAS391 genoom met dat van andere gesequeneerde USA300 isolaten (TCH1516 en FPR3757) hield een beperkt aantal in van variante genen (n=18) die mogelijks verantwoordelijk konden zijn voor het geobserveerde verschil in capaciteit tot biofilmvorming. Het screenen van transposon mutanten die gedisrupteerd waren in één van deze doelwitgenen onthulde één mutant (NE229) die een transposon insertie droeg in SAUSA300_119 (*fakA*) en een verhoogde biofilmvorming vertoonde tot een biomassa vergelijkbaar met UAS391. Transductie experimenten bevestigden dat *fakA*::Tn overeenstemde met een 1.9 tot 4.6-maal verhoging in biofilmvorming afhankelijk van de USA300 stam achtergrond, terwijl complementatie van het TCH1516 wild type fakA allel in UAS391 resulteerde in een 4.3-

maal reductie in biofilmvorming. Deze sequentiële benadering, die bestond uit stamtypering, vergelijking van het genoom en functionele genetische analyse, identificeerde fakA (een recentelijk geïdentificeerd vetzuur kinase in *S. aureus* dat essentieel is voor fosfolipide synthese en een impact heeft op de transcriptie van talrijke virulentiefactoren) als een negatieve regulator van biofilmvorming in *S. aureus* USA300.

Deel 3.4. van hoofdstuk 3 concentreert zich vervolgens op de vraag of biofilm-geassocieerde kandidaatgenen al dan niet kunnen functioneren als kritische determinanten in het pathogeen succes en wijdverspreide prevalentie van MRSA (**artikel 5, hoofdstuk 3**). Genomische sequenering van een ST239 stam (TW20) uit Londen onthulde het bestaan van een nieuw oppervlak verankerde virulentiefactor, SasX (STW20_21850), die zowel kolonisatie als biofilmvorming promoot. Ons onderzoek bevestigde SasX als een kolonisatie-virulentie factor die potentieel aan de basis ligt van het endemische succes van MRSA-ST239 in Azië. We bestudeerden de verspreiding van SasX in MRSA geïsoleerd uit India en Europa, en rapporteerden, voor de eerste keer, het voorkomen van *sasX* en *sasX*-varianten, alsook het *sesI* gen gedragen door *S. epidermidis*, in Indische ST239 en andere MRSA van de CC8 klonale afstamming (5/9). Daarentegen was het voorkomen van sasX beperkt tot slechts enkele ST239 in Europa (2/121). Binnen deze gehele ST239 collectie konden we een nieuwe 'Indische' en 'Servische' clade ontdekken. *SasX* werd gedragen op een intacte ϕSPβ-gelijkende profaag van ~80 kb, terwijl *sesI* werd gedragen op een ϕSPβ-gelijkende profaag van ~118 kb. We identificeerden de insertielocatie van deze profaag ter hoogte van het *yeeE* gen. Onze data bevestigen de disseminatie en diversificatie van *sasX* en *sasX*-varianten in andere ST's dan ST239 in India, alsook de aanwezigheid van nieuwe prevalente ST239 clades in de Indische en Europese ziekenhuisomgeving.

Uiteindelijk reflecteert **hoofdstuk 4** over de gemaakte onderzoeksbevindingen en bespreekt het hoe een verbeterde kennis over de genetische basis van staphylococcale biofilms kan bijdragen tot het gebruik van nieuwe screening methoden, ontdekking van nieuwe geneesmiddelen en de ontwikkeling van geavanceerde biomedische apparatuur om biofilmvorming te voorkomen.

4.5. References

1. Pozzi, C., et al., *Methicillin resistance alters the biofilm phenotype and attenuates virulence in Staphylococcus aureus device-associated infections.* PLoS Pathog, 2012. **8**(4): p. e1002626.
2. Zapotoczna, M., E. O'Neill, and J.P. O'Gara, *Untangling the Diverse and Redundant Mechanisms of Staphylococcus aureus Biofilm Formation.* PLoS Pathog, 2016. **12**(7): p. e1005671.
3. Conlon, K.M., H. Humphreys, and J.P. O'Gara, *icaR Encodes a Transcriptional Repressor Involved in Environmental Regulation of ica Operon Expression and Biofilm Formation in Staphylococcus epidermidis.* Journal of Bacteriology, 2002. **184**(16): p. 4400-4408.
4. Knobloch, J.K., et al., *Biofilm formation by Staphylococcus epidermidis depends on functional RsbU, an activator of the sigB operon: differential activation mechanisms due to ethanol and salt stress.* J Bacteriol, 2001. **183**(8): p. 2624-33.

5. Mashruwala, A.A., A.V. Guchte, and J.M. Boyd, *Impaired respiration elicits SrrAB-dependent programmed cell lysis and biofilm formation in Staphylococcus aureus.* Elife, 2017. **6**.
6. O'Neill, E., et al., *Association between methicillin susceptibility and biofilm regulation in Staphylococcus aureus isolates from device-related infections.* J Clin Microbiol, 2007. **45**(5): p. 1379-88.
7. Rachid, S., et al., *Effect of Subinhibitory Antibiotic Concentrations on Polysaccharide Intercellular Adhesin Expression in Biofilm-Forming Staphylococcus epidermidis.* Antimicrobial Agents and Chemotherapy, 2000. **44**(12): p. 3357-3363.
8. De Backer, S., et al., *Enzymes Catalyzing the TCA- and Urea Cycle Influence the Matrix Composition of Biofilms Formed by Methicillin-Resistant Staphylococcus aureus USA300.* Microorganisms, 2018. **6**(4).
9. Sadykov, M.R., et al., *Tricarboxylic acid cycle-dependent regulation of Staphylococcus epidermidis polysaccharide intercellular adhesin synthesis.* J Bacteriol, 2008. **190**(23): p. 7621-32.
10. DeMars, Z. and J.L. Bose, *Redirection of Metabolism in Response to Fatty Acid Kinase in Staphylococcus aureus.* J Bacteriol, 2018. **200**(19).
11. Sabirova, J.S., et al., *Fatty acid kinase A is an important determinant of biofilm formation in Staphylococcus aureus USA300.* BMC Genomics, 2015. **16**: p. 861.
12. Massé, E., N. Majdalani, and S. Gottesman, *Regulatory roles for small RNAs in bacteria.* Current Opinion in Microbiology, 2003. **6**(2): p. 120-124.
13. Guillet, J., M. Hallier, and B. Felden, *Emerging functions for the Staphylococcus aureus RNome.* PLoS Pathog, 2013. **9**(12): p. e1003767.
14. Chambers, J.R. and K. Sauer, *Small RNAs and their role in biofilm formation.* Trends Microbiol, 2013. **21**(1): p. 39-49.
15. Novick, R.P., et al., *Synthesis of staphylococcal virulence factors is controlled by a regulatory RNA molecule.* EMBO J., 1993. **12**(10): p. 3967-3975.
16. Lindsay, J.A., *Evolution of Staphylococcus aureus and MRSA during outbreaks.* Infect Genet Evol, 2014. **21**: p. 548-53.
17. Planet, P.J., et al., *Emergence of the epidemic methicillin-resistant Staphylococcus aureus strain USA300 coincides with horizontal transfer of the arginine catabolic mobile element and speG-mediated adaptations for survival on skin.* MBio, 2013. **4**(6): p. e00889-13.
18. De Backer, S., et al., *Remarkable geographical variations between India and Europe in carriage of the staphylococcal surface protein-encoding sasX/sesI and in the population structure of methicillin-resistant Staphylococcus aureus belonging to clonal complex 8.* Clin Microbiol Infect, 2019. **25**(5): p. 628 e1-628 e7.
19. Li, M., et al., *MRSA epidemic linked to a quickly spreading colonization and virulence determinant.* Nat Med, 2012. **18**(5): p. 816-9.
20. Lindsay, J.A., *Genomic variation and evolution of Staphylococcus aureus.* Int J Med Microbiol, 2010. **300**(2-3): p. 98-103.
21. Hoiby, N., et al., *ESCMID guideline for the diagnosis and treatment of biofilm infections 2014.* Clin Microbiol Infect, 2015. **21 Suppl 1**: p. S1-25.
22. Tkaczyk, C., et al., *Targeting Alpha Toxin and ClfA with a Multimechanistic Monoclonal-Antibody-Based Approach for Prophylaxis of Serious Staphylococcus aureus Disease.* MBio, 2016. **7**(3).
23. Hilliard, J.J., et al., *Anti-alpha-toxin monoclonal antibody and antibiotic combination therapy improves disease outcome and accelerates healing in a Staphylococcus aureus dermonecrosis model.* Antimicrob Agents Chemother, 2015. **59**(1): p. 299-309.
24. Anderson, M.J., et al., *Alpha-Toxin Contributes to Biofilm Formation among Staphylococcus aureus Wound Isolates.* Toxins (Basel), 2018. **10**(4).
25. Creech, C.B., et al., *Safety, tolerability, and immunogenicity of a single dose 4-antigen or 3-antigen Staphylococcus aureus vaccine in healthy older adults: Results of a randomised trial.* Vaccine, 2017. **35**(2): p. 385-394.
26. Stranger-Jones, Y.K., T. Bae, and O. Schneewind, *Vaccine assembly from surface proteins of Staphylococcus aureus.* Proc Natl Acad Sci U S A, 2006. **103**(45): p. 16942-7.

27. Fowler, V.G., Jr. and R.A. Proctor, *Where does a Staphylococcus aureus vaccine stand?* Clin Microbiol Infect, 2014. **20 Suppl 5**: p. 66-75.
28. Kim, H.K., et al., *Nontoxigenic protein A vaccine for methicillin-resistant Staphylococcus aureus infections in mice.* J Exp Med, 2010. **207**(9): p. 1863-70.
29. Schneewind, O. and D. Missiakas, *Sortases, Surface Proteins, and Their Roles in Staphylococcus aureus Disease and Vaccine Development.* Microbiol Spectr, 2019. **7**(1).
30. Zhang, J., et al., *Antiinfective therapy with a small molecule inhibitor of Staphylococcus aureus sortase.* Proc Natl Acad Sci U S A, 2014. **111**(37): p. 13517-22.
31. Arciola, C.R., et al., *Detection of biofilm formation in Staphylococcus epidermidis from implant infections. Comparison of a PCR-method that recognizes the presence of ica genes with two classic phenotypic methods.* J Biomed Mater Res A, 2006. **76**(2): p. 425-30.
32. Liu, Q., et al., *Targeting surface protein SasX by active and passive vaccination to reduce Staphylococcus aureus colonization and infection.* Infect Immun, 2015. **83**(5): p. 2168-74.
33. Ramasubbu, N., et al., *Structural analysis of dispersin B, a biofilm-releasing glycoside hydrolase from the periodontopathogen Actinobacillus actinomycetemcomitans.* J Mol Biol, 2005. **349**(3): p. 475-86.
34. Chaignon, P., et al., *Susceptibility of staphylococcal biofilms to enzymatic treatments depends on their chemical composition.* Appl Microbiol Biotechnol, 2007. **75**(1): p. 125-32.
35. Izano, E.A., et al., *Differential roles of poly-N-acetylglucosamine surface polysaccharide and extracellular DNA in Staphylococcus aureus and Staphylococcus epidermidis biofilms.* Appl Environ Microbiol, 2008. **74**(2): p. 470-6.
36. Kokai-Kun, J.F., T. Chanturiya, and J.J. Mond, *Lysostaphin as a treatment for systemic Staphylococcus aureus infection in a mouse model.* J Antimicrob Chemother, 2007. **60**(5): p. 1051-9.
37. Kokai-Kun, J.F., T. Chanturiya, and J.J. Mond, *Lysostaphin eradicates established Staphylococcus aureus biofilms in jugular vein catheterized mice.* J Antimicrob Chemother, 2009. **64**(1): p. 94-100.
38. Patil A, M.R., *Role of Extracellular Proteases in Biofilm Disruption of Gram Positive Bacteria with Special Emphasis on Staphylococcus aureus Biofilms.* Enzyme Engineering, 2014. **04**(01).
39. Chao, Y., et al., *Streptococcus pneumoniae biofilm formation and dispersion during colonization and disease.* Front Cell Infect Microbiol, 2014. **4**: p. 194.
40. Marks, L.R., et al., *Streptococcus pyogenes biofilm growth in vitro and in vivo and its role in colonization, virulence, and genetic exchange.* J Infect Dis, 2014. **210**(1): p. 25-34.
41. Brackman, G., et al., *Quorum sensing inhibitors increase the susceptibility of bacterial biofilms to antibiotics in vitro and in vivo.* Antimicrob Agents Chemother, 2011. **55**(6): p. 2655-61.
42. Parsons, J.B., et al., *Identification of a two-component fatty acid kinase responsible for host fatty acid incorporation by Staphylococcus aureus.* Proc Natl Acad Sci U S A, 2014. **111**(29): p. 10532-7.
43. Parsons, J.B., et al., *Metabolic basis for the differential susceptibility of Gram-positive pathogens to fatty acid synthesis inhibitors.* Proc Natl Acad Sci U S A, 2011. **108**(37): p. 15378-83.
44. Parsons, J.B., et al., *Perturbation of Staphylococcus aureus gene expression by the enoyl-acyl carrier protein reductase inhibitor AFN-1252.* Antimicrob Agents Chemother, 2013. **57**(5): p. 2182-90.
45. McCann, M.T., B.F. Gilmore, and S.P. Gorman, *Staphylococcus epidermidis device-related infections: pathogenesis and clinical management.* J Pharm Pharmacol, 2008. **60**(12): p. 1551-71.
46. Moriarty, T.F., J.S. Elborn, and M.M. Tunney, *Effect of pH on the antimicrobial susceptibility of planktonic and biofilm-grown clinical Pseudomonas aeruginosa isolates.* British Journal of Biomedical Science, 2016. **64**(3): p. 101-104.
47. Lebeaux, D., et al., *From in vitro to in vivo Models of Bacterial Biofilm-Related Infections.* Pathogens, 2013. **2**(2): p. 288-356.
48. Lebeaux, D., et al., *In vitro activity of gentamicin, vancomycin or amikacin combined with EDTA or l-arginine as lock therapy against a wide spectrum of biofilm-forming clinical strains isolated from catheter-related infections.* J Antimicrob Chemother, 2015. **70**(6): p. 1704-12.
49. Pletzer, D. and R.E. Hancock, *Antibiofilm Peptides: Potential as Broad-Spectrum Agents.* J Bacteriol, 2016. **198**(19): p. 2572-8.

50. Romano, C.L., et al., *Antibacterial coating of implants in orthopaedics and trauma: a classification proposal in an evolving panorama.* J Orthop Surg Res, 2015. **10**: p. 157.
51. von Eiff, C., et al., *Infections associated with medical devices: pathogenesis, management and prophylaxis.* Drugs, 2005. **65**(2): p. 179-214.
52. Wertheim, H.F.L., et al., *The role of nasal carriage in Staphylococcus aureus infections.* The Lancet Infectious Diseases, 2005. **5**(12): p. 751-762.
53. Datta, R. and S.S. Huang, *Risk of infection and death due to methicillin-resistant Staphylococcus aureus in long-term carriers.* Clin Infect Dis, 2008. **47**(2): p. 176-81.
54. Knight, G.M., et al., *Shift in dominant hospital-associated methicillin-resistant Staphylococcus aureus (HA-MRSA) clones over time.* J Antimicrob Chemother, 2012. **67**(10): p. 2514-22.
55. Sai, N., et al., *Efficacy of the decolonization of methicillin-resistant Staphylococcus aureus carriers in clinical practice.* Antimicrob Resist Infect Control, 2015. **4**: p. 56.
56. Seth, A.K., et al., *Bacteriophage therapy for Staphylococcus aureus biofilm-infected wounds: a new approach to chronic wound care.* Plast Reconstr Surg, 2013. **131**(2): p. 225-34.
57. Cerca, N., R. Oliveira, and J. Azeredo, *Susceptibility of Staphylococcus epidermidis planktonic cells and biofilms to the lytic action of staphylococcus bacteriophage K.* Lett Appl Microbiol, 2007. **45**(3): p. 313-7.
58. Gutierrez, D., et al., *Bacteriophages as Weapons Against Bacterial Biofilms in the Food Industry.* Front Microbiol, 2016. **7**: p. 825.
59. Schuch, R., et al., *Bacteriophage Lysin CF-301, a Potent Antistaphylococcal Biofilm Agent.* Antimicrob Agents Chemother, 2017. **61**(7).
60. Dickey, J. and V. Perrot, *Adjunct phage treatment enhances the effectiveness of low antibiotic concentration against Staphylococcus aureus biofilms in vitro.* PLoS One, 2019. **14**(1): p. e0209390.
61. Yang, L., et al., *Current understanding of multi-species biofilms.* Int J Oral Sci, 2011. **3**(2): p. 74-81.
62. Willems, H.M., Z. Xu, and B.M. Peters, *Polymicrobial Biofilm Studies: From Basic Science to Biofilm Control.* Curr Oral Health Rep, 2016. **3**(1): p. 36-44.

Acknowledgements

First, I would like to thank **Prof. Dr. Malhotra-Kumar** and **Prof. Dr. Goossens** for the amazing opportunity they offered me to work in their laboratory. Prof. Dr. Malhotra-Kumar, thank you for your numerous proof-readings of my articles, guidance, patience, and encouragement. Prof. Dr. Goossens, dank u voor uw aanstekelijke enthousiasme, en uw steun in tijden van crisis.

Daarnaast wil ik het **Fonds voor Wetenschappelijk Onderzoek** bedanken voor de beurs die me de kans gaf dit onderzoek uit te voeren.

I want to thank the members of my doctoral committee; Prof. Dr. Jorens, **Prof. Dr. Ir. Lebeer**, **Prof. Dr. Van Dijck**, **Prof. Dr. Lindsay** and **Dr. Vuong**, for investing their time and efforts in reviewing this thesis.

Ik heb ook het geluk gehad om met andere labo's te mogen samenwerken. **Prof. Dr. Kumar-Singh** of the Laboratory of Cell Biology & Histology (UA), thank you for the nice cooperation. **Prof. Dr. De Greve** van het Structural Biology Brussels (VUB) en Structural & Molecular Microbiology (VUB), en **Prof. Dr. Hernalsteens** van het Viral Genetics Laboratory (VUB), bedankt voor de fijne samenwerking.

Verder wil ik heel graag alle (voormalige) collega's van het laboratorium voor Medische Microbiologie bedanken voor deze onschatbare ervaring die ik nooit zal vergeten. Thank you: **Ann**, **Anne**, **Anupam**, **Bart**, **Britto**, **Christine**, **Daniele, Domenico**, **Fabienne**, **Fien**, **Greet** (Van Kerckhoven), **Hadi**, **Ines**, **Inge**, **Ismail**, **Jasha**, **Jelle**, **Juan Pablo**, **Kenny**, **Konstantina**, **Kevin**, **Julia**, **Lai Ting**, **Lavanya**, **Leen**, **Liesbeth** (Van Heirstraeten), **Matilda**, **Mattia**, **Mayri**, **Melanie**, **Michael**, **Minh**, **Mohamed**, **Pieter**, **Rohit**, **Sien**, **Tuba**, **Veronique**, and **Vincent**.

Liesbeth (Bryssinck), **Anouk**, **Sabine**, **Gert**, **Stalin**, **Kitty**, **Mandy K**. en **Mandy A**., deze thesis zou nooit gelukt zijn zonder jullie continue steun en hulp, vriendelijkheid en de lekkere frietjes. A special thanks goes out to **Tomi** & **Agata** for the unforgettable HGSM-meetings. **Jasmine**, **An** en **Lore**, bedankt voor de lekkere pizza's en ik wil ook **Pien** heel erg hard bedanken om mijn buddy te zijn door dik en dun.

Tenslotte wil ik mijn familie bedanken voor hun interesse, steun en vertrouwen. **Thomas** wil ik bedanken om mijn lichtpuntje te zijn. **Mama**, **papa**, **Vicky** en **bomma**, bedankt voor jullie onvoorwaardelijke steun, jullie inlevingsvermogen, jullie liefde,… Bedankt om er te zijn, altijd.

Deze thesis is evenzeer jullie prestatie als de mijne - Sarah

Addendum: Curriculum vitae

Name: **Sarah De Backer**
Current affiliation: VAXINFECTIO, Laboratory of Medical Microbiology (LMM)
University of Antwerp, Campus Drie Eiken, S6.25
Universiteitsplein 1, 2610 Wilrijk, België
Tel: +32 3 265 93 25
Email: sarah.debacker@uantwerpen.be

Education

2015 – now **Research scholarship Flanders (FWO) navorser – predoctoral mandate**

Universiteit Antwerpen, Wilrijk

Topic: Insight in methicillin-resistant *Staphylococcus aureus* (MRSA) biofilms – Identification of key determinants in biofilm formation of highly pathogenic and globally successful MRSA clones

2014 – 2015 **Junior researcher – BAP (Non-statutory academic personnel)**
Universiteit Antwerpen, Wilrijk

Topic: Insight in methicillin-resistant *Staphylococcus aureus* (MRSA) biofilms – Identification of key determinants in biofilm formation of highly pathogenic and globally successful MRSA clones

2012-2014 **Master in de biomedische wetenschappen**
Universiteit Antwerpen, Wilrijk

Master thesis: Microbiological interactions in an endotracheal tube biofilm and its role in the development of VAP in mechanically ventilated patients.

2009-2013 **Bachelor in de biologie**
Universiteit Antwerpen, Wilrijk

2003-2009 **Wetenschappen – Talen**
Sint-Ritacollege, Kontich

Articles in international peer-reviewed journals

De Backer, S., Xavier, B. B., Vanjari, L., Coppens, J., Lammens, C., Vemu, L., Carevic, B., Hryniewicz, W., Kumar-Singh, S., Lee, A., Harbarth, S., Schrenzel, J.,

Tacconelli, E., Goossens, H., Malhotra-Kumar, S., "*Remarkable geographical variations between India and Europe in carriage of the staphylococcal surface protein-encoding sasX/sesI and in the population structure of methicillin-resistant Staphylococcus aureus belonging to clonal complex 8*", Clinical Microbiology & Infection 2018, pii: S1198-743X(18)30542-1. doi: 10.1016/j.cmi.2018.07.024. Peer review. Impact factor: 5.394.

De Backer, S., Sabirova, J., De Pauw, I., De Greve, H., Hernalsteens, J., Goossens, H., Malhotra-Kumar, S., "*Enzymes catalyzing the TCA- and urea cycles influence the matrix composition of biofilms formed by methicillin-resistant Staphylococcus aureus USA300*", Microorganisms **2018**, 6, 113; doi:10.3390/microorganisms6040113. Peer review. Tracked for impact factor.

Coppens, J., Xavier, B. B., Vanjari, L., De Backer, S., Lammens, C., Vemu, L., Goossens, H. & Malhotra-Kumar, S., "Novel composite *SCCmec* type III element in ST239 MRSA isolated from an Indian hospital.", Journal of Antimicrobial Chemotherapy, dky399, doi: 10.1093/jac/dky399. Peer review. Impact factor: 5.217.

Sabirova, S., Hernalsteens, J., De Backer, S., Xavier, B. B., Moons, P., Turlej-Rogacka, A., H., Goossens, H. & Malhotra-Kumar, S., "*Fatty acid kinase A is an important determinant of biofilm formation in Staphylococcus aureus USA300.",* BMC Genomics, (2015), 16: 861, doi: 10.1186/s12864-015-1956-8. Peer review. Impact factor: 3.73.

Articles under submission in international peer-reviewed journals

Hotterbeekx, A., Sonoda, A. T., De Backer, S., Bielen, K., Lammens, C., Jorens, P. G., Kumar-Singh, S., Goossens, H., & Malhotra-Kumar, S., "*Virulence, growth and biofilm formation by Pseudomonas aeruginosa is enhanced by clinical isolates of Staphylococcus epidermidis*", submitted to Applied and Environmental Microbiology.

Oral presentations in international meetings

De Backer, S., De Greve, H., Lammens, C., Goossens, H., Hernalsteens, J., & Malhotra-Kumar, S., "*TCA cycle intermediate malate stimulates biofilm formation in methicillin-resistant Staphylococcus aureus USA300*", ECCMID 2018 (28th edition), Madrid, Spain (21-24 April 2018), **oral presentation**.

De Backer, S., Xavier, B. B., Vanjari, L., Coppens, J., Lammens, C., Vemu, L., Schrenzel, J., Tacconelli, E., Goossens, H. & Malhotra-Kumar, S., "*Genomic context of a colonization and pathogenicity determinant, sasX, in methicillin-resistant Staphylococcus aureus.*", ECCMID 2016 (26th edition), Amsterdam, The Netherlands (9-12 April 2015), **oral presentation**.

Sabirova, J. S., De Backer, S., De Pauw, I., De Greve, H., Hernalsteens, J., Goossens, H. & Malhotra-Kumar, S., "*Enzymes catalyzing the urea and TCA cycles are important determinants of biofilm formation in methicillin-resistant Staphylococcus aureus USA300.",* ECCMID 2015 (25th edition), Copenhagen, Denmark (25-28 April 2015), **oral presentation**.

Vlaeminck, J., Xavier, B.B., De Backer, S., Kumar-Singh, S., Goossens, H., Malhotra-Kumar, S. "*Staphylococcus aureus persister cells show repressed arginine biosynthesis by downregulation of argG and argH*", ECCMID 2019 (29th edition), Amsterdam, the Netherlands (13-16 April 2019), **oral presentation**.

Poster presentations in international meetings

De Backer, S.**,** De Pauw,I., Hernalsteens, J., Sabirova, J., De Greve, H., Goossens, H. & Malhotra-Kumar, S., "*The role of MecR1 in biofilm formation by methicillin-resistant Staphylococcus aureus USA300.",* ECCMID 2016 (26th edition), Amsterdam, The Netherlands (9-12 April 2015), **eposter presentation**.

De Backer, S., Xavier B.B., De Greve, H., Kumar-Singh, S., Goossens, H., Hernalsteens, JP., Malhotra-Kumar, S. "*Biofilms formed by pandemic methicillin-resistant Staphylococcus aureus clones show upregulation of the arginine deiminase pathway*", ECCMID 2019 (29th edition), Amsterdam, the Netherlands (13-16 April 2019), **poster presentation**.

De Backer, S., Vanmarsenille, C., Vermeulen, W., Holappa, K., De Greve, H., Goossens, H., Hernalsteens, J., & Malhotra-Kumar, S., "*Screening of a bursa aurealis transposon library identified major protein families involved in biofilm formation by Staphylococcus aureus USA300*", ECCMID 2017 (27th edition), Vienna, Austria (22-25 April 2017), **poster presentation**.

De Backer, S**.**, Xavier, B. B., Vanjari, L., Vemu, L., Goossens, H. & Malhotra-Kumar, S., "*Dissemination of the colonization and virulence determinant, sasX, among Indian and European methicillin-resistant Staphylococcus aureus.*", ECCMID 2015 (25th edition), Copenhagen, Denmark (25-28 April 2015), **poster presentation**.

De Backer, S., Vanmarsenille, C., Hernalsteens, J., Xavier, B. B., De Greve, H., Goossens, H. & Malhotra-Kumar, S., "*Stage-dependent changes in matrix composition of biofilms formed by methicillin-resistant Staphylococcus aureus UAS391_USA300*." European Congress on Microbial Biofilms 2015 (Eurobiofilms, 4th edition), Brno, Czech Republic (23-26 June, 2015), **poster presentation** .

Hotterbeekx, A., De Backer, S., Moons, P., Lammens, C., Ieven, M., Vandenbroek, E., Jorens, P., Kumar-Singh, S., Goossens, H. & Malhotra-Kumar, S., "*Differential effects*

of biofilm supernatant of Pseudomonas aeruginosa and Serratia marcescens on biofilm formation of clinical Staphylococcus epidermidis isolates." European Congress on Microbial Biofilms 2015 (Eurobiofilms, 4th edition), Brno, Czech Republic (23-26 June, 2015), **poster presentation**.